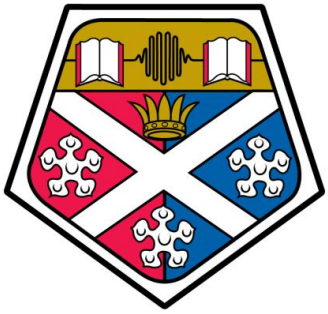

Power Quality Enhancement in Distribution Networks with Distributed Generation

A thesis presented for the degree of

Doctor of Philosophy

At the University of Strathclyde

by

Piyadanai Pachanapan

Supervisor: Dr. Olimpo Anaya-lara

Power Systems Research Group

Department of Electronic and Electrical Engineering

University of Strathclyde

Glasgow, United Kingdom

2012

Declaration of author's rights

This thesis is the result of the author's original research. It has been composed by the author and has not been previously submitted for examination which has led to the award of a degree.

Signed: _____ Date: _____.

Acknowledgements

First, I would like to thank my principal supervisor Dr.Olimpo Anaya-lara in providing guidance and useful comments throughout my PhD study. Without Dr. Olimpo, my goal of submitting my thesis would not have been accomplished. Thanks also to my second supervisor Professor K.L. Lo for his guidance and support. He also gave me a good opportunity to join and work in power systems research group in institute for energy and environment, for 4 years. Many thanks also to Dr. Adam Dysko who took care of me while Dr. Olimpo had been away for a year in Norway, and gave me a good chance to join a project with Scottish Power.

Second, I would like to thank the Royal Thai Government and Faculty of Engineering, Naresuan University for the scholarship and their financial support.

Third, special thanks to Dr. Thamvarit Singhavilai and Dr. Grain Philip Adam for the guidance to pursue my PhD study. Many thanks to Umarin Sangpanich, Kanogkan Leerojanaprapa, Karantarat Nakwa and Chanpen Phokaew and her family for their emotional support and encouragement during my study in Glasgow. Also, thank to Dr. Burin Tharavichitkun for warming support especially during my starting time in UK. Moreover, thank to all Thai students that I have met in Glasgow and Scotland which they make my life likes home while I am studying in the place very far from Thailand.

Last but not least, I am very grateful to thank my family back home, my mother (Dusaddee) and my brothers (Danuwat and Chatpong), for their understanding, support, caring thought and greatest love.

Piyadanai Pachanapan

September 2012

Abstract

This thesis investigates and proposes novel solutions to enhance voltage quality in medium networks with increased distributed generation (DG) penetration, focusing on voltage level variations and harmonic distortion. A new hierarchical distributed voltage control structure is proposed for DG to facilitate autonomous integrated Volt-VAr control in medium networks with DG. It is implemented especially in converter-connected DG, and in addition to enhancing voltage quality, the proposed controller also reduces the need to install new compensation devices. A decentralised active voltage control is developed for DG units to provide short and long-term voltage compensation by manipulating their reactive power output. Local controllable zones (LCZs) are introduced and used to determine the voltage control boundaries for each DG unit, and a methodology is introduced to allow LCZ adapt and follow network changes in real time. The performance and value of the proposed LCZ identification method and voltage control approaches are demonstrated based on load-flow and transient simulations, under various network operating scenarios conducted in DigSILENT *PowerFactory*. A droop control and a coordinated controller between DG units and other voltage controllable devices is presented to enhance voltage controllability whilst minimizing voltage interaction between devices, in case more than one DG unit, in the same LCZ, supports voltage control at the same time.

The proposed coordinated controller applies to DG units, and also to DG units and other voltage compensators such as the modern on-load tap changer (OLTC) and the solid-state transformer (SST). In this context, DG provides primary support, and the other devices concentrate on providing secondary voltage support. Also, a DG structure combining energy storage systems (ESS) is proposed to enhance voltage quality by controlling not only the reactive power output from the DG unit, but also either active or reactive power output of ESS, thus allowing the voltage control to be more effective in a wider range of scenarios. The control and operation of DG in cooperation with a voltage regulator (VR) is also investigated. The voltage regulator is assumed as the secondary voltage support to provide slow voltage control to a wider area, including LCZs, located behind its secondary side. Furthermore, the substation's OLTC can give the slow voltage support similar to the voltage regulator but it provides the wide-area voltage control to cover the whole network including those buses which do not belong to any LCZs. The coordinated voltage controller approach

presented is demonstrated under various network operating scenarios using case studies based on the IEEE 33-bus radial distribution network.

Harmonic distortion across the network when the number of converter-connected DG is increased is also investigated in the thesis. It is found that the increase of this type of DG can raise the level of harmonic distortion to above the statutory limits. A generic approach is adopted to reduce the harmonic injection from converter-connected DG units and non-linear loads, using a phase-shifting technique. By changing the vector group between transformers that connect either converter-connected DG or non-linear loads is operated off-line for self-harmonic cancellation, without physically modifying the existing converter unit. The case study is based on the typical 17-bus medium voltage Dutch network. The performance of the proposed harmonic mitigation solution is examined under various scenarios based on harmonic load flow calculations performed on the distribution network modelled in the harmonic domain.

Table of contents

List of figures

List of Tables

List of symbols and abbreviations

List of symbols

$[\partial V/\partial P]$	Voltage sensitivity matrix from the change of active power
$[\partial V/\partial Q]$	Voltage sensitivity matrix from the change of reactive power
$\hat{f}_1$	Amplitude of the fundamental frequency
$\hat{f}_h$	Amplitude of the harmonic
f_h	Considered frequency
f_s	Switching frequency
f_t	Tune frequency
h	Harmonic order
i_d, i_q	The feedback currents of voltage source converter in the *dq* synchronous rotating reference frame
$i_{d,ref}$, $i_{q,ref}$	The reference currents of voltage source converter in the *dq* synchronous rotating reference frame
$\mathbf{I_h}$	Vector of the nodal harmonic current injections at consider frequency *h*
$\mathbf{J}$	Jacobian matrix
K_{dq}	Derivative gain of droop controller
K_{droop}	*V*-*Q* droop coefficient
k_o	Constant factor (depends on the modulation method)
K_{pq}	Proportional gain of droop controller
m	Modulation index
P	Active power
P_G	DG supplies active power
P_{st}	Short-term flicker index
Q	Reactive power
Q_f	The quality factor
Q_G	DG supplies reactive power
Q_{gen}	Reactive power being dispatched by the DG unit
Q_{res}	Available reserved *Q* in a DG unit
$T_{DG,ref}$	Time period for updating the voltage reference
THD_I	Total current harmonic distortion

THD_V	Total harmonic distortion of the bus voltage
V	Voltage
$V_{ac,\,ref}$	Voltage reference of voltage source converter controller
V_{DB}	Dead band voltage
V_{DG}	Voltage level at DG bus
$V_{DG,lower}$	DG lower limit voltage
$V_{DG.upper}$	DG upper limit voltage
$\mathbf{V_h}$	Vector of the resulting harmonic voltages at consider frequency *h*
V_{mod}	Voltage modulation signal
$V_{OLTC,lower}$	Lower limit of OLTC's voltage control at the substation
$V_{OLTC,upper}$	Upper limit of OLTC's voltage control at the substation
$V_{re,lower}$	Lower limit for remote voltage control of voltage regulator
$V_{re,max}$	Maximum voltage level of remote measurements
$V_{re,min}$	Minimum voltage level of remote measurements
$V_{re,upper}$	Upper limit for remote voltage control of voltage regulator
V_s	Voltage at the point of common coupling
$V_{stat,lower}$	Lower statutory voltage limit
$V_{stat,upper}$	Upper statutory voltage limit
V_{sub}	Voltage level at the secondary side of substation
$V_{sub,lower}$	Lower limit of acceptable voltage level at the substation
$V_{sub,upper}$	Upper limit of acceptable voltage level at the substation
V_t	Voltage at the terminal of voltage source converter
V_{VR}	Voltage level at the secondary side of VR
$V_{VR,lower}$	Lower limit of acceptable voltage level at secondary side of VR
$V_{VR,upper}$	Upper limit of acceptable voltage level at at secondary side of VR
$\mathbf{Y_h}$	Network admittance matrix at considered frequency *h*
ΔP	Value of chanigng active power in controllable DG or ESS
ΔP_{DG}	Available real power support from DG
ΔQ	Value of chanigng reactive power in controllable DG or ESS
ΔQ_{DG}	Available reactive power support from DG
ΔV	Votlage error between voltage reference and voltage feedback of VSC
$\Delta \mathbf{V_{CN}}$	Vector of voltage variations in critical buses
ΔV_i	Voltage change in all buses due to a DG perturbation
Δv_s	Instantaneous voltage variations at point of common coupling
ω	Angular velocity

ω_0	Source frequency
δ	Phase voltage angle

List of abbreviations

AC	Alternating current
ADA	Advance distribution automation
AVR	Automatic voltage regulator
CHP	Combined heat and power
CSC	Current source converter
D	Delta winding connection
DC	Direct current
DG	Distributed generation
DLC	Distribution line carrier
DMS	Distribution management system
DNO	Distribution network operator
DSTATCOM	Distribution static compensator
DVR	Dynamic voltage restorer
ESS	Energy storage system
GA	Genetic algorithm
GIS	Geographic information system
GPS	Global positioning system
GTO	Gate turn-off thyristor
HV	High voltage
ICE	Internal combustion engine
ICT	Information and communication technology
IED	Intelligent electronic device
IGBT	Insulated gate bipolar transistor
IP	Internet protocol
IVVC	Integrated Volt-Var control
LAN	Local area network
LCZ	Local controllable zone
LV	Low voltage
MAS	Multi-agent systems

MV	Medium voltage
OBDD	Ordered binary decision diagram
OLTC	On load tap changer
p.f.	Power factor
PCC	Point of common coupling
PD controller	Proportional derivative controller
PI controller	Proportional integral controller
PLL	Phase locked loop
PMU	Phasor measurement unit
PST	Phase-shifting transformer
PV	Photovoltaic
PWM	Pulse width modulation
QT	Quality-threshold
rms	Root-mean-square
RTU	Remote terminal units
SCADA	Supervisory control and data acquisition
SST	Solid state transformer
SVC	Static var compensator
TCP	Transmission control protocol
TCR	Thyristor controlled reactor
THD	Total harmonic distortion
TSC	Thyristor switched capacitor
VR	Voltage regulator
VSC	Voltage source converter
WAN	Wide area network
WLS	Weighted least squares estimation
Y	Wye winding connection

Chapter 1
Introduction

1.1 Introduction

Electrical power generation is being changed from centralised to decentralised generation over the last decade. The main driver behind this change is the growing concern of climate change and the requirements to reduce carbon dioxide emissions from conventional fossil power plant, by using small and dispersed generation called distributed generation (DG), which consists of small distributed generators and renewable energy sources. In addition, DG technologies include small-scale wind turbines, photovoltaic (PV) arrays, internal combustion engine (ICE) and micro combined heat-and-power (μCHP) [1]. Moreover, energy storage systems (ESSs) and custom power devices are currently being installed into distribution networks either in medium voltage (MV) or low voltage (LV), with the aim to enhance power generation and network performance.

The worldwide growth of DG was predicted in [1] from less than 5% sharing in 2001 to approximately 15 % share of worldwide generation capacity in 2008. Furthermore, this literature also shows that the installed capacity of micro-turbine has increased from less than 20 MW (<500 units) to more than 150 MW in 2011 (>3500 units). In Europe, the highest share of DG generation is from CHP [2]. This reference also shows that Denmark, Portugal, Spain and the Netherlands are countries with high penetration level of DG, where DG shares approximately 20-30% of overall energy production (in each country) in 2006. In case of renewable energy, the wind energy integration around the world in 2005 is reported in [3], which shows that the growth of wind energy integration has raised dramatically all around the world especially in European countries.

Although DG can provide various benefits to network operation [4], it also poses significant challenges in terms of power quality [5]. These challenges affect directly how much DG can be installed. Additionally, new DG connections can affect the voltage profile in the system and raise the voltage level outside statutory limits in some buses. The uncertain characteristic of intermittent renewable resources, particularly wind and solar, can cause voltage and power fluctuation problems. Furthermore, unlike conventional synchronous generation plant, many types of new DG technologies are interfaced to the network through power electronic

converter devices such as PV, small-scale wind turbine and μCHP, which can become a harmonic source and can increase power losses in the network.

This thesis investigates the power quality problems in distribution networks due to increased DG penetration. Many power quality enhancement solutions have been investigated and proposed. Conventional compensation devices such as capacitor banks are employed to improve the power quality but their slow speed of response and lack of adaptability limit their application to steady-state voltage variations. Modern power conditioning devices can provide fast controllability and adapt to changes in network conditions. However, they are costly. Using the support from DG is a promising approach to improve power quality especially the voltage quality. Converter-based DG, which tends to increase in future networks, and has the potential to support short- and long-term voltage variations. Therefore, DG with voltage control capability is being developed to assist enhancing voltage quality and to minimise the impact that increased DG penetration may have on it.

Novel control structures, which consist of decentralised and centralised control systems, are introduced in this thesis to manage the control and operation of DG units and other controllable devices across the network with the aim to enhance power quality and to comply with established standards (e.g. IEEE 519-1992, IEEE 1547 and IEEE 1159-2009), and Grid Codes in different countries particularly in terms of harmonic distortion, voltage flickering, and short- and long-term voltage variations. In addition, the decentralised control is mainly provided by using DG, whereas the centralised control is operated from the substation. The coordinated approach between decentralised and centralised control is proposed to increase the controllability and to prevent interactions between controllable devices.

This chapter is set out to give an overview of technical solutions to improve power quality in distribution networks. Solutions for voltage level improvement are firstly reviewed, and then those for harmonic mitigation. From the review, research gaps are identified: 1) previous research has aimed to use DG for steady-state voltage control rather than dynamic voltage control, and coordination between DG and other controllable devices is lacking; and 2) harmonic mitigation solutions are required when the number of converter-based DG increases, where less costly solutions are preferred to expensive active filters.

1.2 Review of power quality improvement solutions in distribution networks with distributed generation

This review is split into two parts. The first part discusses voltage level improvement approaches in distribution networks with DG connection. Selected literature is brought to show a variety of possible voltage level control methods. The second part addresses the challenging issues of harmonic pollution when a large amount of new power electronic-interfaced DG technology connects to the distribution network. The possible solutions for harmonic mitigation also are discussed.

1.2.1 Review of voltage level improvement solutions

At present, distribution networks with DG are operated in a passive way. Most DG is installed as 'fit and forget' and cannot participate in active voltage control. Centralised control provided by the OLTC at the substation [6] is used to regulate the voltage profile for the whole network. However, this approach has limitations when dealing with short-term disturbances due to the rather slow response of the tap changer, making it hard to comply with international standards such as the IEEE 1159-2009 [7]. Also, existing decentralised voltage control is based on capacitor banks and voltage regulators located in specific areas of the network [8]. Power conditioning devices (also called custom power devices), such as the distribution static compensator (DSTATCOM), can provide fast decentralised voltage compensation, but are very costly [9].

DG can provide decentralised voltage controllability by adjusting either its active power (P) or its reactive power (Q) output [10]-[12]. If DG is operated as firm generation, constant P output is preferred and the voltage is therefore compensated from injection or absorption of Q. The integrated Volt-Var control (IVVC) from the conventional synchronous generator type DG is operated by the excitation system. However, using excitation has various limitations due to the stability issues of the stator and rotor windings [13]. The slow response of the governor is also an issue, which can cause big power swings after the disturbance is cleared [14].

Converter-connected DG technologies, such as CHP, large PV plants and small wind farms, are another option for active decentralised voltage control [15]. An oversized DG is required to provide extra Q for voltage support. Although the oversize causes more investment, the Q

support from converter-connected DG is already enforced by Grid Codes in some countries, such as Germany [16], for either steady-state or dynamic voltage control. The fast automatic voltage controllability from converter-connected PV plant is demonstrated and examined via simulation and field test verifications in [17].

A coordinated voltage controller is required when a group of voltage controllable devices is installed in the network. The coordinated strategy aims to enhance voltage controllability and to optimise the operation of controllable devices to avoid the 'hunting effect' that may occur from the interaction between voltage controllers. The coordinated voltage control has already been employed in several distribution network applications including: coordinated control among DG units [18],[19], between voltage regulators and capacitor banks [8], among voltage regulator and DG [20], the substation's OLTC and capacitor banks [21], the substation's OLTC and microgrid [22] and a lot of researchers are working on coordinated control among the substation's OLTC and DG [23]-[34].

The coordinated voltage control between the substation's OLTC and DG is used in active network management in many ways: supplying minimum *Q* from DG [23]-[25], dealing with the intermittency of DG resources [26], and increasing the penetration level of DG [27]. Additionally, the critical locations which have voltage problems can be determined by: 1) using forecasting information of load demand and generation profile [28]; 2) using distribution state-estimation from on-line remote measurements [29]-[31] (for which communication links are required). However, the time interval for updating the new OLTC and DG set-points takes several minutes (i.e. about 5 to 15 minutes) due to the limit of forecasting data and time consumed in the state-estimation process. For real-time voltage control, information of the controlled voltages is directly sent from remote measurements at critical and pilot buses [32]-[34] (i.e. at the substation and DG buses). However, this method provides voltage control only in those buses where measurements are available.

From the above literature review, it is found that the coordinated voltage level control between DG and other controllable devices is mostly applied for steady-state voltage control rather than dynamic voltage control. The optimal operation for voltage regulation, which is steady-state voltage control, requires time up to several minutes (i.e. up to 15 minutes), which depends on the speed of the communication system and processing units, to analyse the network conditions and to update the new set point of voltage controllable devices. The lack of speed of some controllable devices also causes the network to be updated slowly. It is found that the network still can meet the voltage disturbances, particularly short-duration variations and flicker during the gap (several minutes) for updating the new set-points of

controllable devices. This means that fast voltage support is required to mitigate this problem using custom power devices (in case of conventional solution).

This thesis aims to look at the voltage control performance by adding the decentralised dynamic voltage controllability from the DG, mainly from inverter-based DG, to deal with short- and long-term voltage variations such as sag, swell, flicker, under and over voltage, to complete the gap during each iteration of the routine voltage regulation process, as can be seen in Figure 1.1. The primary support uses DG to provide fast voltage control locally by supplying *Q*. DG can cooperate with other fast controllable devices such as ESSs and smart distribution transformers in order to enhance decentralised voltage controllability. Moreover, wide-area voltage controllable devices, such as the voltage regulator or substation's OLTC, will operate as the secondary support if the support from DG is insufficient. In addition, information and communication technology (ICT) plays an important role in this control approach and is used for exchanging information between voltage controllable devices for coordinated voltage control and to deal with disturbances in real time.

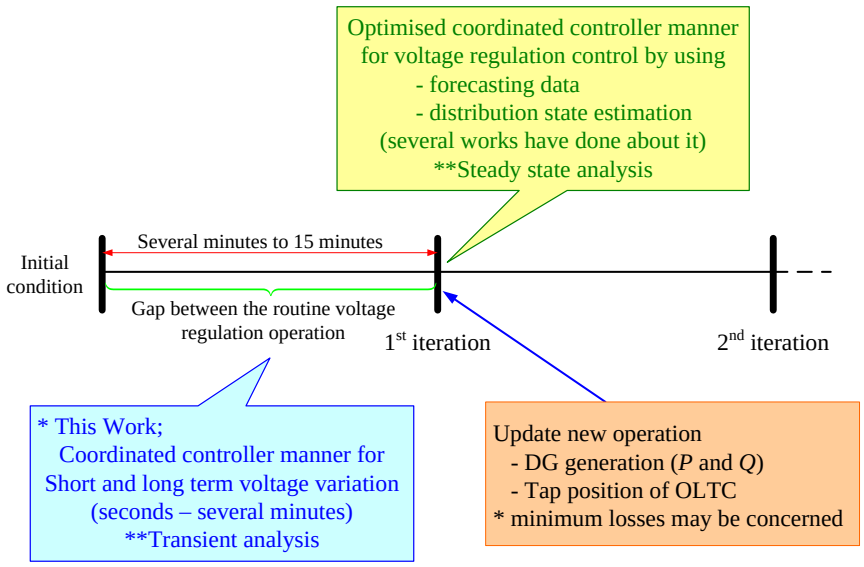

Figure 1.1. Approach proposed in this thesis for voltage level improvement.

1.2.2 Review of harmonic mitigation solutions

The high penetration of power electronic-interfaced DG may increase the level of harmonic current injections into the network, which may cause voltage distortion over the statutory limits, such as the IEEE 519-1992 [35]. Also, the increase of harmonics can limit the number

of allowed DG to connect to the network [36], apart from other problems such as power loss and voltage rise. Although passive filters can mitigate the harmonic distortion, they may lead to resonances [37]. Furthermore, the mix of large non-linear loads and converter-connected DG units in the same MV network complicates harmonic mitigation as it may need to deal with various harmonic frequencies. Multi-harmonic frequencies from different switching frequencies of non-linear loads and converter connected DG units make difficult the design of filters, especially for the addition of new DG units. Several filters may be required to eliminate multi-harmonic frequencies, which may be very expensive.

The active filter is an alternative harmonic filtering technology, which can provide on-line harmonic mitigation at the point of connection by injecting a compensated signal to achieve clean voltage and current waveforms. Hence, it can deal with voltage harmonic variations, which vary continuously due to changes in the number of non-linear loads and converter-connected DG in the network [38]. However, this adaptive filter function requires of advanced control algorithms and processing, which make this filter still not cost effective at the present time. Also, it is difficult to determine the optimal filter location involving complex studies.

The harmonic mitigation technique presented in this thesis aims to use the existing devices in the network as a first option, rather than installing new components (i.e. active filter). As power converters may come from different manufacturers and have different specifications, the mitigation techniques presented adopt a generic approach avoiding modifications on the structure and control of conventional converter units. A potential harmonic mitigation solution is to use the phase-shifting control technique [39]. This technique may be applied to MV networks by changing the vector group of the transformer of each converter unit, interfaced either to DG or to customer loads, to shift the phase angle among harmonic sources. In case the mitigation from this technique is insufficient, additional filters may be required. However, the size of additional filters should be smaller, which means a cheaper investment.

1.3 Research aim and objectives

The aim of this thesis is to develop a new control structure and strategy to enhance the power quality (i.e. voltage level and harmonic) of distribution networks with high penetration of DG, especially inverter-interfaced DG. The solutions proposed present the following characteristics:

a) Avoid installing new power conditioning devices which are very costly (or install as few as possible).

b) Use fast voltage controllability from converter-connected DG as a key role to deal with short- and long-term voltage variations.

c) Use DG, energy storage systems, smart distribution transformers and voltage regulator to provide decentralised voltage control, and use the OLTC substation transformer to provide centralised voltage control to support a wider area.

d) Coordinate the control operation between DG and other controllable devices to reduce interactions and to increase the control performance.

e) Apply the phase-shifting technique among power electronic-based DG and non-linear loads to reduce the level of harmonic distortion in the network.

1.4 Research methodology

The research methodology used to enhance the power quality in distribution networks with high penetration of DG is split into two major parts: voltage level control and harmonic mitigation. The key developments for voltage level control are as follows:

1. Hierarchical and distributed voltage control structure, which includes advanced distribution automation (ADA) technology, and voltage control using the support from DG.

2. Procedure to indentify "local controllable zones (LCZs)", which are smaller voltage controllable areas to illustrate the distributed voltage support capability from DG.

3. DG voltage controller to provide both static and dynamic voltage support.

4. Procedure to coordinate between voltage controllers of DG and other controllable devices to increase voltage support capability, and to avoid voltage interactions between them.

In case of harmonic mitigation solutions, a procedure is developed to apply the phase-shifting technique among harmonic sources, which are either DG or customer loads, to mitigate harmonic pollution, instead of installing new harmonic filters.

1.5 Contributions of the thesis

The major contributions of this thesis are:

1. A voltage control structure which integrates the decentralised voltage support, from mainly DG units, and the centralised voltage support at the substation in medium-voltage distribution networks. In addition, local controllable zones are identified to demonstrate the decentralised voltage controllable areas.

2. Development of a new methodology for decentralised voltage control by using the support from power electronic-interfaced DG technology to deal with short- and long-term voltage changes, in a similar way to conventional power conditioning devices.

3. Development of a new methodology for voltage coordinated controller between DG units and other controllable devices such as the voltage regulator, and the OLTC distribution and substation transformers, which can enhance voltage quality with small interactions among those voltage controllers.

4. Development of a new methodology for harmonic mitigation to avoid installing new compensation devices.

5. Demonstration of those methodologies by using power system simulation package, such as DIgSILENT *PowerFactory*, based on IEEE 33-bus distribution system and the typical Dutch MV network.

1.6 Organisation of the thesis

The thesis is organised in seven chapters.

Chapter 2 explores the power quality problems which may happen in distribution networks with high penetration of DG. Voltage level improvement by using centralised and decentralised voltage controls is discussed. Additionally, the approach of using voltage support from DG is explained. Solutions for harmonic mitigation of converter-connected DG are also surveyed in this chapter.

The concept of the hierarchical distributed control structure for voltage quality enhancement is introduced in Chapter 3. The concept of advanced distribution automation implemented

for this approach is developed and the technology requirements are discussed. The process of adaptive LCZ identification is described. Moreover, the performance and value of the proposed control approach are demonstrated under various network operating scenarios.

Chapter 4 describes the control algorithm and operation of DG to provide decentralised voltage control. The performance of DG while providing voltage support is demonstrated for different types of voltage disturbances, both short- and long-term voltage variations, based on transient simulations. Test results compare the performance with and without voltage support from DG. Moreover, the coordinated controller between DG units is discussed, to avoid interactions, if several DG units are installed in the same LCZ.

Apart from the control coordination between DG units, the coordinated controller between DG and other controllable devices is introduced in Chapter 5. In addition, DG can coordinate the voltage support with ESSs, solid-state transformer, OLTC distribution transformer, and voltage regulator to enhance the decentralised voltage level controllability. Alternatively, DG can coordinate with the centralised voltage controller at the substation, such as the substation's OLTC, for wide-area voltage control, and to reduce the number of tap-changing operation of the OLTC substation transformer. Test results, from computer simulations, are also discussed in this chapter.

Chapter 6 presents the harmonic mitigation, among the group of DG or large non-linear loads connected to the same circuit, by using the phase-shifting technique. The mathematics of harmonic mitigation by phase shifting is explained. The adaptation of this technique to distribution networks is also addressed. Harmonic distortions of the whole network are calculated based on harmonic load flow simulation, which requires modelling the distribution network in the harmonic domain.

Finally, Chapter 7 presents conclusions and suggestions for future work.

1.7 Publications

1. P. Pachanapan, O. Anaya-Lara, K. L. Lo, 'Agent-based control for power quality enhancement in highly distributed generation networks', the 44th Universities Power Engineering Conference (UPEC), Glasgow, UK, 2009.

2. P. Pachanapan, A. Dysko, O. Anaya-Lara, K. L. Lo, 'Harmonic mitigation in distribution networks with high penetration of converter-connected DG', 2011 IEEE PES PowerTech, Trondheim, Norway, 2011.

3. P. Pachanapan, A. Dysko, O. Anaya-Lara, G. Burt, K.L. Lo, 'Decentralised Controller for Flicker Mitigation in Converter-connected DG Networks', the 21st International Conference and Exhibition on Electricity distribution (CIRED), Frankfurt, Germany, 2011.

4. P. Pachanapan, A. Dysko, O. Anaya-Lara, G. Burt, K.L. Lo, 'Decentralised Controller to Mitigate Short-Term Voltage Variations in Distribution Networks with High Penetration of DG', the 17th Power Systems Computation Conference (PSCC), Stockholm, Sweden, 2011.

5. P. Pachanapan, O. Anaya-Lara, A. Dysko, K.L. Lo, 'Adaptive Zone Identification for Voltage Level Control in Distribution Networks with DG', IEEE Transactions on Smart Grid, In-press, August 2012.

6. P. Pachanapan, O. Anaya-Lara, A. Dysko, K.L. Lo, 'Coordinated Voltage Controller with Droop Control among Converter-connected DG in Distribution Networks' IEEE Transactions on Sustainable Energy, submitted July 2012.

7. P. Pachanapan, O. Anaya-Lara, A. Dysko, K.L. Lo, 'Coordinated Voltage Controller for Voltage Quality Enhancement in Distribution Networks with DG' IEEE Transactions on Smart Grid, submitted September 2012.

1.8 References

[1] H. B. Puttgen, P. R. MacGregor, and F. C. Lambert, "Distributed generation: semantic hype or the dawn of a new era?," *IEEE Power and Energy Magazine*, vol. 1, no. 1, pp. 22-29, Jan. 2003.

[2] A. L'Abbate, S. Peteves, and G. Fulli, "Challenges for DG integration in Europe - status and potentials vary by country," *Current Issue-Congeneration & On-Site Power Production*, vol. 8, 2007.

[3] "WINEUR Project: Wind energy integration in the urban environment," Intelligent Energy, Europe, 2005.

[4] A. A. Bayod-Rújula, "Future development of the electricity systems with distributed generation," *Energy*, vol. 34, pp. 377-383, 2009.

[5] N. Jenkins, J. B. Ekanayake, and G. Strbac, *Distributed Generation*, 1st ed. The Institution of Engineering and Technology, 2010, pp. 12-16.

[6] H. Leite, H. Y. Li, N. Jenkins, and P.F.Gale, "Real-Time Voltage Regulation of Distribution Networks With Distributed Generation," in *17th International Conference on Electricity Distribution (CIRED)*, Barcelona, 2003, pp.1- 5.

[7] "IEEE Recommended Practice for Monitoring Electric Power Quality," *IEEE Std 1159-2009 (Revision of IEEE Std 1159-1995)*, pp. c1-81, 2009.

[8] M. J. Krok and S. Gene, "A coordinated optimization approach to Volt/VAr control for large power distribution networks," in *American Control Conference (ACC), 2011*, pp. 1145-1150.

[9] E. Acha, V. Agelidis, O. Anaya, and T. J. E. Miller, *Power Electronic Control in Electrical Systems*, 1 ed.: Newnes, 2002, pp. 320-336.

[10] T. Sansawatt, L. F. Ochoa, and G. P. Harrison, "Integrating distributed generation using decentralised voltage regulation," in *Power and Energy Society General Meeting, 2010 IEEE*, Minnesota, pp. 1-6.

[11] P. N. Vovos, A. E. Kiprakis, A. R. Wallace, and G. P. Harrison, "Centralized and Distributed Voltage Control: Impact on Distributed Generation Penetration," *Power Systems, IEEE Transactions on*, vol. 22, pp. 476-483, 2007.

[12] K. Tanaka, M. Oshiro, S. Toma, A. Yona, T. Senjyu, T. Funabashi, and C. H. Kim, "Decentralised control of voltage in distribution systems by distributed generators" *Generation, Transmission & Distribution, IET*, vol. 4, pp. 1251-1260, 2010.

[13] M. Braun, "Reactive power supply by distributed generators," in *Power and Energy Society General Meeting - Conversion and Delivery of Electrical Energy in the 21st Century, 2008 IEEE*, Pittsburgh, pp. 1-8.

[14] Y. Hu, Z. Chen, and H. McKenzie, "Voltage Source Converters in Distributed Generation Systems," in *Electric Utility Deregulation and Restructuring and Power Technologies, 2008. DRPT 2008. Third International Conference on*, 2008, pp. 2775-2780.

[15] M. H. J. Bollen and A. Sannino, "Voltage control with inverter-based distributed generation," *Power Delivery, IEEE Transactions on*, vol. 20, pp. 519-520, 2005.

[16] A. Notholt, "Germany's New Code for Generation Plants connected to Medium-Voltage Networks and its Repercussion on Inverter Control," in *International Conference on Renewable Energies and Power Quality*, Valencia, Spain, 2009.

[17] L. Huijuan, L. Fangxing, X. Yan, D. T. Rizy, and J. D. Kueck, "Adaptive Voltage Control With Distributed Energy Resources: Algorithm, Theoretical Analysis, Simulation, and Field Test Verification," *Power Systems, IEEE Transactions on*, vol. 25, pp. 1638-1647, 2010.

[18] V. Arcidiacono, M. Chiandone, and G. Sulligoi, "Voltage control in distribution networks using smart control devices of the Distributed Generators," in *International Conference on Clean Electrical Power (ICCEP)*, 2011, Ischia, Italy, pp. 738-743.

[19] M. E. Baran and I. M. El-Markabi, "A Multiagent-Based Dispatching Scheme for Distributed Generators for Voltage Support on Distribution Feeders," *Power Systems, IEEE Transactions on*, vol. 22, pp. 52-59, 2007.

[20] M. E. Elkhatib, R. El-Shatshat, and M. M. A. Salama, "Novel Coordinated Voltage Control for Smart Distribution Networks With DG," *Smart Grid, IEEE Transactions on*, vol. 2, pp. 598-605, 2011.

[21] F. A. Viawan and D. Karlsson, "Combined Local and Remote Voltage and Reactive Power Control in the Presence of Induction Machine Distributed Generation," *Power Systems, IEEE Transactions on*, vol. 22, pp. 2003-2012, 2007.

[22] A. G. Madureira and J. A. Pecas Lopes, "Coordinated voltage support in distribution networks with distributed generation and microgrids," *Renewable Power Generation, IET*, vol. 3, pp. 439-454, 2009.

[23] O. Richardot, A. Viciu, Y. Besanger, N. Hadjsaid, and C. Kieny, "Coordinated Voltage Control in Distribution Networks Using Distributed Generation," in *Transmission and Distribution Conference and Exhibition, 2005/2006 IEEE PES*, Dalian, 2006, pp. 1196-1201.

[24] A. Viehweider, B. Bletterie, and D. Burnier de Castro, "Advanced coordinated voltage control strategies for active distribution network operation," in *Electricity Distribution - Part 1, 2009. CIRED 2009. 20th International Conference and Exhibition on*, Prague, 2009, pp. 1-4.

[25] M. Biserica, B. Berseneff, Y. Besanger, and C. Kieny, "Upgraded coordinated voltage control for distribution systems," in *PowerTech, 2011 IEEE*, Trondheim, pp. 1-6.

[26] L. F. Ochoa and G. P. Harrison, "Minimizing Energy Losses: Optimal Accommodation and Smart Operation of Renewable Distributed Generation," *Power Systems, IEEE Transactions on*, vol. 26, pp. 198-205, 2011.

[27] L. F. Ochoa, C. J. Dent, and G. P. Harrison, "Distribution Network Capacity Assessment: Variable DG and Active Networks," *Power Systems, IEEE Transactions on*, vol. 25, pp. 87-95, 2010.

[28] F. A. Viawan and D. Karlsson, "Coordinated voltage and reactive power control in the presence of distributed generation," in *Power and Energy Society General Meeting - Conversion and Delivery of Electrical Energy in the 21st Century, 2008 IEEE*, 2008, Pennsylvania, pp. 1-6.

[29] F. Bignucolo, R. Caldon, and V. Prandoni, "Radial MV networks voltage regulation with distribution management system coordinated controller," *Electric Power Systems Research*, vol. 78, pp. 634-645, 2008.

[30] M. Fila, D. Reid, G. A. Taylor, P. Lang, and M. R. Irving, "Coordinated voltage control for active network management of distributed generation," in *Power & Energy Society General Meeting, 2009. PES '09. IEEE*, Alberta, Canada, pp. 1-8.

[31] A. Kulmala, A. Mutanen, A. Koto, S. Repo, Ja, x, and P. rventausta, "RTDS verification of a coordinated voltage control implementation for distribution networks with distributed generation," in *Innovative Smart Grid Technologies Conference Europe (ISGT Europe), 2010 IEEE PES*, Gothenburg, pp. 1-8.

[32] T. Pfajfar, I. Papic, B. Bletterie, and H. Brunner, "Improving power quality with coordinated voltage control in networks with dispersed generation," in *Electrical Power Quality and Utilisation, 2007. EPQU 2007. 9th International Conference on*, Barcelona, pp. 1-6.

[33] A. D. T. Le, K. M. Muttaqi, M. Negnevitsky, and G. Ledwich, "Response coordination of distributed generation and tap changers for voltage support," in *Australasian Universities Power Engineering Conference (AUPEC), 2007*, Perth, Australia , pp. 1-7.

[34] R. Caldon, S. Spelta, V. Prandoni, and R. Turri, "Co-ordinated voltage regulation in distribution networks with embedded generation," in *Electricity Distribution, 2005. CIRED 2005. 18th International Conference and Exhibition on*, 2005, Turin, pp. 1-4.

[35] "IEEE recommended practices and requirements for harmonic control in electrical power systems," *IEEE Std 519-1992*, 1993.

[36] A. Bhowmik, A. Maitra, S. M. Halpin, and J. E. Schatz, "Determination of allowable penetration levels of distributed generation resources based on harmonic limit considerations," *Power Delivery, IEEE Transactions on*, vol. 18, no. 2, pp. 619–624, 2003.

[37] N. Jenkins, R. Allan, P. Crossley, D. Kirschen, and G. Strbac, *Embedded generation*, 1st ed. London, United Kingdom: The Institution of Engineering and Technology, 2000, pp. 142-146.

[38] E. Acha, M. Madrigal, *Power systems Harmonics: Computer modeling and analysis*, 1st ed. John Wiley & Sons, 2001, pp. 333-335, 353-358.

[39] A. Baggini, *Handbook of Power Quality*. Chichester, UK: John Wiley & Sons, Ltd, 2008, pp. 248-251.

CHAPTER 2

Overview of Power Quality Issues in Distribution Networks with DG

2.1 Introduction

Power quality refers to the degree to which power characteristics align with the ideal sinusoidal voltage and current waveforms [1]. Utilities are expected to supply the quality of power that meets the needs of the customer, where the quality is measured in terms of voltage stability (i.e. voltage collapse or interruption), and the "purity" of voltage and current [2]. The terms and definitions of each type of voltage quality disturbance in distribution networks are explained in the standard IEEE 1159–2009 [3], and can be classified in 7 categories, including: transient, short- and long-term duration variations, imbalance, waveform distortion, voltage fluctuations and power frequency variations, as summarised in Appendix A (Table A.1). The research in [4] found that the main voltage disturbance (about 92%) is voltage sags with amplitude drops up to 50% and duration below 2 seconds. From the technical report in [5], the origin of voltage disturbances in conventional distribution networks, without DG, may occur from short circuit, start-stop events of the large machines, or the penetration of non-linear loads, as summarised in Appendix A (Table A.2).

Although DG can provide benefits in terms of increasing power generation and environment improvement, it can also either decrease or increase the power quality, depending on the particular conditions. Two main aspects are of concern: 1) voltage variation, and 2) harmonic distortion of the network voltage [6]. With the increase of power quality disturbances, a distribution network operator (DNO) may find it difficult to maintain power quality levels within statutory limits, indicated in international standards such as IEEE 519-1992 [7] (for voltage variation), IEC 61000-3-6 [8] (for harmonic assessment) and IEEE 61000-3-7 [9] (for voltage flicker compatibility).

In this chapter, the power quality challenges in distribution networks with high penetration of DG are discussed. Conventional solutions to improve power quality, either voltage variations or harmonics in present medium voltage (MV) networks are reviewed. The use of DG to enhance power quality in distribution networks is also explained.

2.2 Power quality impacts of DG in distribution networks

The increased penetration of DG can cause power quality problems in distribution networks especially, in the voltage. There are 5 possible types of power quality disturbances associated to DG connection [10]: 1) voltage variations, 2) voltage flicker, 3) voltage imbalance, 4) harmonic distortion and 5) direct current injection.

2.2.1 Voltage variations

In traditional distribution networks, without DG, the power flow is in one direction, from the substation to the customer loads. However, the injection of active power, *P*, from DG affects the power flow direction and the voltage level of the network. Moreover, the start of a large induction machine-based DG unit consumes reactive power, *Q*, which may cause a voltage sag if compensation equipment and soft-starter devices are not installed.

The change in the voltage level when DG is injecting active and reactive power to a certain location of a radial distribution feeder, as shown in Figure 2.1, can be explained as follow.

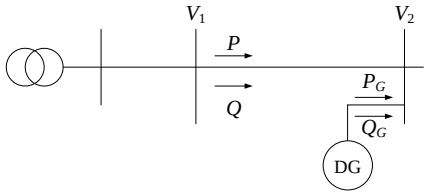

Figure 2.1. A simple radial distribution network with DG for voltage variation analysis.

Without DG, the voltage drop, ΔV, can be written as in (2.1). The derivation of this equation is presented in Appendix B.

$$\Delta V = V_1 - V_2 = \frac{PR + QX}{V_2} \tag{2.1}$$

where *P* and *Q* are the active and reactive power sent from bus 1, respectively. *R* and *X* are the resistance and the inductive reactance of the circuit, respectively. In per unit, the voltage at the DG bus can be assumed as 1.0 p.u., so (2.1) can be approximated as:

$$\Delta V = PR + QX \tag{2.2}$$

In the case that DG supplies active and reactive power, P_G and Q_G, respectively, to the system, then (2.2) can be written as:

$$\Delta V = (P - P_G)R + (Q - Q_G)X \tag{2.3}$$

It is found that the injection of apparent power from DG can reduce the term (P-P_G) and (Q-Q_G), thus the value of ΔV decreases. Then, the voltage at the DG bus (bus 2) will increase. As DG usually operates at unity power factor, with Q_G equals to zero, the voltage change is mostly due to the active power injected from DG. The voltage rise can be reduced if DG absorbs the reactive power. Reference [6, p.14] also suggests that the impact on voltage change from the reactive power produced by DG is more efficient on MV overhead lines than on underground cables, because of a high ratio of X/R of their impedances.

2.2.1.1 Long-term voltage variations

From the definition in IEEE 1159-2009, the long-term voltage variations mean that the rms voltage level changes from the nominal value for a time greater than 1 minute. Over voltage is the main concern in distribution networks with DG. From (2.3), during light load conditions, the value of load demand may be lower than the power injected from DG. Hence, the term (P-P_G) can become negative with V_2 higher than V_1. It is found that the voltage rise at the DG bus depends on the load condition and the power supplied by DG. The over voltage problem in MV networks tends to increase when a large number of DG connects to the network.

As every distribution network operator has an obligation to supply voltage within specific limits, such as ±3% of nominal [52], the amount of DG installed on any feeder is limited to ensure that the DG connection will not cause the voltage profile to deviate from these limits. An example of rules that have been used to guide the maximum capacity of DG in medium voltage networks is shown in Table 2.1 [6, p.14]. However, the limit of DG capacity will be different from country to country depending on their Grid Code's specifications.

Table 2.1. Design rules used as an indication for DG connection [6, p.14].

Network location	Maximum capacity of DG
Out on 11 kV or 11.5 kV network	2-3 MVA
At 11 kV or 11.5 kV busbars	8 MVA
On 15 kV or 20 kV network and busbars	6.5-10 MVA
Out on 63 kV or 90 kV network	10-40 MVA

2.2.1.2 Short-term voltage variations

The short-term voltage variations mean a deviation of the rms voltage from the nominal for a time greater than 0.5 cycles of the power frequency but lower than or equal to 1 minute [3]. Apart from a short circuit, a voltage sag (or dip) can happen in MV networks due to the start-up of fixed-speed wind turbines. This is because induction machines require reactive power to develop the rotating magnetic field. Hence, there is an initial magnetising inrush transient, which is similar to that when a transformer is energised. The depth and time duration of the voltage sag depend on the size and rotor speed of the machine.

The sag behaviour during start-up of an induction generator is also explained by using (2.3). The negative reactive power absorbed by the induction generator makes the term (Q-Q_G) to increase, while the active power is just starting to being injected. Then, the value of ΔV may increase and then V_2 becomes lower than the initial condition which has no power generation from those induction generators. Moreover, local shunt capacitors are connected in parallel with the induction generator to provide reactive power compensation and to improve the power factor. However, the size of these capacitors needs to be properly designed to prevent self-excitation operation [6, p.56].

2.2.2 Voltage fluctuations and flicker

Voltage fluctuations are defined as a series of voltage changes or a cyclical variation of the voltage envelope, which changes in the range of 0.1% to 7% [3]. In addition, voltage fluctuation is an electromagnetic phenomenon while flicker is an undesirable result of the voltage fluctuation in some loads such as light bulbs. However, these two terms are often linked together in many standards [11, pp.136-137].

Voltage fluctuations may be due to the fluctuation in power delivery by DG in distribution networks caused by: 1) the intermittency of renewable sources such as wind and solar, and 2) the improper converter design, which does not have sufficient energy storage to smooth out the power output from DG [10]. In case of a wind turbine, the switching operation which is mainly from the start-up can produce high reactive power transients that cause voltage sags, as explained in Section 2.2.1.2. This voltage variation may not be periodical due to the variability of the wind speed profile. Fixed-speed wind turbines are of more concern than

variable-speed ones. Even though the soft-starter circuit is applied to this type of wind turbine, some inrush transients still occur.

Active power fluctuations from a wind turbine in continuous operation also cause voltage fluctuations. In addition, the active power fluctuations can be caused by tower shadow, yaw errors, wind eddies or fluctuations in the control system. In case of the fixed-speed wind turbine, the main reason for flicker is the wake of the tower, when the power output of the turbine is reduced each time a rotor blade passes the tower. This effect causes periodical power fluctuations with a frequency of about 1 Hz [12, p.108]. However, the level of flicker from continuous operation may be less critical compared with the voltage fluctuation from switching operation of wind turbine.

It can be seen that the voltage fluctuation can be one factor that limits the size and number of wind turbines that can be connected to the network. Flicker introduced by wind turbines must be below the standard limits such as IEEE-P1453 and IEEE 61000-3-7.

2.2.3 Voltage imbalance

A three-phase system is imbalanced when the rms values of the phase voltages are not equal. The degree of imbalance is defined by using the ratio of the negative sequence component to the positive sequence component, usually expressed as a percentage [3], see (2.4). The unbalanced condition can increase heating in three-phase induction machines [4]. It also causes excessive thermal stress and harmonic distortion in power electronic equipment [10],[13]. Mathematically, the voltage imbalance ratio is represented by:

$$\%\ \text{Imbalance} = \frac{|V_{neg}|}{|V_{pos}|} \times 100\% \qquad (2.4)$$

where $|V_{pos}|$ is the magnitude of the positive sequence voltage and $|V_{neg}|$ is the magnitude of the negative sequence voltage.

Moreover, from [3], the imbalance using the preferred definition can be determined using only phase-to-phase (or line-to-line) rms measurements without angle as follow:

$$\%\ \text{Imbalance} = \sqrt{\frac{1-\sqrt{3-6\beta}}{1+\sqrt{3-6\beta}}} \times 100\% \qquad (2.5)$$

where $$\beta = \frac{|V_{AB}|^4 + |V_{BC}|^4 + |V_{CA}|^4}{\left(|V_{AB}|^2 + |V_{BC}|^2 + |V_{CA}|^2\right)^2} \quad (2.6)$$

The long-term voltage imbalance in three-phase MV networks may be due to the operation of large single-phase loads such as induction furnaces and traction motors loads. On the other hand, the voltage imbalance may come from the unbalanced connection of single-phase DG such as roof-top PV systems and μCHP in LV networks. The unbalanced generation from a group of single-phase DG can make the network become unbalance, even when the loads are balanced.

The short-term unbalance can happen under many disturbance conditions, such as asymmetrical short-circuits [11]. Also, the single-phase sag from starting large-single phase induction generators may create a transient voltage unbalance.

2.2.4 Harmonic distortions

Harmonic disturbances normally come from equipment with a non-linear characteristic particularly power electronic devices. These cause the steady-state current and voltage waveforms to distort from an ideal sine wave by adding frequencies which are integer multiples of the fundamental frequency, as can be seen in (2.7). The effect of harmonic pollution increases power losses in distribution networks and electric rotating machines [11, p. 221].

The decomposition of a distorted waveform can be written as:

$$\begin{aligned} f(x) &= \frac{a_0}{2} + a_{(1)}\cos x + b_{(1)}\sin x + a_{(2)}\cos 2x + b_{(2)}\sin 2x + ... + \\ &\quad + a_{(n)}\cos nx + b_{(n)}\sin nx + ... \\ &= \frac{a_0}{2} + \sum_{n=1}^{\infty} a_{(n)}\cos nx + \sum_{n=1}^{\infty} b_{(n)}\sin nx = \frac{a_0}{2} + \sum_{n=1}^{\infty} c_{(n)}\sin\left(nx + \phi_{(n)}\right) \end{aligned} \quad (2.7)$$

where $f(x)$ is a generic periodic waveform, a_0 is the DC component, and $a_{(n)}, b_{(n)}$ are the coefficient of the series, calculated as in (2.8) :

$$a_0 = \frac{1}{\pi}\int_0^{2\pi} f(x)dx \qquad a(n) = \frac{1}{\pi}\int_0^{2\pi} f(x)\cos(nx)dx \qquad b(n) = \frac{1}{\pi}\int_0^{2\pi} f(x)\sin(nx)dx$$

$$c_{(n)} = \sqrt{a_{(n)}^2 + b_{(n)}^2} \qquad \phi_{(n)} = \arctan\frac{a_{(n)}}{b_{(n)}} \quad (2.8)$$

where n is an integer number between 1 and infinity.

Additionally, harmonic sources such as cyclo-converters, induction furnaces and arcing devices also cause inter-harmonics, which are non-integer multiples of the fundamental frequency. The effects of inter-harmonics are interference in the power line carrier signals and introduction of visual flicker in display devices. Furthermore, most modern DG and ESSs are connected via power converters, which can cause harmonics injection into the distribution networks. Even thought passive filters can be used, this can increase the possibility of harmonic resonances in the system [3].

There are two main converter types used to interface DG: 1) current source converter (CSC) and 2) voltage source converter (VSC). The CSC uses thyristor technology with firing angle control. The harmonics in the AC output waveforms drawn by a q-pulse rectifier is determined as [14, p.317]:

$$f_h = k \cdot q \pm 1 \tag{2.9}$$

where k = 1,2,3,…, so a three-phase six-pulse converter generates the 5^{th}, 7^{th}, 11^{th}, 13^{th} … harmonics.

The VSC uses gate turn-off thyristors (GTO) or insulated-gate bipolar transistors (IGBT) and sinusoidal pulse-width modulation (PWM) operating at a high switching frequency (f_s). It generates an output voltage waveform with harmonics positioned in a form of sidebands to the switching frequency as follow [15, pp.222-229]:

$$f_h = k \cdot f_s \pm m \cdot f_1 \tag{2.10}$$

where m = 2, 4, 6, ... when k = 1,3,5…
and m = 1, 3, 5, ... when k = 2,4,6…

The level of voltage harmonics is specified by many international standards such as the IEEE 519-1992, which influences the number of converter-connected DG that can be installed.

2.2.5 Direct current injection

Power converter-interfaced DG or ESSs may also inject DC current into the network, if they are connected directly without an isolation transformer [16]. The DC current injection causes the rising in total harmonic distortions from the converter-connected DG. It also impacts

transformers and other magnetic elements causing saturation and torque ripple in induction machines [10]. Although the DC current injection can be mitigated by proper DG control, this issue is still a concern in the case of high-penetration of converter-connected DG units.

2.3 Conventional solutions to improve voltage level

There are at present various solutions to improve the voltage level in MV networks. Voltage compensation devices now can operate automatically rather than manually. Most traditional compensation devices could deal only with the steady-state voltage control and were mainly used to prevent the voltage drop during high-load demand. Modern power conditioners, which use power electronics, can support both dynamic and static voltage control.

2.3.1 On-load tap changer transformer

The on-load tap changer (OLTC) is an automatic tap-changing controller, which does not cut the electricity off before changing the tap position. It can change the tap of the transformer step-by-step to control the secondary voltage at the desired value. The speed of the tap-changing operation depends on the tap-changing mechanism process, which may take from several seconds to minutes per step. The OLTC can be installed at either the high-voltage winding or the low-voltage winding, as shown in Figure 2.2, where *Tap* is the tap setting in per-unit (p.u.).

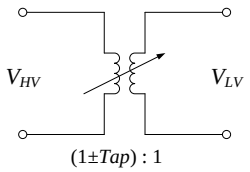

$$V_{LV} = \frac{1}{(1 \pm Tap)} \times V_{HV}$$

(a) Tap changer modelled at HV side

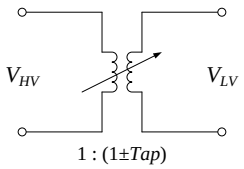

$$V_{LV} = (1 \pm Tap) \times V_{HV}$$

(b) Tap changer modelled at LV side

Figure 2.2. Tap changer transformer models.

Two types of OLTC transformers are discussed in this section: 1) OLTC substation transformer and 2) OLTC distribution transformer. Both are step-down transformers, that is, HV/MV and MV/LV transformers, respectively.

2.3.1.1 OLTC substation transformer

The OLTC transformer at the substation aims to compensate the voltage drop along the MV feeders. It is a centralised voltage control which provides steady-state voltage support to the whole network. Tap-changer types and control operations are explained in detail in [17, pp. 497-508]. In distribution networks without DG, the tap position is adjusted to lift up the secondary voltage of the transformer to avoid the voltage drop below the allowable limit at the end of the feeder especially during high loading conditions. However, the connection of DG may cause voltage rise (see Section 2.2.1) during light load conditions, which may exceed the allowable limit. Figure 2.3 shows the voltage change from tap changing between two MV feeders with and without DG.

The automatic tap changer prevents the voltage to go above the statutory limit, but it can only provide steady-state voltage support due to its limited speed of response. The optimal tap position should be set properly to ensure that the voltage level of every feeder connected to the substation is still within the allowed voltage variation range. For example, from Figure 2.3, while avoiding voltage rise in feeder#2, which has DG connection, by changing the tap position to reduce the voltage at the sending end, other feeders that have no DG (i.e. feeder#1) should not face under voltage problems due to the voltage drop.

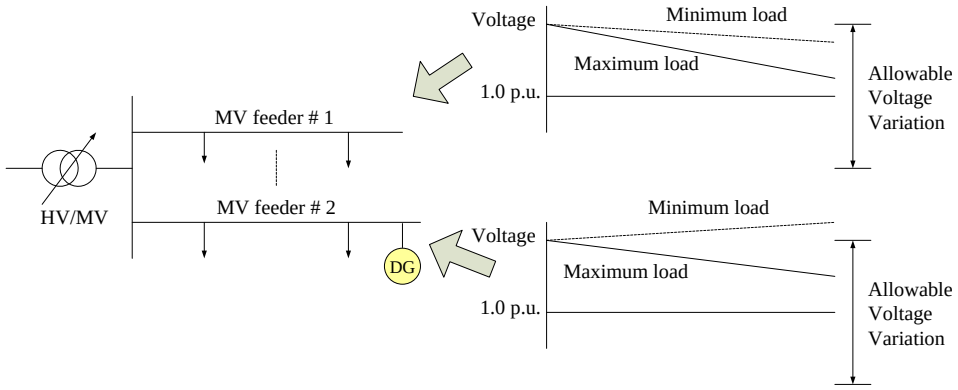

Figure 2.3. Voltage change along MV feeders with OLTC at substation transformer.

2.3.1.2 OLTC distribution transformer

The OLTC distribution transformer (MV/LV transformer), is used to compensate the voltage along LV feeders. At present, this type of OLTC can adjust the tap position manually and normally setting the tap to raise the voltage up to avoid voltage drop during the high loading

conditions. However, the connection of DG at the LV network may cause voltage rise problems during light load conditions. The voltage control by using OLTCs at substation and distribution transformers along a radial feeder is shown in Figure 2.4 [6].

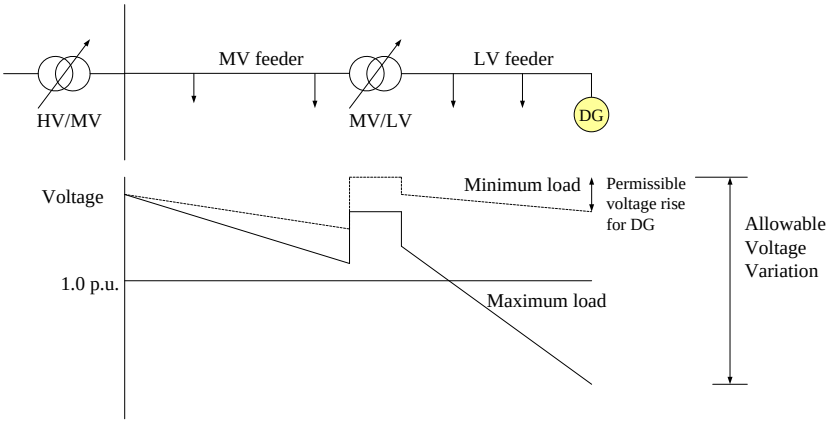

Figure 2.4. Voltage variations down a radial feeder by OLTCs at substation and distribution transformers.

Modern OLTC distribution transformers, using vacuum switches or power electronic switches, can provide automatic voltage controllability for the MV/LV system with faster response than that of more conventional mechanical OLTCs [18],[19]. In addition, they can support dynamic voltage control to deal with short-term variations and flicker [20], and can be used to protect sensitive loads at the LV side. Also, the local voltage control from OLTC distribution transformers may reduce the centralised voltage control from the substation.

2.3.2 Capacitor bank

The capacitor bank is a set of shunt capacitors connected to the network with the aim to supply the reactive power for either voltage control or power factor correction. It is usually installed in specific locations mainly to compensate the voltage drop along MV radial feeders. The voltage can be controlled step-by-step until the voltage level reaches the desired value or remains within the statutory range, as demonstrated in [21].

From (2.3), the Q compensation from shunt capacitors, which have no active power injection, can reduce the term (Q-Q_G) and consequently decrease the value of voltage drop, ΔV. Therefore, it can increase the voltage level at the point of connection. Similarly, the active power injected from DG also can improve the voltage profile, so the number of capacitor banks may be reduced in distribution networks with penetration of DG.

2.3.3 Voltage regulator

The voltage regulator (or step voltage regulator), VR, is a kind of OLTC transformer which can adjust the tap position automatically to improve the voltage profile along MV radial feeders. It is installed in series between two line sections, and aims to provide voltage regulation at the secondary side. The conventional voltage regulator can adjust the tap only with one direction of power flow, which is normally from primary side to secondary side, to compensate for voltage drops during high-loading conditions. The tap position is fixed when reverse power flow occurs, so it cannot deal with the voltage rise in case that DG is connected. Therefore, a new type of voltage regulator has been developed which can change tap positions to control the voltage when it detects the reverse power flow condition, such as in [22]. The communication system is assumed available to let the VR knows the voltage level at specific locations instead of using the estimation. This can allow increasing the level of DG penetration. The type of voltage regulator is shown in Figure 2.5.

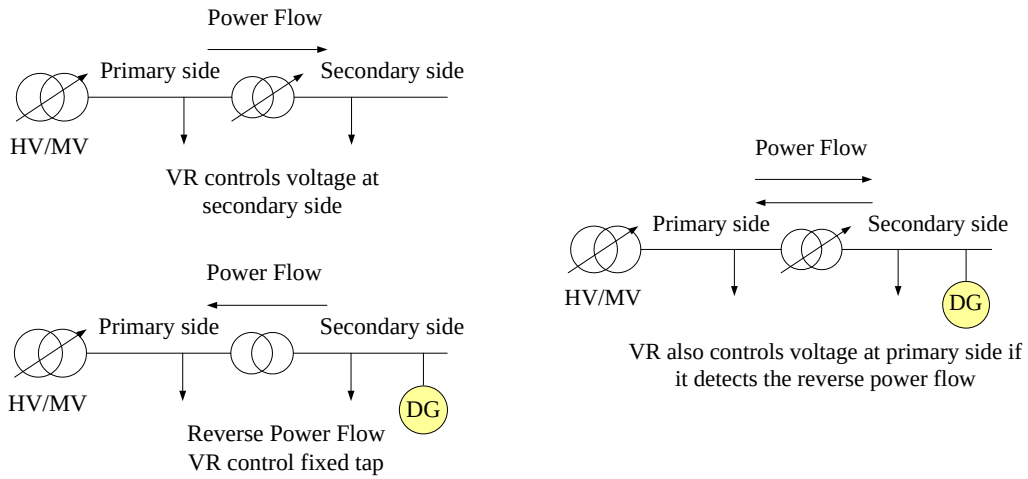

(a) Conventional voltage regulator (b) Modern voltage regulator

Figure 2.5. Types of voltage regulation to improve voltage along MV feeder [22].

2.3.4 Static var compensator

The static var compensator, SVC, is a variable susceptance which can provide fast reactive power compensation into the network. The susceptance of the SVC is controlled by adjusting the thyristor firing angle, α. It can support either static or dynamic voltage control at PCC,

and provides other benefits [15, p.300] including: 1) improvement of voltage stability, 2) enhancement of transient stability limit and 3) provision of power oscillation damping.

The SVC may be designed using fixed capacitors in parallel with a thyristor-controlled reactor (TCR), or a TCR in parallel with a thyristor-switched capacitor (TSC), as shown in Figure 2.6. Thyristor control can provide continuous and smooth reactive power support to the network, and reduce transient over-voltage problems due to the inrush current.

(a) a fixed capacitor with TCR (b) TCR and TSC with a passive filter

Figure 2.6. Typical SVC structure [15, p.301].

From Figure 2.6(a), the SVC can absorb or inject the reactive power by varying the thyristor's firing angle within the range $90° < \alpha < 180°$. The maximum reactive power absorbed by the TCR occurs when the thyristor valves are bypassed, $\alpha = 90°$. On the other hand, when thyristor valves are open, $\alpha = 180°$, the reactive power absorbed by the TCR is zero (maximum reactive power injection from SVC). The available reactance of the TCR, at fundamental frequency, is calculated from [14, p.276]:

$$X_{\text{TCR}} = \frac{\pi X_L}{2\pi - 2\alpha + \sin 2\alpha} \tag{2.11}$$

where X_L is inductance and X_C is capacitance. Furthermore, the SVC equivalent reactance from the parallel combination of TCR and fixed capacitor is

$$X_{\text{SVC}} = \frac{\pi X_C X_L}{X_C\left(2\pi - 2\alpha + \sin 2\alpha\right) - \pi X_L} \tag{2.12}$$

The switching of the thyristor can increase the level of harmonic distortion, especially the harmonics of order 5^{th}, 7^{th}, 11^{th} and 13^{th}, as can be seen from (2.9). A passive filter is therefore required to eliminate those harmonics increasing of size and power loss of the SVC unit (see Figure 2.6(b)). Also, thyristor technology has limited operation bandwidth and its speed of response is slow for modern distribution network requirements [23].

2.3.5 Distribution static compensator

The distribution static compensator, DSTATCOM, is a combination of an SVC and an active power filter, which can compensate reactive power in a minimum of two cycles [23]. It comprises a VSC, a DC capacitor and a coupling transformer, as illustrated in Figure 2.7. The converter converts the DC voltage into a three-phase AC voltage with desired amplitude, frequency and phase, by using GTO or IGBT switches. Multiple converters can be used to reduce harmonics. Moreover, PWM is a popular technique to control the VSC output, giving fast control response and low harmonic emission.

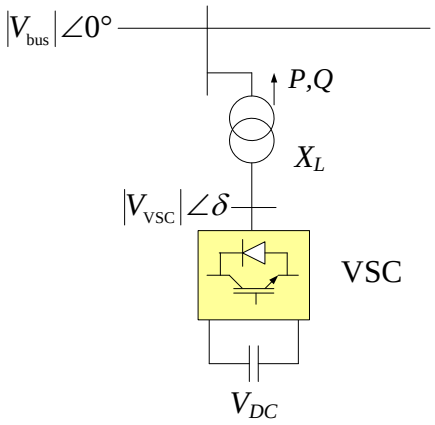

Figure 2.7. DSTATCOM equivalents connected to medium voltage networks [15, p.321].

The reactive power supplied by a DSTATCOM can be controlled by the magnitude difference between the AC system voltage, V_{bus}, and the VSC voltage, V_{VSC}. The active power flow, normally set as zero, can be controlled by the angle, δ, between the AC system and the VSC voltages [15, p.331]. From Figure 2.7, active and reactive powers may be expressed by the following equations:

$$P \approx \frac{V_{bus}V_{VSC}}{X_L}\sin\delta \tag{2.13}$$

$$Q \approx \frac{V_{bus}^2}{X_L} - \frac{V_{bus}V_{VSC}}{X_L}\cos\delta \tag{2.14}$$

where X_L is the equivalent reactance of the transformer and the series reactor.

The DSTATCOM is already employed to improve voltage quality in distribution networks with DG, in many applications such as voltage sag [24], flicker [25], voltage unbalance [26] and harmonics [27].

2.3.6 Dynamic voltage restorer (DVR)

The dynamic voltage restorer, DVR, can be used for active voltage regulation, voltage imbalance improvement and voltage harmonic mitigation at specific locations, such as sensitive load or DG in distribution networks. It consists of a VSC, DC capacitor and a coupling transformer which is similar to the DSTATCOM. In this case, it is installed in series with the AC system, as shown in Figure 2.8.

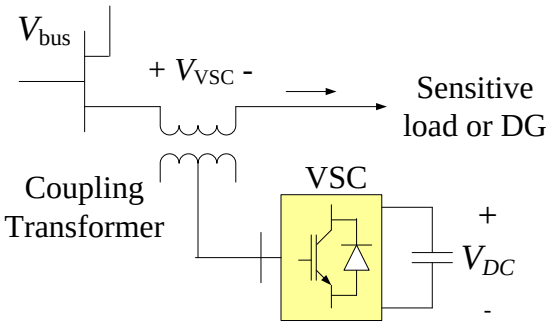

Figure 2.8. Schematic representation of the DVR in distribution networks [15, p.337].

From Figure 2.8, the three-phase AC voltage applied to the sensitive load can be controlled by injecting a compensated voltage from the DVR, V_{VSC}. In addition, the amplitude and phase angle of V_{VSC} can be controlled by the exchanging active and reactive powers between the AC system and the DVR.

This device may be used to compensate voltage fluctuations, which may be due to start-up and shut-down of intermittent renewable energy DG units [28].

2.4 Conventional solution to mitigate harmonic distortions

There are several solutions to mitigate harmonics in distribution networks. Widely used solutions are: line reactor, passive and active filters.

2.4.1 Line reactor

A line reactor (or line choke) is a three-phase series reactor installed between the AC system and a harmonic source, either a non-linear load or converter connected DG. In many cases, the coupling transformer may be used as the line reactor. It is a low-cost solution which can

reduce the line current harmonics, especially high-order harmonics. However, it obviously increases the voltage drop and losses in the network. A reasonable size of reactor needs to be considered, and the recommended size should be between 3% to 6% impedance [29]. This value of the % impedance is calculated from:

$$\% \text{ Impedance} = \frac{\sqrt{3} \times I \times X}{V} \times 100 \tag{2.15}$$

where I is the fundamental load current flowing though the line reactor, X is the reactance at fundamental frequency of the line reactor and V is the line-to-line voltage.

2.4.2 Passive filter

Passive shunt filters are a very popular solution to mitigate the propagation of harmonic currents. It consists of passive components including inductor, capacitor and resistor, which presents a low impedance to the harmonic at its tuned frequency. Several passive filters can be connected in parallel to mitigate multi-harmonic components. However, attention should be paid in terms of sizing and losses in passive filters for multi-harmonics mitigation, and poor designs may lead to harmonic resonance in the network.

(a) Single-tuned filter (b) High-pass filter

Figure 2.9. Typical passive filters [14, p.65].

Two types of passive filters are discussed in this section, single-tuned and high-pass filters. Single-tuned filters are commonly used to mitigate low-order harmonics. They consist of a series resistor, inductor and capacitor, as illustrated in Figure 2.9(a), tuned to a particular harmonic frequency. In addition, they become a very low impedance by-path at the tuned frequency, f_t. The tuning characteristic of this filter can be described by using the quality factor, Q_f, given by

$$Q_f = \frac{hX_L}{R} \tag{2.16}$$

where h is the tuned harmonic, R is the resistance and X_L is the rated reactance. The typical value of Q_f suggested in [14, p.65] should be in the range of $20 < Q_f < 30$.

High-pass filters aim to attenuate high-order harmonics. This filter will bypass a large percentage of all harmonics at or above the corner frequency, where the corner frequency locates at the lower harmonic to be eliminated. However, the single-tuned filter at the tuned frequency can achieve the minimum impedance better than the high-pass filter. The configuration of a high-pass filter is shown in Figure 2.9(b), where the value of quality factor is given by

$$Q_f = \frac{R}{hX_L} \tag{2.17}$$

where the typical value of Q_f is $0.5 < Q_f < 2$, suggested in [14, p.66].

The typical frequency response of these two types of passive filters is shown in Figure 2.10.

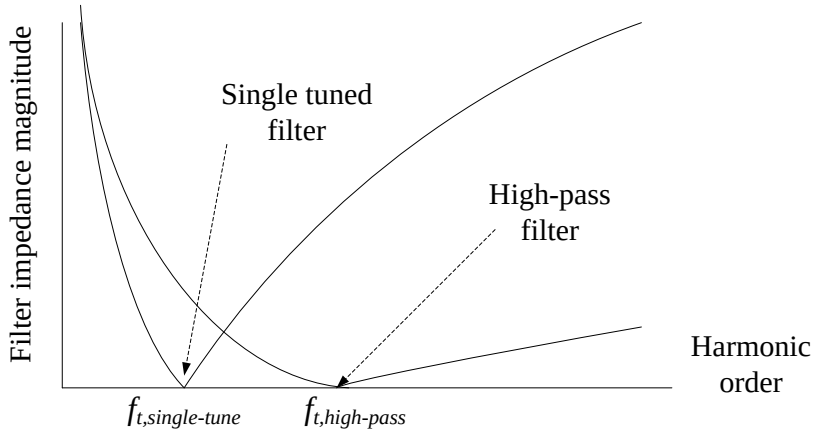

Figure 2.10. Frequency response of passive filters [14, p.66].

2.4.3 Active filter

The active filter is a self-adaptive filter which can mitigate harmonics on a wide frequency band. The active filter is connected in parallel with the network, at the location of the harmonic source and uses power electronic devices such as VSC to control the harmonic elimination, as illustrated in Figure 2.11. It can be seen that power conditioning devices such as the DSTATCOM may also be used for harmonic mitigation [27].

From Figure 2.11, the harmonic current waveform induced from either non-linear loads or converter-connected DG, at the point-of-common-coupling (PCC), is compensated by using the VSC to produce a current waveform which is in anti-phase to the unwanted component in the harmonic current. This technique can make the supply current, from the grid, to be nearly sinusoidal with a little amount of harmonics.

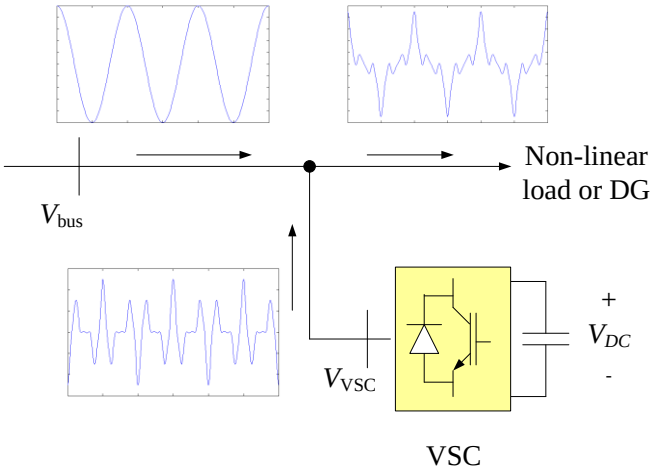

Figure 2.11. Shunt active filter [15, p.356].

2.5 Voltage quality enhancement by using DG

Although voltage rise is one of the main obstacles for increasing the level of DG penetration in MV networks, the voltage level may be controlled by adjusting active and reactive powers from the controllable DGs. Most DG now is operated with fixed active power generation while reactive power is set as zero, or at constant power factor. This is mainly because many network operators worry that the voltage control from DG may cause unintended islanding [30]. However, the unintended islanding can be prevented by modifying the islanding detection such as integrating the rate-of-change of frequency function in parallel with conventional voltage and frequency protections to trip DG units when needed [31].

Furthermore, many Grid Codes already establish fault ride-through capabilities of DG connected to the distribution networks such as wind turbine, which require DG to stay connected to the network during a fault [32]. If DG can provide fast voltage control, it can be used to support short-term voltage variations while DG is forced to stay connected.

The voltage level can be controlled by changing the active power supplied from DG, to prevent the voltage rise during light load conditions. However, fixed active power generation

is preferred when stability and economic issues are concerned. This means that the main voltage control is using the exchange of the reactive power between the AC network and DG.

Two types of DG which can support voltage control are discussed in this section: synchronous machine-based DG, and power electronic-based DG.

2.5.1 Voltage level control by using synchronous machine-based DG

Synchronous machine-based DG such as combined heat-and-power (CHP) generation can provide voltage control by controlling the reactive power output through the excitation system. The steady-state equivalent circuit of the synchronous machine is shown in Figure 2.12 (taken from [53]). The voltage generated by this machine is determined from:

$$V = E_f - jIX_S \tag{2.16}$$

where V is the terminal voltage, E_f is the internal field voltage (function of the field current) and X_S is the synchronous reactance, I is the armature current and δ is the rotor angle.

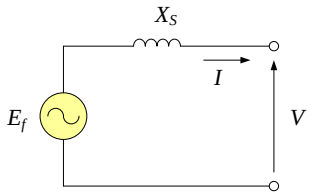

Figure 2.12. Steady-state equivalent circuit of a synchronous generator [53].

Assume a synchronous generator is connected to a fixed voltage source (or infinite bus). E_f can be controlled via the field current. If $E_f > V$, it results in export of reactive power, and power factor, $\cos\varphi$, will be lagging, as can be seen in Figure 2.13(a). This condition is called over-excited. On the other hand, when $E_f < V$, called under-excited, it absorbs reactive power and power factor will be leading, as illustrated in Figure 2.13(b).

From the load flow calculation between two buses in Appendix B, the active and reactive powers delivered to the system is

$$VI^* = P + jQ = \frac{E_f V}{X_s}\sin\delta + j\left(\frac{E_f V}{X_s}\cos\delta - \frac{V^2}{X_s}\right) \tag{2.17}$$

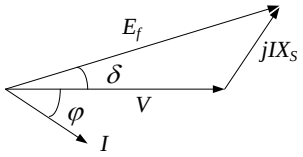

(a) Over-excited condition

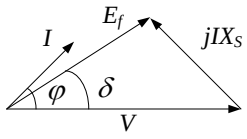

(b) Under-excited condition

Figure 2.13. Phasor diagrams of synchronous generator connected to the network (fixed terminal voltage) [53].

The operating chart of synchronous generator drawn from the phasor diagram of (2.17) is shown in Figure 2.14. However, there are various limits applied as follow [33]:

a) Prime mover limit, P_{max}, which is the maximum power available from the prime mover.
b) The stator limit, S_{max}, which is the maximum current rating of the stator to avoid over heating of the armature coils.
c) The rotor limit, Q_{max}, which is the maximum excitation to avoid over heating of the field winding.
d) The under excitation limit, Q_{min}, which is the minimum excitation for stability and to avoid over heating at the armature end winding.

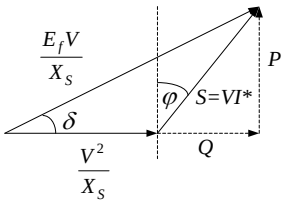

(a) Phasor diagram of apparent power

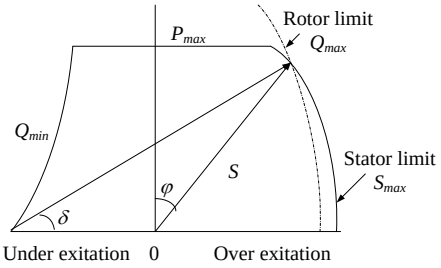

(b) Operation limits

Figure 2.14. The operating chart of synchronous generator connected to the network [53].

In normal conditions, the synchronous machine-based DG is operated under fixed active power and unity power factor. The active power output and/or frequency can be controlled by using the governor which can adjust the torque on the generator's turbine shaft. On the other hand, the reactive power and/or the terminal voltage can be controlled by adjusting the excitation system which includes power factor controller and automatic voltage regulator

(AVR). Many types of excitation systems such as brushless and static systems are explained in [34]. The typical controller of a synchronous machine-based DG is illustrated in Figure 2.15 (taken from [6]). The feedback signals of speed, voltage and current outputs of the generator are measured and sent back to the governor and AVR via transducers.

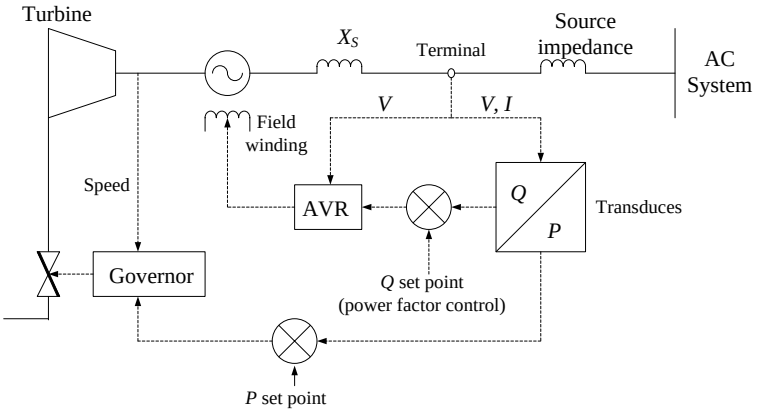

Figure 2.15. Typical control of a synchronous machine-based DG [6].

2.5.2 Voltage level control by using converter-connected DG

There are two main structures of converter-connected DG. Firstly, the system employs one grid-side inverter connected with a DC input power generation such as PV, fuel cell or battery. The grid-side converter will transform the DG power generation from DC to AC. Figure 2.16, shows a general structure of a grid-side inverter-interfaced with DG system. Other type of converter-connected DG, as shown in Figure 2.17, uses two back-to-back converters interfaced with the AC input generation, such as small wind turbine or micro-turbine. The input side converter converts power generation from AC to DC, and then the grid-side converter converts back from DC to AC synchronously with the grid frequency.

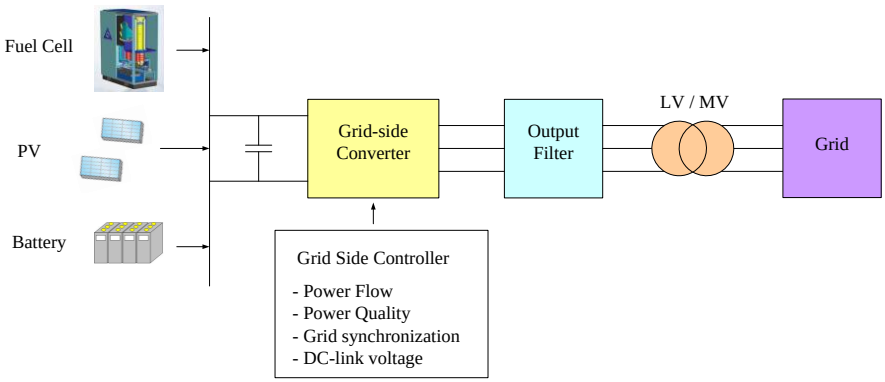

Figure 2.16. Structure of grid-side inverter interface with DG.

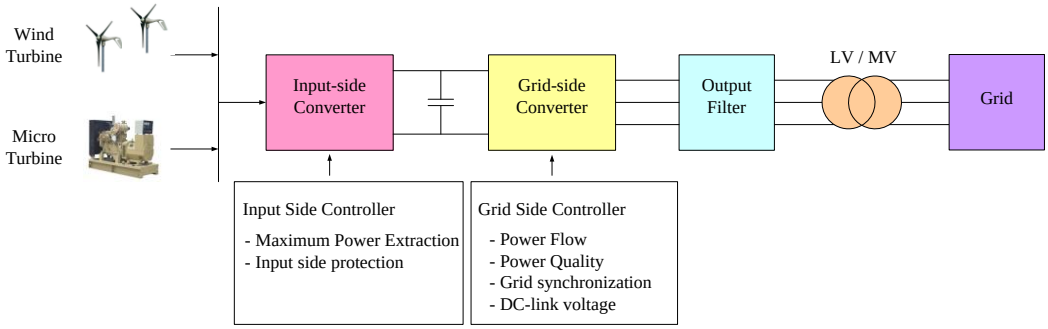

Figure 2.17. Structure of back to back converters interface with DG [44].

The grid-side converter is the main device used to interact with the AC network. Therefore, the simple structure of converter-connected DG can be considered as only grid-side VSC interfaced with the DC circuit [35], as shown in Figure 2.18. Additionally, the DC circuit represents the DG generation and is modelled by a DC voltage source or DC current source connected to a capacitor. The losses in the DC circuit are represented as a parallel resistance. The *P* and *Q* exchange between the network and the grid-side inverter causes variations of the DC voltage, especially when a DC current source is used. Therefore, to reduce this problem, proper design of capacitor and DC voltage controller is necessary to ensure that the level of DG voltage ripple is acceptable.

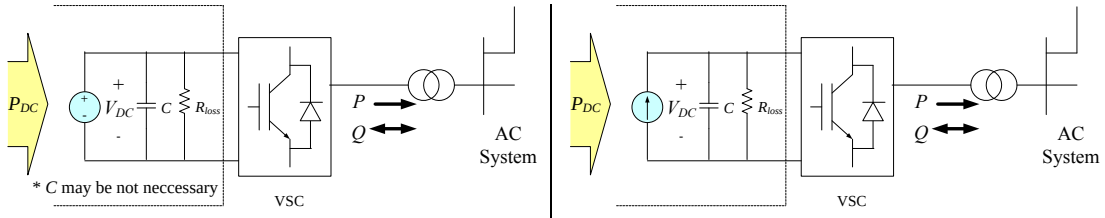

(a) using DC voltage source

(b) using DG current source

Figure 2.18. Simplified equivalent circuit of converter-connected DG [35].

From Figure 2.18, the structure of converter-connected DG is also similar to the DSTATCOM (see Figure 2.7). While DSTATCOM may only compensate reactive power, converter-connected DG may control both active and reactive power at the same time. The general concept of using converter-connected DG to support active voltage control is explained in [36], where the voltage controllability may depend on the rating of the grid-side inverter. It also suggested that the reactive power supported from DG should be high enough to give sufficient voltage control but small enough to prevent hunting among neighbour DG units.

The reactive power capability from grid-side converter is considered from the maximum apparent power, S_{max}, which depends on the size of the grid-side converter, and the actual active power transfer, P_{act}, from the inverter. The maximum possible reactive power supply from the converter-connected DG, $|Q|_{max}$ can be written as [33]:

$$|Q|_{\max}(t) = \sqrt{S_{\max}^2 - P_{act}^2(t)} \tag{2.18}$$

However, P and Q are also limited by the DC voltage and the rated current of power switches or other limiting element in the grid interface [37]. The P and Q control capability of converter-connected DG, including the generation limits, is shown in Figure 2.19 [33].Additionally, some Grid Codes may limit the value of Q support by defining the minimum value of power factor (i.e. power factor at least 0.95 for Germany's Grid Code).

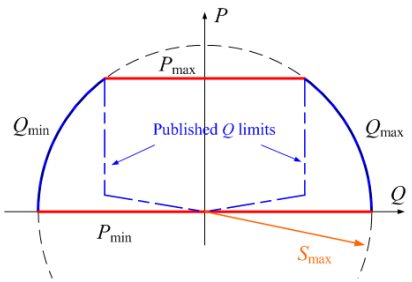

Figure 2.19. The operating chart of inverter-based DG connected to the grid [33].

In case of intermittent DG such as solar and wind, from (2.18), the variable P generated from DG influences the change of Q capability. However, the change of the energy resource may be in the range of minutes, so it is still able to use intermittent DG to support short-term voltage variations with changes in the range of seconds. Moreover, if DG is operated at rated active power generation near the maximum capacity of the grid-side converter, then there is no reserved Q capacity left for supplying reactive power. Therefore, over-sizing of the grid-side converter is required to allow the DG to have some available Q to support power factor and/or AC voltage control.The P and Q from the three-phase converter-connected DG can be controlled by adjusting the switching functions of the VSC. The PWM technique is widely used to this aim. The basic carrier-based sinusoidal PWM compares a high-frequency periodic triangular waveform, called the carrier signal, with a slow-varying waveform known as the modulating signal [38, pp.25-26]. The space-vector PWM [41, p.93] is another PWM technique where switching functions are considered based on eight possible switching states. This PWM has the advantage of reducing switching losses.

The power output of the grid-side converter can be controlled using voltage or current control, see Figure 2.20 [38, Ch.8]. In case of voltage-controlled VSC, the power output of the DG is controlled by adjusting the amplitude and phase of the converter output voltage, V_{VSC}, with respect to the AC system voltage, V_{bus}. The power outputs can be determined from (2.13) and (2.14), which shows a coupling between P and Q. An extra coupling inductor may be required, in addition to the transformer reactance, to control the power flow. In addition, the errors from comparing the reference of P and Q and the feedback signals are used to generate the required amplitude and phase angle of the converter's terminal voltage, which are $|V|$ and δ, respectively. Thus, the modulating signal, V_{mod}, is created with respect to the feedback of grid voltage to generate the required switching signals via the PWM controller (see Figure 2.20(a)).

In case of the current-controlled VSC, the current flow is controlled instead of the converter's terminal voltage, and the addition of the series inductor may not be needed for power flow control. The errors between the reference and the feedback of active and reactive powers are used to generate the required current values. After comparing the required current and the actual current, the error signal is passed on to the current controller and PWM blocks to create the desired switching signals (see Figure 2.20(b)). Additionally, the voltage outputs of the VSC can be controlled by using the voltage controller instead of the reactive power controller [39], or installing an additional voltage controller as the outer controller in cascade with the reactive power controller.

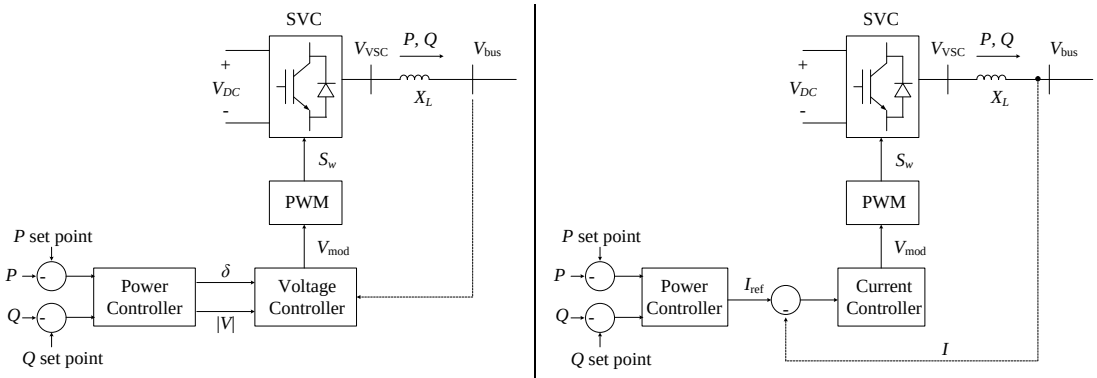

(a) Voltage controlled grid-side VSC

(b) Current controlled grid-side VSC

Figure 2.20. Basic voltage and current control of the grid-side VSC [38, Ch. 8].

It is also found that P and Q controls in the current controlled VSC are separate, as the current outputs can be controlled independently from the AC voltage which depends on the control algorithm. Therefore, power factor and/or AC voltage output can be controlled whilst

P is kept constant [40]. Other advantages of current control are better performance and provision of fast response [41]. The research work in [40] also recommends using the current control method to operate the converter-connected DG for voltage and/or *Q* support.

2.6 Harmonic mitigation from converter-connected DG

The penetration of converter-based DG may increase the harmonic level above the statutory limits. Several techniques are already implemented to mitigate harmonics from this type of DG, including 1) advanced converter control, 2) multi-module converter units, 3) multi-legs converter and 4) multi level converter.

2.6.1 Advanced converter control

Examples of advanced control techniques for harmonic mitigation are as follows;

- Selective harmonic elimination technique (or programmed PWM) adjusts the switching angles to eliminate particular harmonics [14, p.342]. In addition, the required switching angles can be determined by using the off-line optimised strategies especially more than one harmonic order need to be eliminated.
- Harmonic voltage damping and harmonic current compensation functions can be integrated with the controller of converter-connected DG, as secondary functions [42]. The harmonic voltage damping is used to control harmonic of voltage output from DG. On the other hand, if DG is connected in parallel with a non-linear load, the harmonic current compensation provides the harmonic currents compensation of an adjacent non-linear load.
- Converter-connected DG which uses the repetitive control (or natural frame control) can offer better waveform quality than using conventional current control [43]. It offers a better alternative for voltage tracking, which can deal with voltage harmonics simultaneously and also several disturbances. The controller can provide two control objectives: 1) control *P* and *Q* supplied to the grid and 2) maintain voltage output, at the same time. The repetitive voltage controller can be designed based on the H_∞ method to achieve robust performance or stabilisation [44].

Although these advanced control techniques provide a good control performance and reduce harmonics, the design is more complicated and the controller is more complex.

2.6.2 Multi-module converter units

The grid-side converter of DG can comprise several converter modules in parallel rather than using only one single unit, as can be seen in Figure 2.21. This structure provides the voltage harmonic mitigation at the electromagnetic interface level, where output voltages of individual units are connected together, with no need to increase switching frequencies in the PWM control scheme [14, p.345]. In addition, the harmonic mitigation is achieved by providing the phase shifting between individual units, where phase-shifted angles are determined according to the harmonics to be cancelled out.

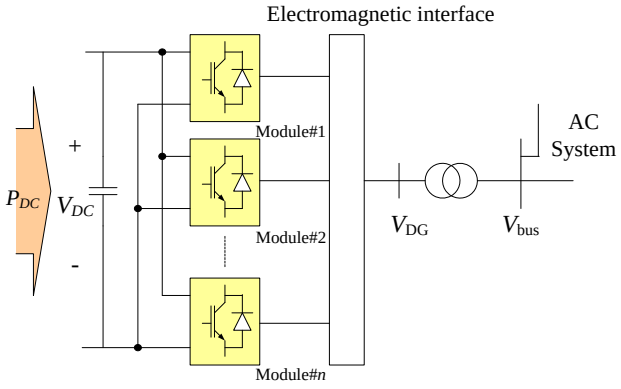

Figure 2.21. DG interface with multi module PWM grid side converters [14, p. 345].

The phase shifting between converter modules can be performed by using zig-zag or phase-shifting transformers. On the other hand, shifting the carrier signals of each PWM control scheme is also possible for harmonic mitigation at the secondary side of the coupling transformer. Furthermore, the circulating currents among converters should be addressed if the connection of converters is non-isolated between the AC and DC system. This connection pattern can form a closed zero sequence current path in the system [45].

2.6.3 Multiple legs converter

The use of converters with multiple legs in parallel is similar to the paralleling converter modules in the previous section. This technique is aimed for MV or LV high-power

applications such as PV and wind power systems [45], where paralleling legs within each pole of converters can possibly increase the current handling capacity, as well as decrease harmonics in the output. The structure of multiple-legs VSC is illustrated in Figure 2.22.

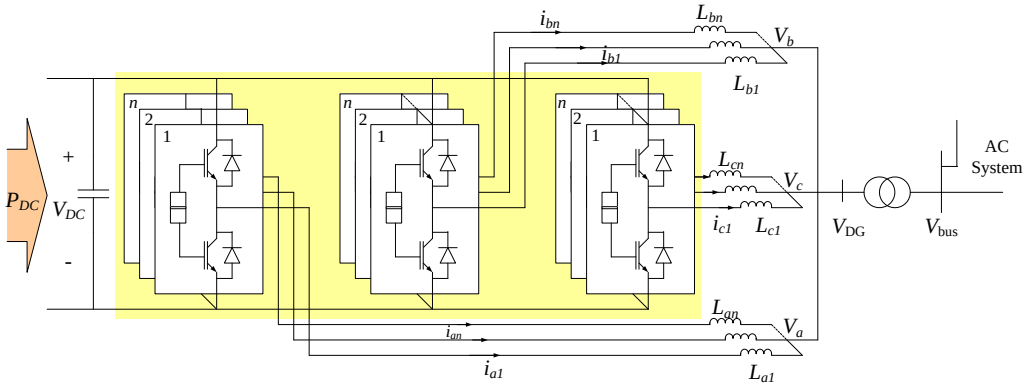

Figure 2.22. Three-phase VSC with multiple legs in parallel [45].

To operate the multiple-leg converter, a current sharing mechanism is required to ensure that currents or powers sharing among the legs of each pole of the converter are equal. In addition, there are two control loops: 1) an external loop that controls the total current of the converter, and 2) internal loops, where the number of controllers depends on the number of legs, to control the current sharing among legs of a same phase [46]. The output harmonics can be eliminated by using phase displacement among the carrier signals of paralleling legs in the same phase, where a PWM pattern is generated independently of each leg in the same phase.

2.6.4 Multi-level converter

A better power quality can be achieved by using the multi-level converter instead of the conventional 2-level converter. The output voltage waveform of the 3-level converter is more similar to a sinusoidal voltage compared with the output voltage of 2-level converter, as examined in [47], [48].

There are two types of 3-level voltage source converter: 1) the flying-capacitor converter, and 2) the diode-clamped converter, as can be seen in Figure 2.23. The additional capacitors are required in the flying-capacitor converter, where the voltage at the capacitor is controlled to adjust the third voltage level. The design of flying-capacitor converter is described in detail in [49]. On the other hand, the diode-clamped converter requires two capacitors to split

the DC link voltage and 6 clamped diodes connected to the neutral point voltage level between those two capacitors.

To operate the flying-capacitor converter, the easiest technique is using the natural balancing achieved by applying phase-shifted switching signals among legs in the same phase, at approximately the same duty cycle [50]. Additionally, the phase-shifted carrier PWM is usually used to create switching signals in the natural balancing strategy. Phase-disposition PWM is another technique which can provide better output waveforms compared with the outputs from the phase-shifted carrier PWM, so this is the preferred method for a flying-capacitor converter. The examination of natural balancing properties of multilevel converter operating under phase-disposition PWM is investigated in [51]. In case of the diode-clamped converter, the switching operation uses the phase-shifted technique which is similar to the flying-capacitor converter [48]. The controller of the neutral point voltage in the DC-link (i.e. between the two capacitors) is required to deal with voltage fluctuations from either the charging or discharging of the capacitors [47].

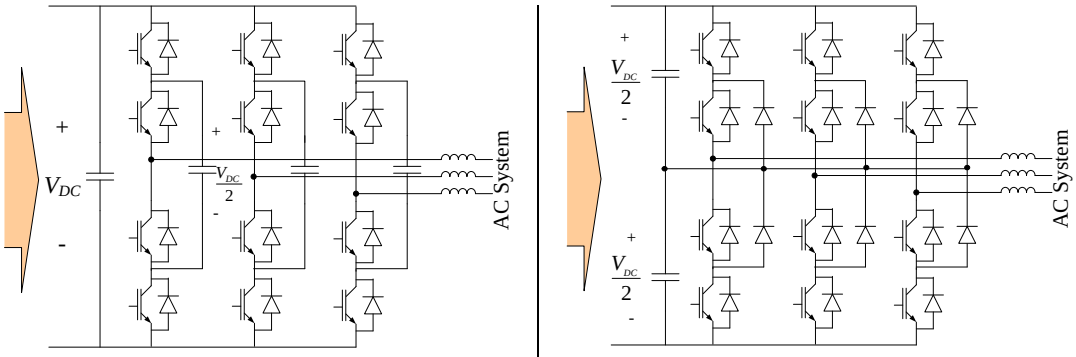

(a) 3-level flying capacitor converter

(b) 3-level diode clamped converter

Figure 2.23. Typical three-level converters [47].

From Section 2.6.2 to 2.6.4, although those innovative converter structures provide the benefit in harmonic mitigation, they pose the significant issues in terms of cost, reliability and power losses. The cost is higher than conventional converter because of those converter structures required more additional devices, such as transformer windings and switching devices, and more complex control schemes. The number of devices that has been increased also makes the failure probability higher, which means that the reliability will be decreased. Furthermore, the additional transformer windings raise the loss in transformer in case of

multi-module converter units. The switching loss also increases due to the increase of switching devices in case of multiple legs converter and multilevel converter.

2.7 Conclusions

This chapter discusses the power quality issues which are possible to arise from the DG connection in distribution networks. It is found that two main issues are of concern: 1) voltage level variations, and 2) harmonic pollutions. The reverse power flow from DG and the intermittency of renewable DG can cause voltage rise and fluctuations, respectively. The impact of single-phase DG connected in LV networks may increase the voltage imbalance condition in the MV network. Moreover, the penetration of converter-connected DG can raise the level of harmonic distortion in the network.

Voltage level improvement by using additional compensation devices and DG's voltage control were introduced. The substation's OLTC can provide steady-state voltage support for a wide area in distribution networks. The modern OLTC distribution transformer which uses power electronic or solid-state devices can support either short- or long-term voltage variations in LV networks. Shunt capacitors and voltage regulators can be used as a decentralised voltage control to deal with slow voltage changes in specific locations especially at the middle and at the end of the feeder. Moreover, power conditioners such as SVC, DSTATCOM and DVR are able to provide decentralised voltage control with fast response. Apart from using compensation devices, synchronous machine-based DG and converter-based DG can also be used to support voltage control by injecting or absorbing reactive power. The converter-connected DG is able to provide fast voltage control similar to power conditioning devices. However, oversize of DG may be required to have sufficient reactive power available for voltage control proposes. Using DG for voltage control reduces the installation of new compensation devices, and allows increasing the penetration level of DG in distribution networks.

The harmonic pollution from non-linear loads and power electronic interfaced DG can be mitigated by installing line reactors, and passive and active filters. The line reactor is used to reduce harmonic currents. The active filter can adapt to all harmonic variations due to changes in network conditions, while the passive filter is able to eliminate only particular harmonics, which depend on the tuned frequencies of the filter. However, installing filters may not be enough with high penetration of inverter-interfaced DG connected in the network, so enhanced harmonic elimination from individual DG units may be required.

Converter-connected DG can reduce its output harmonics by using VSC instead of CSC. Advanced converter control, rather than conventional voltage and current controlled strategies, may be applied to enhance harmonics mitigation. Innovative VSC structures have also been developed to improve performance and minimise harmonics generation.

2.8 References

[1] A. Bayod-Rújula, "Future development of the electricity systems with distributed generation," *Energy*, vol. 34, pp. 377-383, 2009.

[2] L. A. Schienbein and J. G. DeSteese, "Distributed Energy Resources, Power Quality and Reliability - Background," Pacific Northwest National Laboratory, Richland, WA. January 2002, pp. 23.

[3] "IEEE Recommended Practice for Monitoring Electric Power Quality," *IEEE Std 1159-2009*, 2009.

[4] A. D. Almeida, L. M. J. Delgado, and P. Quality, "Power Quality Problems and New Solutions," in *International Conference on Renewable Energies and Power Quality (ICREPQ)*, Vigo, 2003, pp. 1-9.

[5] P. Ferracci, "Power Quality," *Schneider Electric Cahier Technique no. 199*, p. 36, 2000.

[6] N. Jenkins, J. B. Ekanayake, and G. Strbac, *Distributed Generation*, 1st ed. The Institution of Engineering and Technology, 2010, pp. 15-16.

[7] "IEEE recommended practices and requirements for harmonic control in electrical power systems," *IEEE Std 519-1992*, 1993.

[8] "Electromagnetic Compatibility (EMC) – Part 3-6: Limits – Assessment of emission limits for the connection of distorting installations to MV, HV and EHV power systems", *IEC/TR 61000-3-6*, Ed. 2.0 , Feb. 2008.

[9] "Electromagnetic Compatibility (EMC) – Part 3-7: Limits – Assessment of emission limits for the connection of fluctuating installations to MV, HV and EHV power systems", *IEC/TR 61000-3-7*, Ed. 2.0 , Feb. 2008

[10] GE Corporate Research and Development, "DG Power Quality, Protection and Reliability Case Studies Report," National Renewable Energy Laboratory (NREL),Colorado, NREL/SR-560-34635, Aug. 2003.

[11] A. Baggini, *Handbook of Power Quality*. Chichester, UK: John Wiley & Sons, Ltd, 2008.

[12] T. Ackermann, *Wind Power in Power Systems*, 1st ed. John Wiley & Sons, Ltd, 2005.

[13] V. Gosbell, S. Perera, and V. Smith, "Technical Note No.6 - Voltage Unbalance", Integral Energy Power Quality & Reliability Centre at the University of Wollongong," 2002.

[14] E. Acha and M. Madrigal, *Power Systems Harmonics: Computer Modelling and Analysis* Wiley-Blackwell, 2001.

[15] E. Acha, V. Agelidis, O. Anaya, and T. Miller, *Power Electronic Control in Electrical Systems* 1ed.: Newnes, 2002.

[16] L. Gertmar, P. Karlsson, and O. Samuelsson, "On DC injection to AC grids from distributed generation," in *European Conference on Power Electronics and Applications*, Dresden, 2005, pp. 1-10.

[17] C. Bayliss, *Transmission and Distribution Electrical Engineering*, 2nd ed. Newnes, 1999, pp. 497-508.

[18] C. Oates, A. Barlow, and V. Levi, "Tap changer for distributed power," in *Power Electronics and Applications, 2007 European Conference on*, 2007, pp. 1-9.

[19] P. Bauer and S. W. H. de Haan, "Electronic tap changer for 500 kVA/10 kV distribution transformers: design, experimental results and impact in distribution networks," in *Industry Applications Conference, 1998. Thirty-Third IAS Annual Meeting. The 1998 IEEE*, Missouri, pp. 1530-1537.

[20] I. Melnik, F. Provoost, and W. Bos, "Intelligent Distribution Substation Improves Power Quality," in *21st International Conference on Electricity Distribution (CIRED)*, Frankfurt, 2011, pp. 1-4.

[21] "IEEE Guide for the Protection of Shunt Capacitor Banks," *IEEE C37.99-1990*, no. 91, 1991.

[22] S. Taniguchi and S. Uemura, "Problems of SVR Operation in Large Penetration of Photovoltaic Power Generation and Proposal of Improve Operation," in *21st International Conference on Electricity Distribution (CIRED)*, Frankfurt, 2011, pp. 1-4.

[23] M. Noroozian, N. a. Petersson, B. Thorvaldson, A. B. Nilsson, and C. W. Taylor, "Benefits of SVC and STATCOM for electric utility application," in *2003 IEEE PES Transmission and Distribution Conference and Exposition*, 2003, pp. 1143-1150.

[24] N. Roy and M. Hossain, "Voltage profile improvement for distributed wind generation using D-STATCOM," in *Power and Energy Society General Meeting, 2011 IEEE*, Michigan, pp. 1-6.

[25] T. Sun, Z. Chen, and F. Blaabjerg, "Flicker Mitigation of Grid Connected Wind Turbines using STATCOM," in. *Second International Conference on Power Electronics, Machines and Drives, 2004. (PEMD)*, Edinburgh, pp. 175-180.

[26] S.-J. S. Tsai and Y. Chang, "Dynamic and Unbalance Voltage Compensation Using STATCOM," in *Power and Energy Society General Meeting - Conversion and Delivery of Electrical Energy in the 21st Century, 2008 IEEE*, 2008, pp. 1-8.

[27] B. Singh and S. Kumar, "Modified Power Balance Theory for control of DSTATCOM," in *2010 Joint International Conference on Power Electronics, Drives and Energy Systems & 2010 Power India*, New Delhi, 2010, pp. 1-8.

[28] P. Li, W. Wang, H. Cui, S. Wang, X. Yang, and Y. Zhao, "The application of voltage direct detection method based on mathematical morphology in distribution network with DG," in *Industrial Electronics and Applications (ICIEA), 2010 the 5th IEEE Conference on*, 2010, Taichung, Taiwan, pp. 967–972.

[29] G. Sandoval and J. Houdek, "A Review of Harmonic Mitigation Techniques." New Berlin, Milwaukee, pp. 1-17, 2005.

[30] R. C. Dugan, M. F. McGranaghan, S. Santoso, and H. W. Beaty, *Electrical Power Systems Quality*, 2nd ed. New York: McGraw-Hill, 2002, pp. 373-435.

[31] H. Zeineldin and E. El-Saadany, "Impact of DG interface control on islanding detection and nondetection zones," *Power Delivery, IEEE Transactions on*, vol. 21, no. 3, pp. 1515-1523, 2006.

[32] F. Iov, A. D. Hansen, P. Sørensen, and N. A. Cutululis, *Mapping of grid faults and grid codes*, Riso National Laboratory, Riso-R-1617 (EN), July. 2007.

[33] M. Braun, "Reactive power supply by distributed generators," in *IEEE Power and Energy Society General Meeting - Conversion and Delivery of Electrical Energy in the 21st Century*, Pittsburgh, 2008, pp. 1-8.

[34] P. Kundur, *Power System Stability and Control*. McGraw-Hill Professional, 1994, Chapter 8.

[35] I. Papic, "Mathematical analysis of FACTS devices based on a voltage source converter Part 1: mathematical models," *Electric Power Systems Research*, vol. 56, no. 2, pp. 139-148, Nov. 2000.

[36] M. H. J. Bollen and A. Sannino, "Voltage control with inverter-based distributed generation," *Power Delivery, IEEE Transactions*, vol. 20, no. 1, pp. 519-520, 2005.

[37] M. Chinchilla, S. Arnalte, J. Burgos, and J. Rodriguez, "Power limits of grid-connected modern wind energy systems," *Renewable Energy*, vol. 31, no. 9, pp. 1455-1470, 2006.

[38] A. Yazdani and R. Iravani, *Voltage-Sourced Converter in Power Systems: Modeling, Control and Applications*, 1st ed. John Wiley & Sons, Ltd, 2010.

[39] F. Magueed and H. Awad, "Voltage Compensation in Weak Grids Using Distributed Generation with Voltage Source Converter as a Front End," in *2005 International Conference on Power Electronics and Drives Systems*, 2005, vol. 1, pp. 234-239.

[40] S. H. Ko, S. R. Lee, H. Dehbonei, and C. V. Nayar, "Application of voltage-and current-controlled voltage source inverters for distributed generation systems," *Energy Conversion, IEEE Transactions on*, vol. 21, no. 3, pp. 782–792, 2006.

[41] M. P. Kazmierkowski, F. Blaabjerg, and R. Krishnan, *Control in Power Electronics (Selected Problems)*. Academic Press, 2002, Chapter 4.

[42] B. Renders, K. De Gussemé, W. R. Ryckaert, and L. Vandevelde, "Converter-connected distributed generation units with integrated harmonic voltage damping and harmonic current compensation function," *Electric Power Systems Research*, vol. 79, no. 1, pp. 65-70, 2009.

[43] B. Renders, K. De Gussemé, W. R. Ryckaert, and L. Vandevelde, "Converter-connected distributed generation units with integrated harmonic voltage damping and harmonic current compensation function," *Electric Power Systems Research*, vol. 79, no. 1, pp. 65-70, Jan. 2009.

[44] T. Hornik and Q.-C. Zhong, "Control of grid-connected DC-AC converters in distributed generation: Experimental comparison of different schemes," in *Compatibility and Power Electronic (CPE)*, Babajoz, Spain, 2009, pp. 271-278.

[45] I. Jaskulski, I. Gabe, and J. da Costa, "Space Vector Modulation Extended to Voltage Source Converters with Multiple Legs in Parallel," *Power Electronics and Applications, 2007 European Conference on*, Aalborg, 2007, pp. 1-10, 2007.

[46] I. W. Jaskulski, H. Pinheiro, and L. Mariotto, "Multi-Leg Voltage Source Converter for Grid Connected Wind Turbines," *2007 International Conference on Clean Electrical Power*, pp. 229-235, 2007.

[47] T. Petter, H. Raffel, and B. Orlik, "Multi-level converter power unit," in *European Conference on Power Electronics and Applications*, Dresden, 2005, pp. 1-10.

[48] T. J. Hammons, *Renewable Energy*. INTECHopen, 2009, chapter 15, pp. 271–296

[49] D. Krug, M. Malinowski, and S. Bernet, "Design and comparison of medium voltage multi-level converters for industry applications," in *Industry Applications Conference, 2004. 39th IAS Annual Meeting. Conference Record of the 2004 IEEE*, 2004, vol. 2, pp. 781–790.

[50] R. H. Wilkinson, T. a. Meynard, and H. du Toit Mouton, "Natural Balance of Multicell Converters: The General Case," *IEEE Transactions on Power Electronics*, vol. 21, no. 6, pp. 1658-1666, Nov. 2006.

[51] B. P. McGrath and D. G. Holmes, "Enhanced Voltage Balancing of a Flying Capacitor Multilevel Converter Using Phase Disposition (PD) Modulation," *Power Electronics, IEEE Transactions on*, vol. 26, no. 7, pp. 1933–1942, 2011.

[52] Engineering Recommendation P28, "Planning limits for voltage fluctuations caused by industrial, commercial and domestic equipment in the UK", The Electricity Council, September 1989.

[53] N. Jenkins, R. Allan, P. Crossley, D. Kirschen, and G. Strbac, *Embedded generation*, 1st ed., the Institution of Engineering and Technology, 2000, Chapter 4.

Chapter 3

Voltage Control Structure for Distribution Networks with DG and Technology Requirements

3.1 Introduction

Electrical power and network control are typically the responsibility of centralised services that control several areas from the substation. There is no participation from consumers and generation units in the operation and management of the network. Conventional distribution networks have mostly unidirectional power flows and passive operation. However, the integration of DG is unlikely to be made without changes to the distribution network structure, planning and operating procedures [1]. The distribution network management will be transformed from passive to active operation where DG can be controlled, by either the substation, or individually to support voltage control in the network.

A voltage control structure which can manage active voltage support from DG and other voltage controllable devices in distribution networks is proposed in this chapter. This control structure aims to integrate Volt-Var control to the centralised and decentralised voltage control performed by the OLTC at the substation, and modern converter-connected DG technology, respectively. Other voltage controllable devices such as DSTATCOM or ESSs can also be integrated in this control using a coordinated approach. New technologies such as real-time monitoring and communication systems are required to fulfil the advanced distribution automation function implicit to this voltage control structure.

DG with voltage controllability can provide localised voltage support for both steady-state and dynamic voltage disturbances, as explained in Chapter 2. Due to the fast voltage controllability of converter-based DG, the decentralised voltage control is selected as the primary voltage support to specific locations in the network. The substation's OLTC provides the secondary voltage support because the control response from the substation is much slower than that of the DG units. A hierarchical distributed control structure is implemented to support the integrated Volt-Var control between decentralised and centralised control systems. The distribution network is split into smaller areas termed as

"*Local controllable zones (LCZs)"* to illustrate the voltage controllable areas that can receive the support from DG units. The DG units within a zone should be able to satisfy the zone's voltage compensation requirements without affecting the voltage level of the buses external to that zone. A coordinated control algorithm is developed to control the operation of a group of DG units and the substation to support voltage control with less interaction (or called *hunting*) between them.

LCZs can enhance the visibility of voltage controllable locations and can be used for real-time monitoring to illustrate the possible locations in the network that can receive voltage support from DG. The DNO can also use the information of LCZs for planning and operating the active network management especially the active voltage control. The size of LCZs can be adapted automatically to follow changes of network conditions such as the change of DG output, and network configuration. The methodology proposed for LCZ identification is based on voltage sensitivities and the availability of *Q* support from DG.

3.2 Voltage control structure for distribution networks with DG

The increased utilisation of DG causes the electricity system to change from a centralised to a decentralised structure with numerous small generators and renewable energy sources. Therefore, the control structure in MV networks needs to be restructured to coordinate the active control from *distributed controllers* (i.e. DG used for decentralised control), and *central controllers* (i.e. the substation's OLTC used for centralised control). To meet this objective, a hierarchical distributed control structure is introduced with the aim to improve the voltage level of the whole network.

A hierarchical distributed control structure, originally introduced for voltage control in transmission systems [2], is proposed to allow DG units to provide voltage support in distribution networks. This control structure is already applied in many DG applications including: islanding operation [3], electricity trading [4] and protection schemes [5].

3.2.1 Distributed control system in distribution networks with DG

In the case of DG integration into distribution networks, distributed control can be applied in addition to centralised control in the network. It is employed in many applications such as voltage support, frequency control and power trading [2, Ch.11].

The distributed voltage control of distribution networks can be implemented by dividing a network into several LCZs, where each LCZ consists of at least one distributed voltage controller, as can be seen in Figure 3.1. In addition, the voltage controller can be either DG, ESS or power conditioners which can provide voltage support automatically. In the case of a radial network topology, which has feeders steaming out from the substation and several laterals connected to each feeder, the LCZs are located at the laterals.

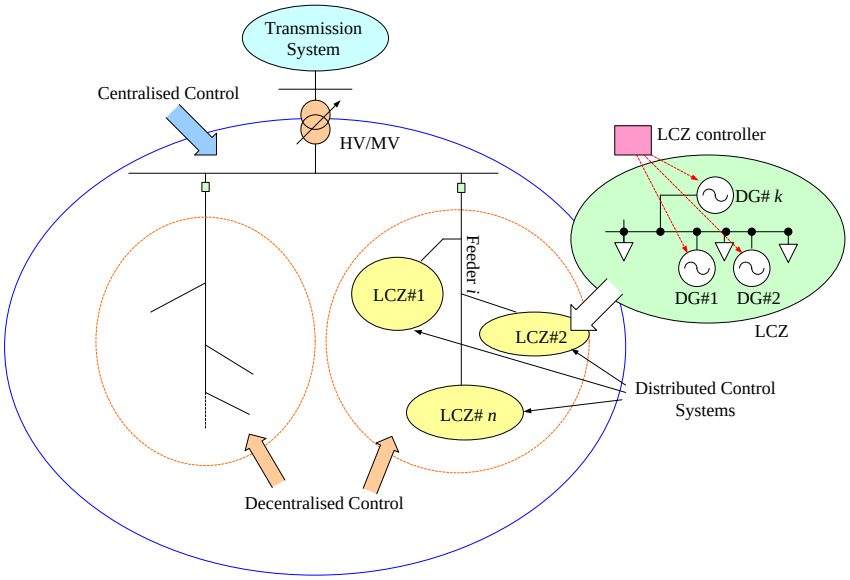

Figure 3.1. Distributed control structure of distribution network.

The voltage control system in each LCZ should be implemented with minimised interactions among adjacent control areas. If more than one DG unit is in the same zone, coordination among DG units may be required to minimise the interaction between them. Each LCZ has an individual master unit called *the LCZ controller* is used as the communication gateway or/and used as the decision maker to operate the group of DG units in the same zone, depending on the application. Additionally, the LCZ controller has either the intelligent processing unit or computer, to make control decisions, and to analyse data.

3.2.2 Hierarchical distributed voltage control structure

The hierarchical distributed voltage control structure integrates the decentralised and the centralised control. The bus's voltages located inside each LCZ can be regulated directly through the Volt-Var control from DG and compensation devices in a specific location of the network. Additionally, DG is used as the primary support while the central voltage controller at the substation will provide secondary support if the primary support from the decentralised control is insufficient. The control centre at the substation can update the network condition by using the sampling data from the LCZs, and adjust the set-point of distributed controllers, if possible, to optimise and maintain the network operating in the desired conditions.

The proposed hierarchical distributed control is shown in Figure 3.2. The MV network is split into LCZs, where a zone consists of DG and other controllable devices, such as ESSs, which can provide voltage control to buses inside that zone. A control algorithm is designed to coordinate the operation of the DG units and other controllable devices, and also to coordinate the operation between LCZs through the higher-level controller at the substation via the communication links. Moreover, the LCZ controller, in this work, is assumed as a data concentrator unit which has on-line monitoring capabilities to exchange data with other neighbouring zones and with the substation as required by the control algorithm.

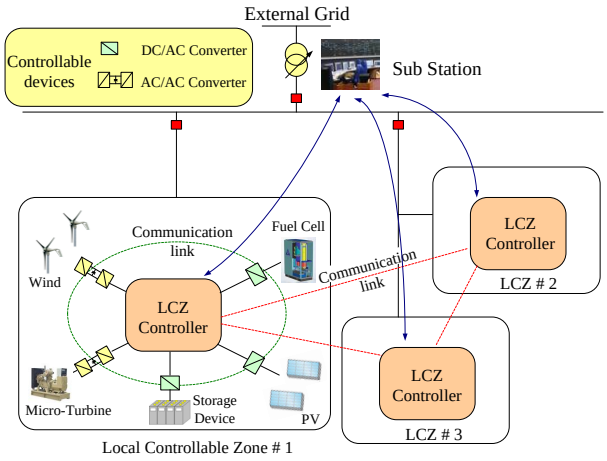

Figure 3.2. Hierarchical distributed voltage control structure in DG networks.

A self-sustained, fully-controlled DG unit such as a micro-turbine is preferable in a voltage control scheme as it can remain operational at all times unlike some other intermittent renewable sources (e.g. PV or wind turbine). However, due to the adaptable nature of the proposed zone identification scheme the best use of available sources is always guaranteed.

The hierarchical distributed control structure consists of three main layers which can be explained as follow:

- *Reactive layer*: This is the bottom layer aiming for decentralised voltage control, so DG is the key device in this layer. The distributed controller can respond with fast speed and perform self-healing actions that need immediate response especially for short-term voltage variations. It has direct communication links among DG units within the same layer.

- *Coordination layer*: The LCZ controller is used for this middle layer with the aim to exchange information, especially the measuring and status data, among zones and the higher layer. This controller may select only the important data due to limitations in the bandwidth capacity of the communication system.

- *Deliberative layer*: It is the top layer which prepares the higher level commands by using information of the network. This layer, located at the substation, has the ability to manage all information and to carry out actions to achieve the voltage control objectives. This layer can provide information about the network conditions and to update the new set points of DG and controllable devices located in the lower layers.

The voltage control strategy consists of three stages:

- *Primary support*: It is a decentralised voltage support from the automatic voltage controllers especially from DG or power conditioning devices, without control commands or support from the substation. The control response is fast, usually in the range of several seconds. The support in this stage can mitigate localised voltage quality problems such as short- and long-term voltage variations, and voltage flicker.

- *Secondary support*: This stage is operated automatically when the support from the primary stage is insufficient. This control response is normally slower than the primary stage, usually several seconds to minutes. The voltage controller of this stage starts after the primary support to avoid interactions among voltage controllers. Therefore, only long-term voltage variation can be supported from this stage. The OLTC distribution transformer and voltage regulator can be used as the secondary voltage controller for decentralised voltage control, to support the voltage control at specific buses when voltage support from DG may not be enough.

- *Tertiary support*: This stage aims to optimise the voltage profile of the whole network, operated by the main computer unit in the control centre at the substation.

The online monitoring data from each LCZ is sent to the substation via the LCZ controller. Then, the results from the optimisation analysis are used to set up the new operating points of voltage controllers across the network. The updated set-points of controllable DG units are sent back to LCZs via the LCZ controller. The tertiary support is a cycle operation in the range of several minutes to 15 minutes, depending on the speed of the communication system and processing units.

3.3 Technology requirement for advanced distribution automation: Voltage control case

Many applications of advanced distribution automation technologies, such as fault location, isolation, service restoration and, in this work, voltage control, have been developed for smart distribution networks. There are many technology requirements to make distribution networks with DG smart enough to facilitate automated voltage control across the network. Although this section is not the main contribution of this research, it can provide the idea how to implement the hierarchical distributed voltage control structure based on the distribution automation platform.

3.3.1 Automatic voltage control system

The hardware platform for automatic voltage control system in distribution networks with DG consists of four main parts including;

1) Supervisory control and data acquisition (SCADA)
2) Smart measurements
3) Information and communication technology (ICT)
4) Global positioning system (GPS)

SCADA is the equipment and procedures for controlling remote stations from a master station. The master station is the control centre at the substation and the remote stations are on-site remote terminal units (RTU) such as the substation's OLTC and LCZ controller of each LCZ. It also includes the digital control equipment, sensing and telemetry equipment and two-way communications to and from the master stations and the remotely controlled stations [6]. Application of SCADA for active distribution management in the distribution networks with DG is presented in [7].

The block diagram of SCADA system for automation voltage control is shown in Figure 3.3. The measurement equipments, the LCZ controller and the DG controller are assumed as the intelligent electronic device (IED). Additionally, IED is the recent distributed automation device which incorporates one or more processors with the capability to receive or send data from or to external sources, as explained in [6]. It can be integrated with protection, control and data acquisition functions to reduce costs, size and eliminate redundant equipment and databases.

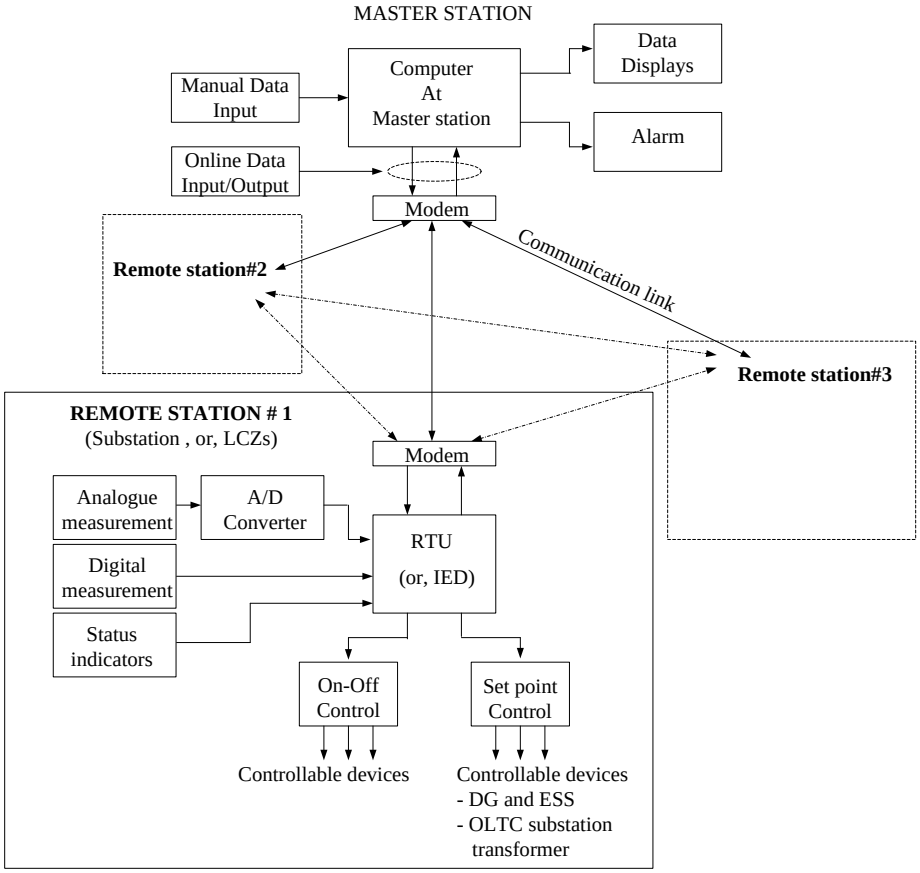

Figure 3.3. SCADA system for voltage control in distribution networks.

The smart measurement devices (e.g. the phasor measurement unit, PMU, but it is very costly) can be installed in specific locations especially at a DG bus and critical buses (such as the bus that has high load consumption, or the bus at the end of a feeder). The measuring data is sent to other LCZs and to the control centre via communication links. The hardware platform used by the measurement system is illustrated in Figure 3.4. The group of LCZ and the substation can be synchronised by using the satellite clock time reference from GPS. Present commercial GPS can provide the synchronising signal with accuracy in the range of 1 μsec [8]. The GPS offers a possibility for tracking the real-time dynamic behaviour across

the network with the same time reference. Moreover, this reference time is also used to synchronise with the substation's monitor and control system and IEDs across the network.

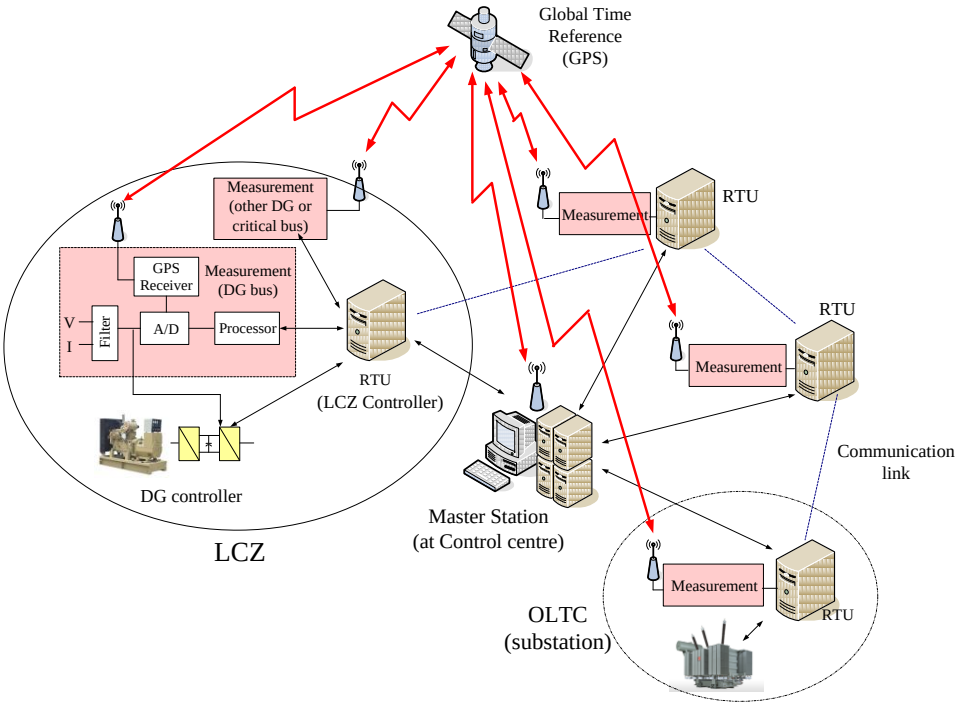

Figure 3.4. Hardware platform used by the network measurement system.

In each LCZ, the measurement information (i.e. voltage, current, active and reactive powers) obtained from a group of measurement devices, in the same zone, is sent to the LCZ controller. Hence, data is sent to the master station unit at the substation for global data processing, including the state estimation or it can be sent to other zones to supporting a coordinated control strategy. The communication link between measurement device, DG controller and LCZ controller should be flexible and adapt to LCZ's changes. Therefore, wireless communications are preferred where possible.

3.3.2 Real-time monitoring and display for future distribution networks

Distribution networks are required to become more visible to enhance network control, operation, and management, allowing DNOs to know the network condition in real-time. In traditional distribution networks, the DNO can monitor power only downstream to each feeder and the busbar voltage at the substation. The lack of online measuring devices and ICT makes it difficult to know the real-time network conditions. However, these technologies are developing, presenting better performance and becoming cheaper.

The network condition is determined by using the information from online measurements by using PMUs across the network. All monitoring data is sent and processed at the main computer in the control centre, which includes the state estimator and zone identification algorithm. Then, the updated information is displayed at the control centre and sent to LCZ controllers for updating their own zone. Additionally, the updated information, including a new set-point or on-off command for rescheduling the DG unit, may be sent to specific zones to maintain the network within the desired condition.

The concept of display system can be developed based on GIS system [2, Ch.12]. The GIS provides the graphic of the real-time network condition drawn from the geography map where the distribution network is located. The geography map can be taken from the recent updated satellite map. Furthermore, the voltage profile of the whole network can be indicated by using different colours or using contour graph, where different colours mean different voltage level. The idea of display system based on GIS is illustrated in Figure 3.5. The GIS can also link with the SCADA system to support the control operation straight from the DNO. The display system can be also integrated with internet and mobile communication systems to offer remote access.

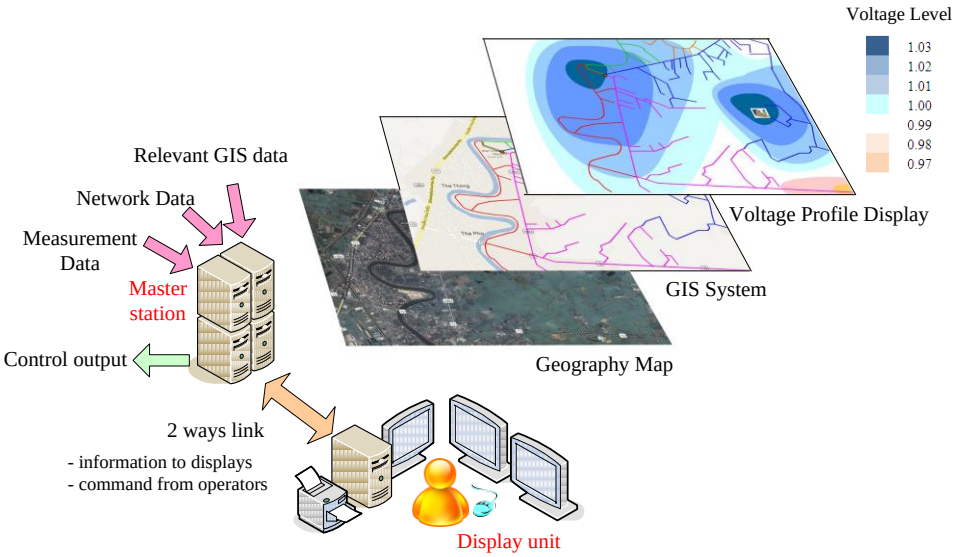

Figure 3.5. Concept of GIS display.

An LCZ can be displayed in graphic form as one layer of the GIS system. Different zones can be used in different colour or marked with different number. Alternatively, the LCZs can be presented by the simple non-graphic form based on the spread-sheet display. This form can be used as the summarised report of the real-time network monitoring. Moreover, it can be displayed via the internet browser for online access. The important information includes

the number of the zone, the DG bus and the LCZ memberships. An example of displays in forms of graphic and spread-sheet is shown in Figure 3.6. (**Note:** Figure 3.5 and Figure 3.6 are used to demonstrate the concept of display system to support the voltage control in distribution networks, but it is not implemented in this work).

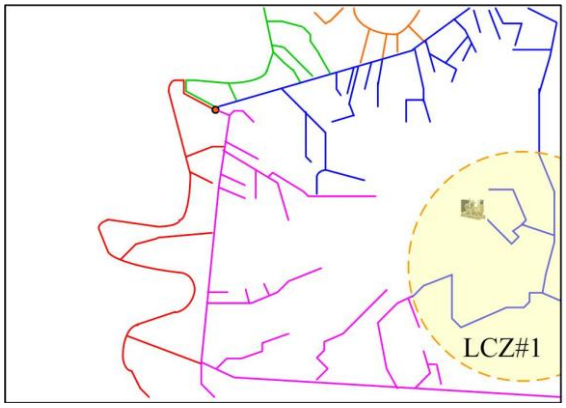

(a) Graphic display

Date xx/xx/20xx Time xxxxx No. of Zone (1)

Zone	No. of Bus	No. of DG	Vth (p.u.)
1	5	1	0.015

Buses

Bus Number	Bus Type	base kV	V (p.u.)	Feeder	Zone	Zone name
105	Load	11	1.02	1	1	GLA_01_z01
106	DG	11	1.03	1	1	GLA_01_z01
107	Load	11	1.02	1	1	GLA_01_z01
108	Load	11	1.01	1	1	GLA_01_z01
109	Load	11	1.01	1	1	GLA_01_z01

Generators

Gen. bus no.	base kV	V(p.u.)	Pgen (MW)	Qgen (MVar)	Qres (Mvar)
106	11	1.03	1	0	0.5

(b) Non-Graphic display

Figure 3.6. Concept of LCZ output display.

3.3.3 Information and communication technology requirements

There are many technology requirements to enable the communication capabilities among controllable devices in the proposed hierarchical distributed voltage control structure. [2, Ch.2] suggested that traditional centralised control and monitoring systems of distribution networks, without decentralised control, need high performance computing systems to let the control meet rigid time requirements. Furthermore, expensive and complex communication systems to transfer data to the control centre are required. Local faults or system malfunction can reduce the reliability of communication networks in centralised control. Conversely, the integration of the distributed control systems can improve the reliability of the communication network where the splitting of one control system into several individual control systems can separate the effect from local faults and malfunctions within the related local control area.

A distributed control system is defined as a physical arrangement for distributed processing that is usually a computer network located across the distribution network. A distributed processing unit can be the LCZ controller, and also the DG controller. The LCZ controller can also be used for information acquisition capturing all sorts of relevant information from a network of sensors inside the LCZ, and then sharing them to other zones and the

substation. Moreover, the communication network should be able to support the coordinated control among distributed control systems located around the network. In [2, Ch.2], it is recommended that communication systems for decentralised control should be designed to operate properly in the presence of limited, unreliable communication links, and often in the absence of a central control mechanism.

A local area network (LAN) can be selected as the communication system to link among controllers at the same location such as in the substation or individual LCZ. On the other hand, a wide area network (WAN) is employed to manage two-way data flow between the control centre at substation and the LCZs in a large-scale distribution network. The requirements for this communication system suggested in [9] are that it should be secure, scalable, and interoperable. Furthermore, the data transmission system should have adequate latency, sufficient bandwidth and necessary coverage.

Many communication protocols are developed to define the rules and regulations for the real-time data transmission between communication devices according to the distribution automation, as suggested in [33], [34]. The transmission control protocol (TCP)/Internet protocol (IP) is the most widely used protocol architecture at present. Modbus is a messaging protocol providing communication between devices connected over several buses and network. DNP 3.0 gives the rules for substation computer and master station computers to communicate data and control commands. IEC 60870-5-101 is a general protocol providing a messaging structure for RTU-IED communication. Moreover, IEC 61850 is an open standard for communication within substations to ensure the interoperability of substation equipments. IEC 62056 and ANSI C12.22 are two set standards that describe open communication systems for smart meters/measurements [34].

3.3.4 Distributed control technologies

For the decentralised voltage control especially the primary and secondary voltage support (see Section 3.2.2), the distributed controllers should operate automatically by their own decision without the command from the central control centre at the substation. Autonomous and intelligent control technologies such as multi-agent systems (MAS) can be applied to enhance the decentralised control ability in many power system applications [10],[11]. MAS is a distributed network of intelligent hardware and software agents that work together to achieve a global goal [2, p.36]. Agents represent individual entities where each agent is

modelled as an autonomous participant with independent strategies to achieve its objective. Moreover, the decisions of the controllers should have a certain degree of intelligence and each unit can interact with other participant controller units. These increase the system scalability necessary to accommodate system changes.

MAS can be applied into the proposed voltage control structure by indentifying the central controller, LCZ controllers and controllable DG units, as agents in MAS environment. Despite each agent is intelligent, it is difficult for individual agents to achieve a goal in terms of the voltage control especially in the complex network. Therefore, MAS should be operated as a group of agents which can perform wide-area control through autonomous and cooperative actions of agents [2, p.36]. The architecture of MAS can be designed matching with the three-layers of the hierarchical distributed control structure in Section 3.2.2, where agents on different layers will communicate with each other for further interchanging their information.

3.3.5 Distribution state estimator engines

The state estimator engine, which is located in the control centre at the substation, is used to extend the observability of the network condition in real time. Although state estimation is still rarely applied to distribution systems, this tool tends to be indispensable for DNOs to monitor and manage the control operation of a distribution network with DG [2, Ch.11]. The state estimation process makes use of redundant actual measurements and pseudo-measurements (i.e. the approximate data of load consumption) to estimate the value of the network state variables, such as voltage level and voltage angle, with the respective uncertainty. However, there is less redundancy in the measurements in distribution systems, unlike in transmission networks, so the state estimation algorithm between them is different. Choices of state estimation algorithms are examined in [12]. It is found that the weighted least squares estimation (WLS) algorithm is suitable for distribution networks. Although the accuracy of estimation results is still quite poor at present, with the increase of installed smart meters in the future can improve the state estimation performance. The mathematical algorithm of state estimation in power system is explained in Appendix D.

The optimal location of actual measurements is also important. Presently, it is impossible to install measurement equipments to all buses in the network due to the cost issue, especially remote measurements that require a reliable transmission channel. Measurement data

plausibility checks should be made to avoid the incorrect information from the actual measurements. The possible measurement locations and sensing data may be as follows:

- Substation (local measurement): *V* at the bus bar, *P* and *Q* flow of each feeder branch and the transformer's tap position.
- DG (remote measurement): *V*, *P* and *Q*
- Power conditioning devices (remote measurement): *V* and *Q*
- Critical buses (remoter measurement): *V*

where *V* is voltage, *P* is active power and *Q* is reactive power. The local measurement means the sensing system is located in the same area with the control centre (i.e. the substation). On the other hand, the remote measurement means the sensing system is located somewhere else in the network apart from the substation.

The experience of applying distribution state estimation for the distribution network with DG in [13] found that a large number of load pseudo-measurements and satisfactory load models are key factors to the voltage estimate accuracy and convergence. Furthermore, adding of load forecasting techniques for assessing the correct pseudo-measurement can improve the accuracy of the results [14].

The distribution state estimator will be installed in the control centre at the substation, which can estimate the entire system from a wide area point of view. A high performance computer is required to process massive live-stream data from both actual and pseudo measurements with, possible short time estimation (i.e. in range of several minutes), to deal with real-time monitoring and control of the distribution network with DG. Moreover, the state estimator engine must be integrated with SCADA or a distribution management system (DMS) to provide automatic control capability. It can link to GIS system to display the network conditions for the DNO including voltage profile and LCZs. The approach of distribution state estimator in the central control centre is shown in Figure 3.7.

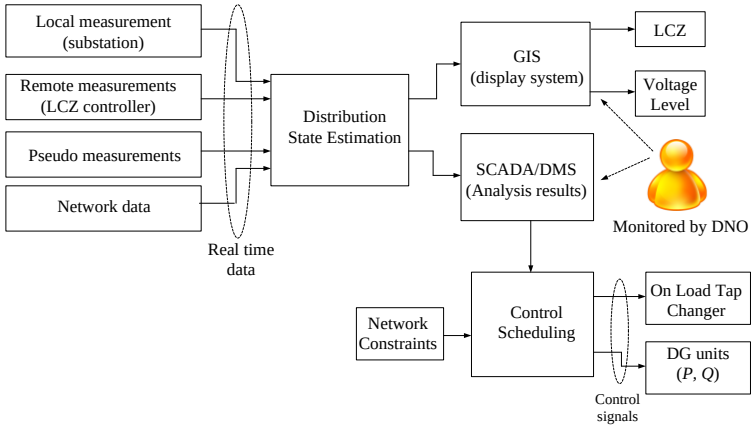

Figure 3.7. Distribution state estimator system in the central control centre.

3.4 Local control zone identification

The LCZs are defined based on the network configuration including number, size and location of DG. Many network partition techniques already proposed in power system applications, both transmission and distribution networks, will be reviewed in this section. In this work, the LCZ identification is determined from the ratios of voltage sensitivity across the network and the DG voltage control capability, which should be enough to handle the voltage changes of bus members inside the LCZ. The details of voltage sensitivity calculation and the methodology to define the LCZ are discussed. Furthermore, the adaptive zone identification is proposed to update the zone in real time according to changes in network conditions over time.

3.4.1 Review of network partition techniques in power systems

There is no unique solution for splitting a large power system in many smaller areas. Different techniques are suitable for different applications such as voltage control, stability and islanding.

The multi-level graph partitioning algorithm [15] is developed for power system islanding and network reconfiguration, with the aim to avoid blackouts in the network [16],[17]. The network is modelled as an edge-weighted graph, where the weight of an edge is the absolute value of the active power flow through the line. The multilevel partitioning scheme is operated in three stages which do not partition the original graph directly. The results are small areas, where each area has the power balance between load and generation.

Splitting strategies for large-scale power systems can be determined by using an ordered binary decision diagram (OBDD) method [18]. The graph theory and boolean algebra are applied in this method to search for the proper islanding areas whilst satisfying many constraints in each island. The islanding areas are searched based on OBDD which satisfy generation-load balance constraints. Moreover, the modified OBDD method [19] can provide short search time to find feasible splitting strategies in real time. In addition, a system is partitioned into several sub-networks, and the paralleling processing technique is applied to search the proper islanding areas in each sub-network at the same time.

The *V-Q* curve can be used for network partition in voltage stability assessments [20],[21]. The amount of aggregated reactive power support (i.e. reactive reserve basin) of each voltage control area is assessed. If the voltage change in the voltage control area is higher than the value of voltage support from the reactive reserve basin, a group of buses in that area will intend to meet the voltage collapse. The *V-Q* curve minima is defined to each zone where buses having similar *V-Q* curve minima can be grouped into the same area.

The electrical distance is often used for network partitioning in secondary voltage control [22],[23], and voltage security assessment [24]. It is the coupling degree of two nodes with regards to voltage and reactive power behaviour between them. The value of electrical distances of all buses is considered from transforming the sensitivity matrix (taken from power flow calculations). If the distance value between buses is small, this means that these two buses are high voltage correlated and the voltage change of one bus will affect directly the other bus. Therefore, a set of buses which have close electrical distances can be grouped together into a separate area. Several methods are proposed to defining a zone boundary from measuring the electrical distance, some of which are described as follow:

- The border of each zone can be classified by using a hierarchical classification algorithm [25]. The DG or compensation devices can be defined as the centre of each zone. The zone radius is introduced and any buses that have electrical distance between themselves and the centre bus within the range of the zone radius will be grouped into the same zone. The voltage response to the perturbation of various reactive power resources is also used to determine the zone boundary range [26].

- The network can be partitioned by using a hierarchical clustering algorithm [2, Ch.9]. This is a bottom up clustering method that treats each bus as an independent zone, and then merges the two nearest buses or zones at each step, by determining the electrical distance, until every bus is in a single zone. However, it does not

guarantee that each bus in the zone is directly connected to some other buses in terms of physical connection. The number of zones can be observed by using clustering indices (e.g. global silhouette index, Davis-Bouldin index, Dunn's index and C index) rather than the network operator's experience [27].

- In case of a large network partitioning, it is found that the *K*-mean clustering algorithm performs better than the hierarchical clustering algorithm, as demonstrated in [28]. It is a top-down approach which divides a complete network into *K* clusters and then adjusts those clusters based on some criteria. The initial *K* clusters are created randomly in the network and the centroid of each cluster is then defined. Each bus re-assigns itself to the nearest centroid based on the electrical distance, which will change the size of each cluster. Consequently, the centroids are relocated in every iteration process. The method iterates until the clusters are stable whilst the location of the centroid of each cluster remains unchanged.

- The genetic algorithm (GA) is also examined in [28], which can solve the non-connected clusters problem that occurs in hierarchical and *K*-mean clustering algorithms, particularly in case of large systems. The initial cluster centres are generated by selecting a set of random buses and then iteratively allowing each cluster centre to envelop neighbouring buses until all buses are included in exactly on cluster. Despite the clustering method being quite effective, it requires substantial computation resource and it is time consuming.

In this work, the LCZs are defined as smaller areas in the distribution network which receive voltage support mainly from DG. This means that only selected buses are grouped into the LCZ. Two key factors should be included into the zone identification, which are the network configuration and the available *P* and *Q* support from DG. The LCZs can be identified directly from the sensitivity matrix of the network which provides the voltage behaviour to a change of *P* or *Q* between two buses. The voltage response of all buses due to the support from each DG unit can be used to determine the zone boundary. The threshold voltage value can be used to define the group of buses associated to each zone.

3.4.2 Voltage sensitivities due to DG units

The ratios of voltage sensitivity among buses are different and depend on the resistance and reactance of the lines and the network topology [29]. In this work, the voltage sensitivity to a

change of either P or Q injection at a DG bus can be used to identify the LCZs. The sensitivity matrix can be determined from the Jacobian matrix, **J**, calculated from the Newton-Raphson power flow equation, as explained in Appendix B. It is found that the voltage magnitude and phase angle, which are V and δ, respectively, are state variables that change according to P and Q perturbations at a specific DG bus. The sensitivity matrix can be written as:

$$\mathbf{J}^{-1} = \begin{bmatrix} \partial\delta / \partial P & \partial\delta / \partial Q \\ \partial V / \partial P & \partial V / \partial Q \end{bmatrix} \tag{3.1}$$

The sub-sensitivity matrices $[\partial V/\partial P]$ and $[\partial V/\partial Q]$ represent the change in the bus's voltage magnitude to a change in P and Q injection at a DG bus, respectively. Each sub-matrix has $n \times n$ size, where n is the number of buses in the network. The voltage change in all buses due to a DG perturbation (ΔP_{DG} and ΔQ_{DG}) at bus m, can be estimated as follows:

$$\left[\Delta V_i\right] \approx \left[\partial V_i / \partial P_m\right] \cdot \Delta P_{DG,m} + \left[\partial V_i / \partial Q_m\right] \cdot \Delta Q_{DG,m} \tag{3.2}$$

where i is the bus number (1,2, …n). The size of ΔV_i, $[\partial V_i/\partial P_m]$ and $[\partial V_i/\partial Q_m]$ are $n \times 1$. n means the number of buses in the network, and m is the bus where the DG is connected. It was found that DG units can provide significant voltage support to buses with high sensitivities, while they have little impact on those with very small sensitivities.

3.4.3 Local zone identification methodology

Some clustering algorithms are proposed which aim to define the voltage controllable areas from the voltage sensitivity matrix, such as quality-threshold and voltage coupling index algorithms [30]. Those approaches determine the group of buses by comparing the voltage sensitivities or voltage coupling index (i.e. calculated from the voltage sensitivity matrix) with a threshold value. Therefore, the concept of network clustering by using threshold is adopted in this work to identify the buses associated with each LCZ.

As the main contribution to voltage support is achieved by controlling the Q output of the DG unit, the zone contains those buses where the Q injection from DG units has a high impact on the voltage profile. The Q support available in each DG unit, ΔQ_{DG}, is calculated from:

$$\Delta Q_{DG} = \begin{cases} |Q_{res}| - Q_{gen}, \text{ to increase voltage level} \\ |Q_{res}| + Q_{gen}, \text{ to reduce voltage level} \end{cases} \quad (3.3)$$

where Q_{res} is the available reserved Q in a DG unit (either at leading or lagging p.f.), and Q_{gen} is the reactive power being dispatched by the DG unit. The value of ΔQ_{DG} is not constant and depends on the network conditions over time. ΔQ_{DG} is used to find the change in the bus voltage according to (3.2). Furthermore, ΔQ_{DG} also depends on the voltage control (for both short- and long-term duration), which aim to increase the voltage level, in case of a voltage sag, or to reduce the voltage level, in case of a voltage swell.

The buses associated with each LCZ are determined using the *thresholding operation* (adopted from the fundamental theory of image processing [31]). In grey-scale image applications, the thresholding operation chooses some of the pixels (i.e. the samples of an original image) as the foreground to make up the objects of interest, and the rest as background. Certain grey tone values can be selected as threshold values to separate the grey-scale image into groups. In the simplest case, a single threshold value is chosen. All pixels whose gray tone values are greater than, or equal to the threshold values become foreground pixels.

The bus at which DG is connected is set as the *centre* of each zone. The threshold value of voltage change, ΔV_{th}, is defined to identify the buses on which the DG control has the highest impact, and therefore, should be grouped into the same zone. The value of ΔV_{th} is set by the system operator and it should be reasonable to allow proper dynamic voltage compensation within the zone with little voltage interaction with other buses external to the zone. From the voltage sensitivity results obtained from (3.2), the buses with a voltage change higher than the assumed threshold ($\Delta V > \Delta V_{th}$) are counted as members of the LCZ. The buses that are not included in any zone are assumed to receive little support from the DG units in case of voltage variations, and are not included in the control scheme. The following criteria are applied in case of any overlap between zones:

1) If there are a few buses belonging to more than one zone, they are associated to the closest zone according to the highest voltage change, ΔV.
2) In case that the overlapping area covers the DG bus of each zone, these zones are merged together. Therefore, some zones may contain more than one DG unit.

When there is lack of voltage support from DG units, the ungrouped buses excluded from the control scheme will have to rely on other forms of voltage compensation, such as static

compensators. However, if fast response is not required, the ungrouped buses may receive conventional voltage support from the substation's OLTC.

3.4.4 Real – time adaptive zone identification

Because network conditions change all the time, the LCZs are not fixed and can be identified autonomously in response to changes in network conditions. To this aim, it is assumed that live-stream monitoring data from PMUs and the central controller at the substation are available. A state estimator is then used to calculate consistent load flow results that fit real-time measurements and pseudo measurements (estimated data for load consumption), as explained in Section 3.3.5. The Jacobian matrix can be obtained from the load flow calculation process to update the sensitivity matrix, and the zone is identified following the algorithm introduced in the previous section. The flow chart diagram for the LCZ real-time identification process is shown in Figure 3.8.

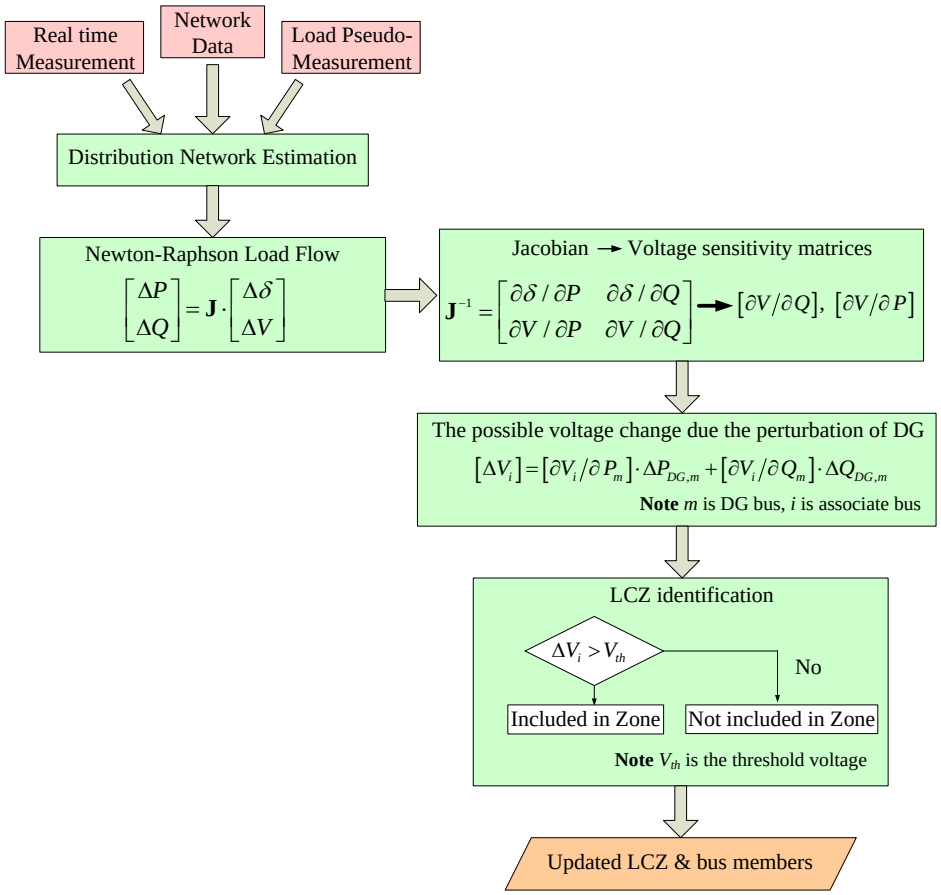

Figure 3.8. Flow chart of the real-time adaptive LCZ identification method.

The network state estimation cycle is up to 15 minutes depending on the speed of ICT to transmit and process data. New settings of Q_{gen} may be required in some DG units to meet the optimal voltage profile and address power losses. Therefore, the available Q, ΔQ_{DG}, may change in each cycle which can affect directly the size of an LCZ.

In case DG is using renewable resource (i.e. PV and wind turbine), the intermittent power generation from DG also causes the variation of its available Q support, as determined from (2.18). Hence, in this case, the state estimation cycle should be fast enough (i.e. in range of several minutes) to update network conditions and LCZs corresponding to the uncertain generation characteristics of this type of DG.

Due to the growing interest in distribution automation, the increase of online measurement and communication link expected in the near future provides the results from the state estimation more accuracy compared to presently available state estimator. In this research, however, it is assumed that load and DG profiles are known at every location. Hence, the state estimation of the network is not included and the sensitivity matrix is directly extracted from the load flow engine (in DIgSILENT *PowerFactory*).

3.5 Test system and base case study

The performance and value of the proposed zone identification approach are demonstrated under various operating scenarios. Only the steady-state conditions are examined in this chapter to show the idea of defining LCZs based on voltage sensitivity matrix and available Q support from DG.

The study is based on the IEEE 33-bus distribution system shown in Figure 3.9. The system data including line parameters and load connections can be found in Appendix K (Section K.1). The dashed lines are tie lines (normally open). For this study, two 1-MW DG units, working at unity p.f., are connected to the network. The total load is 3.75 MW and 2.30 MVar. The voltage at the substation is set to 1.01 p.u. It was initially found from load flow calculations that the connection of DG units at buses 11 and 29, produces minimum network losses and enhance the voltage profile, following the algorithm in [32]. Hence, this network condition is assumed as the base case for the simulation studies.

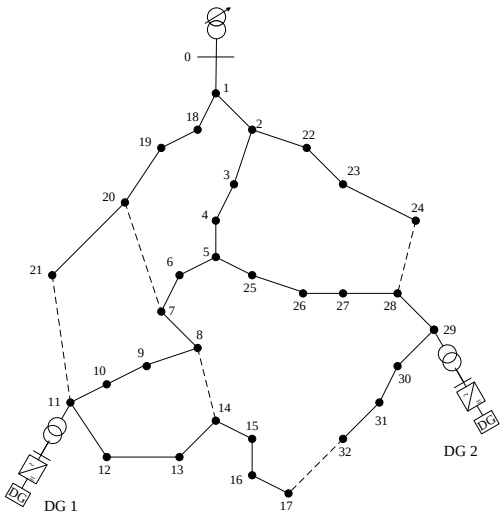

Figure 3.9. IEEE 33-bus radial distribution system.

The 2 DG units are assumed as converter-connected type and modelled by the grid-side VSC connected to a DC source. Each DG unit has a capacity $Q = \pm 1$ MVar (p.f. ≥ 0.707, leading and lagging), which means $Q_{res} = \pm 1$ MVar. Details of the control system of the DG units grid-side VSC are provided in Chapter 4.

If both DG units operate at unity p.f. ($Q_{gen} = 0$), from (3.3), the available Q is $\Delta Q_{DG} = 1$ MVar (either to increase or decrease the voltage level). From the voltage sensitivity matrix, $[\partial V/\partial Q]$, the change of bus voltage, ΔV, due to a Q perturbation (1 MVar) from both DG units at bus 11 and 29 is shown in Figure 3.10.

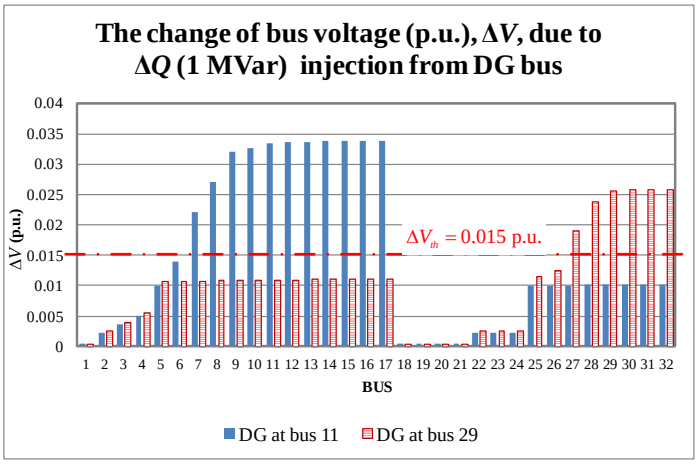

Figure 3.10. Change of bus voltage due to DG perturbations at buses 11 and 29.

It was found that DG units connected at buses 11 and 29 can provide a maximum voltage compensation of about ± 3.4% and ±2.6%, respectively. The voltage threshold, ΔV_{th}, defines

the minimum voltage support capability that a DG unit can provide to a bus in that zone. The ΔV_{th} should be high enough to minimise voltage interactions with other zones. For example, the ΔV_{th} is chosen as 0.015 p.u., because of the DG unit will, at least, be able to provide ±0.015 p.u. voltage support to all bus members in the zone with little interactions among two zones for this particular network condition. The DG can be set to start voltage compensation when the change of voltage at the DG bus is more than ± 1.5%. It is important to note that a disturbance inside the zone boundary affects directly the DG bus voltage, and there is no need for the communication system to sense signals from any other buses. The LCZs membership is shown in Table 3.1.

Table 3.1. Detail of LCZs for the base case

Zone	DG bus	DG priori	Bus members
1	11	1st at bus 11	7,8,9,10,11,12,13,14,15,16,17
2	29	1st at bus 29	27,28,29,30,31,32

The *V*-*Q* curves in Figure 3.11 show that the change of reactive power 1 MVar impacts the change of bus's voltage in LCZ#1 and LCZ#2 to higher than 0.015 p.u. (>ΔV_{th}), whereas the voltages of non-member buses (e.g. buses 6 and 26) can change less than the threshold value with the same amount of reactive power change. From these *V*-*Q* curves, it can be confirmed that the support of 1 MVar from DG unit to the bus member in the same LCZ should be sufficient to compensate the voltage level, at least 1.5%.

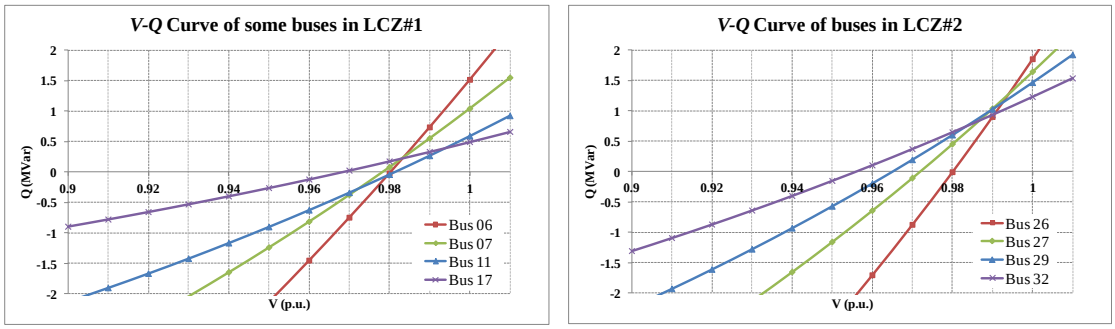

(a) *V*-*Q* curves of some buses in LCZ#1 (b) *V*-*Q* curves of some buses in LCZ#2

Figure 3.11. *V*-*Q* curves of specific buses in the test base case.

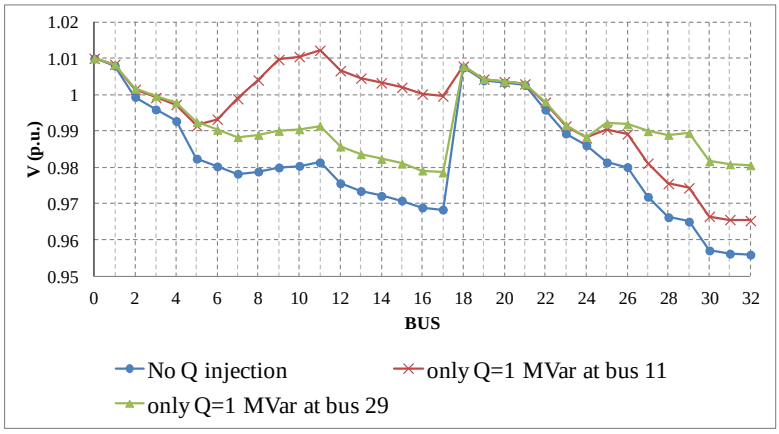

Figure 3.12. Voltage responses (steady-state) from the *Q* injection at buses 11 and 29 in the base case scenario.

From the load flow calculation, the voltage profile due to a change of *Q* injection at buses 11 and 29, (ΔQ_{DG} =1 MVar), is shown in Figure 3.12. It was found that the major voltage change occurs only in buses inside the zone. There is a very small voltage interaction between LCZs, less than 1.0 %, hence the zones can be assumed to be essentially decoupled, especially for short-term voltage control where the disturbance duration is very short.

3.6 Further simulations and results

The test system is also examined in three different scenarios, including the change of network operating points, network topology and the number of DG units, to demonstrate the adaptive zone identification method.

3.6.1 Case 1: change in network operating conditions

For this case, it is assumed that the network operates in heavy load conditions. The load connected to each bus increases 150 % compared to the base case, causing a decrease in the voltage level of the whole network as shown in Figure 3.13. It is found that the voltage level of bus 31 and 32, which are in LCZ#2, is nearly lower than 0.9 p.u.

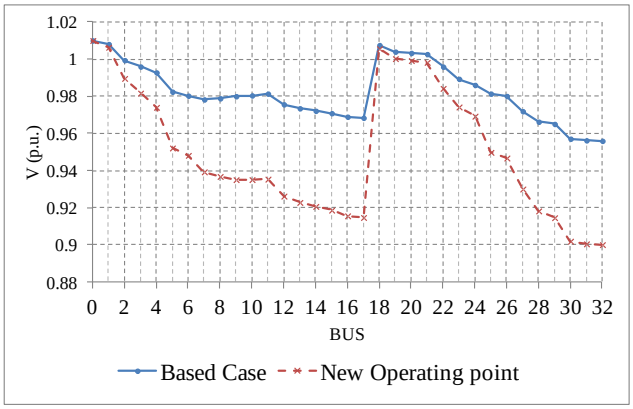

Figure 3.13. Voltage profiles of case 1 compared with the base case.

From the voltage sensitivity matrix, if both DG units still keep operating at unity p.f. (Q_{gen} = 0 and ΔQ_{DG} = 1 MVar), the response of bus voltage, ΔV, which can happen from Q support (1 MVar) of both DG units at bus 11 and 29 under the heavy load conditions is shown in **Error! Reference source not found.**. It is found that the voltage sensitivities are not much different between the two cases in LCZ#1. On the other hand, the load increase causes the voltage sensitivities to have a slight change in LCZ#2. Therefore, if ΔV_{th} = 0.015 p.u., it is found that the LCZs membership remains unchanged from the base case (see Table 3.1).

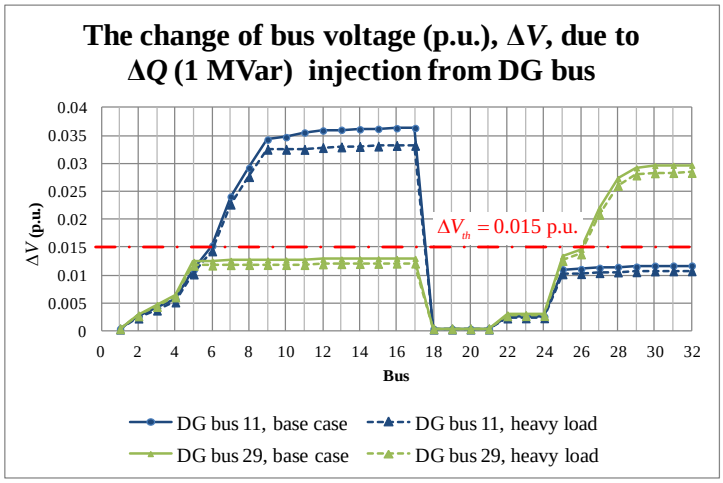

Figure 3.14. $\Delta V/\Delta Q$ sensitivity from DG at buses 11 and 29 of case 1 compared with the base case.

From Figure 3.13, it can be seen that the voltage drop under heavy load conditions is quite serious in some locations, especially at the end of the feeder in LCZ#2. Hence, the network operator can send the commands from the control centre at the substation to both DG units to adjust their reactive power outputs to support the voltage level of the whole network. In this case, it is assumed that each DG change its reactive power injections from 0 to 0.3 MVar

(Q_{gen}= 0.3 MVar and ΔQ_{DG} = 0.7 MVar). Additionally, in practice, the new set-point of each DG unit can be obtained from the optimisation analysis (i.e. satisfy voltage profile and minimum losses). The improvement of voltage profile due to the support of both DG units is shown in Figure 3.15, where it can be seen that the bus voltages in LCZ#1 and LCZ#2 increase approximately 1%.

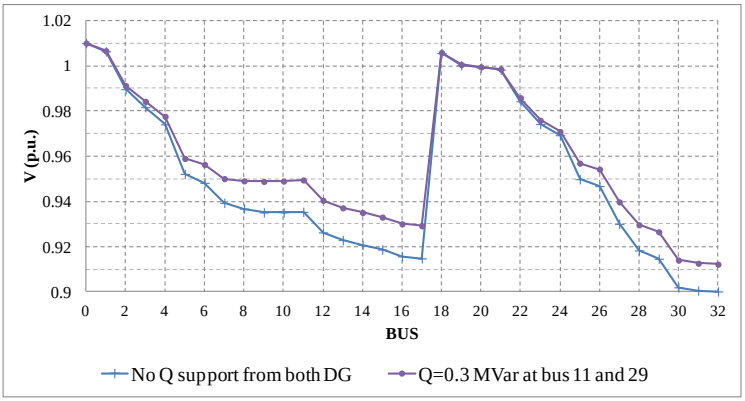

Figure 3.15. Voltage profiles under the heavy load condition with and without DG support.

The new operating point of each DG impacts to its available Q that can compensate other voltage disturbances, where ΔQ_{DG} reduces (in case to increase voltage level). The new LCZs have to be redefined following the new voltage sensitivities of the network during the heavy load condition and each DG unit has Q_{gen} = 0.3 MVar and ΔQ_{DG} = 0.7 MVar. Then, the update of voltage sensitivities corresponding to the 0.7 MVar injections from both DG units at bus 11 and 29 is illustrated in Figure 3.16. It can be seen that the level of voltage compensation, in each zone, is reduced due to the decrease of available Q support of each DG unit. Compared to Table 3.1, if ΔV_{th} = 0.015 p.u., it is found that the bus membership of LCZ#1 remains unchanged whereas the size of LCZ#2 becomes smaller compared to the case where the DG units operate at unity p.f., and bus 27 is not included in the zone. This means that bus 27 can receive the voltage support from DG2 less than 1.5%. The new LCZs membership is shown in Table 3.2.

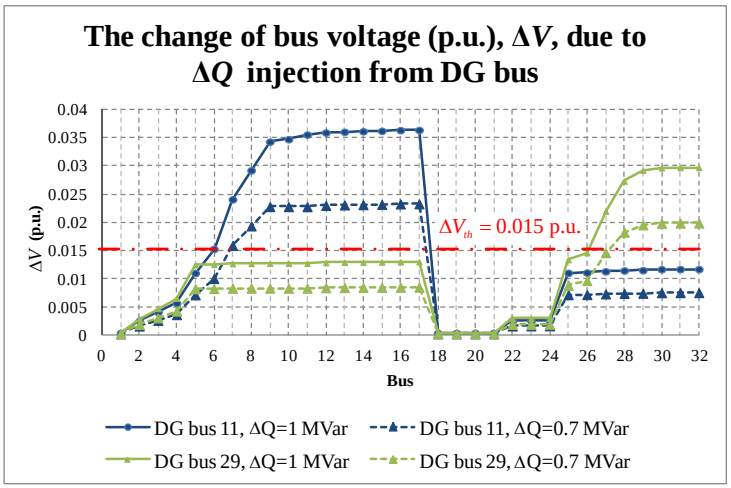

Figure 3.16. ΔV from injecting ΔQ from DG at buses 11 and 29 at new operating points compared with the case where DG units operate at unity p.f.

Table 3.2. New LCZs for the heavy load condition case with DG's new operating point.

Zone	DG bus	DG priori	Bus members
1	11	1st at bus 11	7,8,9,10,11,12,13,14,15,16,17
2	29	1st at bus 29	28,29,30,31,32

From the load flow calculation, the voltage profiles due to the change of Q injection from DG units, from 0.3 to 1 MVar (corresponding to ΔQ_{DG} =0.7 MVar), at buses 11 and 29, is shown in Figure 3.17. It is found that DG1 and DG2 can support voltage control in new LCZ#1 and LCZ#2, respectively, to more than the ΔV_{th} value at 1.5%, as can be seen in Figure 3.17(b). It can be seen that the new LCZ#2 does not include bus 27 because the voltage support from DG2 is less than the ΔV_{th} value.

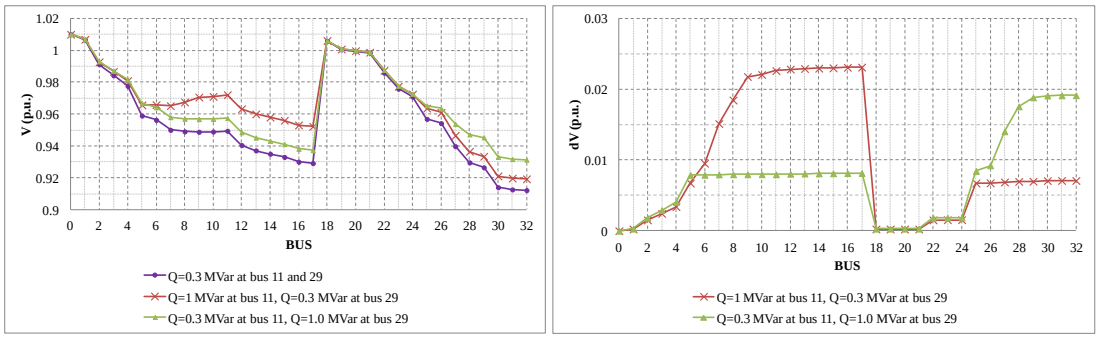

(a) Voltage Response Profile (b) Derivative Voltage Profile

Figure 3.17. Voltage response and derivative voltage profiles when each DG is operated under the new operating point (i.e. heavy load, Q_{gen} = 0.3 MVar and ΔQ_{DG} =0.7 MVar).

3.6.2 Case 2: change in network topology

The network in Figure 3.9 is changed from the original base case by disconnecting the line between buses 2 and 22, and connecting the tie-line between buses 24 and 28. The condition of the substation, DG units and load demand remains the same as that of the base case. The voltage profile and voltage sensitivity from the DG at buses 11 and 29, with Q_{gen}= 0 MVar, are illustrated in Figure 3.18 and Figure 3.19, respectively.

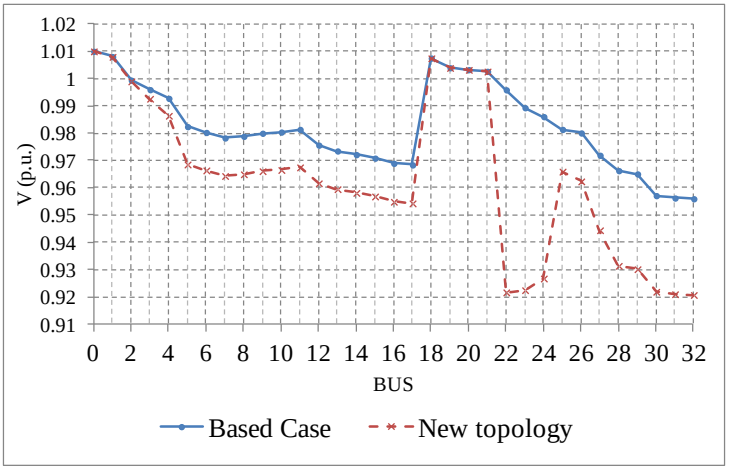

Figure 3.18. Voltage profile in case 2 compared with the base case.

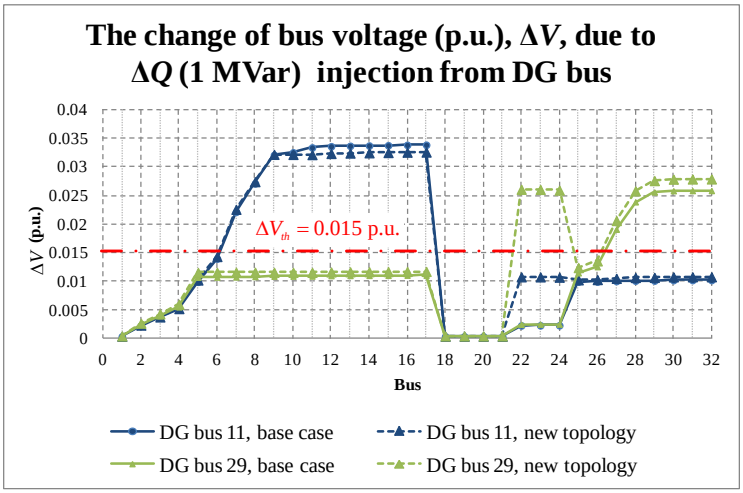

Figure 3.19. Δ*V*/Δ*Q* sensitivity (p.u./MVar) from DG at buses 11 and 29 compared with the base case.

The new network topology has different voltage sensitivities from the base case, especially for the LCZ#2 as the change occurs very near to DG2, rather than DG1. It was found that the *Q* injection from DG at bus 29 can support the voltage change at buses 22, 23 and 24 more

than in the base case. It is observed that, in this case, DG2 has the capability to exercise voltage control in more buses. Furthermore, the size of LCZ#2 needs to be adapted according to the change in voltage sensitivity. In the case that ΔV_{th} is defined as 1.5 %, the new bus members in each LCZ are shown in Figure 3.20.

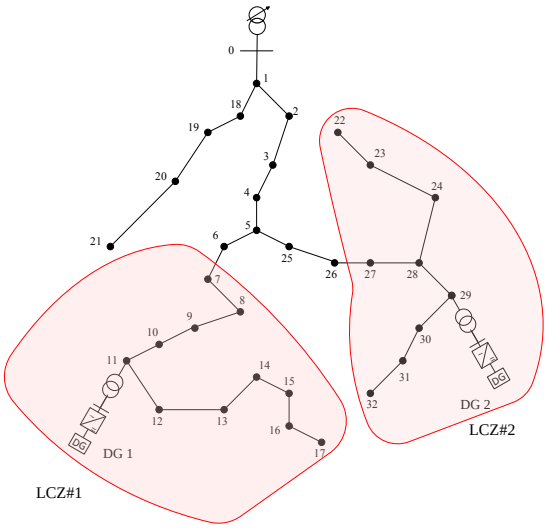

Figure 3.20. LCZs for the new network topology.

The influence of supplying ΔQ = 1 MVar from each DG unit on the voltage profile is shown in Figure 3.21. The change of voltage inside the zone is very high compared to that outside the zone. The voltage interaction between zones is small, less than 0.01 p.u., and hence could be ignored.

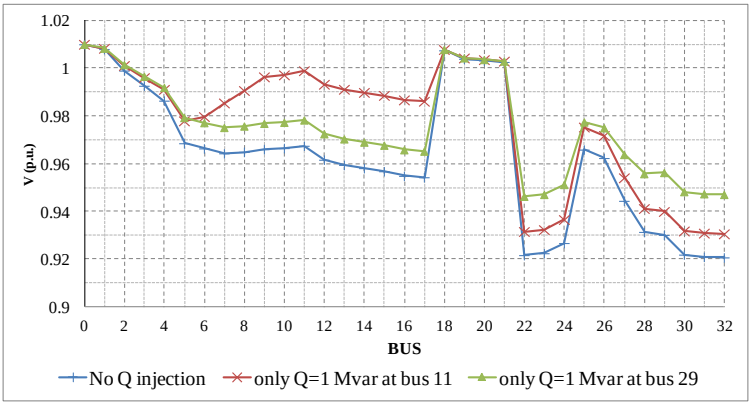

Figure 3.21. Voltage response (steady state) from the *Q* injection at buses 11 and 29 in the modified network topology case.

3.6.3 Case 3: Increase of DG Capacity

In this case, the network condition is the same as in the base case, and a new DG (DG3) is connected to bus 7, and supplies P= 1 MW at unity p.f. The Q reserve of this DG is ±0.5 MVar (p.f. ≥ 0.89, leading and lagging). As shown in Figure 3.22, an additional DG unit causes an increase in the voltage profile compared to the base case. The voltage sensitivities from the Q injection at each DG bus are shown in Figure 3.23, where the ΔQ of DG1 and DG2 is 1 MVar and the ΔQ of DG3 is 0.5 MVar. It was found that the voltage support from DG3 is about one third of DG1, because its available Q reserve is smaller. Therefore, DG3 can be grouped into LCZ#1, following the LCZs identification in Section 3.4.3, as indicated in Figure 3.24.

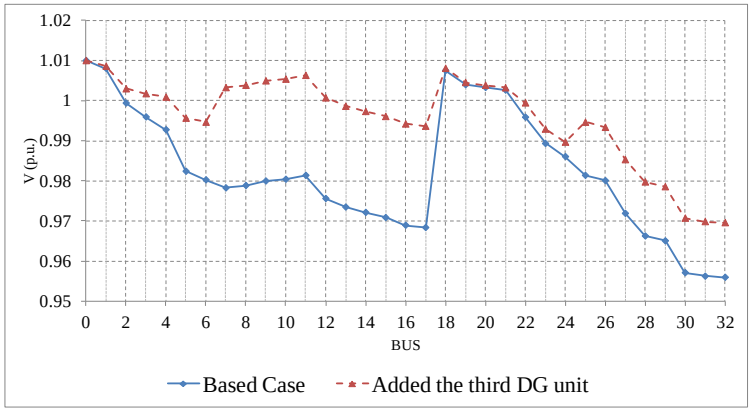

Figure 3.22. Voltage profile after adding new DG3 at bus 7.

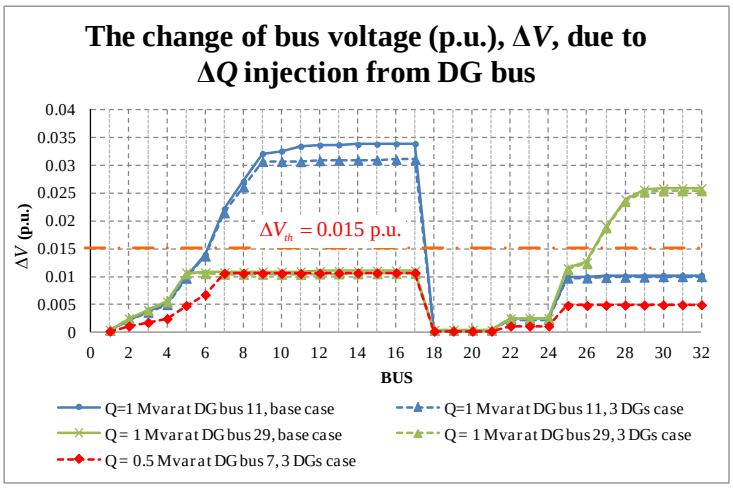

Figure 3.23. $\Delta V/\Delta Q$ sensitivities from DG at bus 11, 29 and 7 compared with the base case.

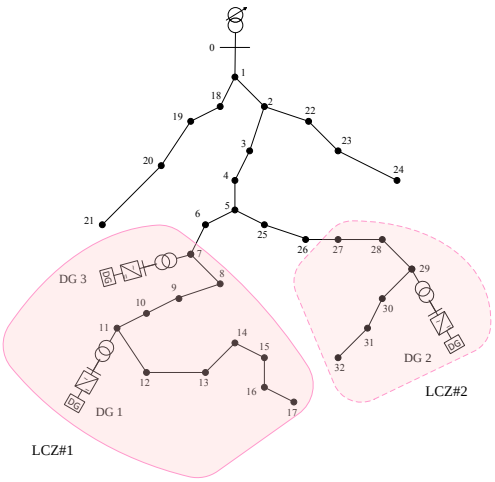

Figure 3.24. LCZs when 3 DG units are connected into the network.

The influence of supplying ΔQ = 1 MVar from DG1 and DG2, and ΔQ = 0.5 MVar from DG3, on the voltage profile is shown in Figure 3.25. The change of voltage inside LCZ#1 and LCZ#2 is very high compared to that outside the zone. In LCZ#1, the voltage support from DG1 has more impact on the bus members of LCZ#1 than the support due to DG3. Voltage interactions between DG1 and DG3 are observed, which can cause the hunting between the voltage controllers of these DG units. Hence, voltage oscillations may be introduced in the zone if the group of voltage controllers in the same zone, provide voltage compensation at the same time. The hunting between voltage controllers can be prevented by applying a coordinated controller or by adding a droop controller, as it will be discussed and demonstrated in Chapter 4.

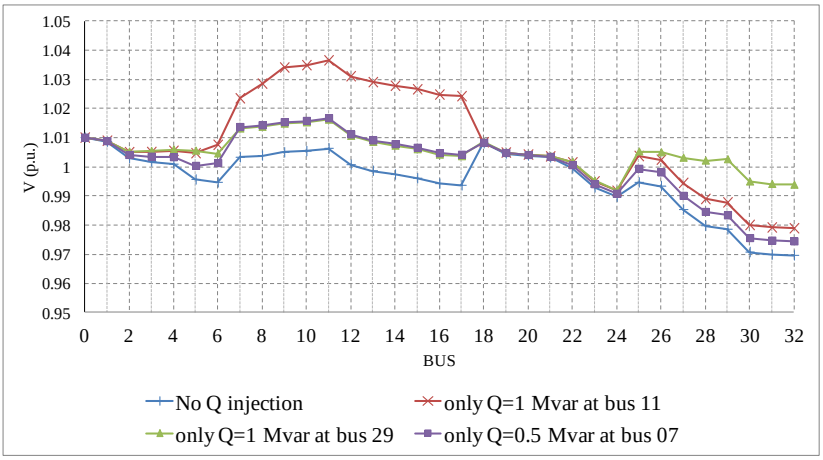

Figure 3.25. Voltage response (steady state) from the Q injection at buses 7, 11 and 29 in the case with increased DG penetration.

3.7 Conclusions

The chapter has shown that a hierarchical distributed voltage control structure can be applied to facilitate the autonomous integrated Volt-Var control in distribution networks with DG connection, especially the converter-connected DG type. The DG aims to provide the decentralised short-term voltage support, while the substation's OLTC provides a centralised voltage control to cover the long-term voltage regulation across the network. In addition, many advanced technologies are required to implement the voltage control structure and fulfil the automatic control ability, such as real-time monitoring, intelligent processing unit and communication system.

The case studies showed that the LCZs identification by assessing the voltage sensitivity and the available reactive power reserve of DG units maintains a certain level of voltage interaction between zones. However, this interaction was not significant and the zones operation and control remained very much independent of each other.

The LCZs can be adapted to follow changes in network operating conditions and topology. To achieve this adaptive feature, online measurements, a communication system and a state estimator are required to monitor the network condition in real time. Results from load flow and steady-state simulations demonstrated that the LCZs can be adapted to handle the change of network condition under different scenarios. The steady-state voltage variations can be controlled efficiently by using the decentralised voltage control, where distributed controllers such as the converter-connected DG can provide local voltage control in specific areas of the distribution network.

Looking ahead, the LCZs can enhance the network and DG visibility to the distribution management system. For example, the network operator can use historical information about changes in the LCZs for the purposes of planning and operating the active network in terms of voltage control and identification of the preferred locations for additional DG connections.

3.8 References

[1] A. Bayod-Rújula, "Future Development of the Electricity Systems with Distributed Generation," *Energy*, vol. 34, no. 3, pp. 377-383, 2009.

[2] M. Shahidehpour and Y. Wang, *Communication and Control in Electric Power Systems: Applications of Parallel and Distributed Processing*: Wiley-IEEE Press 2003. Chapter 9.

[3] D. Lei, P. Zhencun, C. Wei, and P. Jianye, "An Integrated Automatic Control System for Distributed Generation Hierarchical Islanding," in *Power System Technology, 2006. PowerCon 2006. International Conference on*, Chongqing, 2006, pp. 1-6.

[4] K. Kok, C. Warmer, R. Kamphuis, P. Mellstrand, and R. Gustavsson, "Distributed control in the electricity infrastructure," in *Future Power Systems, 2005 International Conference on*, Amsterdam, 2005, pp.1- 7.

[5] N. Perera and A. D. Rajapakse, "Agent-Based Protection Scheme for Distribution Networks with Distributed Generators," in *IEEE Power Engineering Society General Meeting, 2006.* Quebec, 2006, pp.1- 6

[6] T. Gonen, *Electric Power Distribution System Engineering*, 2nd ed.: CRC Press, 2007.

[7] P. Järventausta, S. Repo, A. Rautiainen, and J. Partanen, "Smart Grid Power System Control in Distributed Generation Environment," *Annual Reviews in Control*, vol. 34, no. 2, pp. 277-286, 2010.

[8] A. P. S. Meliopoulos, F. Zhang, and S. Zelingher, "Power System Harmonic State Estimation," *Power Delivery, IEEE Transactions on*, vol. 9, no. 3, pp. 1701–1709, 1994.

[9] G. O'Malley, J. Wu, and N. Jenkins, "Technical Requirements of Smart Electric Power Distribution Networks in the UK," in *45th International Universities Power Engineering Conference (UPEC)*, Cardiff, *2010*, pp. 1-6.

[10] S. D. J. Mcarthur et al., "Multi-Agent Systems for Power Engineering Applications — Part I: Concepts , Approaches , and Technical Challenges," *Power*, vol. 22, no. 4, pp. 1743-1752, 2007.

[11] S. D. J. Mcarthur et al., "Multi-Agent Systems for Power Engineering Applications — Part II: Technologies, Standards, and Tools for Building Multi-agent Systems," *Power*, vol. 22, no. 4, pp. 1753-1759, 2007.

[12] R. Singh, B. C. Pal, and R. A. Jabr, "Choice of Estimator for Distribution System State Estimation," *Generation, Transmission & Distribution, IET*, vol. 3, pp. 666-678, 2009.

[13] V. Thornley, N. Jenkins, and S. White, "State Estimation Applied to Active Distribution Networks with Minimal Measurements," in 15th *Power Systems Computation Conference (PSCC)*, Liege , 2005, pp. 1-7.

[14] F. Bignucolo, R. Caldon, and V. Prandoni, "Radial MV Networks Voltage Regulation with Distribution Management System Coordinated Controller," *Electric Power Systems Research*, vol. 78, pp. 634-645, 2008.

[15] G. Karypis and V. Kumar, "Multilevel K -way Partitioning Scheme for Irregular Graphs," *Journal of Parallel and Distributed Computing*, vol. 129, pp. 96-129, 1998.

[16] C.-gen Wang et al., "Power System Islanding Based on Multilevel Reduced Graph Partitioning Algorithm," *43rd International Universities Power Engineering Conference*, Padova, 2008, pp. 1-6.

[17] J. Li, "Power System Reconfiguration Based on Multilevel Graph Partitioning," *PowerTech, 2009 IEEE*, Bucharest, 2009, pp. 1-5.

[18] K. Sun and D. Zheng, "Splitting Strategies for Islanding Operation of Large-Scale Power Systems using OBDD-Based Methods," *Power Systems, IEEE Transactions*, vol. 18, no. 2, pp. 912-923, 2003.

[19] K. Sun and D. Zheng, "Searching for Feasible Splitting Strategies of Controlled System Islanding," *IEE Proceedings - Generation, Transmission and Distribution*, vol. 153, no. 1, 2006.

[20] R. A. Schlueter, "A Voltage Stability Security Assessment Method," *IEEE Transactions on Power Systems*, vol. 13, no. 4, pp. 1423-1438, 1998.

[21] M. K. Verma and S. C. Srivastava, "Approach to Determine Voltage Control Areas Considering Impact of Contingencies," *IEE Proceedings - Generation, Transmission and Distribution*, vol. 152, no. 3, pp. 1-9, 2005.

[22] P. Lagonotte, J. C. Sabonnadigre, J. Y. Leost, and J. P. Paul, "Structural Analysis of The Electrical System Application to Secondary Voltage Control in France," *Power Systems, IEEE Transactions*, vol. 4, no. 2, pp. 479-486, 1989.

[23] M. Shaaban, "Improved Regional Coordination of Generation Voltage Control," in *Power and Energy Conference, 2008. PECon 2008. IEEE 2nd International*, Johor Bahru, 2008, no. 8, pp. 175–179.

[24] H. Liu, A. Bose, and V. Venkatasubramanian, "A Fast Voltage Security Assessment Method using Adaptive Bounding," in *Power Industry Computer Applications, 1999. PICA'99. Proceedings of the 21st 1999 IEEE International Conference*, California, 1999, vol. 15, no. 3, pp. 325–330.

[25] J. Zhong, E. Nobile, and A. Bose, "Localized Reactive Power Markets using The Concept of Voltage Control Areas," *Power Systems, IEEE Transactions on*, vol. 19, no. 3, pp. 1555-1561, 2004.

[26] Z. Li, Y. Liu, and R. Liu, “Network Partition for Distributed Reactive Power Optimization in Power Systems,” *IEEE International Conference on Networking, Sensing and Control* (*ICNSC*), Hainan, 2008, pp. 6-9.

[27] L. Cai-hao and D. Xian-zhong, “A Clustering Validation Based Method for Zone Number Determination in Network Partitioning for Voltage Control,” *Universities Power Engineering Conference (UPEC)*, Bristol, 2004, pp. 727-731.

[28] S. Blumsack, P. Hines, and M. Patel, “Defining Power Network Zones from Measures of Electrical Distance,” *IEEE Power & Energy Society General Meeting*, Alberta, 2009, pp. 1-8.

[29] M. Kashem, “Distributed Generation as Voltage Support for Single Wire Earth Return Systems,” *Power Delivery, IEEE Transactions*, vol. 19, no. 3, pp. 1002-1011, 2004.

[30] K. Rogers, R. Klump, and H. Khurana, “Smart-Grid-Enabled Load and Distributed Generation as a Reactive Resource,” *Innovative Smart Grid Technologies (ISGT)*, Gothenburg, 2010, pp. 1-8.

[31] L. G. Shapiro and G. C. Stockman, *Computer Vision*, 1 ed.: Prentice Hall, 2001, pp. 97-99.

[32] A. Kazemi and M. Sadeghi, "Distributed Generation Allocation for Loss Reduction and Voltage Improvement," in *Asia-Pacific Power and Energy Engineering Conference, 2009. APPEEC 2009*. Wuhan, pp. 1- 6.

[33] J. Northcote-Green and R. Wilson, *Control and automation of electrical power distribution systems*, 1st ed. CRC Press, 2006. Chapter 7.

[34] J. Ekanayake, K. Liyanage, J. Wu, A. Yokoyama, and N. Jenkins, *Smart grid: technology and applications*, 1st ed. John Wiley & Sons, Ltd, 2012. Chapter 2.

Chapter 4

Dynamic Voltage Control in Distribution Networks using DG

4.1 Introduction

This chapter demonstrates the capabilities of DG to provide dynamic voltage support. Converter-connected DG technologies, such as large photovoltaic plants and small wind farms, are the preferred type of DG for this purpose due to the fast voltage controllability provided by the converter interface [1]. The voltage control provided by DG acts on the reactive power exchanged with the network using an integrated Volt-Var control loop to support either short-term or long term variations.

The converter interface is typically based on the voltage source converter, VSC, which uses IGBTs or GTOs. In this work, a closed-loop current control in the *dq* reference frame is used to control the *P* and *Q* output of the VSC. PWM is used to switch the VSC. A voltage control loop is added to the VSC controller to enhance the voltage support capabilities.

The dynamic performance of VSC-based DG is demonstrated via transient simulations. The case studies examine different voltage disturbance scenarios including short-term variations (e.g. voltage sag and swell), long-term variations (e.g. under and over voltages), voltage flicker and temporary voltage imbalance. After receiving support from DG, the voltages are measured and assessed following international standards such as the IEEE 1159-2009 and IEEE 61000-3-7. The voltage compensation provided by converter-connected DG is compared to that provided by DG based on synchronous machines and also to that provided by compensation devices such as the DSTATCOM.

A coordinated control based on time delay is proposed to reduce the voltage interactions among DG units. This technique allows DG units to provide voltage support in a sequential manner, one-by-one, according to their ranking order (based on their influence on the voltage level and their speed of response). Other proposed solution uses a *V-Q* droop controller, implemented and added to the main voltage controller of the DG unit, aiming to decrease the voltage oscillations among DG units when the disturbance is cleared.

4.2 Modelling of converter-connected DG and control System

The model of converter-connected DG interfaced with the AC grid is discussed in this section. The detail of the VSC control structure and the implementation of the voltage measurement/tracking system are explained.

4.2.1 VSC based DG Modelling

The converter-connected DG is modelled by considering a VSC connected to a DC circuit, as shown in Figure 4.1 (taken from [2]). The sinusoidal PWM technique has been used to create the sinusoidal output voltage waveform. The DC circuit is represented by a DC voltage source connected in parallel with a capacitor. The losses in the DC circuit are represented as a parallel resistance. The converter is interfaced with the AC network via a smoothing reactor and a step-up transformer. A shunt filter is also used to filter low-order harmonics in the output waveform.

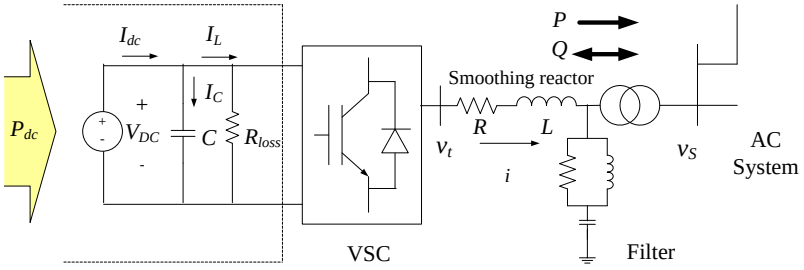

Figure 4.1. Simplified model of VSC-AC network [2].

From [2], the approximate AC terminal voltage, v_t, of the VSC can be calculated as

$$v_t(t) = m(t)\frac{V_{dc}(t)}{2} - v_d(t) + harmonics \qquad (4.1)$$

where m is the modulation index, which can be adjusted independently by the PWM control. v_d is the voltage drop to account for the switching losses.

The model of the DG grid-side converter is implemented in DIgSILENT *PowerFactory* for transient studies assuming balanced network conditions, where only positive sequence components are considered. The converter is modelled using an average model at fundamental frequency.

From equation (4.1), the line-to-line, rms voltage output of the VSC can be written as

$$\begin{aligned} v_{t,\alpha}(t) &= k_{\mathrm{o}} m_{\alpha}(t) V_{dc}(t) \\ v_{t,\beta}(t) &= k_{\mathrm{o}} m_{\beta}(t) V_{dc}(t) \end{aligned} \tag{4.2}$$

where $v_{t,\alpha}$ and $v_{t,\beta}$ are the real and imaginary part of the rms terminal voltage, respectively. Similarly, m_{α} and m_{β} are real and imaginary part of the modulation index, respectively. k_{o} is a constant factor that depends on the modulation method. k_{o} is $\sqrt{3}/\left(2\sqrt{2}\right)$ in case of the Sinusoidal PWM [3].

4.2.2 VSC-based DG control structure

The simplified control structure of the grid-side VSC is implemented as shown in Figure 4.2 (taken from [20]). Details of the power and current controls of the VSC can be found in Appendix E (Section E.2). The closed-loop control consists of two cascaded control loops. The outer control loop gives the current set-points to the inner *dq*-frame current control loop. The two current components, i_d and i_q, are controlled separately. The reference value of the *d*-axis current can be provided by the DC voltage or the *P* controller, whilst the reference value of the *q*-axis current is provided by the AC voltage or the *Q* controller, depending on the application. In both control loops the error signals are compensated using PI controllers. The cross coupling between *d*-axis and *q*-axis is neglected as they are considered as disturbances in the system. In this work, the *P* and *Q* controls are selected as the main application which aims to maintain the power generation from DG constant under normal conditions.

The voltages, u_d and u_q from the inner-current controllers are the input signals to the PWM generators, which are limited to ensure that PWM operates in its linear range. Those input voltages will be referred to the modulation index signals, m_d and m_q, in the *dq*-frame, which are converted to the *αβ*-frame and then to the real and imaginary voltages of the VSC calculated using (4.2). Thus, the *dq* voltages of the VSC can be transformed into three-phase voltages by transforming from *αβ*-frame to *abc*-frame. The frequency of the AC system is obtained by using a phase-locked-loop (PLL) for the transformation between *dq*-and *αβ*-frame. The transformations between *αβ*-and *abc*-frame, and between *dq*-and *αβ*-frame are explained in Appendix E (Section E.1).

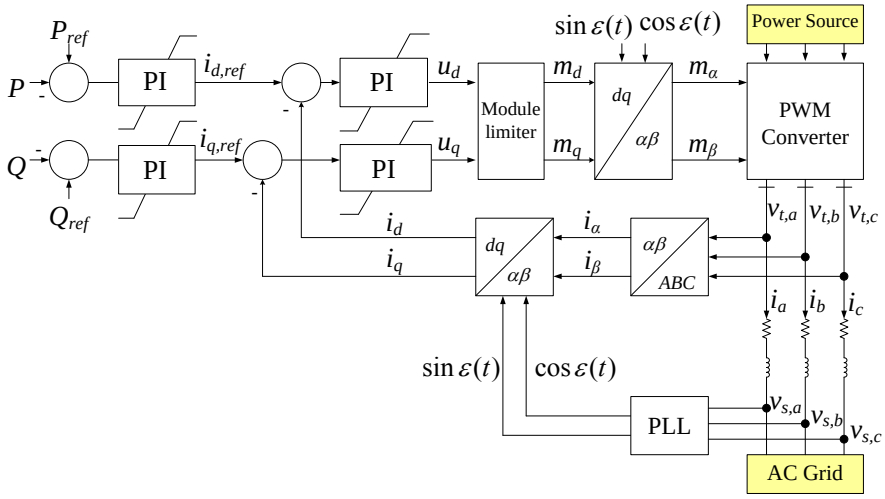

Figure 4.2. Grid-side VSC-based DG control structure [20].

4.2.3 VSC-based DG control system with additional voltage controller

To use converter-connected DG to support the AC voltage control, the grid-side VSC is designed to operate in two modes: *PQ* control and *PV* control. In *PQ* mode, the DG will maintain *P* and *Q* constant while the network is in normal conditions. The *P* and *Q* control in Figure 4.2 is used as the main control structure. The value Q_{ref} can be changed to the updated value of *Q* being dispatched by the DG unit, Q_{gen}. In this mode, modest voltage variations have a minor effect on the management of the DG unit.

On the other hand, in the *PV* mode, the DG units provide active voltage control by adjusting their *Q* output. The voltage controller is added as an optional outer control loop of the *Q* controller, which can be connected or disconnected from the main controller depending on the level of the feedback voltage signal. VSC-based DG can enter the *PV* mode automatically when the level of voltage change is greater than the dead-band value, V_{DB}, or when it is out of the statutory limit. The PI controller with limiter function is used as the compensator. The limiter function is used to limit the amount of *Q* support from DG to avoid overloading the VSC. The control structure of the *PV* mode and the rule base to switch the controller between *PQ* to *PV* mode are shown in Figure 4.3. In this work a constant DC voltage source is assumed, hence there is no need to implement a DC voltage control loop.

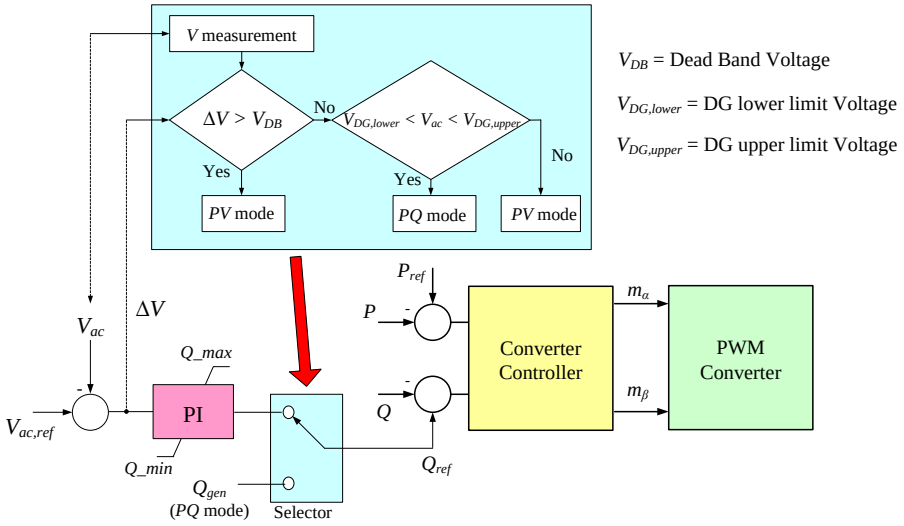

Figure 4.3. Control structure of *PQ* and *PV* modes.

4.2.4 Voltage measurements and tracking System

From the AC voltage controller in Figure 4.3 (see detail in Appendix E (Section E.2.3)), the feedback voltage, V_{ac}, is sent back from the AC grid to the AC voltage controller via the voltage measurement device [4]. The magnitude of the feedback voltage is compared with the AC voltage reference. The reference value is adaptable according to the changes in network conditions over time. Therefore, the tracking system is developed to update the new reference value.

Under balanced conditions, the magnitude of the feedback voltage (rms) is calculated from the real and imaginary parts of the positive sequence voltage at the PCC, given by

$$V_{ac}(t) = \sqrt{\left(v_{s,\alpha}(t)\right)^2 + \left(v_{s,\beta}(t)\right)^2} \tag{4.3}$$

where $v_{s,\alpha}$ and $v_{s,\beta}$ are the real and imaginary parts of the rms voltage at the PCC, respectively.

In case of unbalanced conditions, the magnitude of the feedback voltage (rms) is calculated as follow:

$$V_{ac}(t) = abs\left\{\frac{1}{3}\left[v_{s,a}(t) + \left(-\frac{1}{2} + j\frac{\sqrt{3}}{2}\right)v_{s,b}(t) + \left(-\frac{1}{2} - j\frac{\sqrt{3}}{2}\right)v_{s,c}(t)\right]\right\} \tag{4.4}$$

where $v_{s,a}$, $v_{s,b}$ and $v_{s,c}$ are the phase-to-ground voltages, in p.u.

Real-time voltage measurements are required to deal with dynamic changes in the network. Furthermore, the voltage reference, $V_{ac,ref}$, needs to be updated according to changes in network conditions. The time period for updating the voltage reference, $T_{DG,ref}$, should be small enough (less than a second is desirable) to ensure that short-term voltage variations can be captured. The voltage reference value will remain constant as the previous updated value when the AC voltage controller detects that the voltage change, ΔV, is higher than the V_{DB}. On the other hand, the voltage reference changes to the upper or lower limit when the voltage level is out of the upper or lower limit (i.e. $V_{DG,lower}$ and $V_{DG,upper}$), respectively, in order to keep the long-term voltage variation within the statutory limit. The voltage tracking system is implemented as shown in Figure 4.4. The flowchart of the tracking system to update the value of voltage reference in every cycle is shown in Figure 4.5.

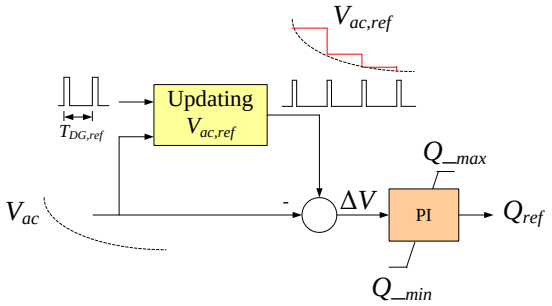

Figure 4.4. Voltage tracking system in the AC voltage controller.

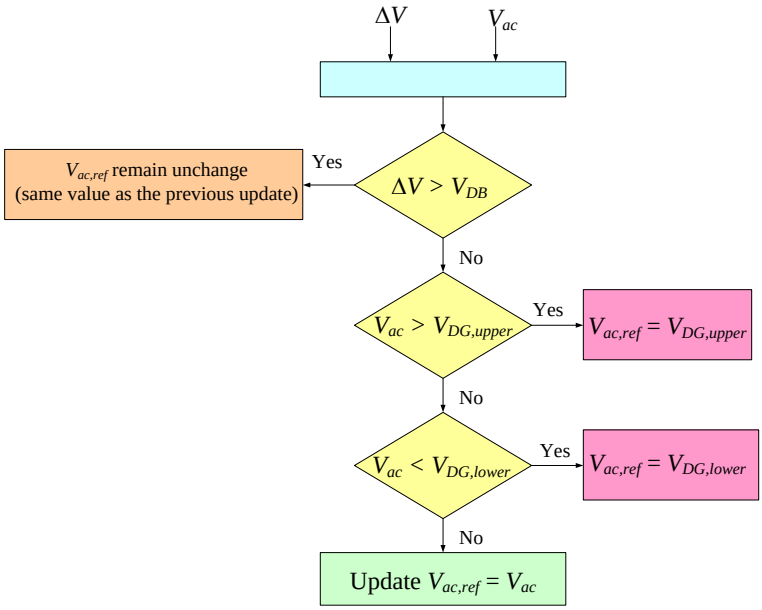

Figure 4.5. Flow chart of the tracking system to update the voltage reference.

4.3 Dynamic voltage support from a single converter-connected DG

In this section, the dynamic performance of voltage support from converter-connected DG and the proposed LCZ are examined under difference scenarios. The case study assumes a single VSC-based DG interfaced with the MV network. Short- and long-term voltage variations are investigated. Moreover, the experience of using DG as the remote voltage controller to support voltage control at a specific bus is presented.

4.3.1 Test system

The test system is the IEEE 33-bus distribution network described in Section 3.5. A 1-MW converter-connected DG is connected at bus 11, as shown in Figure 4.6. It has a capacity Q = ± 1 MVar (p.f. ≥ 0.707, leading and lagging), which means Q_{res}= ± 1 MVar. The DG unit is assumed to operate at unity p.f. at the initial condition. The network demand is the same as in Section 3.5, whilst the secondary voltage at the substation (bus 0) is set to 1.045 p.u. to have a 1.0 p.u. voltage at the DG bus.

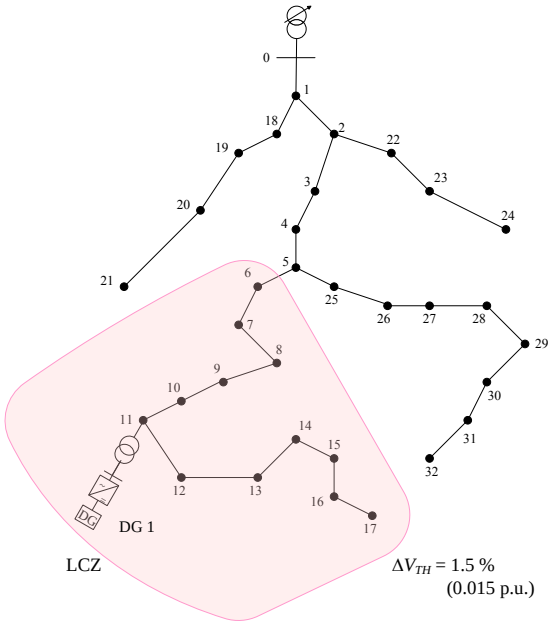

Figure 4.6. The test system for studying the dynamic of converter-connected DG.

The voltage profiles across the network for voltage sag and swell studies are illustrated in Figure 4.7(a). From the voltage sensitivity matrix, the change of bus voltage, ΔV, due to a Q perturbation (1 MVar) from both DG units at bus 11 is shown in Figure 4.7(b). Moreover,

the LCZ is defined by using the zone identification algorithm in Section 3.4.3. In case that the threshold voltage, ΔV_{th}, is 1.5 p.u., the group of bus members that belong to the LCZ are defined as the area indicated in Figure 4.6.

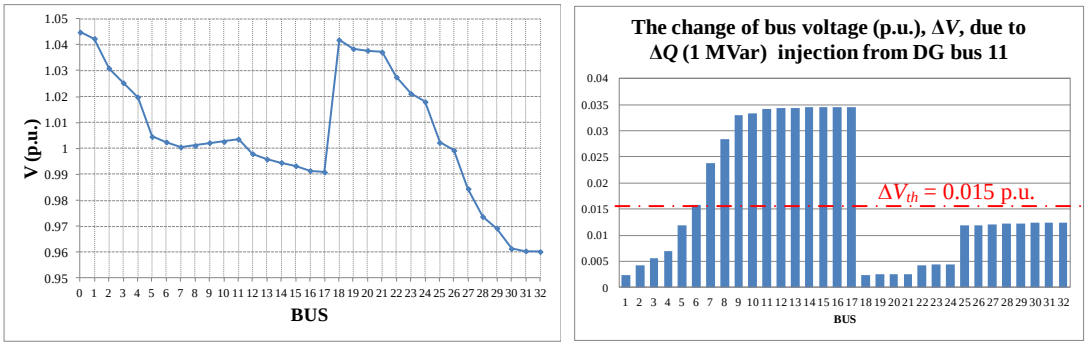

(a) Voltage Profiles

(b) change of bus voltage due to DG perturbations at buses 11

Figure 4.7. Voltage profiles and the change of bus voltage due to DG perturbations at bus 11.

The PI controller gains can be selected using root-locus or Ziegler and Nichols tuning methods [5]. These tuning methods are typically used in the initial design stage, and later a fine tuning is conducted to obtain the final settings (typically done by trial and error). The details of the VSC parameters including the PI controllers' gains and the stability test of DG controllers are given in Appendix E (Section E.3).

4.3.2 Short-term Voltage Control

The dynamic behaviour from the voltage support of converter-connected DG during short duration variations is demonstrated in this section. Four different scenarios are examined including voltage sag, voltage swell, voltage flicker and temporary voltage imbalance.

4.3.2.1 Voltage sag and swell

The dynamics of voltage support operation by DG is examined in the event of voltage sags and swells. The dynamic performance of the critical buses in the LCZ including DG buses and the bus at the end of the feeder is demonstrated. The V_{DB} of converter-connected DG is set to 0.015 p.u. to start the voltage control when the level of voltage change is greater than 1.5%. In case of the voltage sag, it is simulated via a three-phase short circuit through a high impedance at bus 13 (see detail in Appendix L, Section L.1), starting at t=0.5 sec and

finishing at *t*=2 sec. The results show the comparison between the variation of the bus voltage for the DG operating in *PQ* mode and *PV* mode. Buses 11, 13 and 17 which are DG bus, disturbance bus and the bus at the end of the feeder, respectively, are shown in Figure 4.8(a). The *P* and *Q* delivered by the DG unit are shown in Figure 4.8(b).

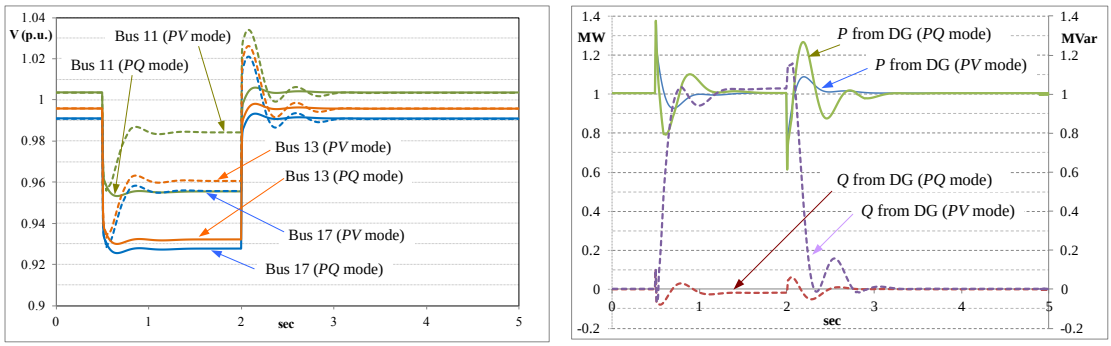

(a) Bus voltage

(b) *P* and *Q* from DG units

Figure 4.8. Key results for the voltage sag simulations.

It was found that when DG operates in *PV* mode, the voltage in LCZ#1 buses increases by about 3% which is nearly the value from the voltage sensitivity calculation in Figure 4.7(b), bringing the voltage level at buses 11, 13 and 17 back within the statutory limit (i.e. ±0.05 p.u. from the nominal voltage). Additionally, the level of actual voltage compensation to those buses is lower than the calculation from the voltage sensitivity because the drop of *Q* between buses needs to be accounted for. The VSC control shows a fast response supplying *Q* to the network in approximately 1 sec (which is fast enough to correct instantaneous and longer-duration variations). The change of *Q* output also interacts with the *P* output because these two values are coupled in the VSC controller, as discussed in Section 4.2.3. Although the DG in *PV* mode provides the benefit of rising up the voltage during the voltage sag, it introduces voltage spikes after the disturbance is cleared because some *Q* is still being supplied by DG. These spikes occur due to the little delay time in the voltage controller. However, the *Q* supplied by the DG will reduce rapidly by the fast control action, allowing the voltage across the zone to recover its nominal value within approximately 1 sec.

The voltage swell is modelled by injecting additional power into the network at bus 13 (see detail in Appendix L, Section L.2), starting at *t*=0.5 sec and finishing at *t*=2 sec. The voltage response in the network is evaluated under the same conditions used for the voltage sag, the results are shown in Figure 4.9(a). The *P* and *Q* delivered by the DG units are shown in Figure 4.9(b).

It is found that the disturbance causes a significant voltage swell in the LCZ where voltage at buses 11, 13 and 17 rises above the statutory limit (i.e. 1.05 p.u.). When operating in *PV* mode, DG absorbs *Q*= -1 MVar. The results show that the voltage level in the LCZ is reduced by about 3.3%. The VSC controller response is again fast (within 1 sec). Some negative spikes can be observed after the disturbance clearance, which are due to the delay response of the DG controller to switch from *PV* mode to *PQ* mode. However, it can be seen that the DG units recover rapidly their original operating condition, allowing the voltage across the zone to return back to the nominal level, in less than 1 sec.

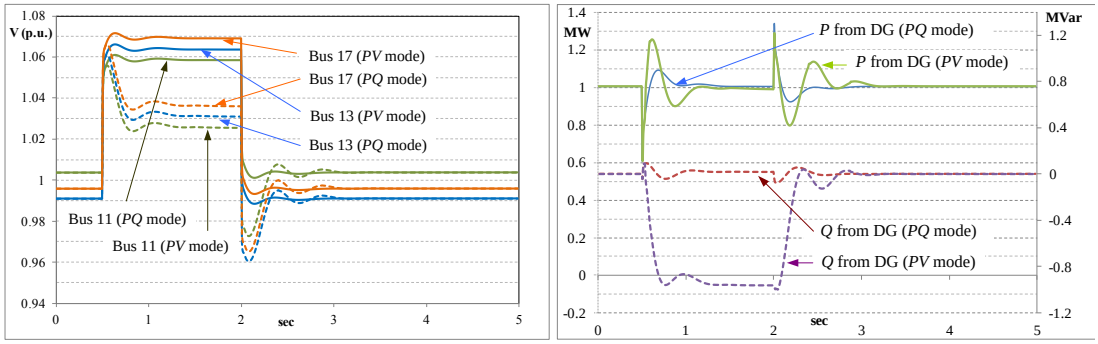

(a) Bus voltage (b) *P* and *Q* from DG units

Figure 4.9. Key results for the voltage swell simulations.

The comparison of voltage control responses between converter-connected DG and conventional synchronous machine-based DG is shown in Figure 4.10, for the voltage sag scenario. The synchronous generator aims to supply 1 MW with ± 1 MVar, equal to the converter-connected DG, which means over sizing is required. Unlike the VSC-based DG, the power factor of the synchronous generator is limited to about 0.8-0.9 due to stability issues. In this case, a 2-MVA and 0.87 p.f. steam turbine generator is used. The IEEE TGOV1 and the IEEE type AC1 excitation system are used as the turbine governor and the AVR, respectively (see details in Appendix F).

From Figure 4.10(a), it is found that the voltage control response from the synchronous generator-based DG is slightly slower than the VSC-based DG which depends on the electromagnetic mechanism and the type of excitation system. The inertia of the generator and the governor control cause oscillations in the voltage and active power during the disturbance and after the voltage support has finished. The swing of *P* in case of using the synchronous generator-based DG is greater than the VSC-based DG, as can be seen in Figure 4.10(b). The capacity of *Q* supplied from the synchronous machine-based DG is limited by the stability limit of the machine especially on the stator winding. Furthermore, the possible

Q support from synchronous machine-based DG is lower than the VSC-based DG, as can be seen in Figure 4.10(c). This can happen because of the limitation in the stability of the machine especially on the field and armature windings (see Section 2.5.1). The change of frequency is relatively small for both two cases because the level of voltage drop is not high and the DG unit remains connected to the grid during the disturbance.

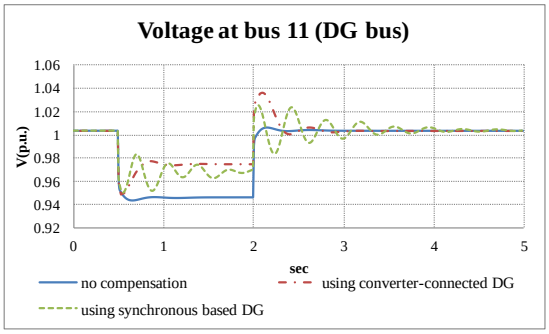

(a) Voltage at DG bus

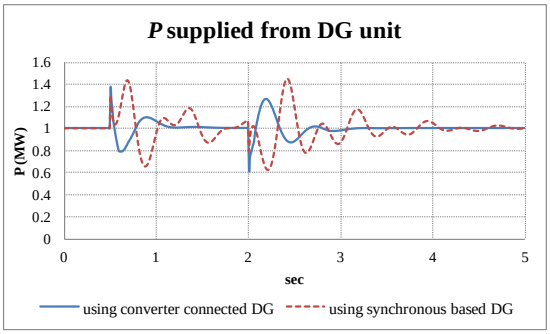

(b) Active power from DG unit

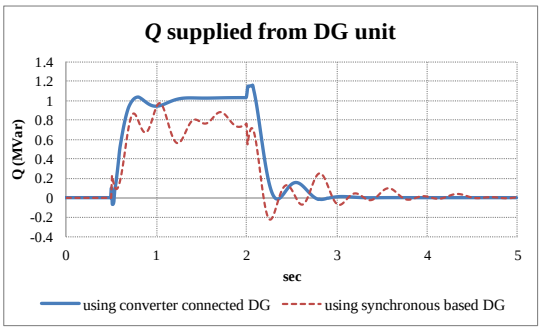

(c) Reactive power from DG unit

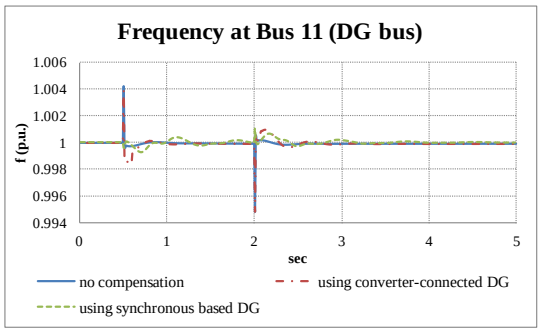

(d) Frequency based on 50 Hz

Figure 4.10. Comparisons of voltage control responses between converter-connected DG and synchronous machine-based DG.

It can be seen that converter-connected DG can provide a better performance in terms of voltage support compared to the synchronous generator-based DG. Therefore, the converter-connected DG should be the preferable type of DG to support the decentralised voltage control in distributed networks.

4.3.2.2 Voltage flicker

Voltage flicker in distribution networks can be generated by intermittent DG sources, such as fixed-speed wind turbines, or industrial loads such as arc furnaces. It can be reduced by installing power conditioning devices such as DSTATCOM. However, this solution is costly

and increases the harmonics injection [6]. Alternatively, converter-connected DG can also provide fast active voltage control as that of dedicated compensation devices, reducing thus network complexity and costs.

Distributed automation control and management based on flicker disturbance mitigation is used across controllable devices, mainly converter-connected DG, to decrease the level of voltage fluctuations. In addition, to maintaining the voltage level at the PCC, assumed as "*local bus*", each converter-connected DG unit aims to provide support to *'remote buses*' where the flicker source may be located especially in the same LCZ with the converter-connected DG, as shown in Figure 4.11.

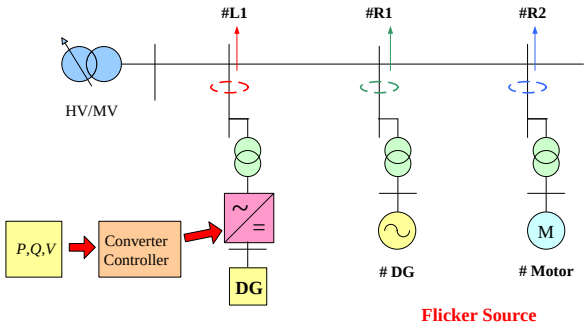

Figure 4.11. Voltage flicker mitigation using converter-connected DG.

The level of flicker is typically measured by using a flickermeter, as presented in terms of the flicker indices, P_{st} and P_{lt}. The standard IEC 61000-4-1 provides the functional and design specifications of a flickermeter [7]. Additionally, P_{st} is a short-term flicker index measured over a period of 10 minutes, and P_{lt} is a long-term index corresponding to a period of 2 hours. Further details of the IEC flickermeter are provided in Appendix G.

The IEC 61000-3-7 standard indicates the compatibility levels for flicker in LV and MV systems as $P_{st} \leq 1$ and $P_{lt} \leq 0.8$, respectively. In this work, only P_{st} is considered. The normalised flickermeter response (P_{st}=1) versus frequency, and the shape of the flicker are shown in Figure 4.12 (taken from [8]).

From the test system in Section 4.3.1, it is assumed that the flicker source is a fixed-speed wind generator connected at bus 7. The value of V_{DB} of converter-connected DG at bus 11 should be small enough to support small voltage variations. If ΔV_{th} is defined as 0.005 p.u. (meaning that the injection of Q from a DG unit can mitigate a 0.5% voltage, at least), the

LCZ can be identified from the voltage sensitivities in Figure 4.7(a) with the result shown in Figure 4.13 (see the area indicated on the diagram). It is found that the size of the LCZ is bigger compared with the previous case, as the amount of voltage support required is smaller (i.e. reducing from at least 1.5% to 0.5%). Moreover, the results in Section 4.3.2.1 showed that the voltage control response of this VSC-based DG is approximately 1 sec, so only low-frequency flicker (≤ 1 Hz) can be mitigated by this solution.

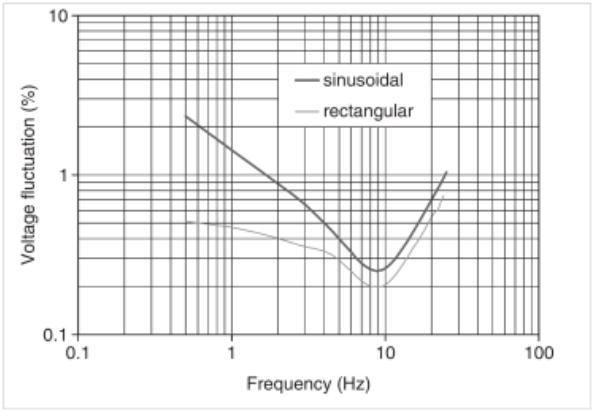

Figure 4.12. Normalised flickermeter response for voltage variation.

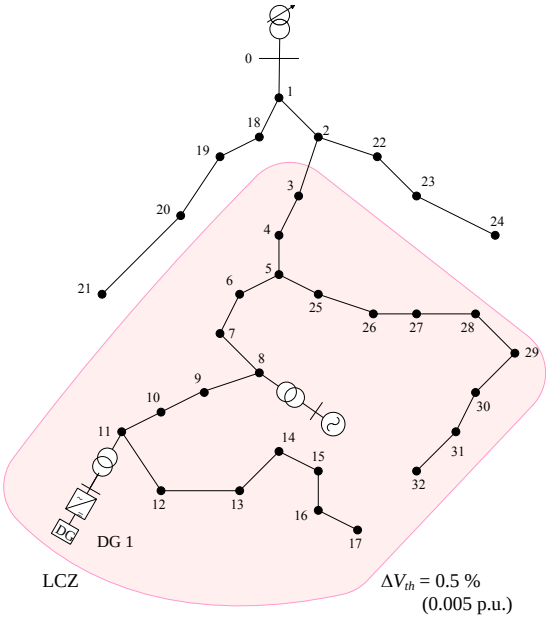

Figure 4.13. Test system for the flicker mitigation study with new LCZ identification.

The flicker voltage is generated from the fluctuation of the DG power output at bus 8. The flicker is assumed to be sinusoidal, with a ±1.0 % voltage variation and frequency of 1 Hz. However, from Figure 4.12, the IEC statutory limit for a 1-Hz sinusoidal flicker is 1.432% [7]. The *V*-*Q* curves of buses 8 and 11 in Figure 4.14 show that the voltage change of ±1 %

at bus 8 can be mitigated by compensating Q around ±0.4 MVar, so the Q capacity of DG (i.e. ±1.0 MVar) is sufficient to mitigate the voltage flicker at bus 8. From Figure 4.7(b) and Figure 4.14, it is found that the values of voltage change due to a change of Q =1 MVar, determined by the voltage sensitivities and V-Q curves between buses 8 and 11 are very similar. Moreover, the V_{DB} of converter-connected DG is set to 0.005 p.u. to support voltage control when the level of voltage change is higher than 0.5%. Two scenarios are presented and discussed to demonstrate the performance of the proposed controller:

Base Case: no compensation from using neither converter-connected DG nor DSTATCOM

Case 1: using converter-connected DG to control flicker at its local bus (bus 11)

Case 2: using only a DSTATCOM (1.0 MVar) at the flicker source bus (bus 8)

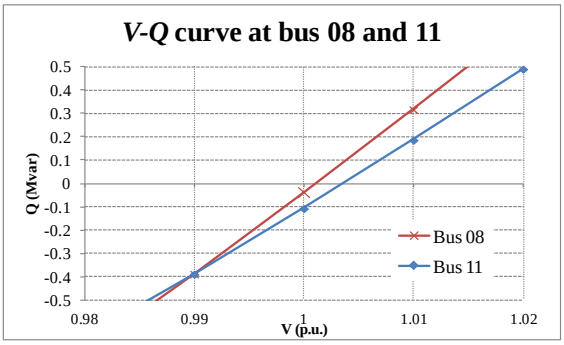

Figure 4.14. V-Q curve at bus 8 and bus 11.

The case study is conducted using rms transient simulations in DIgSILENT *PowerFactory*. The voltage flicker waveforms at buses 8, 11, 24 and 30, for the two scenarios, are shown in Figure 4.15. The Q supplied by the converter-connected DG and the DSTATCOM are shown in Figure 4.16. The P_{st} of 10 minute-flicker waveform is used for flicker assessment. This value is calculated using the IEC flicker measurement simulator (sampling rate 2 kHz), called FlickerSim [9], based on MATLAB software. In addition, the rms voltage flickers, which are simulation results, are converted into sinusoidal voltage flicker waveforms before being used as input of the flickermeter. The P_{st} of essential buses in different scenarios is presented in Table 4.1, for the two scenarios under study.

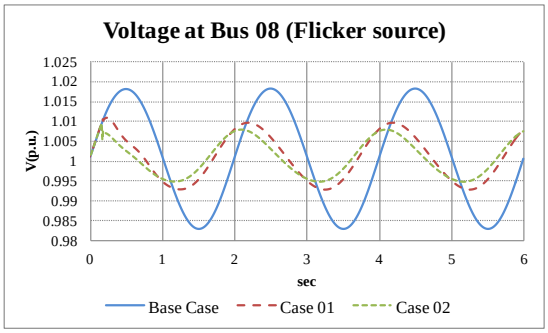

(a) Voltage at bus 8

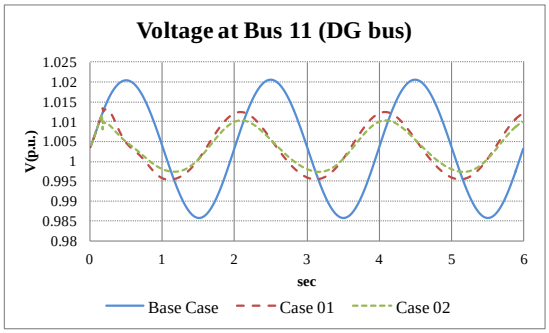

(b) Voltage at bus 11

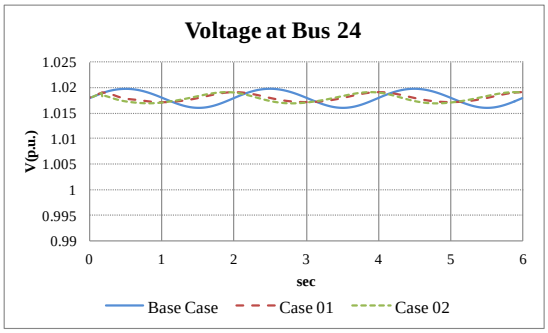

(c) Voltage at bus 24

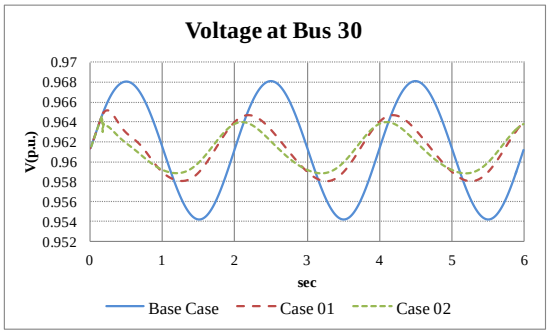

(c) Voltage at bus 30

Figure 4.15. Voltage flicker waveforms in different scenarios

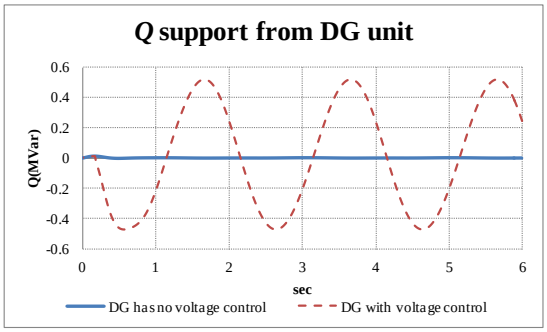

(a) *Q* supported from DG unit

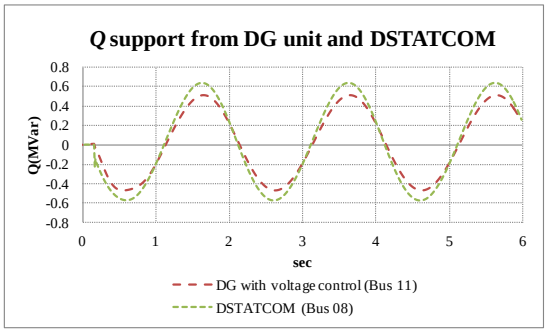

(b) *Q* supported from DSTATCOM

Figure 4.16. *Q* supplied from DG unit and DSTATCOM

Table 4.1. Short-term flicker index, P_{st}, for the three scenarios.

Bus	P_{st} (Short term flicker index)		
	No compensation	case 1: using DG at bus 11	case 2: using DSTATCOM at bus 8
8	1.0504	0.5138	0.4008
11	1.0369	0.5026	0.3954
17	1.0369	0.5026	0.3954
24	0.1143	0.0609	0.0670
30	0.4309	0.2145	0.1674

The results show that the DSTATCOM provides the finest voltage flicker mitigation (e.g. P_{st} is reduced from 1.0504 to 0.4008 at the flicker source bus 8. If the converter-connected DG operating with p.f. $\geq$ 0.707 (leading and lagging) located in the same zone is used to mitigate the flicker, the P_{st} at bus 8 can be reduced by 0.5366 (i.e. about 50%). It is found that both methods can mitigate the flicker level to below the IEC statutory limit (P_{st} = 1).

It was also found that flicker mitigation in buses outside the zone, such as bus 24, is not significant. By way of example, the P_{st} of bus 17, located inside the LCZ, can be mitigated by about 0.5-0.6. On the other hand, the P_{st} of bus 24, which is outside the zone can only be reduced by about 0.05. This is because the voltage sensitivity between the buses outside the zone and the flicker source is small. Furthermore, Figure 4.16, shows that the *PV* mode control effectively allows the DG unit to provide *Q* compensation and dynamic voltage control. The amount of *Q* support from DG is similar to the case using a DSTATCOM.

4.3.2.3 Voltage imbalance

Converter-connected DG can be used to compensate short-time voltage imbalance in the network. Transient voltage imbalances can appear under disturbance conditions especially an unsymmetrical short circuit. The intermittency of single-phase renewable generators in the LV network can cause transient voltage imbalances when they are not connected symmetrically in three phases.

Several techniques are proposed for using VSC-based DG under the transient voltage imbalance condition. Three parallel voltage controllers have been applied, where each voltage controller is used to control the voltage level of individual phases [10]. Negative sequence components should be included in the control system for voltage imbalance compensation. The idea of implementing the controller in positive synchronous reference frame with feed-forward of negative voltage is introduced in [11]. Then, the VSC controller sees the negative sequence voltage as a disturbance. Alternatively, the compensation technique based on the symmetrical component decomposition method is proposed in [10], which tries to neglect the negative sequence by creating the inverse negative sequence in the controller. The dual vector controller is developed in [12],[13], which uses two parallel controllers, one for each sequence, and the reference for the negative sequence controller is set to zero. From the reviews, it is found that the additional controller and the negative sequence measurement are required.

In this work, the imbalance voltage can be detected by DG voltage measurement at the PCC. From (4.13), the magnitude of the voltage output from voltage measurements will change according to the level of voltage imbalance. The VSC controller is still based on the positive sequence component, which means that the main controller remains unchanged, so the negative sequence components are not controlled directly by this controller. Note that this method aims to demonstrate that VSC-based DG can address the light-to-moderate voltage imbalances, and possibly provide some support to improve the voltage during unsymmetrical short circuits. Three scenarios are examined in this section including;

1) Single line-to-ground fault (phase A)
2) Double line-to-ground fault (phase A and B)
3) Line-to-line fault (phase A and B)

To examine the dynamic performance in case of an imbalanced disturbance, the initial conditions for the simulations are taken from Section 4.3.1. The case studies assume an imbalanced disturbance at bus 13, starting at t=0.5 sec and finishing at t=2 sec. The V_{DB} of converter-connected DG is set to 0.015 p.u (1.5 %). The results show the comparison between the variation of three-phase voltages from the DG operating in *PQ* mode and *PV* mode. Buses 11 and 13, which are DG bus and disturbance bus, respectively, are shown in Figure 4.17. The *P* and *Q* delivered from the DG unit are shown in Figure 4.18. Moreover, Figure 4.19 shows the positive and negative sequence voltage of the DG voltage controller, where the positive sequence voltage is the voltage measured at the PCC. The line-to-line voltage levels at buses 11 and 13, and the values of positive and negative sequence voltage which are the comparison with and without voltage support from DG unit, during a disturbance has occurred, are summarised in Table 4.2 and Table 4.3, respectively.

It is found that the DG will provide voltage support when the level of voltage imbalance causes the change of positive sequence voltage (absolute value) at the PCC to be greater than the voltage dead-band (V_{DB}=1.5%), as can be seen in Figure 4.19. All three transient imbalanced scenarios cause the feedback voltage (positive sequence voltage) to be lower than the reference voltage, so positive *Q* support will be required to recover the voltage level back to the desired range. The VSC in this work cannot mitigate the level of negative sequence voltage because the DG voltage controller is designed based on the positive sequence components only. Furthermore, three-phase reactive power is supplied from DG equally (see Figure 4.18). All three-phase voltages have to receive the voltage support from DG, although in some phases it is not necessary. Consequently, the voltage compensation by this DG introduces a voltage rise in some phases compared with the case without the voltage

support, as shown in Figure 4.17. For example, voltages in phase B and C increase when the DG provides voltage support in case of the single line-to-ground fault.

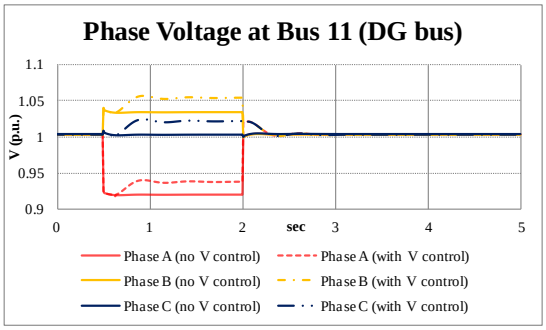

(a) Single line-to-ground fault (Bus 11)

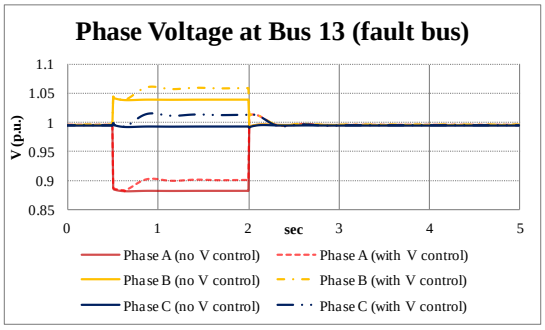

(b) Single line-to-ground fault (Bus 13)

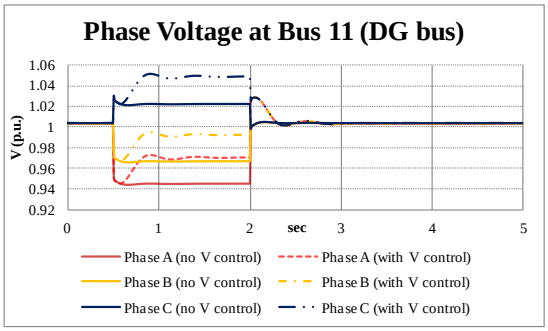

(c) Double line-to-ground fault (Bus 11)

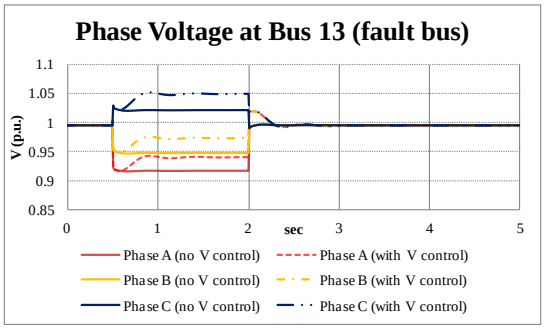

(d) Double line-to-ground fault (Bus 13)

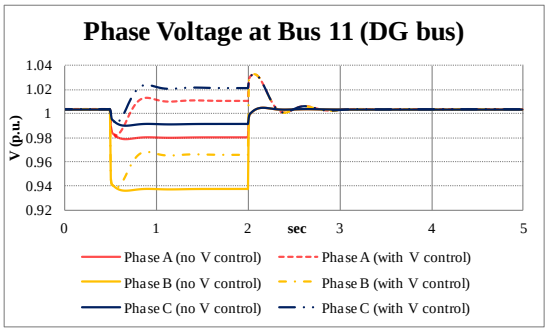

(e) Line-to-line fault (Bus 11)

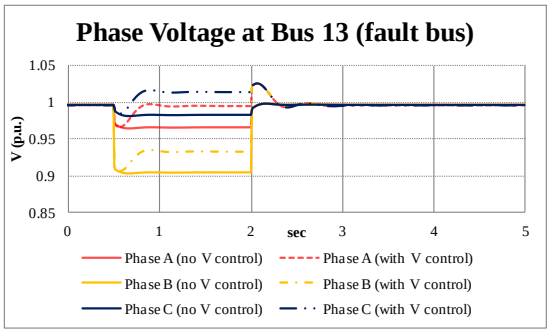

(f) Line-to-line fault (Bus 13)

Figure 4.17. Three-phase voltages at buses 11and 13 in difference scenarios.

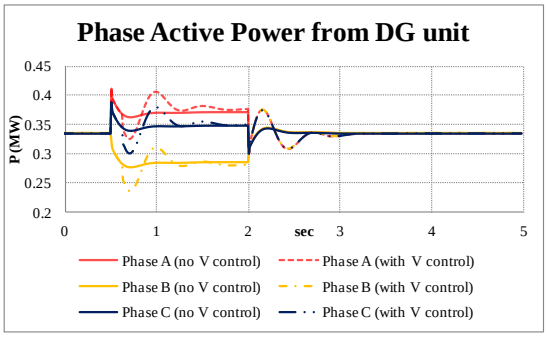

(a) *P* from DG (Single line-to-ground fault)

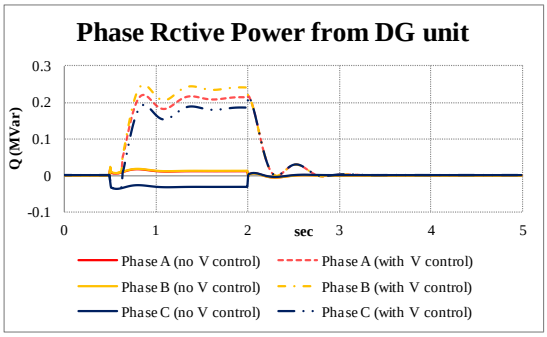

(b) *Q* from DG (Single line-to-ground fault)

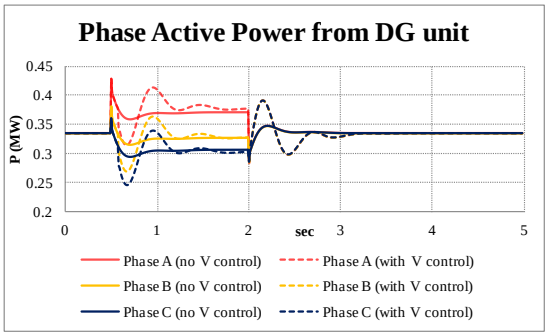

(c) *P* from DG (Double line-to-ground fault)

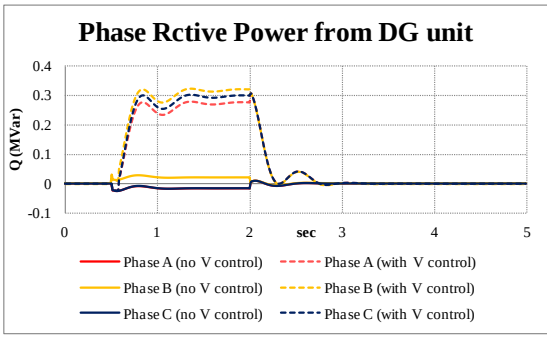

(d) *Q* from DG (Double line-to-ground fault)

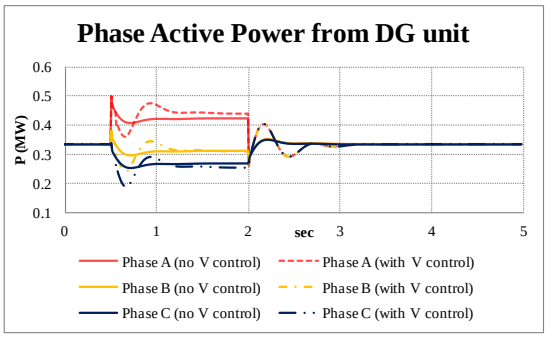

(e) *P* from DG (Line-to-line fault)

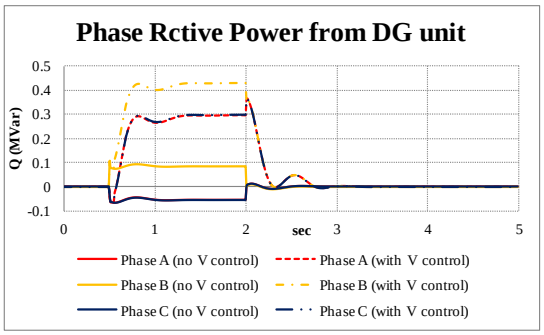

(f) *Q* from DG (Line-to-line fault)

Figure 4.18. Three-phase *P* and *Q* delivered from DG unit.

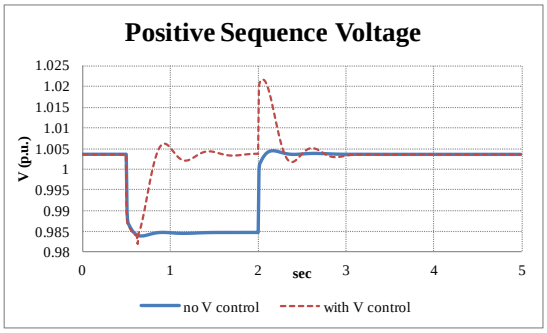

(a) Positive sequence voltage (Single line-to-ground fault)

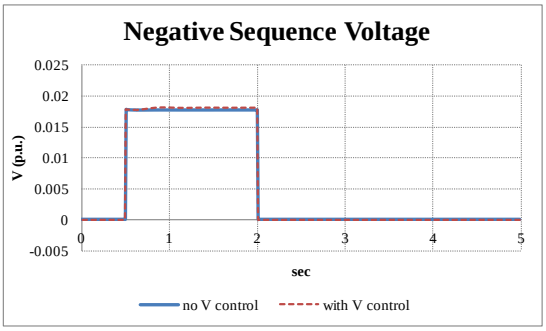

(b) Negative sequence voltage (Single line-to-ground fault)

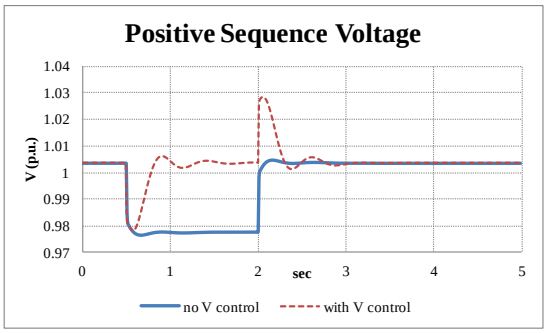

(c) Positive sequence voltage (Double line-to-ground fault)

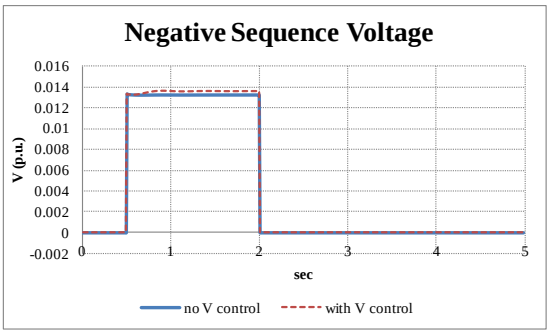

(d) Negative sequence voltage (Double line-to-ground fault)

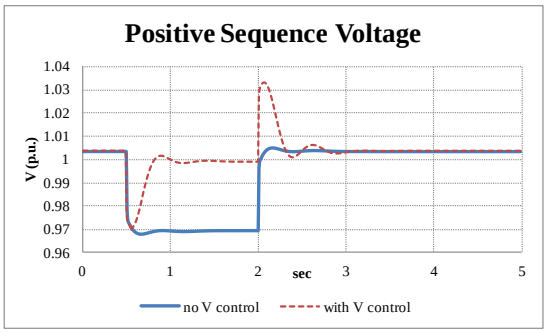

(e) Positive sequence voltage (Line-to-line fault)

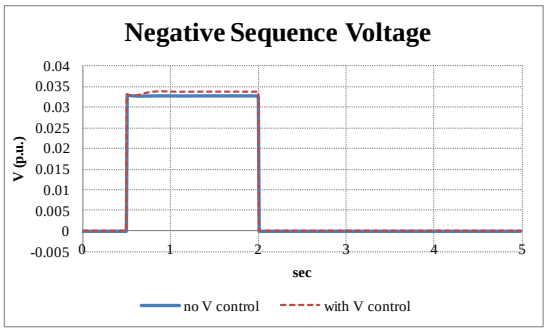

(f) Negative sequence voltage (Line-to-line fault)

Figure 4.19. Positive and negative sequence voltage of the DG voltage controller.

From the summary of voltage levels during a disturbance in Table 4.2 and Table 4.3, the level of imbalance can be assessed by using equations (2.4) and (2.5) in Section 2.2.3. The percent of imbalance at bus 11, calculated by using the information of line-to-line voltages and the absolute values of positive and negative sequence voltage, are shown in Table 4.4. It is found that the level of voltage imbalance decreases slightly after receiving voltage support from the DG unit. The voltage imbalance is improved well in case of the line-to-line fault. The main impact is from the improvement of the positive sequence voltage whilst the negative sequence voltage remains unchanged. The imbalanced voltage compensation can be

better if the voltage controller can control the level of negative sequence voltage to zero. However, the voltage controller will become more complex.

Table 4.2. Line-to-line voltage (p.u.) at buses 11 and 13 during the disturbance.

Disturbance	phase	Voltage (p.u.) at Bus 11		Voltage (p.u.) at Bus 13	
		no voltage control	with voltage control	no voltage control	with voltage control
Single line-to-ground fault	A-B	0.967	0.986	0.946	0.965
	B-C	0.990	1.010	0.978	0.997
	C-A	0.997	1.016	0.989	1.009
Double line-to-ground fault	A-B	0.970	0.996	0.949	0.975
	B-C	0.973	0.999	0.956	0.981
	C-A	0.991	1.017	0.980	1.007
Line-to-line fault	A-B	0.948	0.997	0.919	0.947
	B-C	0.959	0.989	0.938	0.967
	C-A	1.001	1.032	0.997	1.027

Table 4.3. Positive and negative sequence voltage (p.u.) during the disturbance.

Disturbance	Sequence	no voltage control	with voltage control
Single line-to-ground fault	positive	0.985	1.004
	negative	0.018	0.018
Double line-to-ground fault	positive	0.978	1.004
	negative	0.013	0.014
Line-to-line fault	positive	0.969	0.999
	negative	0.033	0.034

Table 4.4. Percent of imbalance comparing with and without DG voltage support.

Disturbance	Using line-to-line voltages, (2.5)		Using positive and negative sequence voltages (2.4)	
	% Imbalance at Bus 11		% Imbalance at Bus 11	
	no voltage control	with voltage control	no voltage control	with voltage control
Single line-to-ground fault	1.44	1.43	1.83	1.79
Double line-to-ground fault	1.06	1.03	1.33	1.29
Line-to-line fault	2.64	2.08	3.41	3.30

4.3.3 Long-term voltage control

Long-term voltage changes are typically due to gradual changes in network demand. Heavy load consumption causes a voltage drop, whilst light load consumption causes a voltage rise. The change of voltage may take time several minutes to being outside the allowed limits. The DG will provide voltage support when the voltage level at the DG bus is approaching the statutory limits (i.e. 0.95 p.u. and 1.05 p.u.). From Figure 4.3, the DG is changed from

PQ to *PV* mode when the voltage level reaches its lower or upper limits which are $V_{DG,lower}$ and $V_{DG,upper}$, respectively. The safety margin gap between DG's voltage limits and network's statutory limits ($V_{stat,lower}$ and $V_{stat,upper}$) is defined to ensure that voltage is controlled sufficiently before it goes out of the statutory limits. The voltage reference ($V_{ac,ref}$) of the DG voltage controller is updated according to changes in network conditions using the tracking system introduced in Section 4.2.7. The voltage reference will remain at the DG upper or lower limit when the voltage level is outside the DG's voltage limits (see Figure 4.5).

The test system and the initial conditions in Section 4.3.1 are used to examine the long-term voltage support provided by DG. The values of $V_{DG,lower}$ and $V_{DG,upper}$ are set as 0.96 p.u. and 1.04 p.u., respectively. The safety margin gap for voltage control is 0.1 p.u. The voltage reference of the DG voltage controller is updated every 0.5 sec. The long-term voltage variation is generated by changing the network's demand as shown in Figure 4.23 (total simulation time is 360 sec). In addition, the change of load demand in this simulation is assumed to be faster than in practice, in order to reduce simulation time and computer memory. The total load demand starts gradually increasing from t=0 sec until t=100 sec causing the voltage level in the network to drop slowly. After t= 100 sec, the load demand will reduce continuously until t= 360 sec. It is found that the voltage starts rising (above the nominal voltage) at t= 221 sec. The transient simulation compares the voltage levels at buses 11 and 17, which are a DG bus, and a bus at the end of feeder. The *P* and *Q* from the DG unit with and without voltage support provision are shown in Figure 4.24.

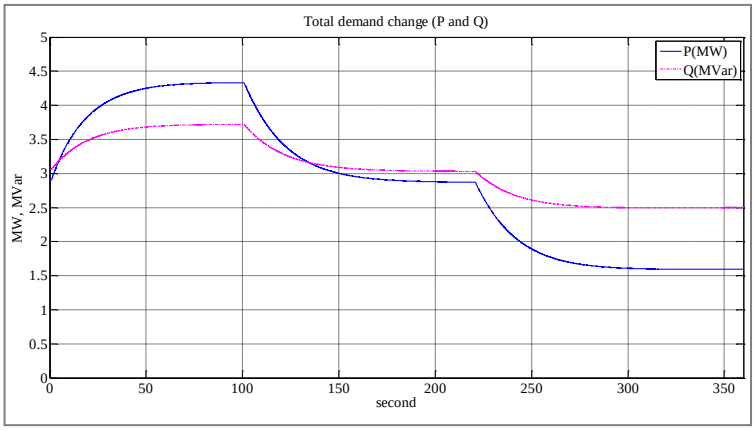

Figure 4.20. Characteristic of total load demand (active and reactive powers) change in the long-term voltage change study.

The results in Figure 4.21 show that the voltage support from DG can prevent the under and over voltage problems at bus 11 due to gradual load changes. The voltage support from DG starts operating when the voltage level at bus 11 reaches the DG's voltage limits, assuming

$V_{DG,lower}$ = 0.96 p.u. and $V_{DG,upper}$ = 1.04 p.u.. The *Q* support from DG is regulated slowly according to the slow voltage change. However, the voltage compensation from DG is insufficient to rescue the voltage level at the end of the feeder, bus 17, from going below the lower statutory limit. This is because the voltage level at this bus is normally lower than that in bus 11 for the same load condition. Also, the available *Q* support from DG is quite limited. Secondary voltage support from the substation's OLTC, or from power conditioning devices may be required in this bus. Figure 4.21(c) shows that the slow *V/Q* compensation from DG does not cause the obvious fluctuation in *P* output. This means the interaction between *P* and *Q* of DG is very little and seems like they are decoupled in the case of long-term voltage control. It can be seen that the DG can be used to support long-term voltage variations in the LCZ successfully in addition to the short-term voltage support.

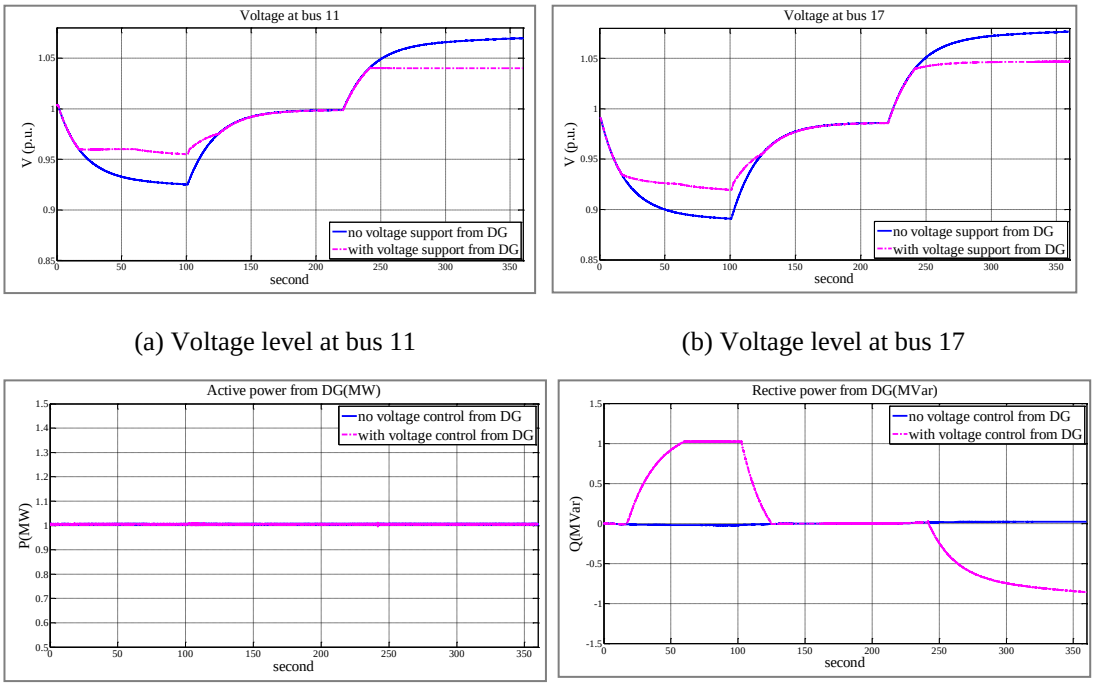

(a) Voltage level at bus 11

(b) Voltage level at bus 17

(c) Active power of DG unit

(d) Reactive power of DG unit

Figure 4.21. Voltage levels and active and reactive powers of DG comparing with and without voltage support from DG in case of the long-term voltage support.

4.3.4 Mixed short- and long-term voltage variations

In this case study, the enhanced voltage controllability of the DG unit is examined under mixed short- and long-term voltage variations in the same scenario. The DG should fully support short-term voltage control if the DG unit has some available reactive power (i.e.

$\Delta Q_{DG} > 0$ MVar). However, during DG long-term voltage control, the amount of available reactive power is reduced because the DG already generates some reactive power for the voltage control. If the DG supplies the reactive power until reaching its maximum limit (i.e. for the under voltage control), where $Q_{gen} = +Q_{res}$ and $\Delta Q_{DG} \sim 0$ MVar, the DG will have no additional reactive power available to support the voltage sag. On the other hand, the DG cannot support the voltage swell if the DG already supports over voltage control until the value of reactive power reaches its minimum limit (i.e. $Q_{gen} = -Q_{res}$).

The test system in Section 4.3.1 is used as the initial condition for the transient simulations. The V_{DB} is set to 1.5% and the DG's voltage limits are 0.96 p.u. and 1.04 p.u., respectively. The disturbances are the combination of short- and long-term voltage variations, as shown in Table 4.5. The simulation results from applying those disturbances are shown in Figure 4.22, which compare the voltage level and reactive power of the DG unit with and without voltage support from DG.

Table 4.5. Detail of mixed disturbance events.

No.	*t*(*s*)	Event
1	1	Start increasing load demand
2	80	Small voltage sag for 3 seconds
3	100	Start decreasing load demand
4	145	Voltage swell for 2 seconds
5	180	Voltage sag for 4 seconds
6	220	Start further decreasing load demand
7	310	Voltage sag for 2 seconds

From Figure 4.22, it is found that the voltage support from DG aims to control the voltage in its DG bus (bus 11), which also enhances the voltage compensation in bus members inside the LCZ. At bus 11, DG can bring the voltage back to the statutory limits, for almost every disturbance event, using *V*/*Q* compensation. It is found that DG cannot provide sufficient voltage support when *Q* has already reached its capacity limit, $\pm Q_{res}$, such as at *t*= 80 sec when the DG has no available *Q* left to compensate the small sag. However, as the voltage has already been raised by the *Q* injection, the voltage suffering from this sag is softer than the case without DG support. Conversely, DG can support the voltage sag compensation at *t*= 310 sec, by injecting *Q* into the network, although the *Q* has been absorbed by DG to prevent the over voltage, because the supporting *Q* for voltage sag is in different direction (from -*Q* to +*Q*). During *t*=125 sec to *t*=220 sec, the *Q* support from DG is zero since the voltage level at bus 11 is within the allowed limits. So, the DG can fully support short-term voltage control both swell and sag at *t*=145 sec and *t*=180 sec, respectively.

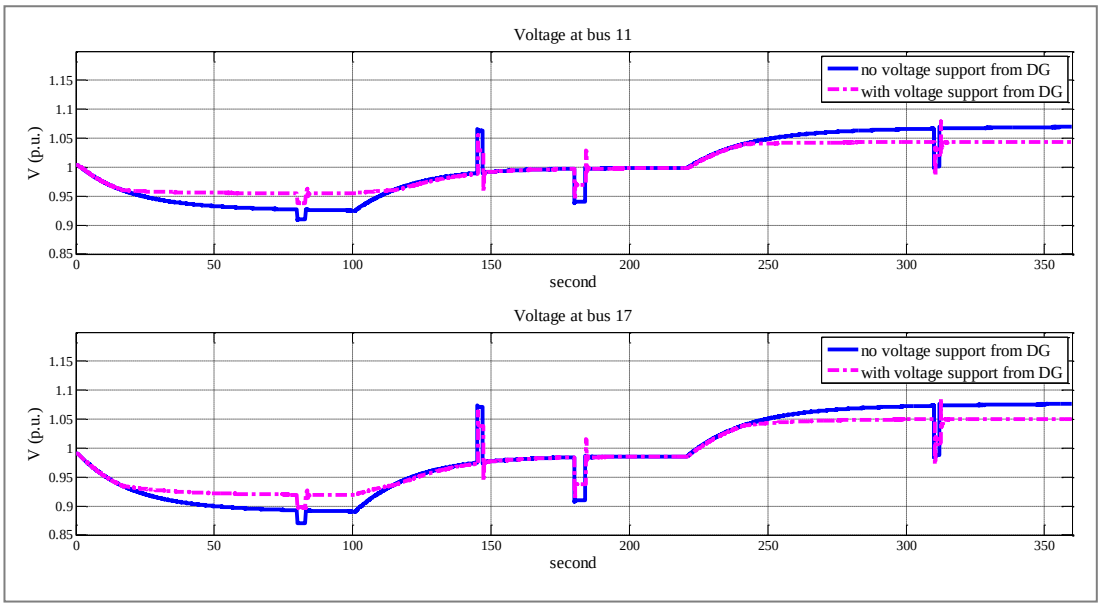

(a) Voltage levels at buses 11 and 17

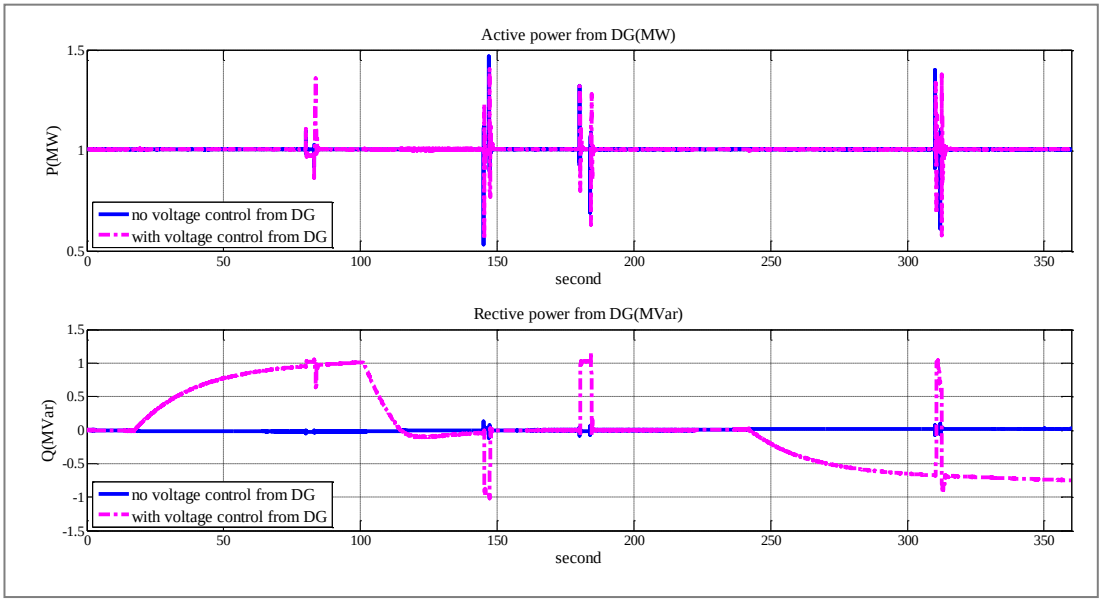

(b) Active and reactive power from DG unit

Figure 4.22. Voltage levels and active and reactive powers of DG comparing with and without voltage support from DG in case of mixed voltage disturbances.

4.3.5 Remote voltage support from DG

The Volt-Var control from DG can be applied directly to a specific bus especially in the same LCZ via remote measurement and communication systems. For example, DG can

provide voltage flicker control directly at the location of the flicker source, and provide long-term voltage control to a critical bus, such as a bus at the end of feeder.

In case of the remote voltage flicker control, it can be examined by using the case study in Section 4.3.2.2. Additionally, DG at bus 11 will compensate the *Q* directly at the flicker source bus 8. The transient simulation is shown in Figure 4.23, which is comparing with the case where DG provides voltage support at its own local bus (DG bus 11). The comparison is summarised by using a flicker index, as shown in Table 4.6. It is found that using remote voltage control can provide better voltage flicker mitigation at the flicker source bus. The *Q* supplied by DG in case of using the remote control is higher than using the local control because the level of voltage fluctuation at bus 8 is higher, and the *Q* is also compensated via the line reactance between the DG and the flicker source. However, from the flicker index, the performance in voltage flicker mitigation is very close between using local and remote controls. It can be seen that the flicker mitigation using converter-connected DG is very effective without communication system requirements, when it is connected near the flicker source, for example a mixed DG system comprising fixed-speed wind generation, and either PV or fuel cells within the same LCZ.

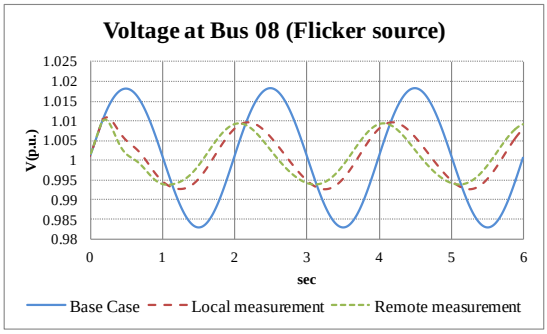

(a) Voltage at bus 8

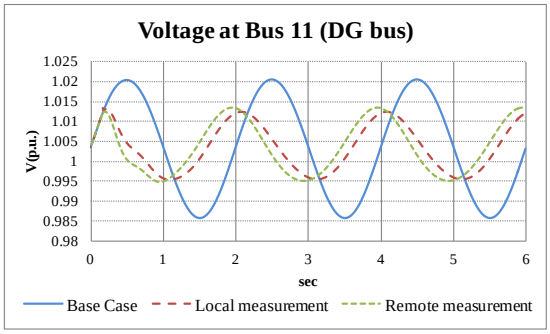

(b) Voltage at bus 11

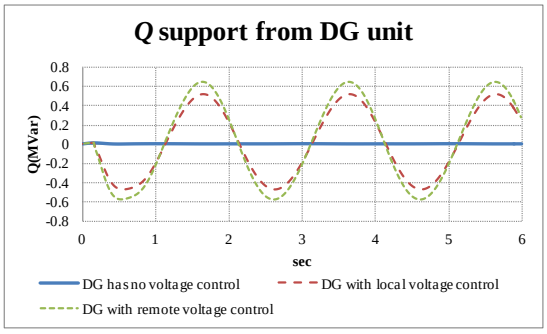

(c) Reactive power from DG

Figure 4.23. Voltage flicker waveforms and reactive power from using DG to control flicker comparing local and remote bus control.

Table 4.6. P_{st} between using DG to control flicker at its local bus and the remote bus.

Bus	P_{st} (Short term flicker index)		
	No compensation	With the local voltage control (bus 11)	With the remote voltage control (bus 8)
8	1.0504	0.5138	0.4689
11	1.0369	0.5026	0.5589
17	1.0369	0.5026	0.5589
24	0.1143	0.0609	0.0773
30	0.4309	0.2145	0.1936

In case of long-term voltage control, the information of voltage measurements at the DG and the remote buses, both in the same LCZ, are sent to the DG voltage controller. The voltage controller will determine the voltage levels among measurement data to find out which bus has the most critical voltage level problem. The remote voltages from the selected buses in the same LCZ are compared to find the values of maximum and minimum voltage level (i.e. $V_{re,max}$ and $V_{re,min}$, respectively). $V_{re,min}$ and $V_{re,max}$ will be re-checked with the voltage level at the DG bus. The supporting voltage control at DG bus is the first priority. Hence, the DG voltage controller allows to support the remote voltage control if the voltage level at DG bus (V_{DG}) is still within its acceptable limit (i.e.. between $V_{DG,lower}$ and $V_{DG,upper}$). The modified control diagram (i.e. adapted from the original voltage controller in Figure 4.3) and the flowchart of the DG voltage controller with remote controllability are shown in Figure 4.24.

The remote long-term voltage control is examined by using the case study in Section 4.3.3. Bus 17 is assumed as the remote voltage control bus, $V_{remote,\text{bus17}}$, located at the end of the feeder which tends to have an under voltage problem. From Figure 4.24, $V_{remote,\text{bus17}} = V_{re,min} = V_{re,max}$, as it is the only remote bus in this case. The voltage measurements at buses 11 and 17 are sent as the inputs to the DG voltage controller at the same time. The simulation results of voltage level at buses 11 and 17 by using DG voltage controller with the remote controllability are shown in Figure 4.25. Figure 4.26 shows the voltage reference of the DG voltage controller and reactive power of the DG unit in this case. It is found that the voltage level at bus 17 is improved by using the remote control from DG at bus 11.

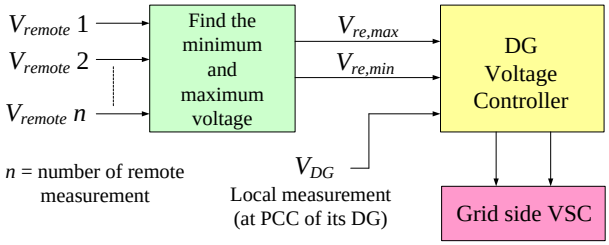

(a) Diagram of DG voltage controller with the remote controllability

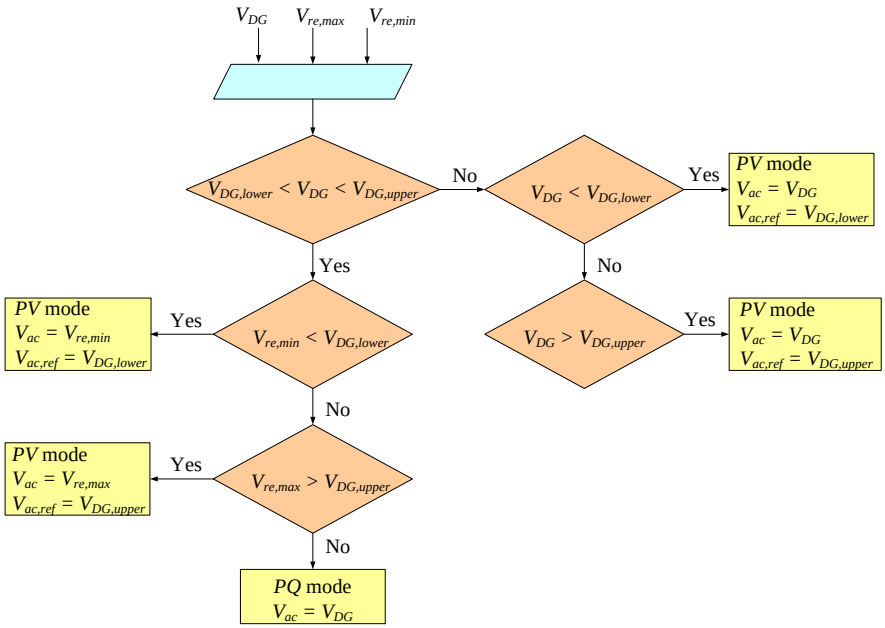

(b) Flow chart diagram of DG voltage controller with the remote controllability

Figure 4.24. Control diagram and flow chart of DG voltage controller with remote controllability.

Figure 4.25 shows that the DG voltage controller remains operating in *PQ* mode as the input is V_{ac}, until t= 7 sec, where the voltage at bus 17 is nearly reaching the statutory limit. Then the voltage input is swapped from bus 11 to bus 17, and the voltage reference is kept constant at $V_{DG,lower}$ = 0.96 p.u.. A little voltage spike during t= 12 sec to t=14 sec occurs when the DG switches from *PQ* mode to *PV* mode and due to the switching between voltage inputs from bus 11 to bus 17. The switching between voltage inputs also impacts on the little spike at the *Q* from DG, as can be seen in Figure 4.26. During t= 19 sec and t = 112 sec, the voltage level at bus 17 cannot be controlled to stay within the statutory limits because the *Q* supplied from DG has already reached the capacity limit whereas the demand continues increasing. In addition, at t= 60 sec, the voltage input is swop from bus 17 to bus 11 due to the voltage level at bus 11 is reaching the lower limit ($V_{DG,lower}$). The DG remains operating under *PV* mode until t= 120 sec aiming to control the voltage level at bus 17 back to the

allowed limits. Hence, during *t*= 120 sec to *t*=150 sec, the voltage input is switched from bus 17 to bus 11 as the voltage at bus 17 is already back to the allowed range. Meanwhile, at *t*= 110 sec, the *Q* output from DG start to decrease slowly until *t*= 150 sec, where the *Q* supplied from DG is zero and DG switches from *PV* mode to *PQ* mode.

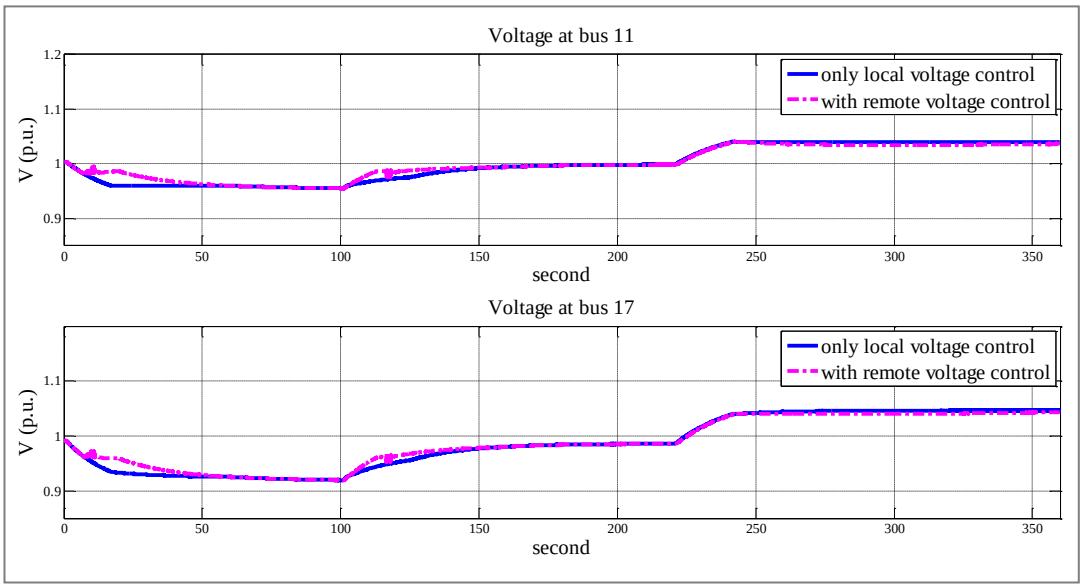

Figure 4.25. Voltage level control by DG unit with remote voltage controllability.

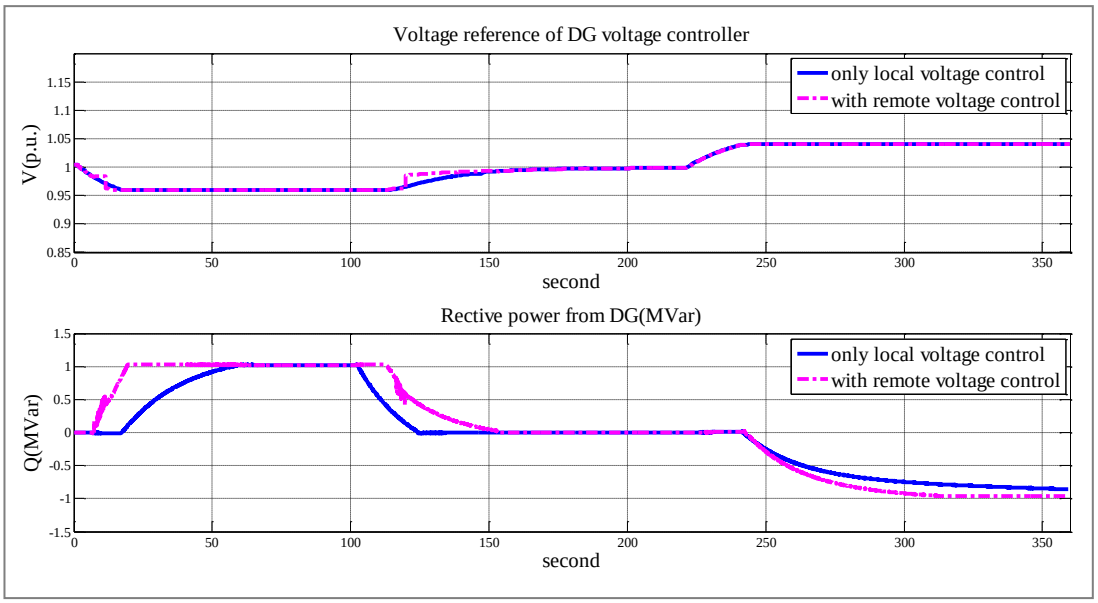

Figure 4.26. Voltage reference of voltage controller and reactive power supported from DG.

Alternatively, DG starts to operate in *PV* mode again at *t*= 242 sec, when the voltage at bus 11 (DG bus) is above the $V_{DG,upper}$ = 1.04 p.u, to prevent the over voltage during the light load condition by absorbing *Q* from the network. It was found that in this case the DG controls

the voltage level at its own bus without remote control to bus 17, because the voltage level at bus 11 is higher than that at bus 17. The input voltage remains using the voltage at the DG bus and the voltage reference is maintained at the value of $V_{DG,upper}$.

It can be seen that DG can support long-term voltage control to specific locations in the same zone, which can enhance the level of voltage quality in the network. However, communication systems are required. The limitation of reactive power capability of DG and the line reactance between the DG bus and the remote bus also restrict the performance of the voltage support provided by the DG unit to a remote bus. Remote voltage control may not be necessary in case the remote bus is very close to the DG bus.

4.4 Dynamic voltage control in distribution networks with multiple converter-connected DGs

This section explains the interaction between voltage controllable DG units and demonstrates the transient behaviour when several controllable DG units are connected to the same feeder in the distribution network. Voltage interactions between LCZs are also examined. The concern of voltage interactions is in the case that more than one DG unit is connected in the same LCZ, where the change in *V/Q* compensation from one DG unit can impact on the voltage change of other DG units.

4.4.1 Voltage interactions among voltage controllable devices

When more than one voltage controllable device within the same zone provide voltage support simultaneously, may give rise to undesired voltage interactions among them. Using the approach in [14] and (3.2), the voltage variation of a critical bus, especially the DG bus, with respect to a change of *P* and *Q* of the controllable DGs and ESSs can be explained as:

$$\Delta \mathbf{V}_{\mathbf{CN}} \approx \left[\partial V / \partial P\right] \cdot \Delta P + \left[\partial V / \partial Q\right] \cdot \Delta Q \qquad (4.5)$$

where $\Delta \mathbf{V}_{\mathbf{CN}}$ is the vector of voltage variations in critical buses. ΔP and ΔQ are the change of active and reactive power in controllable DG or ESS, respectively. $[\partial V/\partial P]$ and $[\partial V/\partial P]$ are the voltage sensitivity matrices of size $[n \times m]$, where n is the number of critical buses and m is the number of controllable devices.

This voltage interaction problem affects directly the voltage controller of the DG grid-side converter making it difficult to maintain the voltage at its set-point value. From Figure 4.1 and Figure 4.2, the dynamic current variations of the grid-side converter including the voltage interaction can be written as:

$$L\frac{di_d(t)}{dt} = \left(v_{t,d}(t)\right) - \left(v_{s,d}(t) + \Delta v_{s,d}(t)\right) - Ri_d(t) + \omega L i_q(t) \tag{4.6}$$

$$L\frac{di_q(t)}{dt} = \left(v_{t,q}(t)\right) - \left(v_{s,q}(t) + \Delta v_{s,q}(t)\right) - Ri_q(t) - \omega L i_d(t) \tag{4.7}$$

where $v_{s,d}$ (t) and $v_{s,q}$ (t) are the instantaneous dq components of the voltage variation at the PCC due to own changes of the DG under consideration. $\Delta v_{s,d}$ (t) and $\Delta v_{s,q}$ (t) are the instantaneous voltage variations at the PCC caused by changes in other controllable devices.

From (4.6) and (4.7), it is found that the interactions at the PCC, v_s+Δv_s, increase the level of voltage variation, and consequently the change in output currents. Then, the DG's terminal voltage, v_t, is changed according to the change of output currents. From the P and Q controllers of VSC in Appendix E (Section E.2.2), the dynamic apparent power exchanged by the VSC with the AC network (including the impact on voltage interactions), can be written as:

$$L\frac{dP(t)}{dt} = -RP(t) - L\omega_0 Q(t) + \frac{3}{2}\left(\left(v_{t,d}(t)\tilde{v}_{s,d}(t) + v_{t,q}(t)\tilde{v}_{s,q}(t)\right) - \left(\tilde{v}_{s,d}^2(t) + \tilde{v}_{s,q}^2(t)\right)\right) \tag{4.8}$$

$$L\frac{dQ(t)}{dt} = -RQ(t) + L\omega_0 P(t) + \frac{3}{2}\left(\tilde{v}_{s,d}(t)v_{t,q}(t) - \tilde{v}_{s,d}(t)v_{t,q}(t)\right) \tag{4.9}$$

where $\tilde{v}_{s,d}(t) = \left(v_{s,d}(t) + \Delta v_{s,d}(t)\right)$ and $\tilde{v}_{s,q}(t) = \left(v_{s,q}(t) + \Delta v_{s,q}(t)\right)$ are the instantaneous voltage variations at the PCC in dq components. From (4.8) and (4.9), it can be seen that voltage interactions from other controllable DG also increase the fluctuation of the P and Q outputs from the DG, apart from the interactions by the coupling between P and Q themselves.

4.4.2 Simulations and results

The test system is taken from the base case in Section 4.3.1. Three 1-MW converter-connected DG units, working at unity p.f., are connected to the network at buses 7, 11 and 23, as shown in Figure 4.27, while the total load demand remains unchanged. The secondary voltage at substation transformer (bus 0) is set to 1.019 p.u. DG1 and DG2, have ± 1 MVar (p.f. ≥ 0.707) extra capacity each, and DG3 has ± 0.5 MVar (p.f. ≥0.89). If unity p.f.

operation is assumed, then from (3.3), the available Q support from those DG units are $\Delta Q_{DG,1} = \Delta Q_{DG,2}$ =1 MVar, and $\Delta Q_{DG,3}$=0.5 MVar, respectively.

The sensitivity matrices are obtained from the load flow calculation in DIgSILENT *PowerFactory*. The change of bus voltage, ΔV, caused by the DGs active and reactive powers compensation support are shown in Figure 4.28. These figures allow analysing the P and Q coupling in the DG controller (see (4.5)). It was found that DG1, DG2 and DG3 can provide a maximum voltage compensation of about ± 3.45 %, ±1.16 % and ±1.04%, respectively. DG2 and DG3 provide only a small amount of V/Q compensation due to the limitation of the network topology and the available Q reserve.

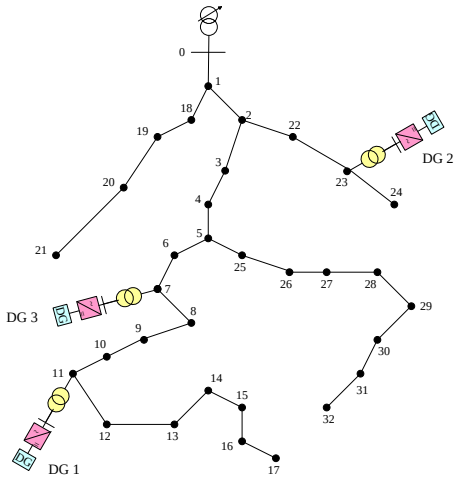

Figure 4.27. The test system in case of multi DG connection.

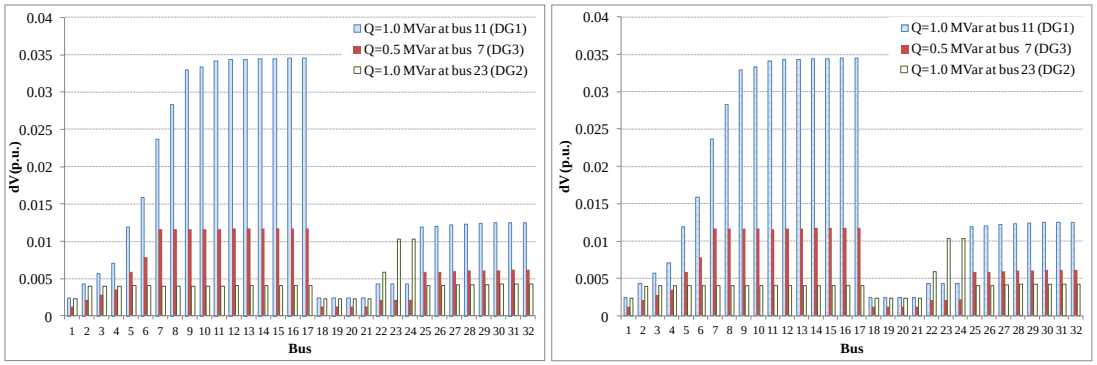

(a) Voltage change from the Q injection from DG (b) Voltage change from the P injection from DG

Figure 4.28. Change of bus voltage from the active and reactive powers injection from DG at buses 7, 11 and 29.

It is found that the level of voltage support influenced from DG3 is about one third of DG1, which provides significant voltage changes at buses 6 to 17 similar to DG1. If ΔV_{th} is defined

as 0.015 p.u. (which means that DG can provide ±0.015 p.u. voltage compensation, at least, for all bus members), the main voltage control comes from DG1 because the available *Q* reserve is greater than DG3, which can cover the voltage control area, the same as from DG3. Therefore, DG1 and DG3 can be grouped into the same zone, as shown in Table 4.7. The aggregated voltage controllability from these two DG units is about ±4.5%. In the case of DG2, which has a small reserve to provide additional compensation, ΔV_{th} is defined as 0.5% in order to provide 0.005 p.u. voltage compensation among buses 23 and 24. This small voltage controllability may be suitable to mitigate small voltage variations, such as flicker.

Table 4.7. Detail of LCZs in case of 3 DG units

Zone	DG bus	ΔV_{th} (p.u.)	DG priori	Bus members
1	07, 11	0.015	1st at bus 11 2nd at bus 07	6, 7,8,9,10,11,12,13,14,15,16,17
2	23	0.005	1st at bus 23	23,24

The voltage profile caused by a change in the *Q* injection at buses 7, 11 and 23 is shown in Figure 4.29. It was found that major voltage changes occur only in associated buses within each zone. There are some voltage interactions between LCZ#1 and LCZ#2, but as they are very small (less than 0.4 %), the zones can be assumed to be decoupled. However, the interaction between DGs in the same zone is evident. This interaction can interfere directly with the voltage controller of each DG converter, if they provide dynamic voltage control at the same time.

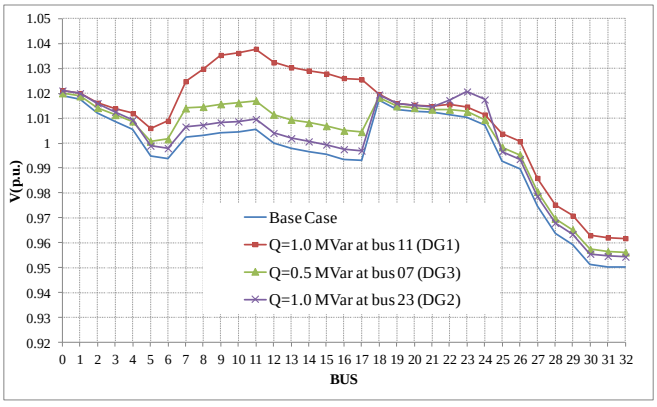

Figure 4.29. Voltage response (steady state) from the *Q* injection at buses 7, 11, 23 comparing with the base case (without compensations).

The DG controllers in LCZ#1 and LCZ#2 are set to start dynamic voltage compensation when the change of voltage at both DG buses is more than the V_{DB} of ± 1.5 % and ± 0.5 %,

respectively. In addition, the value of V_{DB} should not be higher than ΔV_{th} to ensure that LCZ can receive the assumed minimum level of support ΔV_{th}. Moreover, the voltage support is also activated whenever the voltage level is outside the statutory limits (e.g. 0.95 p.u. – 1.05 p.u.). The transient simulation is examined in the event of a voltage sag by applying a small fault (see Appendix L, section L.1) at bus 13 (i.e. in LCZ#1), starting at t=0.5 sec and finishing at t=3.5 sec. The overall simulation time is 6 sec. To demonstrate the impact of voltage interactions, the capability of DG1 and DG3 to provide voltage support in LCZ#1 is analysed in two cases:

1) Only DG1 operates in *PV* mode to support voltage control while DG3 operates in *PQ* mode
2) Both DG1 and DG3 operate in *PV* mode when the voltage changes more than ±1.5%.

Note that both cases assume that there is no coordinated control between DG1 and DG3.

Figure 4.30, shows the key results from these simulations. Figure 4.30(a) and Figure 4.30(b) show the *P* and *Q* of DG1 and DG3, respectively. Voltage interactions between DG1 and DG3 are observed, where the level of interactions increases when both DG units support voltage at the same time. From Figure 4.30(c), it can be seen that when either DG1 or DG3 operate in *PV* mode, DG2 still operates in *PQ* mode (as the voltage change at DG2 bus is well below its V_{DB} of 0.5%). This demonstrates minimum interaction between LCZs. The change of frequency (based on 50 Hz) at each DG bus is very small and within the standard limit (i.e. ±5%) as shown in Figure 4.30(d). The results in Figure 4.30(e) also show that using *Q* support from both DG1 and DG3 units can raise the voltage level better than with DG1 only. Although a post-fault low-frequency voltage oscillation (~ 1 Hz) is observed in the LCZ#1, it recovers back to the steady state after a few seconds. As LCZ#1 and LCZ#2 are essentially decoupled, this post-fault oscillation is not observed in LCZ#2, as can be seen in Figure 4.30(f).

The voltage oscillation occurs as both DG units try to control rapidly the *Q* injection back to the pre-fault value. This change also impacts on the *P* output due to the coupling between *P* and *Q*, as found in (4.8) and (4.9). Consequently, changes in both *P* and *Q* outputs increase the variations in the voltage output. Apart from local interactions between *P* and *Q* in individual DG units, voltage interactions with other DG units will also contribute to increase the level of voltage variation in all DG units, which can be determined by the ratios of voltage sensitivity between those DG buses (see Figure 4.28). These voltage interactions cause a delay in the DG controllers to restore the voltage back to the normal conditions.

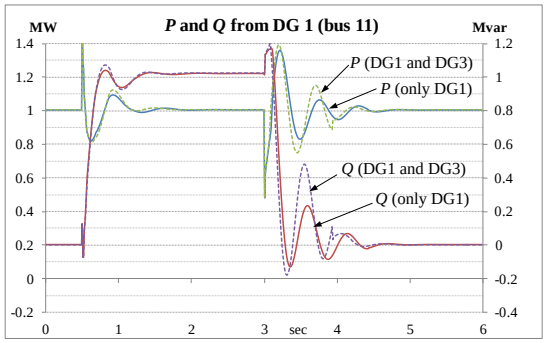

(a) *P* and *Q* from DG1 (LCZ#1)

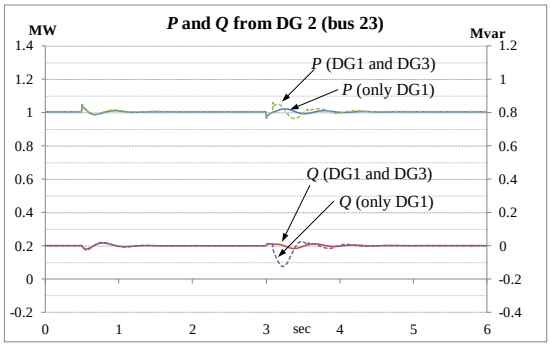

(b) *P* and *Q* from DG3 (LCZ#1)

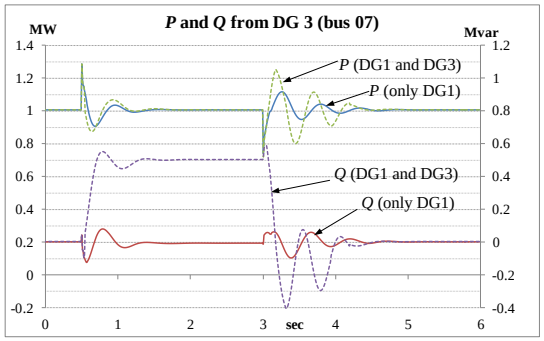

(c) *P* and *Q* from DG2 (LCZ#2)

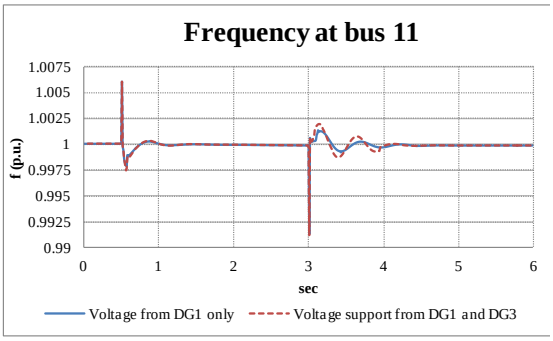

(d) Frequency (p.u.) at DG1 (bus 11)

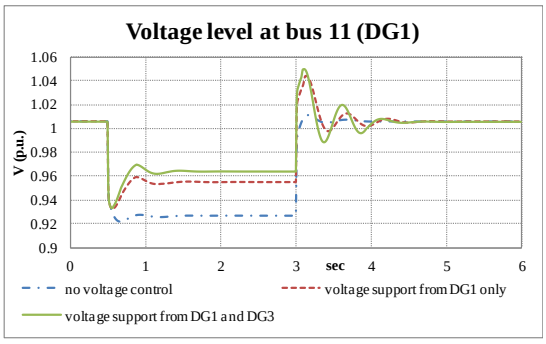

(e) Voltage level at bus 11 (LCZ#1)

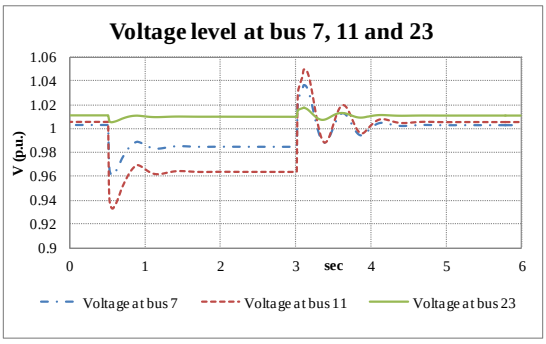

(f) Voltage level at bus 7, 11 and 23 when DG1 and DG3 support voltage control together

Figure 4.30. Transient simulations of voltage control from DG comparing with and without the impact of voltage interactions.

The level of oscillation and recovery time tend to increase when the number of voltage controllable devices, within the same LCZ, increases. It would be desirable to use the minimum number of DG units as long as the voltage is maintained within the limit. This will require a coordinated control and operation among the DG units in the same zone. For this to be achieved and mitigate voltage interactions a distributed coordinated control among the group of DG units within the same LCZ is proposed in this research.

4.5 Coordinated voltage control strategy and droop control among a group of DG units

The operation of the DG units should be properly supervised via a coordinated control to prevent negative interactions among DG units located in the same LCZ, given the situation that more than one unit is providing *V/Q* control at the same time. The coordinated controller aims to reduce the number of DG units providing voltage support, while they still maintain the voltage level within the statutory limits. The coordinated control allows DG units to provide voltage support in a sequential manner, one-by-one, according to their ranking order. The ranking order is determined by the speed of the voltage controller and the available extra *Q* capability. In addition, converter-connected DG is preferred in the case of dynamic voltage control due to the fast action of the power electronic converter. Synchronous generator-based DG may be used only for steady-state voltage control or as a back-up system.

In case that the level of voltage change is high and the duration time is quite long, the above coordinated control may not be enough. Meanwhile, the group of DG units are still required to support voltage control at the same time aiming to address the voltage level problem as much as possible. The *Q-V* droop controller can be added into the DG voltage controller for mitigating the interactions between the *Q* of DG and its voltage at that DG bus.

4.5.1 Coordinated voltage control among DG units

The coordinated controller is applied to DG units in LCZ#1. The ranking to provide voltage support is determined from the available *Q* capacity. Hence, DG1 (ΔQ = ±1MVar) takes the lead to support voltage compensation and is assumed as "*Master controller*". DG3 (ΔQ = ±0.5MVar), is assumed the *"Slave controller"*, and will operate when the voltage support from DG1 is insufficient.

A time delay (assumed as 1 sec) is added into the slave controller to ensure that the support action from DG1 has stabilised (about 0.8 sec). If DG1 can provide all the voltage compensation needed, this means that DG3 does not need to operate in *PV* mode. However, communication systems between *Master DG* and *Slave DG* are required. The operation diagram of the interaction between slave and master controller is shown in Figure 4.31.

In this experiment, the V_{DB} of DG1 and DG3 is defined as 0.015 p.u.. The proposed coordinated control method is examined with the same disturbance condition as the base case in Section 4.4.2. Additionally, the test considers 2 different scenarios: 1) medium voltage change and 2) high voltage change.

The response of each voltage controller including *P* and *Q* in essential voltage buses is shown in Figure 4.32. The results from DG2 are not included as there is very small impact to LCZ#2 from the disturbance in LCZ#1, as found in the previous section (see Figure 4.30(c) and Figure 4.30(f)).

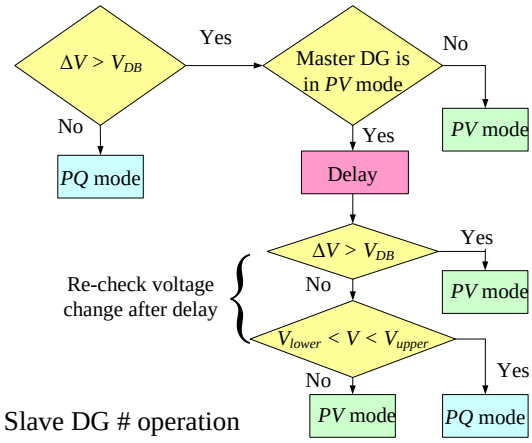

Figure 4.31. Operation diagram of the slave converter-connected DG with coordinated controller method.

The results show that, DG1 will take the first responsibility to mitigate voltage variations in case that a medium voltage change has occurred, which is the case when the voltage drop in LCZ#1 is higher than 1.5%. Hence, the DG3 will delay around 1 sec to make the control decision. It is found that the voltage level is already compensated within the statutory limit, so, DG3 does not need to operate in *PV* mode and only *Q* support from DG1 is sufficient. It can be seen that there are no voltage interactions from other controllable DG units. The small oscillation occurs due to the fast restoration of *Q* back to the initial value after the disturbance is cleared.

In case of a lower retained voltage level, voltage support from DG1 only is not sufficient, as it is found that the voltage level at bus 11 is still below 0.95 p.u. Therefore, after a delay of 1 sec, DG3 needs to inject *Q* into the network to achieve full voltage compensation. Because both DG units are requested to support voltage control, there is a voltage interaction between them. It can be seen that this interaction causes the increase of voltage oscillation after the

disturbance is cleared. Furthermore, the fluctuations in the *P* and *Q* outputs are also increased from the voltage interactions influenced by other controllable DG units.

It was also found that the delay time, 1 sec, of each DG in this coordinated control approach reduces the fast voltage compensation capability. For example, only one DG unit can support voltage control if the high voltage sag duration is less than 1 sec. Therefore, this coordinated controller may be not required if the level of voltage oscillation among DG units is acceptable to maintain the fast voltage support response. A *V*-*Q* droop controller is proposed in the following section to mitigate the voltage interactions when DG units provide voltage support at the same time.

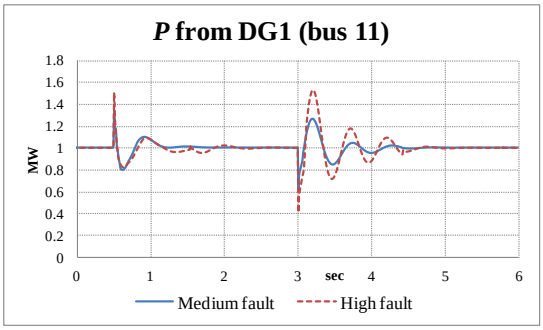

(a) *P* from DG1 (bus 11)

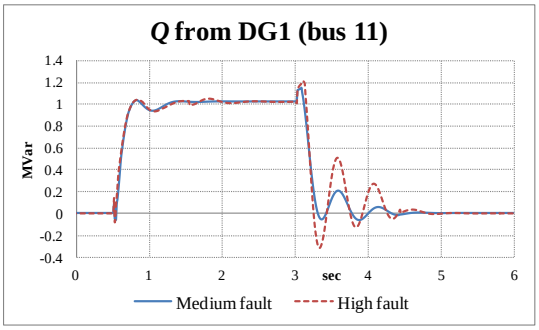

(b) *Q* form DG1 (bus 11)

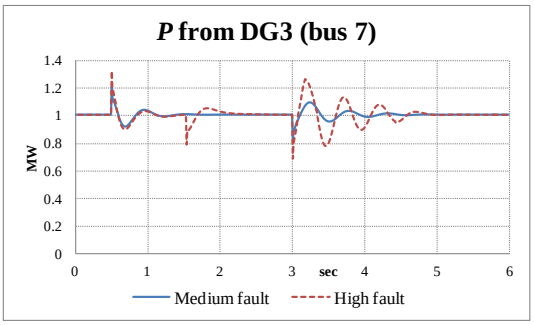

(c) *P* form DG3 (bus 7)

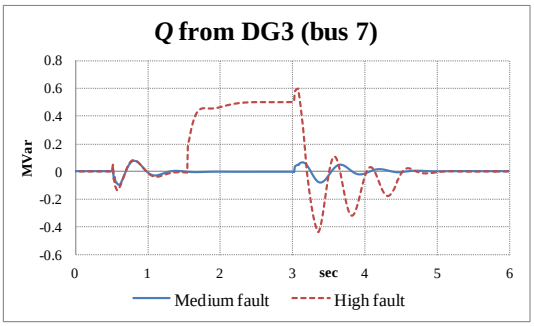

(d) *Q* form DG3 (bus 7)

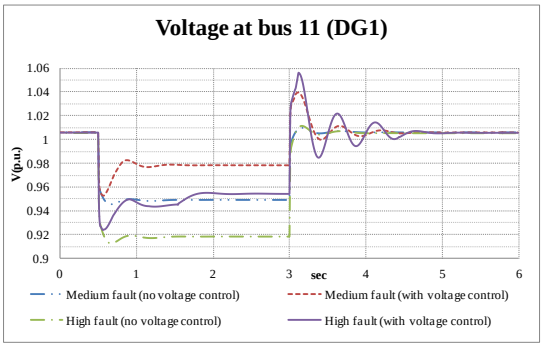

(e) Voltage at bus 11

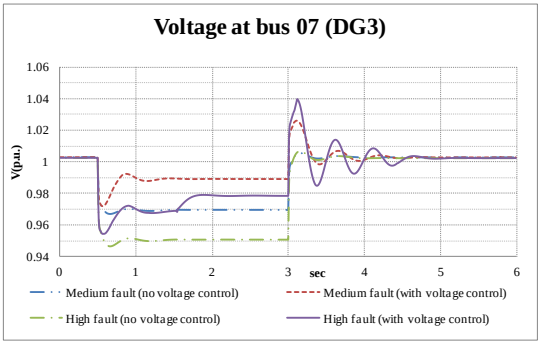

(f) Voltage at bus 7

Figure 4.32. Transient simulations of the proposed coordinated control method.

4.5.2 *V-Q* droop control

The droop control method can be added to the DG controller to damp out the dynamic oscillation between reactive power, *Q*, and bus voltage, *V*, locally. This method has been applied widely in distribution networks based on inverter-interfaced DG, especially using photovoltaic and micro-turbines, to control frequency and voltage in the microgrid in islanding mode [15]-[17]. However, the frequency control (*P-f* droop) is not included in this work. Only voltage control (*V-Q* droop) is considered because the frequency variation is negligible as it is assumed that the network remains connected to the grid. The objective of the *V-Q* droop control in this work is to maintain reasonably uniform voltage during a rapid change of the *Q* output after the disturbance is cleared.

During steady-state conditions, the conventional droop control of converter-connected DG can be analysed from the simple circuit in Figure 4.37. The DG connects to the common bus through the series impedance which is formed from a series filter and a transformer. This impedance is assumed to be highly inductive, which means that $Z \approx X$ and $\theta \approx 90°$. Hence, the active and reactive powers supplied to the grid are:

$$P = \frac{V_t V_s}{X} \sin\phi \tag{4.10}$$

$$Q = \frac{V_t V_s \cos\phi - V_s^2}{X} \tag{4.11}$$

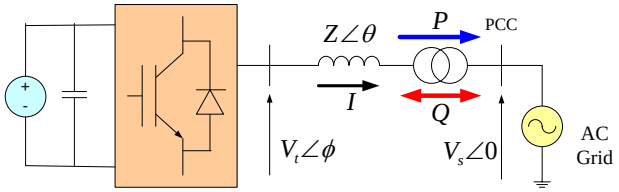

Figure 4.33. Equivalent circuit of grid-side converter-connected to the grid.

According to (4.11), it is found that *Q* mainly depends on the output voltage magnitude. The conventional droop aims to provide the voltage regulation control of PCC, V_s, as a function of *Q*, which can be written as

$$V_s = V_O + K_{droop}(Q - Q_O) \rightarrow K_{droop} = \frac{V_{\min} - V_O}{Q_{\max} - Q_O} \tag{4.12}$$

where V_O and Q_O are the amplitude of the voltage at PCC and reactive power output, under normal conditions, respectively. V_s and *Q* are feedback signals from PCC. K_{droop} is the droop

coefficient which is the negative slope of the *Q*-*V* droop curve. The typical value of the droop coefficient is about 2-5% [17].

The static droop characteristic is shown in Figure 4.34(a). However, it is found that the conventional droop control is similar to the proportional (P) controller, which is deficient in terms of transient response and system stability.

The dynamic performance can be enhanced by adding a derivative (D) controller into the droop control [18], [19]. The voltage variation can be damped following the deviation of the *Q* output as can be seen in (4.13) (where it is possible to modify the transient response). This proposed control also keeps the static droop characteristic. The control diagram of the PD droop controller of the grid-side converter is shown in Figure 4.34(b). It can be seen that the *Q* output will be restricted by the addition of this droop controller.

$$V_s = V_O + K_{pq}(Q_O - Q) + K_{dq}\frac{d(Q_O - Q)}{dt} \tag{4.13}$$

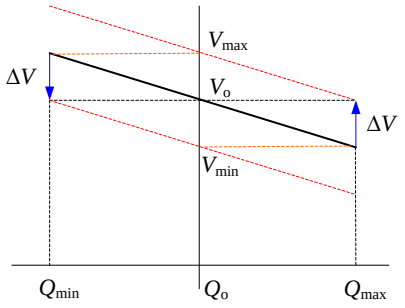

(a) Static *V*-*Q* droop characteristic

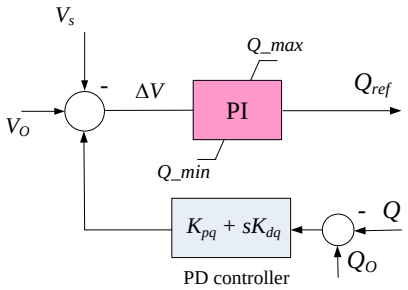

(b) Block diagram of the proposed droop controller

Figure 4.34. Static *V*-*Q* droop characteristic and control system of the propose *V*-*Q* droop controller

The performance of the droop controller is examined based on transient simulations of the high voltage change case from the previous section. The droop controller's gains of this case are illustrated in Appendix E.2. The test compares 3 cases as follow: 1) No droop controller, 2) P-droop controller and 3) PD-droop controller.

The *P*, *Q* and *V* of each DG unit in LCZ#1 are shown in Figure 4.35. It is found that using droop controllers can damp the *Q* and *V* variations from the interactions among DG units in LCZ#1, after the disturbance has been cleared. The level of voltage oscillations is reduced and the time range of oscillations is shorter compared to the case without the droop controller. In addition, the droop with PD control provides effective performance in terms of

reducing the level of variation. The derivative term of the droop controller also gives the benefit of reducing the time consumed to bring the system back to the steady-state condition.

The main damping is from the droop control of DG1 rather than DG3. This means that the DG unit with higher *Q* support capability needs to have the droop controller, whereas the droop controller of small DG units may not be necessary. It can be seen that the addition of the *V*-*Q* droop can allow the group of DG units to support voltage control at the same time with lower voltage interactions. It can be seen that if the droop controller can mitigate the voltage interactions sufficiently, the coordination among DG units may not be necessary.

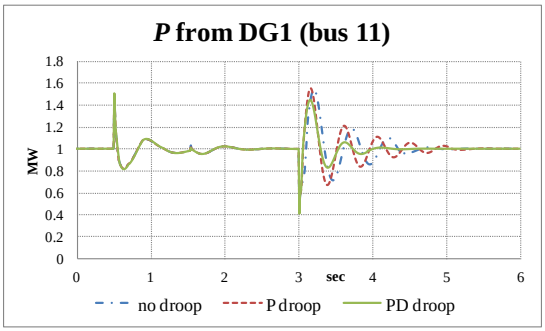

(a) *P* from DG1 (bus 11)

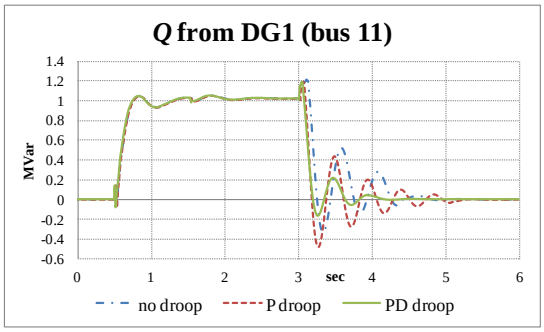

(b) *Q* form DG1 (bus 11)

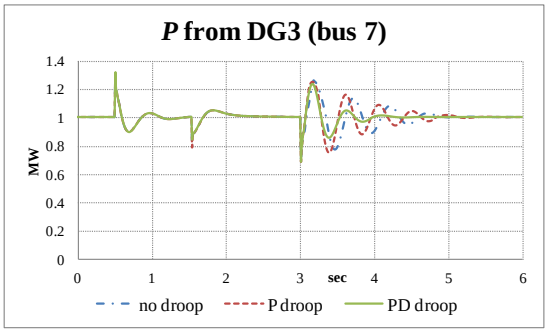

(c) *P* from DG3 (bus 7)

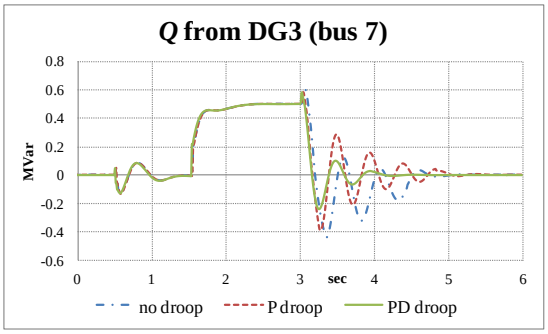

(d) *Q* form DG3 (bus 7)

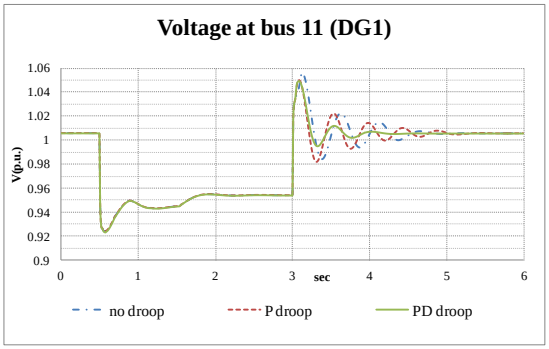

(e) Voltage at bus 11

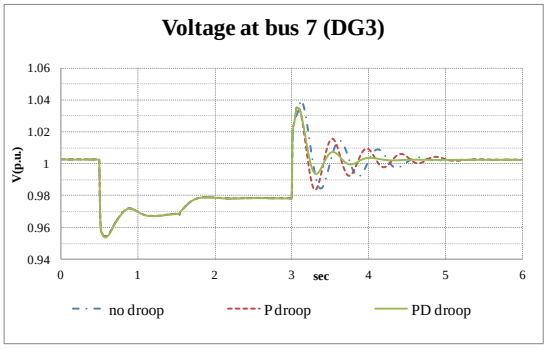

(f) Voltage at bus 7

Figure 4.35. Performance of three different droop controllers.

4.6 Conclusions

This chapter demonstrated the dynamic performance of active voltage control from DG in distribution networks. The voltage source converter-connected DG can be used as a voltage compensation device similar to power conditioning devices. It can achieve short- and long-term voltage control successfully due to the fast action of the power electronic converter. Additionally, the voltage control response of VSC-based DG is fast and smooth, unlike the voltage support from conventional synchronous machine-based DG, which has a slower and more fluctuating response.

Results from transient simulations showed that converter-connected DG can support dynamic voltage control to associated buses located in the same LCZ with DG effectively, under different scenarios including voltage sags and swells, voltage flicker, voltage imbalance and mixed voltage variations. The voltage interactions among LCZs are very small and they can be assumed to be decoupled.

The voltage control from DG can support directly specific locations, such as a bus at the end of feeder in the same LCZ, rather than only control at its PCC. The communication system is required to link between DG and the remote bus. The simulation results showed that the voltage level at the remote bus is improved by using this method. However, the level of improvement may be not much due to the limit of available reactive power support and the reactive power drop along the line. Meanwhile, the remote voltage control may be not necessary in case that the remote bus is very close to the DG bus, or the ratios of *V/Q* sensitivity between bus members are high enough.

Despite the voltage support from DG can provide the benefit of enhancing voltage quality of the distribution network, the voltage interactions among the group of DG located in the same LCZ increase the level of the voltage variation after the disturbance is cleared. Consequently, the voltage controllers have a difficulty of controlling their *Q* and *V* outputs to return to the satisfactory condition. The impact on voltage interaction tends to increase when the number of voltage controllable DG connected into the network has increased.

A coordinated controller approach is proposed to reduce the number of voltage supporting DG units while they still maintain voltage level within the statutory limits. The voltage support from DG units is operated by determining from the ranking order with time lag in each control sequence. This technique concentrates on using the DG with the highest capacity of *Q* available as the first DG unit for supporting the voltage control. On the other

hand, the additional *V-Q* droop controller is then used to reduce the voltage oscillation from the interaction among DG units when they support voltage control at the same time. The simulations show that the effective solution to mitigate voltage interactions between DG units is achieved by adding the PD droop controller. Furthermore, in this case the voltage controller can take less time to bring the voltage back to the steady-state condition after the disturbance has been cleared, compared to the case when there is no droop control.

4.7 References

[1] L. Huijuan, L. Fangxing, X. Yan, D. T. Rizy, and J. D. Kueck, "Adaptive Voltage Control With Distributed Energy Resources: Algorithm, Theoretical Analysis, Simulation, and Field Test Verification," *Power Systems, IEEE Transactions on*, vol. 25, pp. 1638-1647, 2010.

[2] A. Yazdani and R. Iravani, *Voltage-Sourced Converters in Power Systems*, 1 ed.: Wiley, 2010, chapter 8.

[3] *DIgSILENT Technical Documentation: PWM Converter,* DIgSILENT GmbH, 2007.

[4] *DIgSILENT Technical Documentation: Voltage Measurement,* DIgSILENT GmbH, 2007.

[5] D. Xue, Y. Q. Chen, and D. P. Atherton, *Linear feedback control: analysis and design with MATLAB*. Society for Industrial and Applied Mathematics, 2009, chapter 6.

[6] M. Joorabian, D. Mirabbasi, and A. Sina, "Voltage flicker compensation using STATCOM " in *Industrial Electronics and Applications, 2009. ICIEA 2009. 4th IEEE Conference on* 2009, pp. 2273 - 2278.

[7] *IEC 61000-4-15*, "Electromagnetic compatibility (EMC) – Part 4: Testing and measurement techniques – Section 15: Flickermeter – Functional and design specifications" , edition 1.1, updated 2003.

[8] T. Ackermann, *Wind Power in Power Systems*, 1st ed. John Wiley & Sons, Ltd, 2005, pp.82.

[9] Solcept (2012, May), Open Source Flicker Measurement-Simulator [Online]. Available at http://www.solcept.ch/en/embedded-tools/flickersim.html.

[10] S.-J. S. Tsai and Y. Chang, "Dynamic and Unbalance Voltage Compensation Using STATCOM," in *Power and Energy Society General Meeting - Conversion and Delivery of Electrical Energy in the 21st Century, 2008 IEEE*, Pennsylvania, 2008, pp. 1-8.

[11] F. Magueed and J. Svensson, “Control of VSC Connected to The Grid through LCL-filter to achieve Balanced Currents,” in *Industry Applications Conference, 2005, 40th IAS Annual Meeting. Conference Record of the 2005 IEEE*, Hong Kong, pp. 572-578.

[12] M. Bobrowska-Rafał, K. Rafał, and G. Abad, “Control of PWM rectifier under grid voltage dips,” *Bulletin of the Polish Academy of Sciences Technical Sciences*, vol. 57, no. 4, pp. 337-343, 2009.

[13] H.-seok Song, “Dual current control scheme for PWM converter under unbalanced input voltage conditions,” *Industrial Electronics, IEEE Transactions on*, vol. 46, no. 5, pp. 953-959, 1999.

[14] A. Viehweider, B. Bletterie, and D. Burnier de Castro, "Advanced coordinated voltage control strategies for active distribution network operation," in *Electricity Distribution - Part 1, 2009. CIRED 2009. 20th International Conference and Exhibition on*, Prague, 2009, pp. 1-4.

[15] H. Chih-Chiang, L. Kuo-An, and L. Jong-Rong, "Parallel operation of inverters for distributed photovoltaic power supply system," in *Power Electronics Specialists Conference (PESC), 2002.IEEE 33rd Annual*, Queensland. Australia, pp. 1979-1983.

[16] H. Karimi-Davijani and O. Ojo, "Dynamic operation and control of a multi-DG unit standalone Microgrid," in *Innovative Smart Grid Technologies (ISGT), 2011 IEEE PES*, Manchester, 2011, pp. 1-7.

[17] S. Ling, Z. Jianhua, M. Weishi, Y. Qi, and L. Ruoxi, "Study on Control Strategy for Islanded Microgrid Based on Microturbine," in *Asia-Pacific Power and Energy Engineering Conference (APPEEC), 2010*, Sichuan, China, 2010, pp. 1-4.

[18] J. M. Guerrero, L. G. de Vicuna, J. Matas, M. Castilla, and J. Miret, "A wireless controller to enhance dynamic performance of parallel inverters in distributed generation systems," *Power Electronics, IEEE Transactions on*, vol. 19, pp. 1205-1213, 2004.

[19] G. Yajuan, W. Weiyang, G. Xiaoqiang, and G. Herong, "An improved droop controller for grid-connected voltage source inverter in microgrid," in *Power Electronics for Distributed Generation Systems (PEDG), 2010, 2nd IEEE International Symposium on*, Hefei, China, 2010, pp. 823-828.

[20] R. Caldon, F. Rossetto, and R. Turri, “Analysis of dynamic performance of dispersed generation connected through inverter to distribution networks,” *17th international conference on electricity distribution*, Barcelona, 2003, pp. 12–15.

Chapter 5

Voltage Control Coordination between DG and other Voltage Controllable Devices for Voltage Quality Enhancement

5.1 Introduction

The previous chapter demonstrated that converter-connected DG can provide voltage support in distribution networks efficiently. However, the voltage control capability is restricted by the size and available *Q* capacity of DG. The lack of *Q* support from DG causes that the bus members in the LCZ receive only small amount of voltage compensation which may not be enough to stay within the statutory limits if the magnitude of the disturbance is relatively high. To enhance voltage level control in the LCZ, additional voltage controllable devices besides converter-connected DG may be required. These controllable devices should be able to provide active and fast voltage control to deal with either short- or long-term voltage variations. Moreover, the secondary voltage support may be provided for a wider area by the substation's OLTC. It can also enhance the voltage in areas of the network where the decentralised voltage support from DG and other controllable devices is insufficient.

In this chapter, voltage control structures which incorporate converter-connected DG and other voltage controllable devices are introduced and discussed. Advanced energy storage technologies incorporated within the DC bus of the DSTATCOM, such as ultra-capacitor [1], battery [2] and flywheel systems [3], can be used to increase the short-term voltage controllability in the LCZ. This would allow the provision of *P* and *Q* compensation similar to power conditioning devices. Although ESSs can be used to enhance voltage controllability, the voltage interactions between converter-connected DG and ESS-based DSTATCOM are of concern when they are located in the same LCZ and provide voltage support at the same time.

Another solution to improve decentralised voltage controllability is to use a smart distribution transformer [4],[5], to support active voltage control at the secondary side of the transformer at specific buses in the LCZ. Modern OLTCs, using vacuum switches [6], or power electronic switches [7], can provide on-load voltage controllability to the LV system

with faster control response than that of more conventional mechanical OLTCs. The solid-state transformer (SST) has also been developed to improve power quality in distribution networks [8], and microgrids [9], using power electronics technology [10].

The voltage regulator (VR) aims to be used as the secondary voltage controller to provide slow voltage control over the buses located behind the secondary side of the VR [11] to improve voltage level control along the MV feeder. The modern VR can deal with either voltage drop or voltage rise problems. A coordinated voltage controller between DG and VR is implemented to enhance voltage control, in case the VR is located above the LCZs. In addition, the active voltage controllers in the LCZ, such as DG and ESS, provide the primary voltage support to bus members inside the zone (both short- and long-term). Consequently, the VR will support the slow voltage control when the primary support inside the LCZ is insufficient.

For wide-area voltage control, the coordinated voltage controller between DG and the central voltage controller (e.g. the substation's OLTC) is implemented. Despite many coordination techniques between the substation's OLTC and DG have been proposed for various applications, they are mostly applied for steady-state voltage control rather than dynamic voltage control. This work aims to enhance the real-time voltage control using DG for decentralised dynamic voltage support in the LCZ, while the centralised voltage control from the substation is used as secondary voltage support.

Dynamic models of those voltage controllable devices (apart from converter-connected DG) are implemented in this chapter. The dynamic performance of the coordinated voltage control between DG and other controllable devices is demonstrated via transient simulations. The test system is based on the standard IEEE 33-bus distribution network used in previous chapters. The case studies are examined under different voltage disturbance scenarios including short- and long-term variations depending on the type of voltage controllable devices that cooperate with DG. The results compare the voltage control from DG and other controllable devices with and without coordination.

5.2 Voltage control coordination between DG and energy storage systems

ESSs are installed in specific areas to provide temporary energy supply when the power supplied by the main grid has been lost. Conventional ESSs are designed mainly to inject

active power into the network, which aims to maintain reliability of supply in that area. In this section, ESSs based on the DSTATCOM structure are used to support fast voltage control to bus members inside the LCZ, in addition to the voltage support provided by converter-connected DG. Batteries and ultra-capacitors may be installed in the DC bus of the DSTATCOM to exchange both *P* and *Q* with the MV network. The *P* or *Q* compensation from this type of EESs can provide voltage control to its terminal voltage and the buses nearby similarly to power conditioning devices. However, the time length for supporting voltage control depends on the energy storage capacity.

5.2.1 Modelling of the DSTATCOM-ESS

The model of the proposed integrated DSTATCOM-ESS is adopted from [1],[2]. Figure 5.1(a) shows the basic circuit which consists of the voltage source converter, the coupling step-up transformer, the DC bus capacitor, the buck-boost converter (i.e. DC/DC converter) and the energy storage device (e.g. battery or ultra-capacitor). The buck-boost converter and the energy storage can be modelled as a DC voltage source to simplify the model for transient analysis, as shown in Figure 5.1(b). It can be seen that the DSTATCOM-ESS structure is similar to the VSC-based DG introduced in Section 4.2.1. Therefore, the dynamic model of the DSTATCOM-ESS can be assumed as a VSC-based DG which supplies zero *P* and *Q* to the network during normal conditions.

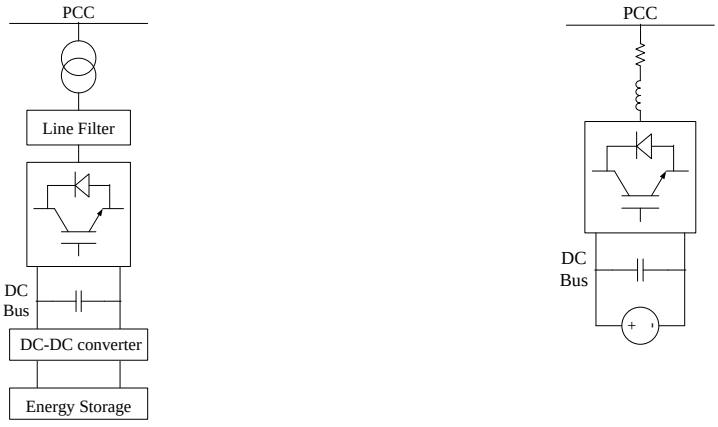

(a) Basic circuit (b) Simplified model

Figure 5.1. Modelling of DSTATCOM integrated with energy storage.

The control outputs of the DSTATCOM-ESS can be *P* and *Q*, AC voltage at the PCC, $V_{ac,}$ and the DC voltage at DC bus, V_{dc}. The sinusoidal voltage output is achieved through

sinusoidal PWM. The VSC controller is developed in the *dq* reference frame (see Section 4.2.4). A constant DC voltage source has been assumed as the energy storage device and buck-boost converter.

The DSTATCOM-ESS can provide voltage support either by *P* or *Q* control. In case *V/Q* compensation is used, the AC voltage controller is added as an optional outer control loop to the *Q* controller. A frequency controller may be connected as an outer control loop to the *P* controller to assist network stability during islanding operation. It is found that the DSTATCOM-ESS structure in this case is similar to the VSC-based DG model (see Figure 4.3 in Section 4.2.3). The *Q* support from the VSC-based DG and the DSTATCOM-ESS at the same time may introduce voltage interactions between them, as examined in Section 4.4. Thus, the coordinated control between DG and the DSTATCOM may be required.

In case that DSTATCOM-ESS is using *V/P* compensation to support voltage control, the AC voltage controller is added as an optional outer control loop of the *P* controller, as illustrated in Figure 5.2. The *Q* controller is set to maintain constant *Q* output.

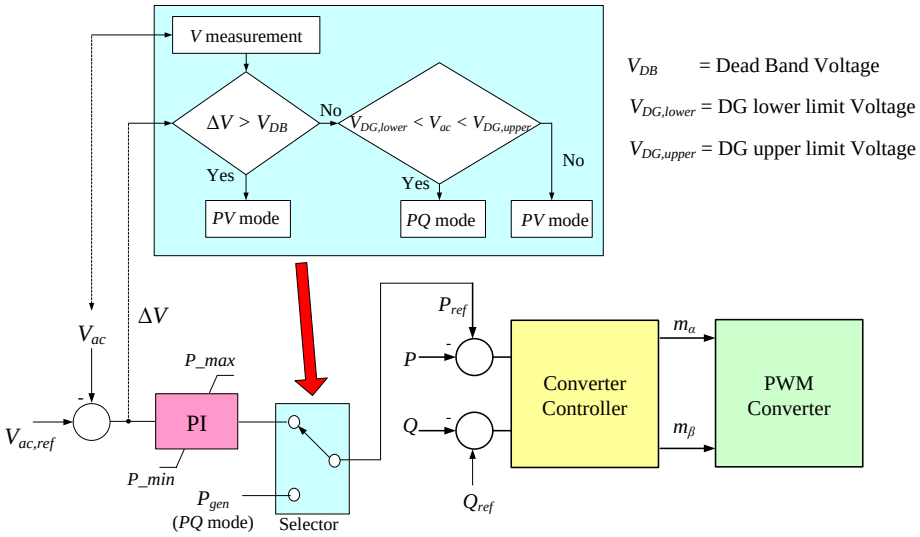

Figure 5.2. Control structure for voltage control by *P* compensation of DSTATCOM-ESS.

5.2.2 Simulations and results

The test system is taken from IEEE 33-bus distribution network with the same network conditions as described in Section 4.3.1. A 1-MW (±1 MVar) converter-connected DG is connected at bus 11 and a DSTATCOM-ESS is connected at bus 17, which is the bus at the end of feeder as shown in Figure 5.3. The size of the DSTATCOM-ESS can be determined

from the *V-P* and *V-Q* curves (see Figure 5.4). It is found that adjusting the *P* output at about 0.13 MW, or *Q* output at about 0.15 MVar can change the voltage level at bus 17 about 0.1 p.u. Therefore, the size of the DSTATCOM-ESS is assumed as 0.4 MVA which can supply either P = ±0.26 MW or Q= ±0.3 MVar into the network (to support voltage compensation approximately ±0.2 p.u.) depending on the voltage controller (e.g. *V/P* or *V/Q* control). The gains of the DSTATCOM-ESS controller are shown in Appendix H.

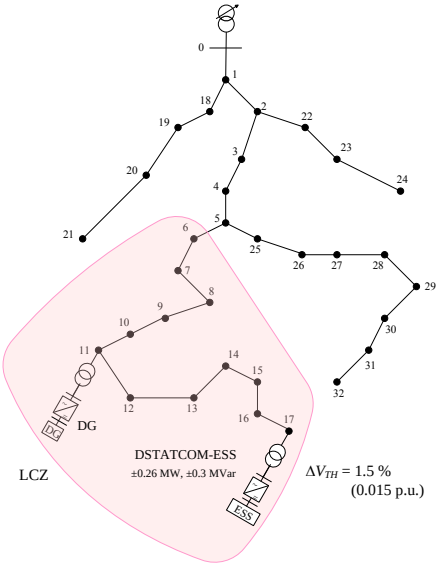

Figure 5.3. Test system for studying the dynamic performances of voltage control by DG and DSTATCOM – ESS.

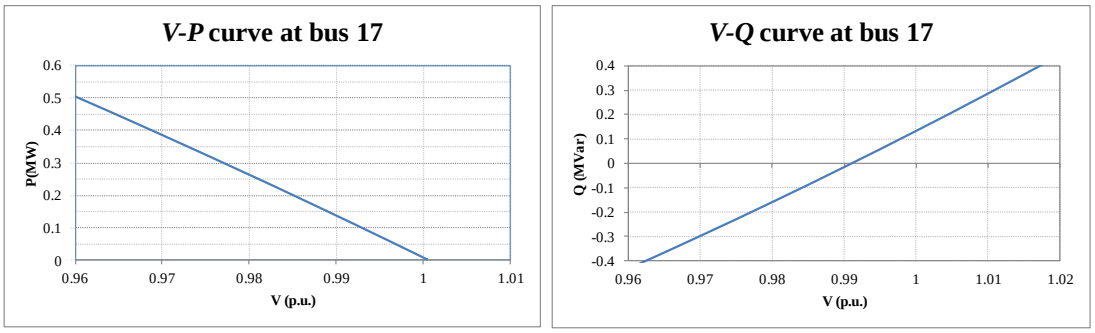

(a) *V-P* curve (b) *V-Q* curve

Figure 5.4. *V-P* curve and *V-Q* curve at bus 17.

The voltage sensitivities from the change of *P* and *Q* at buses 11 and 17 are demonstrated in Figure 5.5. It is found that if the ΔV_{th} is 1.5%, the group of bus members which can receive support from the DG and the DSTATCOM-ESS effectively is defined as the area indicated in Figure 5.3. Furthermore, Figure 5.5 shows that voltage interactions will occur if both buses 11 and 17 inject *P* or *Q* into the network at the same time.

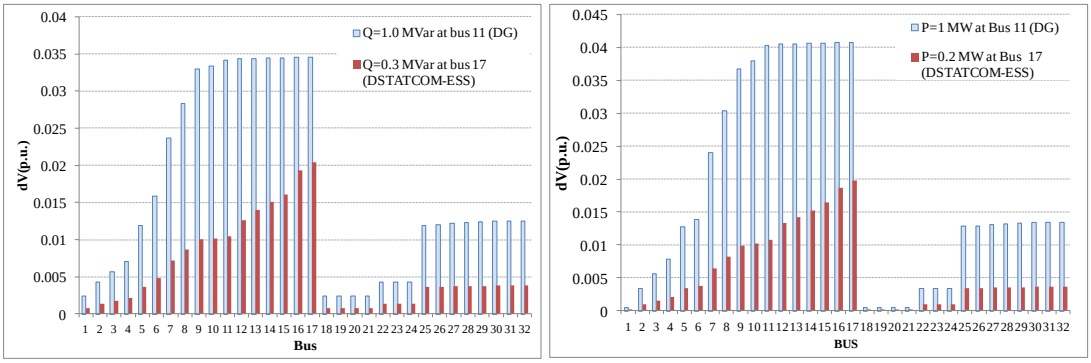

(a) Voltage change from the *Q* injections at buses 11 and 17

(b) Voltage change from the *P* injections at bus 11 and 17

Figure 5.5. Voltage sensitivities from the change of *P* and *Q* at buses 11 and 17.

The transient simulation is examined in the event of a voltage sag by applying a three phase short-circuit through a high impedance in bus 13 in the LCZ, starting at t=0.5 sec and finishing at t=2.0 sec. The overall simulation time is 6 sec. The DG and DSTATCOM-ESS in the LCZ are set to start dynamic voltage compensation when the change of voltage at both DG and DSTATCOM-ESS buses is more than the V_{DB} of ± 1.5 %. The dynamic performance of the DG and DSTATCOM-ESS when providing voltage support in LCZ is analysed in two cases: 1) DG and DSTATCOM-ESS provide *V/Q* compensation, and 2) DG provides *V/Q* compensation while DSTATCOM-ESS provides *V/P* compensation. The results are compared with the base case where only DG provides voltage support.

5.2.2.1 Voltage control by using *Q* compensation of DSTATCOM-ESS

Figure 5.6 shows the *P* and *Q* responses from the DG and DSTATCOM-ESS and the voltage responses at buses 11 and 17. It is found that the coordinated voltage support from DG and DSTATCOM-ESS can improve the voltage level in the LCZ, especially at bus 17, where support from DG only cannot bring the voltage level at bus 17 back within statutory limit (> 0.95 p.u.). In addition, the *Q* support (+0.3 MVar) from the DSTATCOM-ESS can increase the voltage level by 0.02 p.u. which is similar to the value calculated from the *V-Q* curve and voltage sensitivity ratios (see Figure 5.4 and Figure 5.5). However, voltage interactions are observed between DG and DSTATCOM-ESS after the disturbance is cleared as both of them supply *Q* into the network at the same time. The voltage oscillations cause a time delay of about 2 sec in the controllers to restore the voltage back to the steady-state conditions.

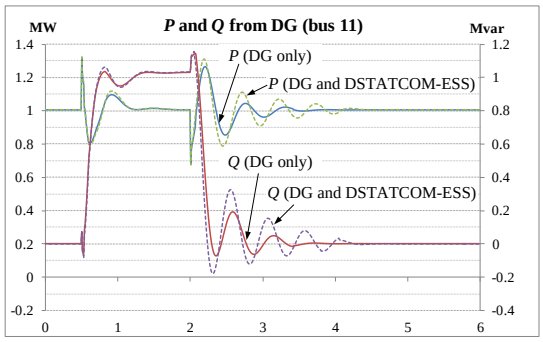

(a) *P* and *Q* from DG

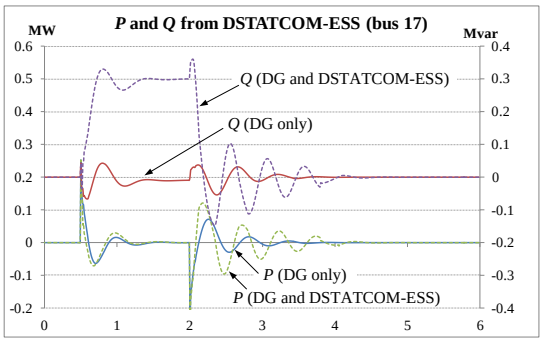

(b) *P* and *Q* from DSTATCOM-ESS

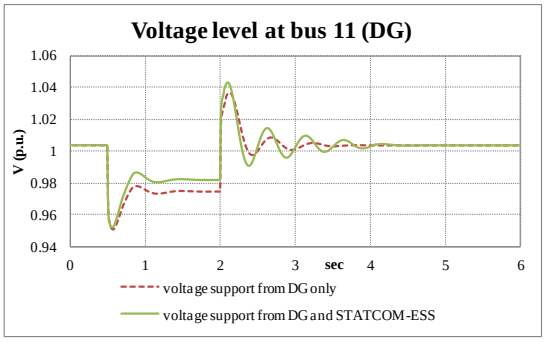

(c) Voltage level at bus 11 (DG bus)

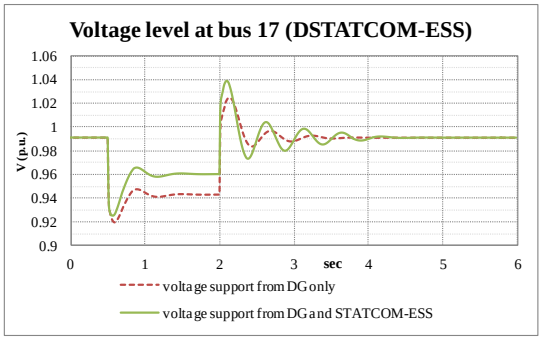

(d) Voltage level at bus 17 (DSTATCOM-ESS bus)

Figure 5.6. Transient simulations of voltage control from DG and DSTATCOM-ESS (both providing *V*/*Q* compensation).

The voltage interactions can be mitigated by using a coordinated voltage controller (with a time delay), or adding a *V*-*Q* droop controller to the VSC controller, as demonstrated in Section 4.5. To keep fast voltage controllability in this case, the *V*-*Q* droop controller is applied to the DG and the DSTATCOM-ESS instead of using a coordinated control technique. The droop controller is designed as a PD controller, as presented in Section 4.5.2, with K_{pq} = 0.01 and K_{dq} = 0.005. Figure 5.7 shows that the *V*-*Q* droop controller can mitigate the level of interaction after the fault is cleared and bringing the controllers back to the normal condition faster.

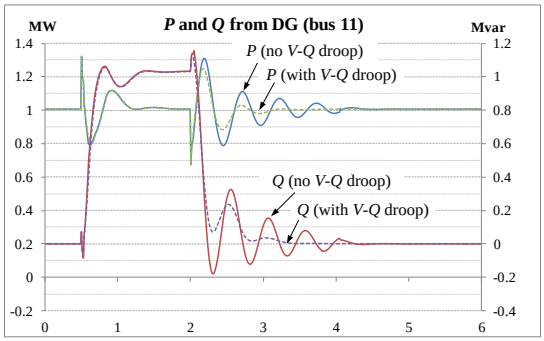

(a) *P* and *Q* from DG

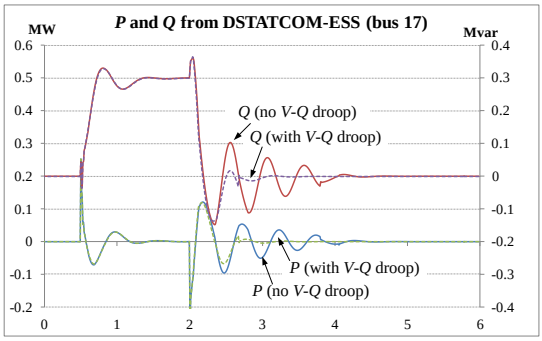

(b) *P* and *Q* from DSTATCOM-ESS

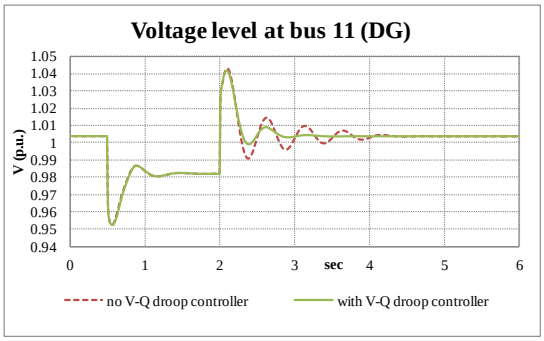

(c) Voltage level at bus 11 (DG bus)

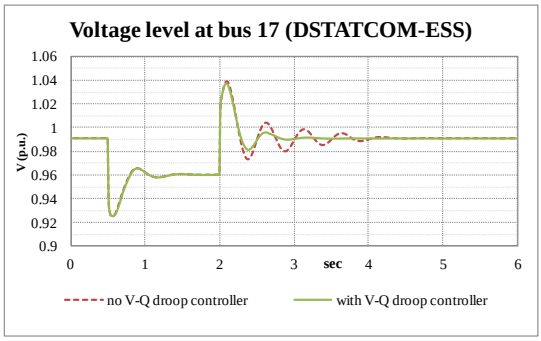

(d) Voltage level at bus 17 (DSTATCOM-ESS bus)

Figure 5.7. Voltage interaction mitigation by using *V-Q* droop controller during voltage control operation from DG and DSTATCOM-ESS (both providing *V/Q* compensation).

5.2.2.2 Voltage control by using *P* compensation of DSTATCOM-ESS

The *P* and *Q* responses from DG and DSTATCOM-ESS and voltage responses at buses 11 and 17 for this case study are shown in Figure 5.8. It is found that the *V/P* compensation from DSTATCOM-ESS can support voltage control in a similar way as when using *V/Q* compensation, as examined in the previous case. Additionally, the extra *P* support (+0.26 MW) from DSTATCOM-ESS can increase the voltage level by 0.02 p.u. which is similar to the value calculated from the *V-P* curve and voltage sensitivity ratios. However, the level of voltage interaction between DG and DSTATCOM-ESS is obviously smaller compared to the case where both DG and DSTATCOM-ESS supply *Q* for voltage control at the same time. This illustrates that the *P* and *Q* controllers of DG and DSTATCOM-ESS are decoupled, and hence, a change of *P* output from DSTATCOM-ESS does not impact significantly the *Q* output from DG. Therefore, the coordinated voltage controller or adding *V-Q* droop controller may be not necessary for this case.

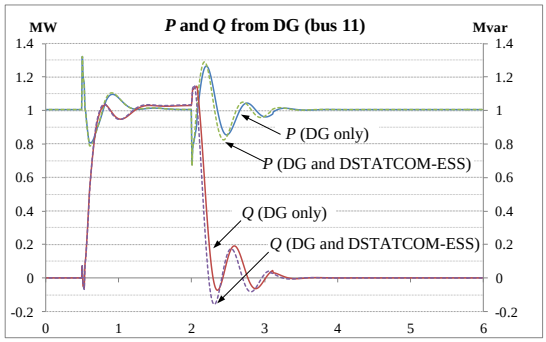

(a) *P* and *Q* from DG

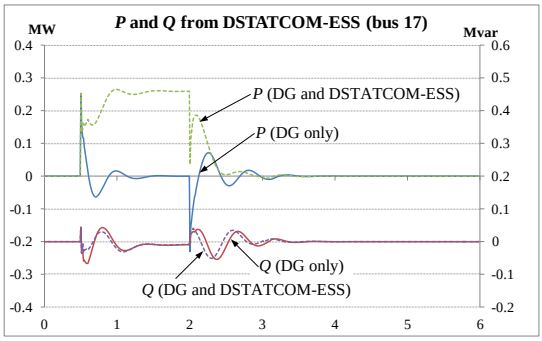

(b) *P* and *Q* from DSTATCOM-ESS

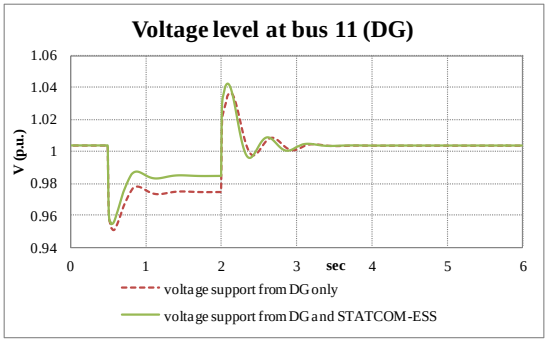

(c) Voltage level at bus 11 (DG bus)

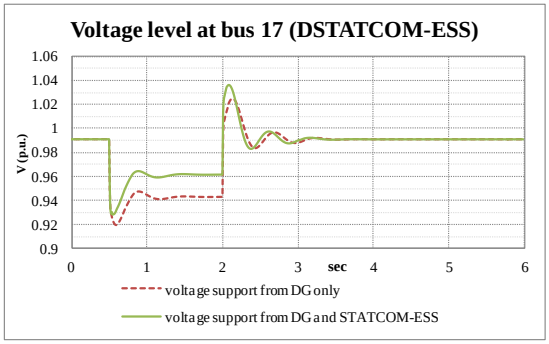

(d) Voltage level at bus 17 (DSTATCOM-ESS bus)

Figure 5.8. Transient simulations of voltage control from DG and DSTATCOM-ESS which are providing *V/Q* compensation and *V/P* compensation, respectively.

5.3 Voltage control coordination between DG and smart on-load tap changer distribution transformer

The smart OLTC distribution transformer supports voltage level control of specific LV networks, such as the bus that connects with sensitive LV loads. The tap position is adjusted after it is found that the voltage level at the LV side of the transformer is not in the allowed limits. Additionally, the voltage level at the LV side is updated by using the voltage tracking system (see Section 4.2.4). The tap position is changed until the voltage level of the LV side is in the statutory boundary, or the tap position reaches the upper or the lower position.

Although the modern OLTC, using vacuum switches [6] or power electronic switches [7], can provide faster control response than the conventional OLTC, the tap changing process, step-by-step, causes a slower voltage control response than that from converter-connected DG. Therefore, the coordinated voltage controller between DG and OLTC distribution transformer is implemented.

5.3.1 Coordinated voltage controller between converter-connected DG and OLTC distribution transformer

The coordinated voltage control structure uses the converter-connected DG to provide fast voltage control inside the LCZ to mitigate short-term voltage variations. Then, the OLTC on distribution transformers operate with a time delay after the converter control, to maintain the voltage level at selected LV buses within the statutory limit, particularly when the voltage support from the DG is not sufficient.

The OLTC aims to control the voltage level of the LV side within the statutory limit, as shown in Figure 5.9. A time delay is introduced in the OLTC operation such that it operates after the converter-connected DG. In addition, the time delay is defined according to the control speed of converter-connected DG, which ensures full DG voltage support before the OLTC starts operating.

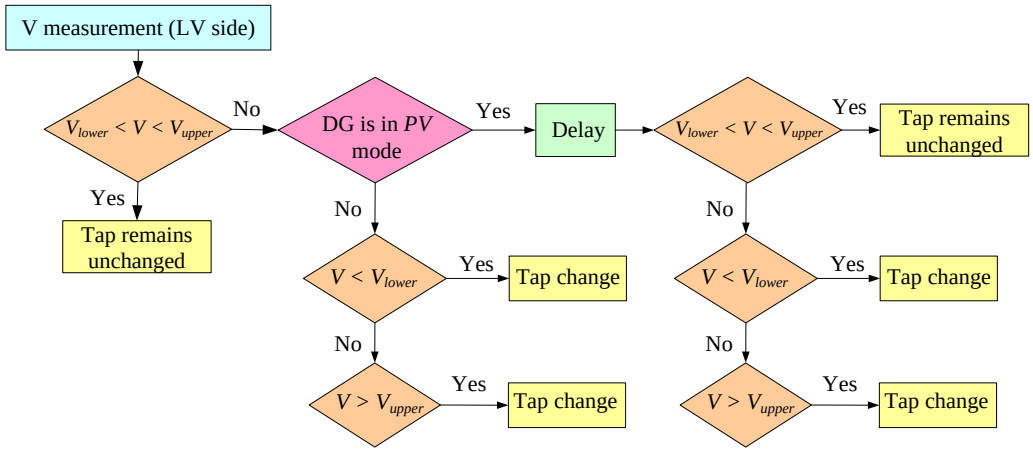

Figure 5.9. Diagram of OLTC control with a time delay.

5.3.2 Simulations and results

The test system is adapted from Section 5.2.2. A 1-MW (±1 MVar) converter-connected DG is connected at bus 11 and an OLTC distribution transformer is connected at bus 17, as shown in Figure 5.10. The OLTC is adopted from [6] which can change the tap position by ±2 taps with a 2.5% voltage change per tap. The voltage measurement at the secondary side of the transformer is updated every 0.5 sec. A relatively fast tap changing process of about 0.1 sec/step is assumed. The tap position will be changed after the voltage level at LV side is

updated and found that the voltage level is staying outside the statutory limits (e.g. between 0.95 and 1.05 p.u.). To coordinate with the DG, the operation of the OLTC is delayed 1 sec to ensure that the voltage support from converter-connected DG is completed, and also to avoid using the OLTC to support a voltage variation of very short duration. The dynamic performance of the coordinated voltage control between the DG and the OLTC distribution transformer is examined in two cases: short- and long-term voltage variations.

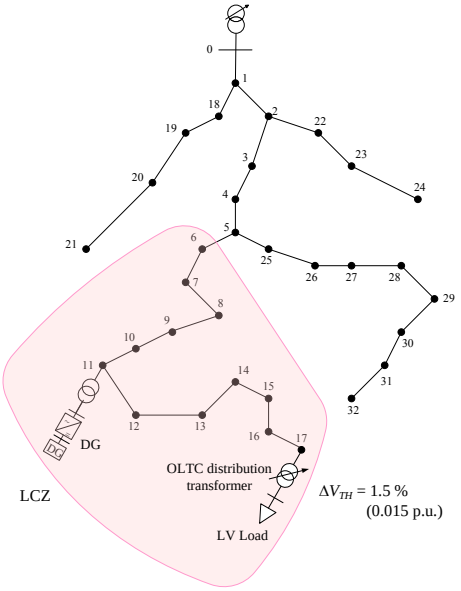

Figure 5.10. Test system for studying the dynamic performances of voltage control by DG and OLTC distribution network.

5.3.2.1 Short-term voltage control

The dynamic performance in the case of short-term voltage variations is examined in the event of a voltage sag by applying a three-phase short-circuit through a high impedance in bus 13, starting at t=0.5 sec and finishing at t=3.0 sec. The overall simulation time is 6 sec. The V_{DB} of DG is set to ±1.5%. The dynamic performance of the DG and OLTC distribution transformer in terms of voltage control is analysed in three cases, including: 1) no voltage support from DG and OLTC, 2) only DG voltage support, and 3) both DG and OLTC provide voltage support.

Figure 5.11 shows the results from transient simulations including voltage level at buses 11 and 17 (primary and secondary sides), the P and Q from the DG unit, and the tap position of the OLTC. It is found that DG is set to take a first responsibility to provide voltage support.

However, voltage support from only DG cannot bring the voltage level at the LV side of bus 17 back into the allowed range (±5%). In consequence, after a delay of 1 sec, the OLTC starts changing the tap position. The tap position needs to step down 2 taps (from 0 to -2) to improve the voltage level at the LV side to above the lower statutory limit (>0.95 p.u.). On the contrary, the voltage level at the primary side of the transformer cannot receive voltage support from the OLTC, so the voltage level is still below the statutory limit and the voltage responses remain unchanged compared to the case where only DG provide voltage support.

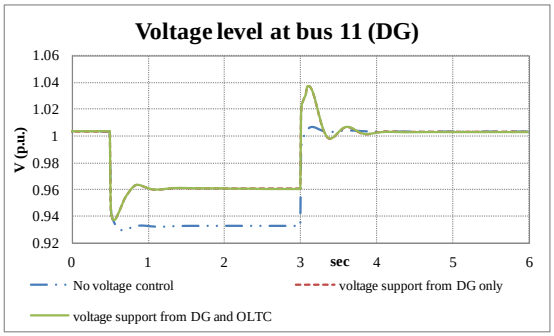

(a) Voltage at bus 11 (DG bus)

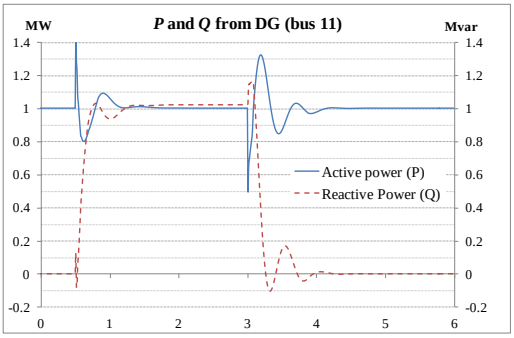

(b) *P* and *Q* from DG

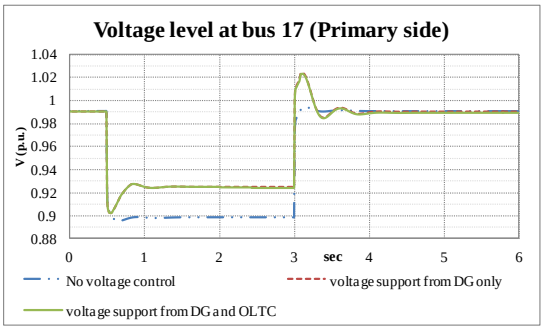

(c) Voltage at bus 17 (primary side)

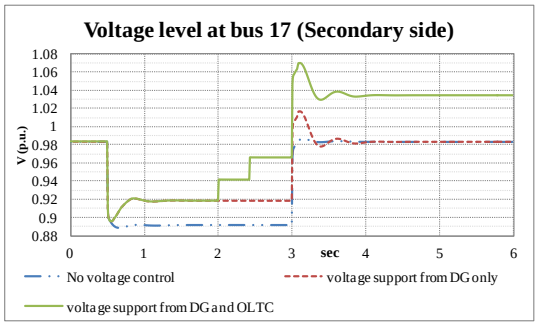

(d) Voltage at bus 17 (secondary side)

Figure 5.11. Results from the coordinated voltage controller between DG and OLTC distribution transformer.

After the fault is cleared, the tap position remains at -2 taps, which causes the voltage level to become higher than before the disturbance had occurred. Although the level of voltage rise from this tap position is not above the upper statutory limit (i.e. 1.05 p.u.), it causes an increase in the power loading of the transformer as shown in Figure 5.12. An optimisation algorithm (i.e. not included in this work), maybe added to the OLTC controller, which can find the optimal tap position that can provide minimum loss whilst maintaining the voltage within allowed limits during the steady-state condition. In this case, it is found that changing the tap to position "0" can give a better performance, the power loading in the transformer is low, and the voltage level is still within the allowed range (see Figure 5.12, after *t*=4 sec and

assuming the tap changing process is 0.6 sec/step). Note that, although adjusting the tap position to "1" can give the lowest power loading, the voltage level is very close to the lower limit.

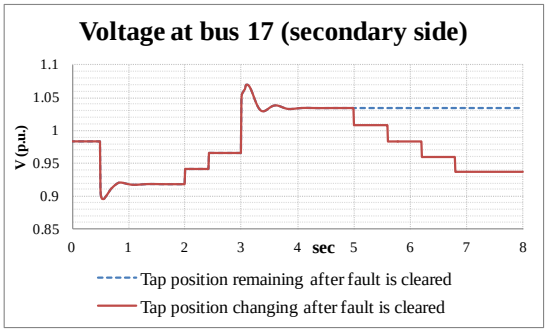

(a) Voltage at bus 17 (secondary side)

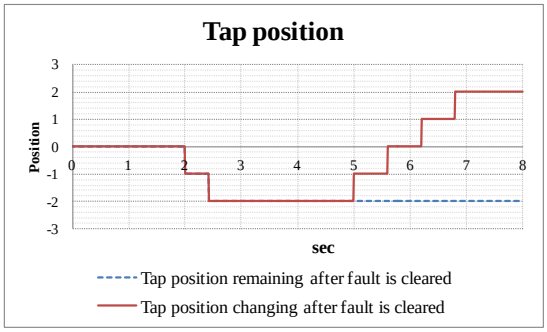

(b) Tap position

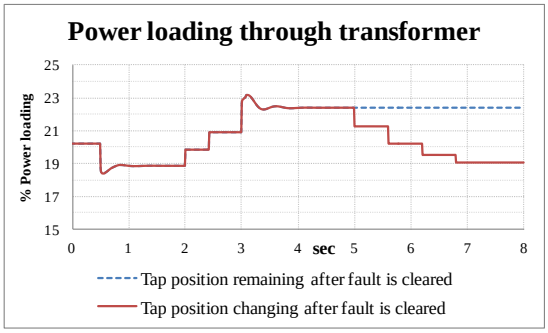

(c) Power loading

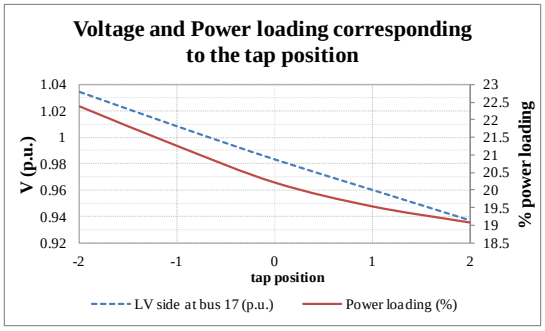

(d) Comparing tap positions with power loading and voltage level

Figure 5.12. Power loading flows through the transformer and voltage level corresponding to the tap position.

It can be seen that the fast tap-changing process of the modern OLTC distribution transformer allows it to deal with short-term voltage variations at the LV side of the transformer effectively. However, the OLTC cannot improve the voltage level at the primary side of transformer. A time delay can be added to operate the OLTC after the converter-connected DG when coordinated control between them is used. The LV side can allow to be operated under slower voltage control because voltage drop level is smaller than the MV. Furthermore, in some Grid Codes, the allowed voltage range of LV network (e.g. ±10%) is looser compared to MV networks (e.g. ±5%).

5.3.2.2 Long term voltage control

The long-term voltage control is examined by applying gradual increase and decrease of the load demand, across the network, as shown in Figure 5.13. The DG will provide voltage support when the voltage level at the PCC is not within the allowed limits, and $V_{DG,\,upper}$ and $V_{DG,lower}$ are set to 1.04 p.u. and 0.96 p.u., respectively. Moreover, the OLTC operates voltage control when the voltage level at the secondary side of the transformer is below 0.95 p.u. or over 1.05 p.u. The OLTC controller will be delayed 1 sec to allow DG to provide voltage support in the first instance. The transient results compare the case where only DG provides voltage support and the case when both DG and OLTC provide voltage support.

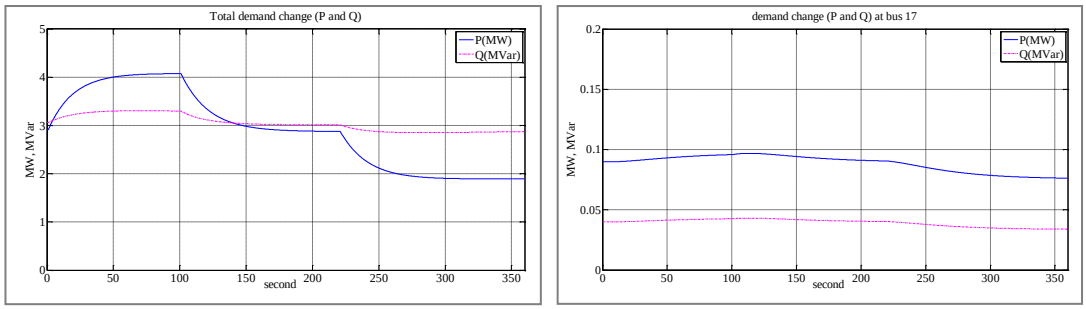

(a) *P* and *Q* of total load demand (b) *P* and *Q* of load demand at bus 17

Figure 5.13. Change of total load demand in case of long-term voltage change.

The voltage level at bus 11 and bus 17 (in the primary side) and the *Q* support from the DG bus are shown in Figure 5.14. The voltage level at the secondary side of transformer and the tap positions of the OLTC are presented in Figure 5.15. The DG starts providing voltage support at t≈20 sec to compensate the voltage drop due to the increase in load demand. It is found that the voltage level at the LV side of the transformer remains outside the allowed limits over some period of time when only DG supports the voltage. The voltage level is lower than 0.95 p.u. during t≈13 sec to t≈120 sec, and nearly above 1.05 p.u. since t≈257 sec.

The results from transient simulations show that the additional support from the OLTC in bus 17 can achieve the voltage level control at the LV side of transformer. The tap-changing process has been operated at t≈21 sec which is after the DG starts to support the voltage. The tap position is stepped down 2 steps, from 0 to -2, to lift up the voltage level when the DG compensation is insufficient. The tap position remains at -2, although the voltage level is back into the allowed range. This can cause a voltage rise at the LV side in bus 17, especially during light load conditions, compared to the case with no voltage support from the OLTC.

Therefore, since $t \approx 248$ sec, the tap position has stepped up 2 steps (from -2 to 0) to control the voltage level back below the upper statutory limit (<1.05 p.u.). It can be seen that the gradual support from DG, in case of long-term voltage control, cannot prevent the voltage at the LV side of the transformer to go below the lower statutory limit (i.e. 0.95 p.u.) during the heavy load demand condition. Hence, the tap changer is operated before the DG provides full *Q* support to the network.

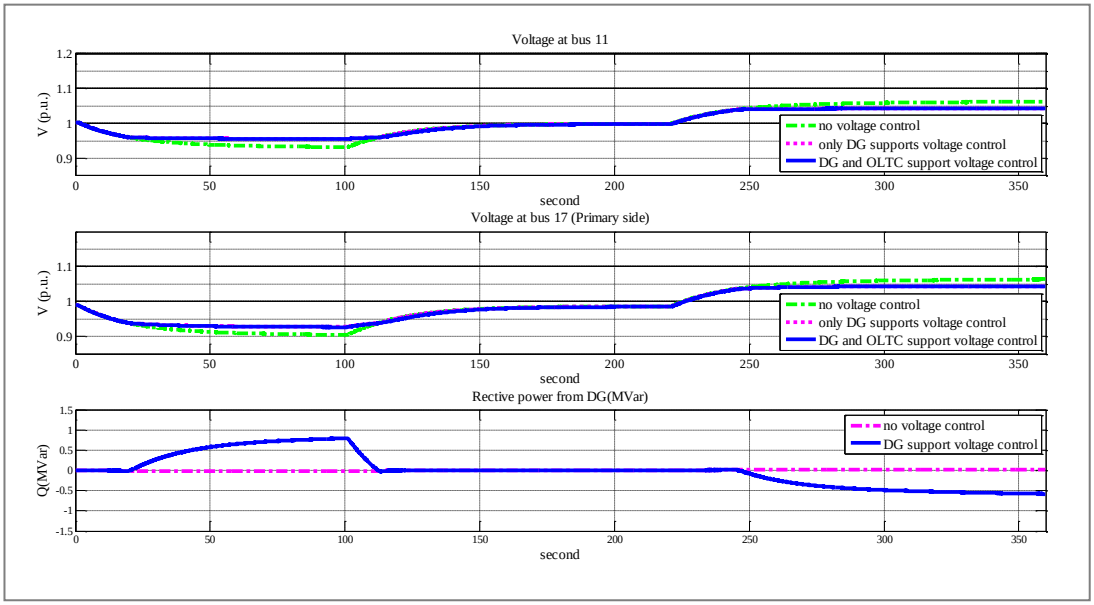

Figure 5.14. Voltage level of buses 11 and 17 (primary side of the transformer) and *Q* support from DG.

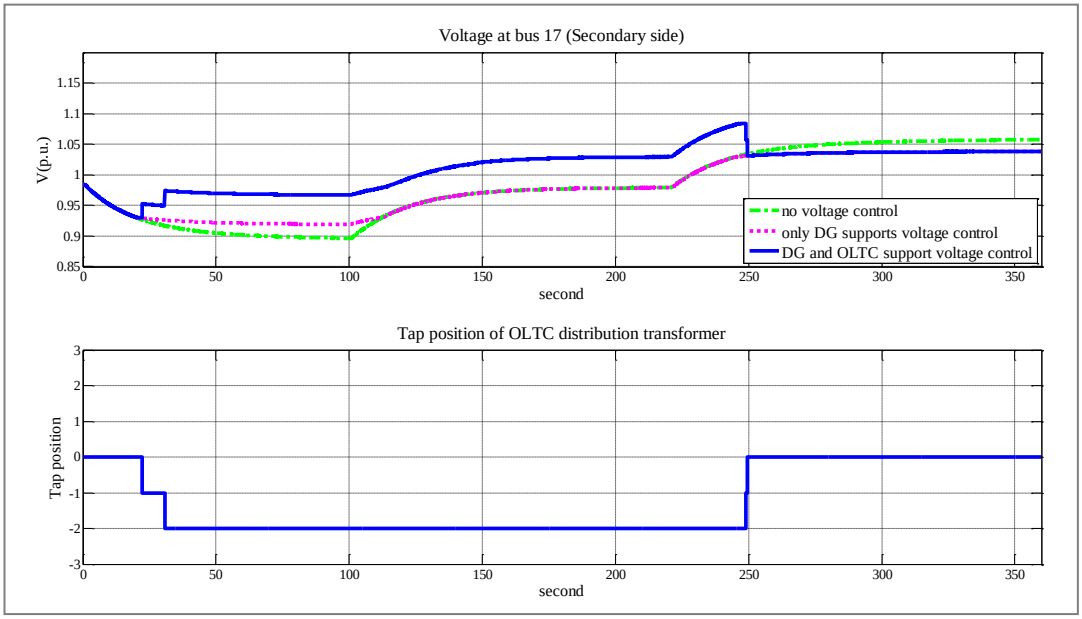

Figure 5.15. Voltage level of LV side of transformer and tap position.

The results illustrate that the coordinated voltage controller can be used to support voltage at specific locations in the LCZ. Despite the OLTC can support voltage only for LV networks, a DG unit with remote controllability can be applied to support the voltage level at the primary side (MV bus) of that transformer.

5.4 Voltage control coordination between DG and solid-state transformer

The SST has been developed to improve power quality and power flow control in the network. Power electronic devices, such as the VSC, are the main control components, which can provide fast voltage control at both MV and LV sides of the transformer.

5.4.1 Modelling of the solid-state transformer

The SST can be used to step up or step down the AC voltage similarly to a conventional transformer. However, power electronic converters and high-frequency transformers are used instead of the traditional 50/60 Hz transformer. The overview of the SST structure is shown in Figure 5.16. It consists of 3 stages including: 1) AC/DC rectifier 2) DC/DC converter and 3) DC/AC inverter [13]. It can be seen that the SST is a back-to-back converter with the DC link regulated by a DC/DC converter [8].

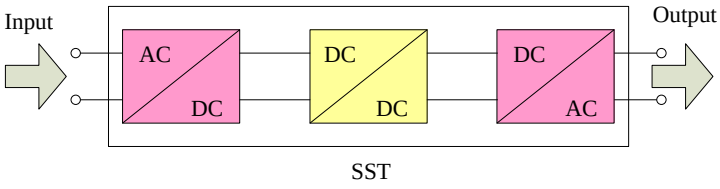

Figure 5.16. Solid state transformer structure.

5.4.1.1 The AC/DC rectifier

The AC/DC rectifier is modelled as the VSC with the shunt DC capacitor to convert a three-phase AC voltage into single-phase DC voltage. The AC voltage control is achieved through the Sinusoidal PWM technique. The rectifier can be operated in 2 modes: 1) power factor control during normal conditions, and 2) active voltage control during voltage disturbances.

In this work, the controller of the rectifier is based on the *dq* reference frame, and consists of two cascaded control loops similar to the VSC controller in Chapter 4. The inner loops control i_d and i_q, and the outer loops are the *P* and *Q* controllers. The AC voltage controller will support voltage control when the level of voltage change is higher than the V_{DB} or the voltage level is outside the allowed limits. Moreover, the DC voltage controller is the outer loop of *P* controller. PI compensators are used in this control system. The control structure of the AC/DC rectifier is shown in Figure 5.17.

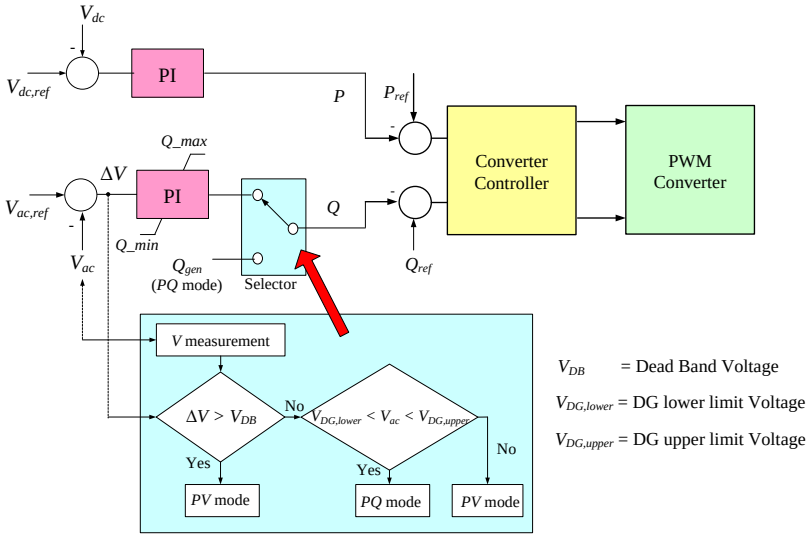

Figure 5.17. Controller of AC/DC rectifier.

5.4.1.2 The DC/AC inverter

The DC/AC inverter is modelled similarly to the AC/DC rectifier with a VSC and shunt DC capacitor. In this work, the controllers of the inverter are designed to control the levels of the input DC voltage and output AC voltage. It consists of two cascaded control loops, where the inner loops are the i_d and i_q controllers, and the outer loops are the DC voltage and AC voltage controllers, as shown in Figure 5.18.

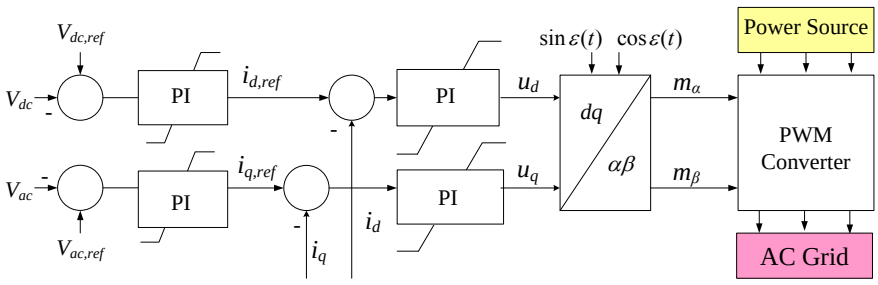

Figure 5.18. Controller of the DC/AC inverter.

5.4.1.3 The DC/DC converter

The DC/DC converter is a buck-boosted converter used to step down or step up the DC voltage at the output side of the SST. The DC/DC converter can be implemented under the dual active bridge structure, which consists of a high-voltage H-bridge, a high-frequency transformer and a low-voltage H-bridge, as shown in Figure 5.19(a) (adopted from [13]). However, to make the model simpler for transient analysis, the conventional buck converter is used to step down the DC voltage (see Figure 5.19(b)), while the DC links, both input and output sides, are controlled by the rectifier and the inverter, respectively. Details of the buck converter based on DIgSILENT Software can be found in [14].

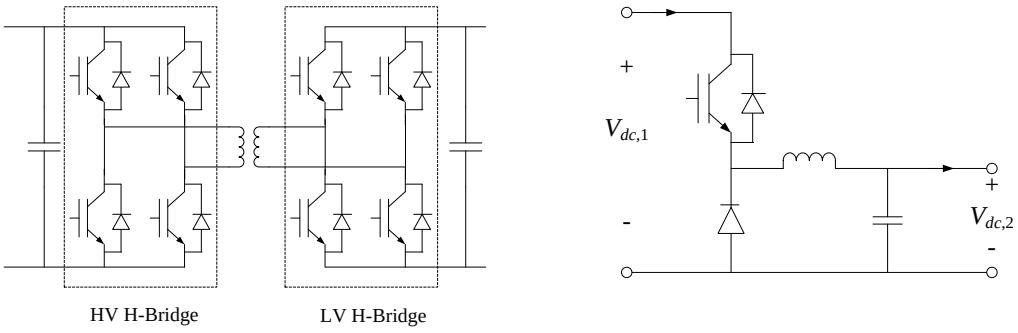

(a) Dual active bridge (b) Buck converter

Figure 5.19. Modelling of the DC/DC converter.

From Figure 5.19(b), the voltage ratio of the DC voltage on the primary side, $V_{dc,1}$, and on the secondary side, $V_{dc,2}$, is defined by

$$\frac{V_{dc,2}}{V_{dc,1}} = \frac{t_{on}}{T_s} \tag{5.1}$$

where $$T_s = t_{on} + t_{off} \tag{5.2}$$

where T_s is the switching period, t_{on} and t_{off} are the time periods when the switch is ON and OFF, respectively.

5.4.2 Simulations and results

The test system is adapted from Figure 5.10 in Section 5.3.2 where a 1-MW (±1 MVar) converter-connected DG is connected at bus 11 and a SST replaces the OLTC distribution transformer at bus 17. The model of the SST in DIgSILENT *PowerFactory* is shown in

Figure 5.20. The parameters of the AC/DC rectifier and the DC/AC inverter are defined following the design guidelines of the VSC presented in Chapter 4. The SST is assumed as 1 MVA to step down the three-phase AC voltage (rms value) from 12.66 kV to 0.44 kV (50 Hz). The rectifier converts the input AC voltage 12.66 kV to 24 kV DC bus. Then, the DC/DC converter steps down the DC voltage from 24 kV to 0.8 kV. The inverter inverts the DC voltage, 0.8 kV, to AC voltage, 0.44 kV. The HV and LV- DC capacitors are 28 μF and 25 mF, respectively. The gain parameters of the SST controllers are given in Appendix H.

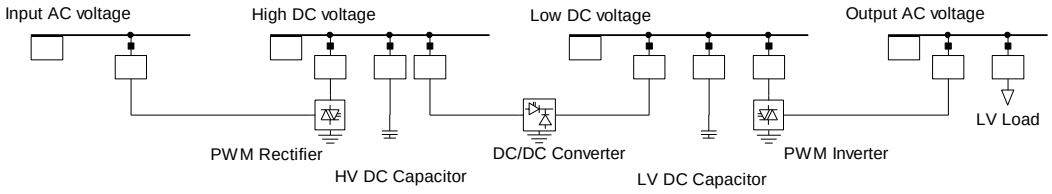

Figure 5.20. Single-line diagram of the SST based on DIgSILENT *PowerFactory*.

The dynamic performance of the coordinated voltage controller between the DG and the SST is examined under both short-term and long-term voltage variations.

5.4.2.1 Short-term voltage control

The dynamic performance in case of short-term voltage variations is examined in the event of a voltage sag by applying a three-phase short-circuit through a high impedance in bus 13, starting at t=0.5 sec and finishing at t=2 sec. The overall simulation time is 6 sec. The V_{DB} of DG and SST is set to ± 1.5%. The rectifier of the SST is allowed to support Q = ±0.5 MVar for voltage compensation. To maintain fast voltage controllability, both DG and SST are allowed to support voltage control at the same time (no time delay between them). The *V*-*Q* droop controller is added to the DG voltage controller to reduce the voltage interactions between the DG and the SST.

The transient results of voltage, P and Q of DG at bus 11, and the input and output AC voltages of SST (bus 17) are shown in Figure 5.21. The P and Q of SST that flow through the rectifier and inverter, and the DC voltages at the HV and LV sides are illustrated in Figure 5.22. Note that the negative power means the converter is absorbing power from the system. It is found that support from DG unit only is insufficient to recover the voltage level at bus 17 (MV) to above the allowed limit (0.95 p.u.). However, the rectifier of SST injects Q=+0.5 MVar can enhance the voltage controllability at this bus, about +0.2 p.u., which can

bring the voltage level of this bus back in the safety limit. The SST voltage control capability can be enhanced by over-sizing the rectifier to increasing the amount of *Q* that can be injected into the network. Figure 5.21(a) and Figure 5.21(b) show that the interactions between the DG and the SST increase when both of them provide voltage support simultaneously.

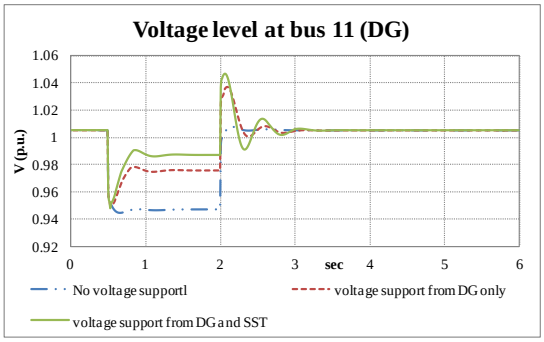

(a) Voltage at bus 11 (DG bus)

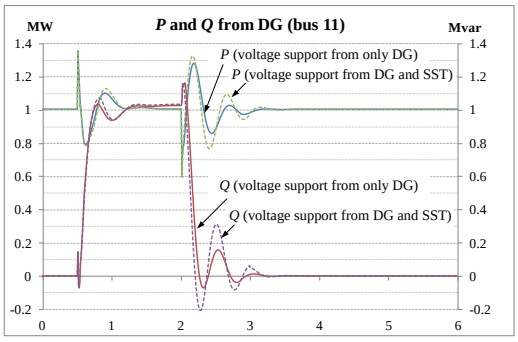

(b) *P* and *Q* from DG

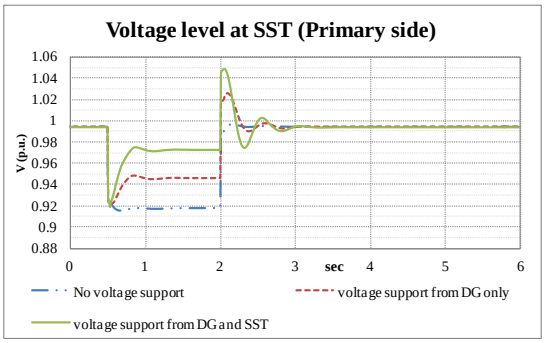

(c) Voltage at the primary side of SST

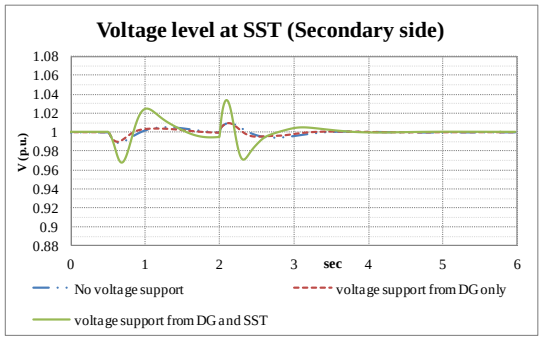

(d) Voltage at the secondary side of SST

Figure 5.21. Voltage levels at buses 11 and 17 and *P* and *Q* from DG unit.

Although the level of the DC voltages at both HV- and LV-DC links is controlled by the DC voltage controllers of the rectifier and inverter, the voltage sag in the network still gives little impact on the variations in the DC voltages at both DC links, as can be seen in Figure 5.22(c) and Figure 5.22(d). Hence, the variation of the DC voltage at the LV side also affects the variation of the output AC voltage at the secondary side of the SST. Despite using the SST to compensate the voltage disturbance causes the increasing of variation of the output AC voltage, the level of voltage change is still within the allowed range, as found in Figure 5.21(d). It is found that the AC voltage controller of the DC/AC inverter keeps the output AC voltage during the disturbance, unlike the conventional transformer where the voltage at the secondary side will change according to the change of voltage at the primary side. It can

be seen that the SST can protect the disturbance from the MV network riding through the LV network.

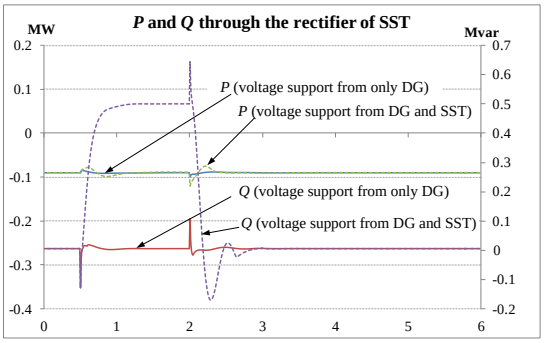

(a) *P* and *Q* through the rectifier

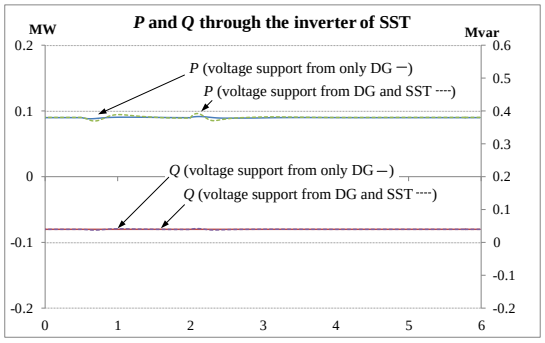

(b) *P* and *Q* through the inverter

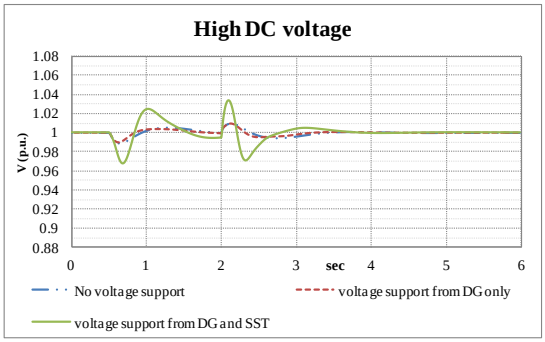

(c) High DC voltage

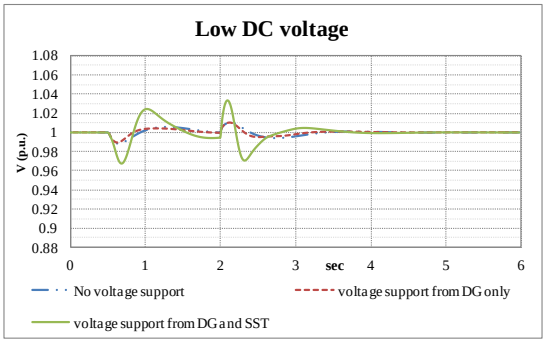

(d) Low DC voltage

Figure 5.22. *P* and *Q* through SST and DC voltages of DC link

5.4.2.2 Long-term voltage control

The long-term voltage control is examined by applying the gradual increasing and decreasing of total load demand, same as in Section 5.3.2.2 (see Figure 5.13). The SST will provide voltage support to the MV bus when the AC voltage at the primary side is below 0.96 p.u. or above 1.04 p.u. The transient results compare between 2 cases: 1) only DG providing voltage support, and 2) both DG and SST providing voltage control.

From transient simulations, the voltage levels at DG bus 11 and the SST (primary and secondary sides of bus 17) are illustrated in Figure 5.23. Figure 5.24 presents the *P* and *Q* support from DG, and the *P* and *Q* flow through the SST. The DC voltages at HV-and LV-DC links are shown in Figure 5.25.

Figure 5.23 shows that the voltage support from DG and the SST rectifier can provide better voltage support especially at the primary side of the SST (i.e. bus 17), compared to the case

where only DG provides voltage support. The SST rectifier injects nearly Q=+0.4 MVar into the MV network, to compensate the voltage drop at bus 17, as found in Figure 5.24. The voltage support from DG and the SST rectifier gives a small impact, in terms of voltage variation, to the voltage levels at the secondary side of the SST and DC links (see Figure 5.25). It is found that there is no much difference between these two cases of voltage support either by using only DG or both DG and SST. In addition, the small voltage variation at the secondary side of the SST is mainly from the change of LV load that connects to this bus, rather than from the change of load demand in MV network.

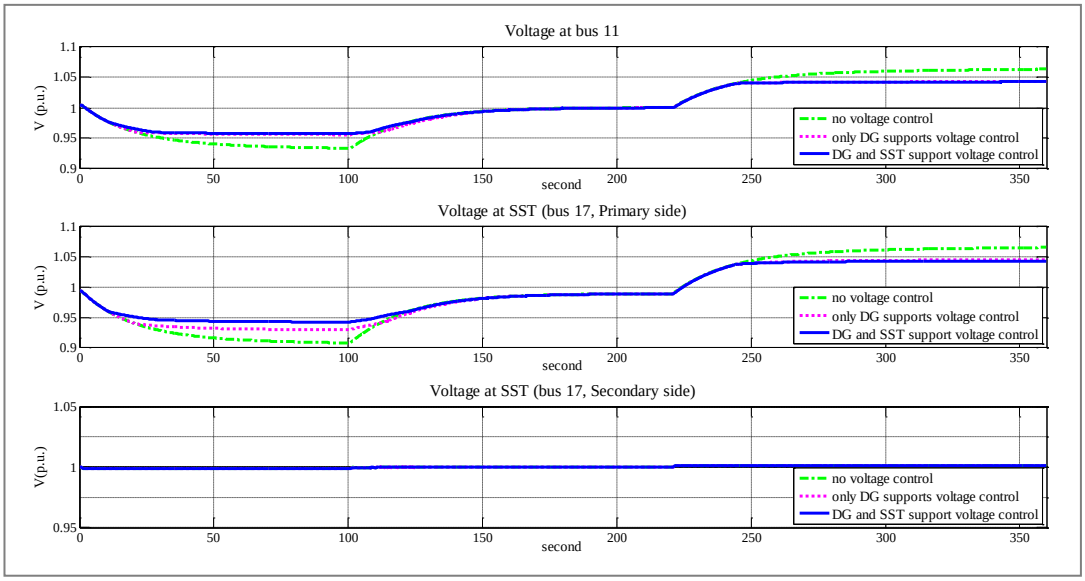

Figure 5.23. Voltages at DG bus and SST buses

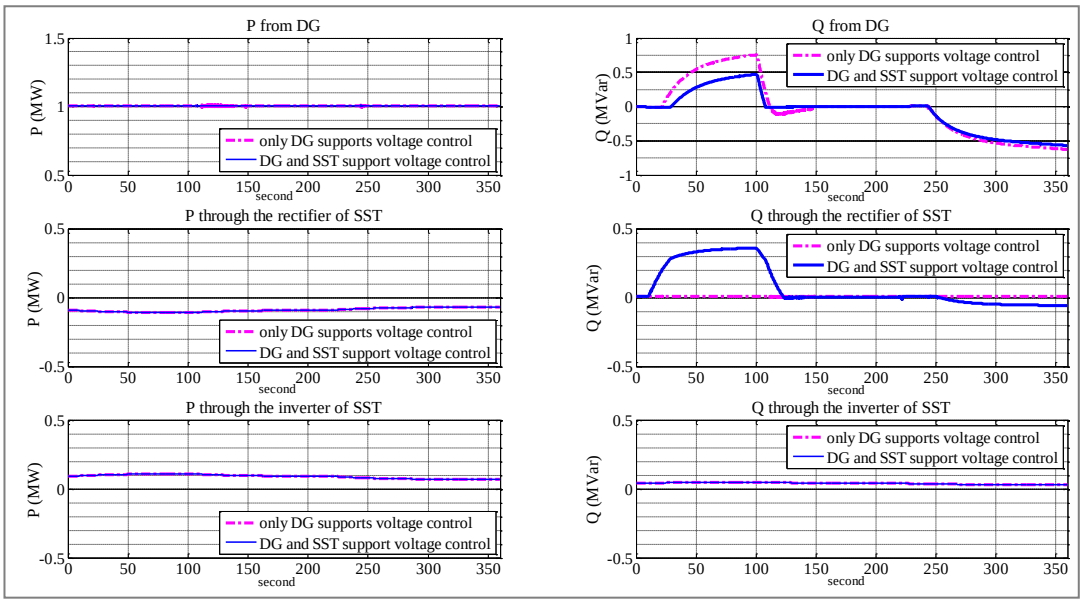

Figure 5.24. *P* and *Q* of DG and *P* and *Q* flow through SST.

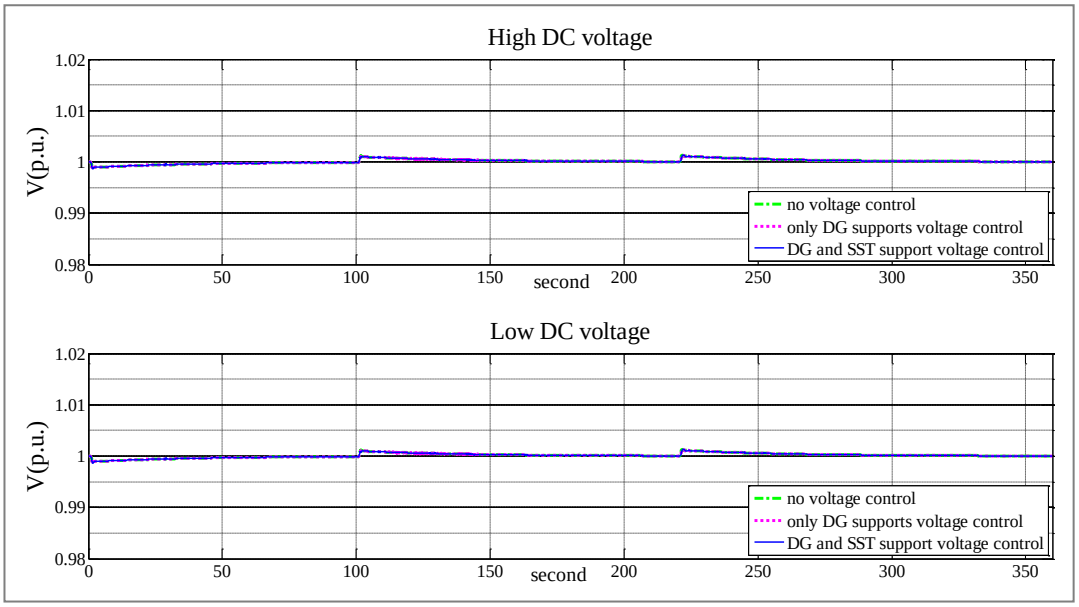

Figure 5.25. DC link voltages of STT

5.5 Voltage control coordination between DG and voltage regulator

In this section, the coordination between DG and VR for voltage level control is introduced. The VR can provide slow voltage support to LCZs connected in the same feeder and located behind the secondary side of the VR. The coordinated controller between DG and VR was already proposed to improve voltage regulation (i.e. steady-state voltage control) in distribution networks [11], [15]. However, in this thesis the coordinated voltage controller is developed with the aim to improve dynamic voltage control.

5.5.1 Coordinated voltage controller between converter-connected DG and voltage regulator

Despite DG can provide voltage control covering the bus members in the LCZ, the limit of DG's *Q* reserve may not be sufficient to rescue the voltage level of some bus members to stay within the statutory boundary. For example, the voltage support from DG is insufficient to compensate the voltage drop of the bus at the end of feeder when the load demand has increased, as found in Section 4.3.3. To enhance voltage controllability, the VR can be used to provide wider voltage control to cover the group of buses located behind that VR. Additionally, those buses include the group of buses that belong to the LCZ and those not

belonging to any LCZ. The VR will provide voltage support by changing the tap position after the DG due to slow speed voltage control from the tap-changing operation. The voltage control structure coordinating DG and VR operation in the distribution network is shown in Figure 5.26.

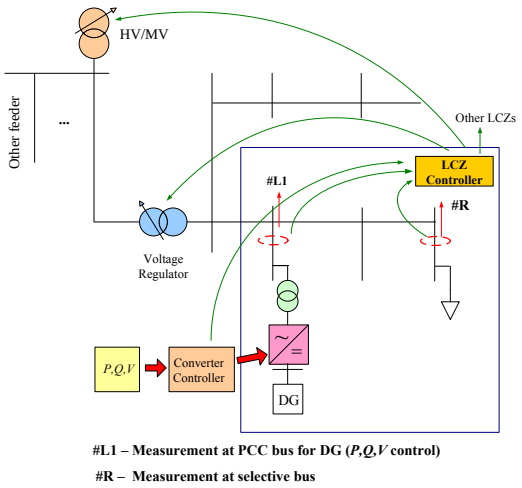

Figure 5.26. Voltage control structure in distribution network with DG and VR.

From Figure 5.26, based on the hierarchical distributed voltage control structure in Section 3.2.2, it can be seen that converter-connected DG provides primary voltage support to bus members in the same LCZ, then VR provides secondary support to specific buses inside that LCZ. Real-time monitoring and control are required to deal with the dynamic voltage variation. The remote measurements from LCZ can be sent to the VR controller via the LCZ controller which is the data concentrator of the LCZ. Additionally, the suggested locations for remote measurements are DG bus and a bus at the end of the feeder [16]. Furthermore, the speed of sensing data from the measuring device to the DG controller should be relatively fast to let DG deal with fast voltage variations whereas the sensing data sent from the LCZ to the VR controller can be slower. The measured data can be transmitted via communication links.

The structure of the VR controller is illustrated in Figure 5.27. Only the group of buses with remote measurements is controlled by the VR. The group of voltage data from remote measurements are compared to find the values of maximum and minimum voltage level (i.e. $V_{re,max}$ and $V_{re,min}$ respectively). Consequently, $V_{re,max}$ and $V_{re,min}$ will be re-checked with the voltage level at the secondary side of the VR. The VR controller allows to adjust the tap only when the voltage level at the secondary side of the VR, V_{VR}, is still within the acceptable range (e.g. 0.95 – 1.05 p.u.) defined as $V_{VR,lower}$ and $V_{VR,upper}$ for lower and upper limits, respectively. Hence the tap position is changed when either $V_{re,max}$ and $V_{re,min}$ is out the

remote voltage control limits, defined as $V_{re,lower}$ and $V_{re,upper}$ to avoid under and over voltage problems. The voltage levels of other buses should not exceed their limit after the tap position of VR is changed. Therefore, the tap will remain unchanged if it is found that hunting between voltage controlled buses has occurred.

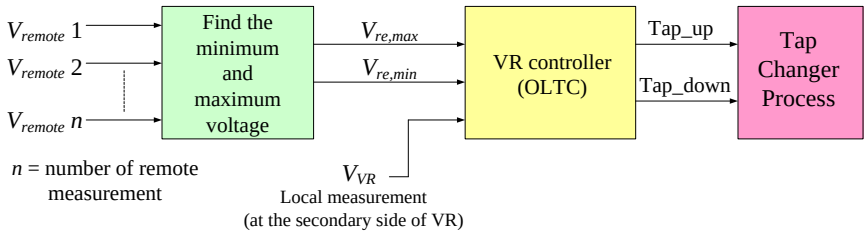

Figure 5.27. VR controller.

The coordinated voltage controller between DG and VR is proposed in two applications depending on the capability of the DG voltage controller: 1) DG cannot provide remote voltage control to other buses and 2) DG has remote voltage controllability.

5.5.1.1 DG cannot provide remote voltage control

In this case, the DG can provide voltage control only at its PCC. Therefore, the voltage compensation from DG may not be adequate to support some buses in the LCZ, especially when those buses are far from the DG unit. The VR will take responsibility to provide wide voltage control and cover those buses by using the data from remote measurements of specific locations in the LCZ. Only slow voltage variations can receive the voltage support from VR. Furthermore, the slow sensing data and the control operation of VR cause it to provide voltage support normally after the DG. A delay time may be added to the VR controller to ensure that DG already supports voltage control into the LCZ and to prevent the VR from supporting short-term voltage variations. However, the VR may not wait until DG support Q reaches the reserve capacity (i.e. $Q = \pm Q_{res}$)

The coordination between DG and VR is implemented by defining the gap between voltage control limits, as shown in (5.3) and (5.4). The gap between the voltage limits of DG and VR should be wide enough to allow the Q compensation from DG to reach its reserve capacity or be used as much as possible, before the VR start the voltage control process.

$$V_{DG,lower} > V_{re,lower} > V_{stat,lower} \quad (5.3)$$

$$V_{DG,upper} < V_{re,upper} < V_{stat,upper} \quad (5.4)$$

where $V_{DG,lower}$ and $V_{DG,upper}$ are the lower and upper limits of DG voltage control. $V_{stat,lower}$ and $V_{stat,upper}$ are the lower and upper statutory voltage limits, established by Grid Codes.

5.5.1.2 DG can provide remote voltage control

In case that DG can provide remote voltage control to other buses, apart from its PCC, the VR can wait until DG provides *Q* support and reaches its reserve capacity. The remote control from DG is expected to reduce the voltage support from VR which can save the number of changing tap position. The main idea of coordinated voltage control in this case is illustrated in Figure 5.28. The margin gap between voltage control limits is still applied in this coordination approach to avoid the hunting between DG and VR.

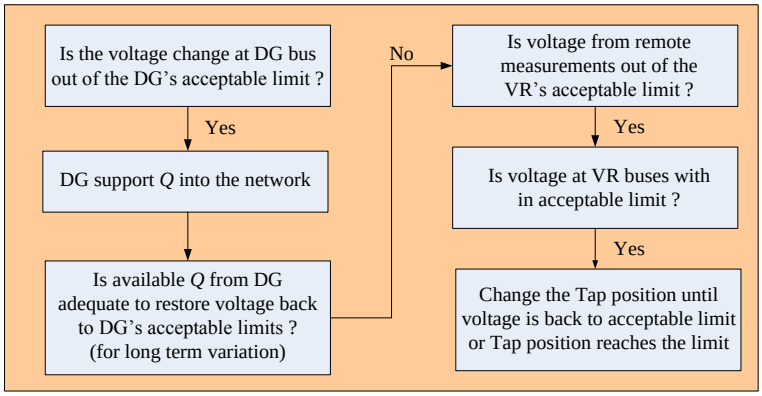

Figure 5.28. Diagram of the coordinated voltage controller between VR and DG with remote controllability.

5.5.2 Simulations and results

The test system is adapted from the IEEE 33-bus distribution network with the same network condition as described in Section 4.3.1. A 1-MW (±1 MVar) converter-connected DG is connected at bus 11 and a VR is connected between buses 5 and 6. The remote measurements are assumed to be installed at a DG bus (bus 11) and at a bus at the end of feeder (bus 17). The measured data is sent to the VR controller by communication system via LCZ controller. The test system in this case is shown in Figure 5.29.

The VR controller scans the information from local and remote measurements every 2 sec while the DG voltage controller scans in every 0.5 second. The VR is designed as "straight

(or type A)" structure with the tap changer on the primary side of the VR [15]. The VR's OLTC has ±8 taps which give a 1.25 % voltage change per tap. The time delay for changing the tap position in each step is assumed to be 10 sec. In addition, the length of time delay is shorter than the recommendation (i.e. 15 sec.) in [17] to make the voltage control response fit to the length of the simulation time window (i.e. 360 sec). To coordinate the voltage controller between DG and VR, the margin gap between voltage control limits of DG and VR is introduced, as shown in Figure 5.30. Both DG and VR are not providing voltage support when the voltage level is in the safety voltage range. The DG starts providing voltage control when the voltage level at its PCC or remote bus is above $V_{DG,upper}$ or below $V_{DG,lower}$. Similarly, the VR provides voltage support when the voltage level of the remote location is above $V_{re,upper}$ or below $V_{re,lower}$. A time delay of 5 sec is added to the VR controller to prevent it from providing short-term voltage support.

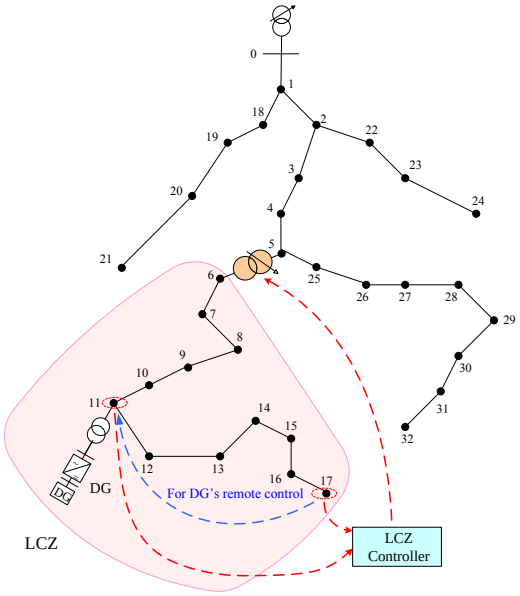

Figure 5.29. Test system for studying the dynamic performances of voltage control by DG and VR.

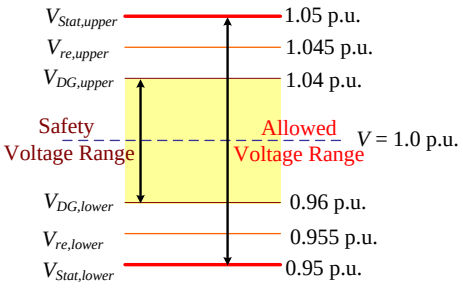

Figure 5.30. Coordinated voltage control limits between DG and VR to preventing the voltage level of the controlled bus to go out of the statutory limits.

The dynamic performance of the coordinated controller strategy between DG and VR is examined based on the slow voltage variations by applying a gradual increasing and decreasing total load demand as in Section 5.3.2.2 (see Figure 5.13). The transient simulations of the coordinated voltage controller aim to study two different cases: 1) VR cooperates with DG with no remote controllability, and 2) VR cooperates with DG to provide remote control to bus 17.

5.5.2.1 DG without remote voltage control and voltage regulator

Figure 5.31 shows the key results from transient simulations which consists of voltage level at buses 11, 17 and the secondary side of VR. The *Q* support from DG and tap position of VR is illustrated in Figure 5.32. It is found that, during the heavy loading condition (voltage level is decreasing), the *Q* support from DG can compensate the voltage level at its PCC (bus 11) successfully, whereas the voltage level at the end of the feeder (bus 17) is still below the lower statutory limit (<0.95 p.u.). The VR can operate as the secondary support to the LCZ including buses 11 and 17 by changing the tap position to adjust the voltage level of its secondary side. The slow data scanning and coordination of voltage limits among DG and VR cause the VR to start the control operation behind the DG. Then, the VR starts to operate at $t \approx 26$ sec, while DG starts to support voltage from $t \approx 20$ sec.

The tap position of the VR will change 5 steps (from 0 to -5) to bring the voltage at bus 17 back within statutory limits, as can be seen in Figure 5.32. The voltage level at bus 17 returns back to the statutory range from $t \approx 62$ sec. However, the tap position remains unchanged despite the network is back to normal condition. The impact of this unchanged tapping can result in the voltage at the secondary side of VR rising above the upper statutory limit (>1.05 p.u.) and then requiring the tap position to be stepped up 1 step, at $t \approx 143$ sec, to reduce the voltage level at this bus. Furthermore, the tap position steps up 3 steps (from -4 to -1), starting at $t \approx 252$ sec, to mitigate the voltage rise problem that occurs at bus 11 during the light load condition. The overall tap changing, both step up and step down, in this case, is 9 steps.

From Figure 5.32, it is observed that the tap changing of VR affects the *Q* support from DG. When the tap position is changed, during the heavy load condition, it also lifts the voltage level at bus 11 up above the $V_{DG,lower}$, causing the DG stops to support *Q* into the network. Hence, the voltages at buses 11 and 17 slightly drop suddenly, so the DG needs to inject *Q* into the network again until the tap of VR is changed to the new position. Then, the *Q*

compensation from DG is stopped and the voltage control is then mainly from the tap changer operation of VR. It can be seen that interactions between the control operation of VR and DG in this case impact on the increasing of tap changing process because DG cannot provide full voltage support before the VR start operating. The hunting between DG and VR can be mitigated by adding remote controllability in DG to support the bus at the end of the feeder (bus 17), as demonstrated in the next section.

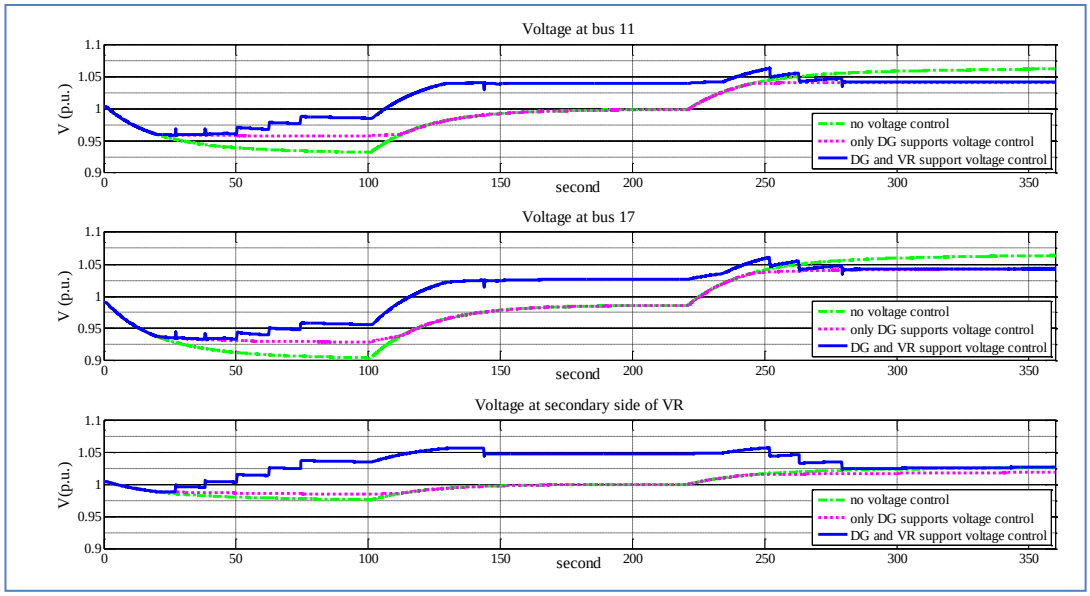

Figure 5.31. Voltage at DG bus and at the end of the feeder in case that DG has no remote controllability.

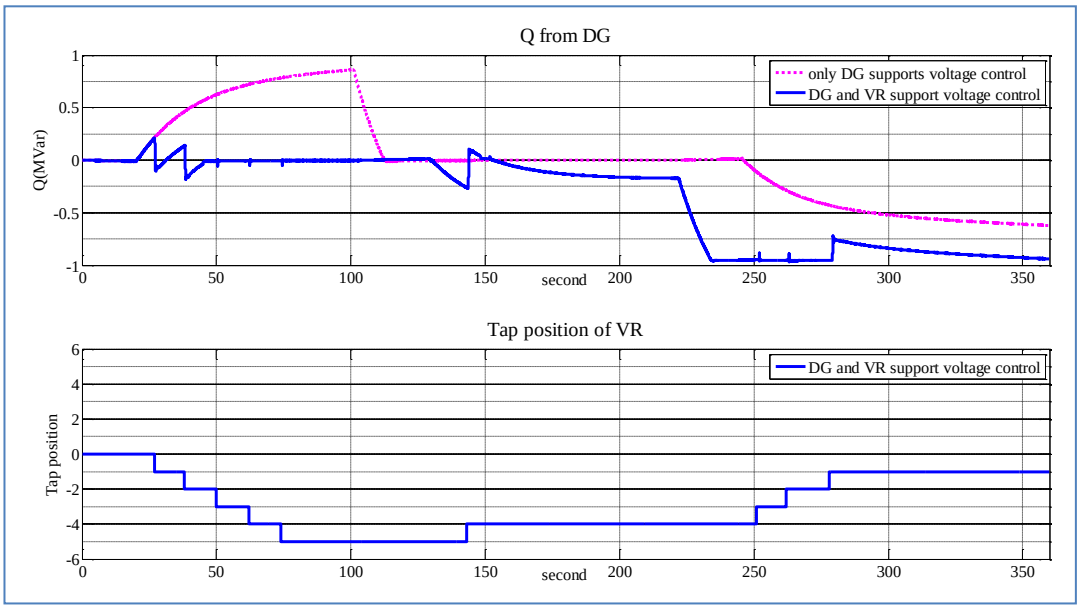

Figure 5.32. *Q* support from DG and tap position of VR in case that DG has no remote controllability.

5.5.2.2 DG with remote voltage control and voltage regulator

The DG with remote voltage control can provide voltage control at bus 17, apart from its PCC, and is used in coordination with the VR. It aims to reduce the controller hunting between DG and VR by allowing DG to provide *Q* support fully before the VR starts supporting the secondary voltage control. Meanwhile, the number of tap changing operations should be reduced. The model of DG with remote control is adopted from Section 4.3.5. The simulation results are compared with the previous case where DG has no remote voltage control capabilities.

Figure 5.33 shows the voltage level at buses 11 and 17 and the secondary side of the VR. It is found that using DG to support voltage control directly to bus 17 gives a better voltage control performance compared to the case where DG has no remote controllability. The DG changes to support voltage bus 17 from $t \approx 9$ sec when it starts to support voltage faster than the previous case. Moreover, DG can provide *Q* support until reaching the maximum *Q* reserve capacity (+1 MVar) before VR starts to support voltage control, as can be seen in Figure 5.34. In consequence, the VR will start to operate at $t \approx 45$ sec after the support from DG is insufficient. With fully *Q* compensation from DG to bus 17, it can reduce the number of tap changing operations from 9 steps, in the previous case, to 5 steps. Furthermore, it is found that the voltage rise problem from the tap remaining unchanged after stepping down to prevent the under voltage does not occur in this case.

It can be seen that the coordinated voltage controller between VR and DG with remote controllability can provide better voltage control performances and the voltage level can remain within the statutory limits (0.95 p.u. – 1.05 p.u.) almost all the time. Furthermore, the support from the VR is reduced which can extend the life time of tap changer and reduce maintenance costs. However, a communication link between DG and remote bus is required.

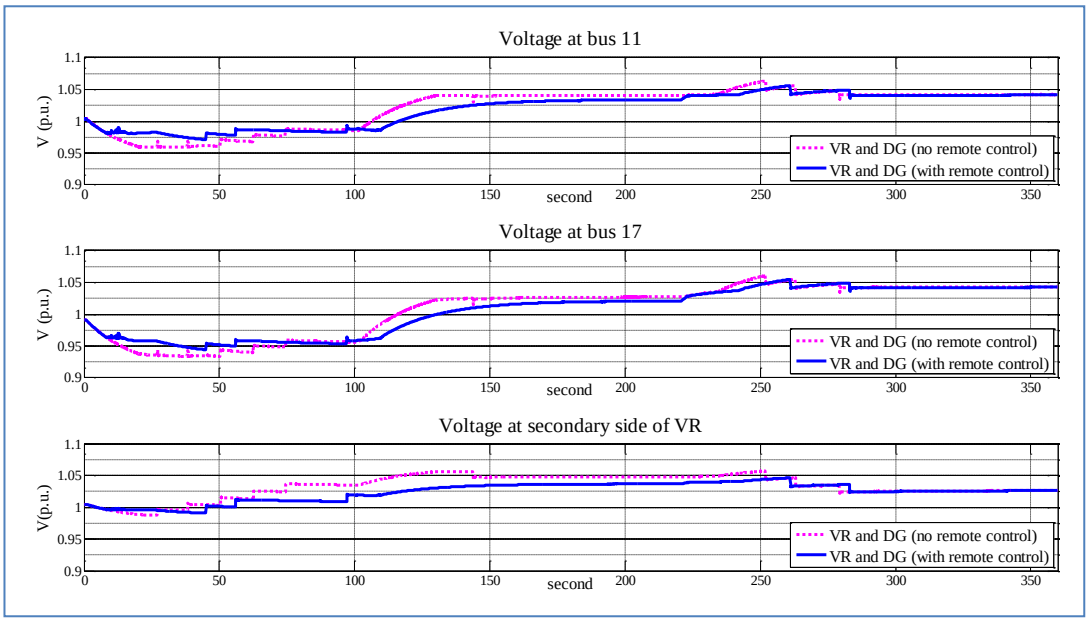

Figure 5.33. Voltage at DG bus and at the end of feeder in case that DG has remote controllability.

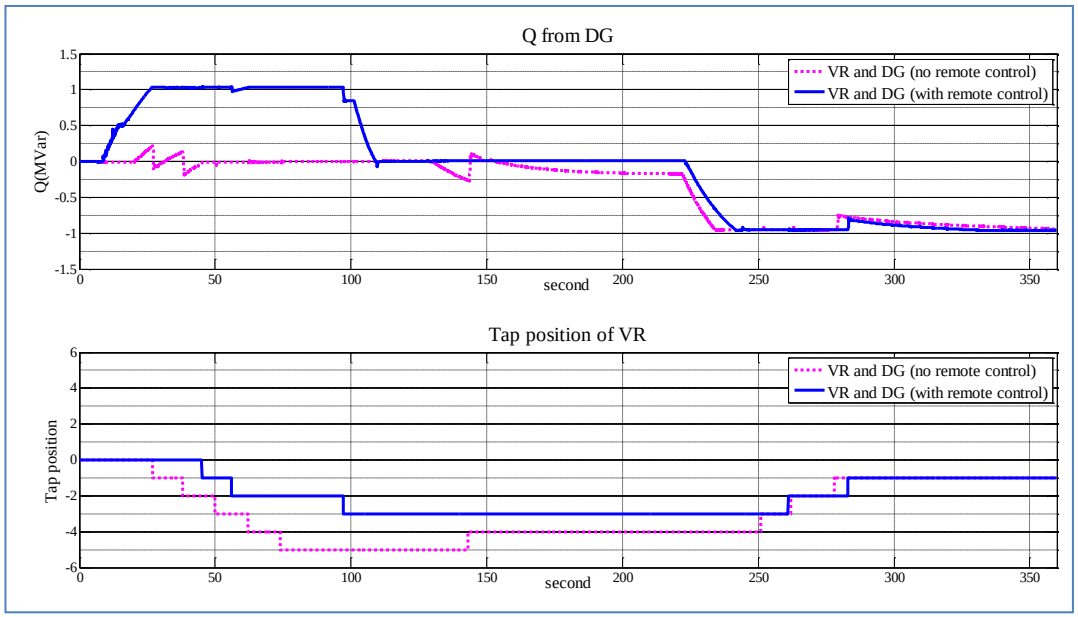

Figure 5.34. *Q* support from DG and tap position of VR in case that DG has remote controllability.

5.6 Voltage control coordination between DG and on-load tap changer substation transformer

The substation's OLTC is the central voltage controller that can provide wide-area voltage support to the distribution network. In addition, the changing of tap position at the substation impacts on the voltage level to all feeders which connect to the same substation. The coordinated voltage controller is required when the group of distributed voltage controllers such as DG is installed in the network to enhance voltage controllability and to avoid the hunting effect that can occurs by the interaction between DG and the substation's OLTC. From the review in Chapter 1, many coordinated voltage controller between these two devices have been developed for steady-state voltage control. Nonetheless, this work proposes the coordinated control structure for dynamic voltage control.

In this section, the structure of coordinated controller strategy between DG and the substation's OLTC aimed for dynamic voltage control is explained. Furthermore, the dynamic performance of the proposed coordinated voltage control is demonstrated based on transient simulations.

5.6.1 Substation's OLTC Controller

The OLTC controller is included in the central control, at the substation, which can provide the automatic long-term voltage control for the whole network. Voltage levels are monitored through local measurement (at its substation) and remote measurements. The data from remote measurements are sent to the controller via a wide-area communication system. The scanning time from all measuring devices takes several seconds which depend on the speed of communication links. Moreover, the time delay for changing the tap in each step is approximately 10 – 30 seconds [16].

The OLTC's controller is illustrated in Figure 5.35. The voltages from remote measurements across the network are compared to find the values of maximum and minimum voltage level ($V_{re,max}$ and $V_{re,min}$, respectively) from specific areas in the network, where only the group of buses with remote measurements is controlled by the substation's OLTC. $V_{re,min}$ and $V_{re,max}$ will be re-checked with the voltage level at the substation. The controller allows to change the tap only if the voltage level at substation (V_{sub}) is still within its acceptable limit (i.e. $V_{sub,lower}$ and $V_{sub,upper}$), which $V_{sub,lower}$ is normally 1.0 p.u. to avoid voltage drop along the

feeder. Hence, the tap position is changed when either $V_{re,min}$ or $V_{re,max}$ is not staying in the OLTC's voltage control limits (i.e. $V_{OLTC,lower}$ and $V_{OLTC,upper}$).

The hunting among remote controllable buses needs to be observed as other buses should not exceed its limit after the tap position is changed. The flowchart of the tap changer operation is shown in Figure 5.36. In addition, the hunting detector is explained in Appendix I.

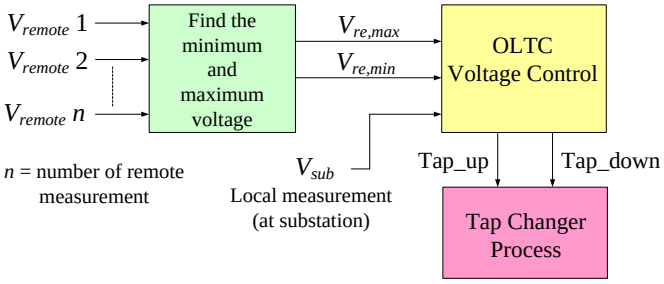

Figure 5.35. Substation's OLTC controller.

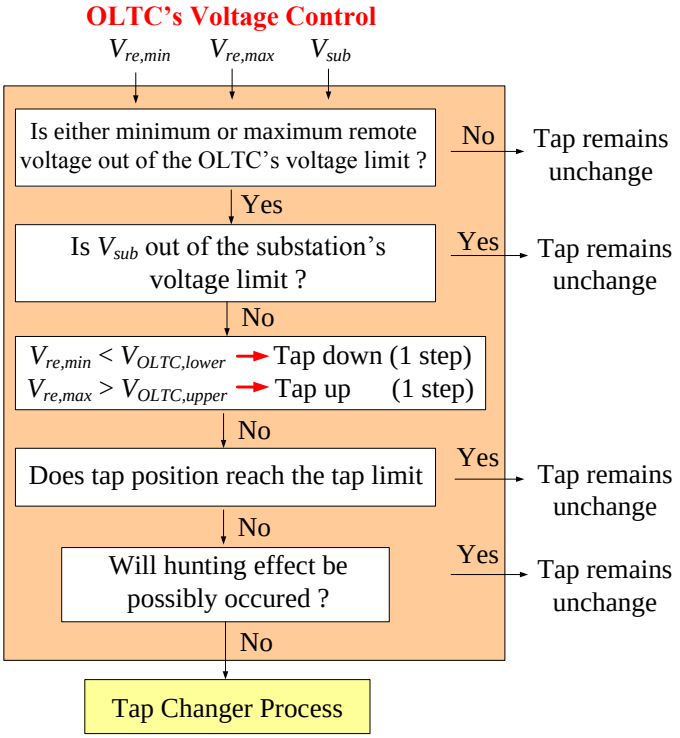

Figure 5.36. Flowchart diagram of the tap changer operation.

5.6.2 Coordinated voltage controller among DG and OLTC Substation Transformer

In this work, the coordinated voltage controller between DG and substation's OLTC is built for real-time voltage control. It is implemented to deal with the voltage change automatically; particularly short- and long-term variations, during the gap of the routine voltage regulation operation (see Figure 1.1 in Section 1.2.1). The coordinated manner is developed based on the hierarchical distributed voltage control structure presented in Section 3.2.2 which is using DG for decentralised dynamic voltage support in the LCZ. Similar to VR, the OLTC substation transformer is the secondary voltage support providing the slower voltage control if it is detected that primary voltage support inside the zone is not sufficient. However, the area that can receive the voltage support from the substation's OLTC is wider than VR, where the other bus voltages should not exceed its limit after the tap changing operation. This effect may lead the OLTC cannot stop the tap changing operation [18].

Real-time monitoring and control are required to deal with dynamic variations. The suggested locations for remote measurements are the controllable DG bus and the outermost bus of the feeder. The process of coordinated voltage controller between DG and OLTC substation transformer is as follows;

1. (start the control cycle) The new set points for all controllable DG and OLTC are determined by the central controller at the substation to optimise the voltage profile, and other issues such as loss minimisation.
2. Update DG and OLTC operations following the new set-points received from the central controller (substation).
3. The voltage changes inside the LCZ will affect directly the DG bus in that zone due to the impact of voltage sensitivity. DG can deal with fast and slow voltage changes, (i.e. from short circuit and load changes respectively). The main voltage support of DG is from supplying *Q*.
4. If *Q* support from DG is insufficient in case of long-term voltage changes, the substation's OLTC can support voltage control by changing the tap position. However, the control response is relatively slow due to time delays which are from voltage scanning and the tap changing process.
5. Buses located outside the LCZ, which DG cannot support, can receive voltage support directly from the substation's OLTC, if there are remote measurements installed.
6. For steady-state voltage regulation, the minimum *Q* of DG is recommended to let DG have enough room for voltage control (nearly unity power factor is preferred). It

means that the *P* curtailment from non-firm DG or the support from ESSs may be required to reduce the *Q* support from DG.

This work focuses in steps 3-5 which can enhance the voltage controllability, apart from the steady-state voltage regulation presented in many previous investigations.

The gap between OLTC's and DG's voltage control limits is defined for coordinated voltage controller among these devices, as shown in (5.5) and (5.6). The gap between OLTC's and DG's voltage limits should be wide enough to ensure that the OLTC will start to operate after DG already support *Q* until reaching its reserve capacity. Furthermore, DG with remote controllability, which can regulate voltage level to other bus (e.g. at the end of the feeder) in the LCZ, can give better voltage control performances and reduce the control operation from the secondary voltage control devices, as examined in Section 5.5.2.2.

$$V_{DG,lower} > V_{OLTC,lower} > V_{stat,lower} \tag{5.5}$$

$$V_{DG,upper} < V_{OLTC,upper} < V_{stat,upper} \tag{5.6}$$

The maximum voltage in the network is usually located either at the substation or at the DG buses [18], during the light loading condition. On the other hand, the minimum voltage normally occurs at the end of the feeder during heavy loading condition. Although, more than one feeder connects to the substation, it is quite unlikely to found that both $V_{re,min}$ and $V_{re,max}$ are outside the OLTC's voltage limits at the same time, as the load consumptions among feeders normally have a similar characteristic during the same period of time.

5.6.2 Simulations and results

The test system is adapted from the IEEE 33-bus distribution network with the same network condition as described in Section 4.3.1. A 1-MW converter-connected DG unit, working at unity p.f., is connected to the network at bus 11. DG is assumed to have remote controllability which can support voltage control to a bus at the end of feeder (bus 17). The remote measurements are located at buses 11 and 32, which are a DG bus, and a bus at the end of feeder which does not belong to any LCZs, respectively. The LCZ controller can switch to sensing the voltage level at bus 17, instead of bus 11, to the central controller if the voltage support from DG is not sufficient. The test system is illustrated in Figure 5.37. The network's allowed voltage boundary, between $V_{stat,lower}$ and $V_{stat,upper}$, is 0.95-1.05 p.u. Moreover, $V_{DG,lower}$ and $V_{DG,upper}$ of the DG voltage controller are set as 0.96 and 1.04 p.u., respectively.

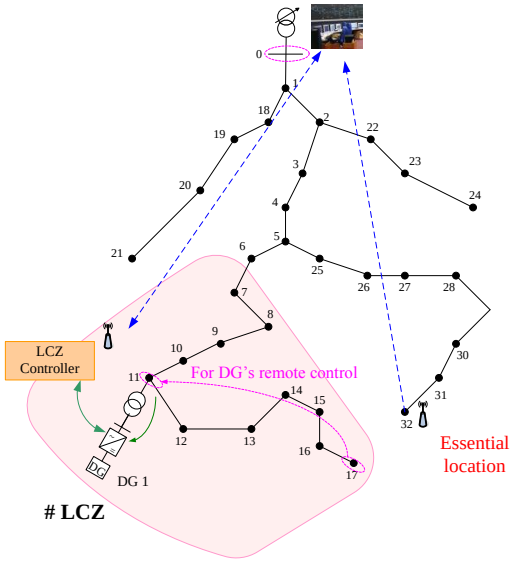

Figure 5.37. Test system in case of coordinated voltage controller between DG and the substation's OLTC.

The substation's OLTC controller scans information from local and remote measurements in every 2 sec, assuming that the fast communication link is feasible. The initial tap position is -2. The allowed voltage limits at the substation are $V_{sub,lower}$ = 1.0 p.u and $V_{sub,upper}$ = 1.12 p.u.. Furthermore, the substation's OLTC has ±12 taps which provide 1 % voltage change per tap. The delay time for changing the tap in each step is 10 seconds. The voltage limits of OLTC controller, $V_{OLTC,lower}$ and $V_{OLTC,upper}$, is between 0.955 p.u. and 1.045 p.u. The OLTC controller will delay 5 sec, after it detects voltage rise or voltage drop problems in the network, to avoid short-term voltage compensations.

The dynamic performance of the coordinated voltage controller between DG and OLTC is examined based on the slow voltage variations by applying a gradual increasing and decreasing total load demand as in Section 5.3.2.2 (see Figure 5.13). The transient simulations compared with and without the secondary support from the substation's OLTC. The key simulation results are illustrated in Figure 5.38 and Figure 5.39, including: the voltage levels at the substation, buses 11, 17 and 32, Q support from DG and the tap position of the substation's OLTC.

The results from transient simulations show that the substation's OLTC can improve the long term voltage controllability especially to the essential buses which do not belong to any LCZs. It is found that changing the tap position can secure the voltage at buses 17 and 32 from the under voltage problem, which is not successful when only DG is used to support voltage control. The DG can support voltage control at bus 17 until $t \approx 40$ sec, and then the

voltage level at bus 17 becomes lower than the statutory limit. In consequence, the LCZ controller will switch to use the sensing data at bus 17, instead of bus 11, and sending it to the central controller to allow bus 17 receiving the voltage control by the substation's OLTC (see the bottom plot in Figure 5.39).

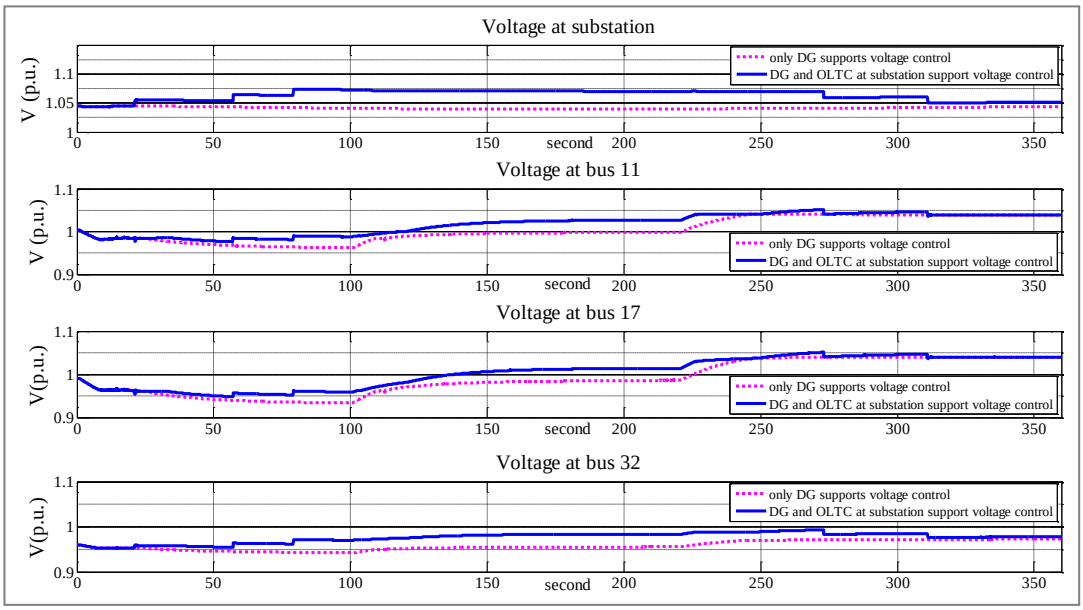

Figure 5.38. Voltage at substation, DG and the end of feeder in case that DG has remote controllability.

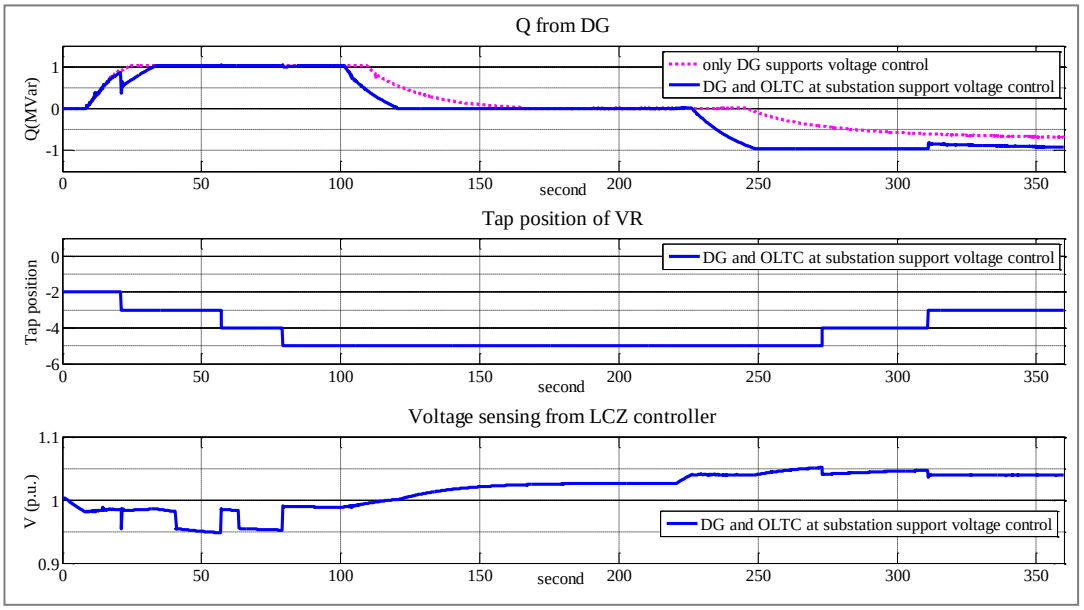

Figure 5.39. *Q* support from DG, tap position and sensing voltage from LCZ controller in case of coordinated voltage controller between DG and substation's OLTC.

Figure 5.39 shows that the tap position is stepping down from -2 to -3 and -3 to -5 to prevent the voltage drop below the statutory limit at buses 32 and 17, respectively. The tap position remains at -5, although the network is back to the normal condition with the *Q* support from DG back to zero. The impact of tap remaining unchanged introduces the over voltage problem to bus 11, starting at $t \approx 260$ sec. Consequently, the tap needs to step up 2 steps, from -5 to -3 (start at $t \approx 273$ sec) to reduce the voltage level at buses 11 and 17 back to below the statutory upper limit. The overall number of tap-changing operation is 5 steps.

It can be seen that the number of tap-changing operation of the OLTC should be as small as possible to avoid voltage interactions in the whole network.

5.7 Conclusions

This chapter presented the coordinated control manner between DG and other voltage controllable devices to enhance voltage controllability in distribution networks, either short- or long-term voltage variations. Voltage controllable devices such as ESSs, modern OLTC distribution transformer and SST can provide fast voltage controllability which can be used as the primary voltage control similar to the converter-connected DG. On the other hand, the VR and the substation's OLTC aim to be used as the secondary voltage control as their control speed is relatively slow. The coordinated voltage control between DG and those controllable devices is implemented to avoid voltage interactions between them and to maximise their voltage controllability.

The results from transient simulations showed that the DG cooperation with those controllable devices enhances the voltage quality and control. The ESS based DSTATCOM structure can accomplish short-term voltage control by compensating either *P* or *Q* into the network. However, in case that using *Q* support the voltage control in the same LCZ with DG, the *V*-*Q* droop controller should be added into the voltage controller to avoid the voltage interactions between DG and DSTATCOM-EES when using them to provide voltage support together at the same time.

The modern OLTC distribution transformer can be used to support fast voltage control at specific bus in the network. This device can provide voltage control only at the LV side of the transformer. Meanwhile the voltage support for the MV network is still from the DG. On the other hand, the SST can support voltage control to the MV and LV sides of the transformer. It aims to keep voltage levels at the LV side constant over time while the

primary side (i.e. MV bus) can be controlled in 2 modes: power factor control and active voltage control. As the voltage at the MV side of the transformer is controlled by *Q* compensation, the *V*-*Q* droop controller should be added to the voltage controller to avoid voltage interactions with the DG in case that they are located in the same LCZ.

The VR is assumed as the secondary support: providing the slow voltage control to cover the buses located behind its secondary side (at the same feeder). It can support long-term voltage control to the LCZ when the *V/Q* compensation from DG is insufficient. The coordinated voltage control limits between DG and VR is introduced to allow voltage controllable devices to support voltage control with different voltage set-points. By this method, the DG and the VR will not provide voltage control at the same time. Moreover, the results showed that DG with remote controllability can provide better voltage control performance when DG provides voltage control in coordination with the VR.

The substation's OLTC, which is the central controller, can be used as secondary support similar to the VR, but it can provide the wide area voltage support across the network. It can support long-term voltage variations that occur to specific buses: inside or outside the LCZs. The bus member inside the LCZ can receive the primary voltage support from the DG while the buses outside the LCZ can receive the support directly from the substation's OLTC. However, the hunting among voltage-controlled buses needs to be addressed, as other buses should not exceed their limits after the tap position has changed.

5.8 References

[1] M. Molina and P. E. Mercado, "Dynamic modelling and control design of DSTATCOM with ultra-capacitor energy storage for power quality improvements," in *Transmission and Distribution Conference and Exposition: Latin America, 2008 IEEE/PES*, Bogota, 2008, pp. 1-8.

[2] M. Molina and P. E. Mercado, "Control design and simulation of DSTATCOM with energy storage for power quality improvements," in *Transmission & Distribution Conference and Exposition: Latin America, 2006. IEEE/PES*, Caracas, 2006, pp. 1-7.

[3] G. Suvire and P. E. Mercado, "Improvement of power quality in wind energy applications using a DSTATCOM coupled with a Flywheel Energy Storage System", *Brazilian Power Electronics Conference, 2009. COBEP'09*, Bonito MS, pp. 58-64.

[4] P. Kadurek, J. F. G. Cobben, and W. L. Kling, “Smart MV/LV transformer for future grids,” in *Power Electronics Electrical Drives Automation and Motion (SPEEDAM), 2010 International Symposium on*, Pisa, 2010, pp. 1700-1705.

[5] I. Melnik, F. Provoost, and W. Bos, “Intelligent Distribution Substation Improves Power Quality,” in *21st International Conference on Electricity Distribution, CIRED*, Frankfurt, 2011, pp.1-4.

[6] C. Oates, A. Barlow, and V. Levi, "Tap changer for distributed power," in *Power Electronics and Applications, 2007 European Conference on*, Aalborg, 2007, pp. 1-9.

[7] P. Bauer and S. W. H. de Haan, "Electronic tap changer for 500 kVA/10 kV distribution transformers: design, experimental results and impact in distribution networks," in *Industry Applications Conference, 1998. Thirty-Third IAS Annual Meeting. The 1998 IEEE*, St. Louis, 1998, pp. 1530-1537.

[8] D. Aggeler, J. Biela, J.W. Kolar, “ Solid-State Transformer based on SiC JFETs for Future Energy Distribution Systems”, in *The Smart Energy Strategies Conference (SES’08),* Zurich, Switzerland, 2008.

[9] X. She, S. Lukic, and A. Huang, “Performance evaluation of solid state transformer based microgrid in FREEDM systems,” in *Applied Power Electronics Conference and Exposition (APEC), 2011 Twenty-Sixth Annual IEEE*, California, 2011, pp. 182-188.

[10] W. Hui, T. Xing-guo, L. Qing-min, and Z. Fei, “Development and applicability analysis of intelligent solid state transformer,” in *Electric Utility Deregulation and Restructuring and Power Technologies (DRPT), 2011 4th International Conference on*, Nanjing, 2011, pp. 1150-1154.

[11] M. Elkhatib and R. El-Shatshat, “Novel Coordinated Voltage Control for Smart Distribution Networks with DG,” *Smart Grid, IEEE Transactions on*, vol. 2, no. 4, pp. 1-8, 2011.

[12] Z. Jiang and X. Yu, “Active Power - Voltage Control Scheme for Islanding Operation of Inverter-Interfaced Microgrids,” in *Power& Energy Society General Meeting*, Alberta, Canada, 2009, pp. 1-7.

[13] T. Zhao, J. Zeng, and S. Bhattacharya, “An average model of solid state transformer for dynamic system simulation,” in *Power & Energy Society General Meeting, 2009. PES ’09. IEEE*, Alberta, Canada, 2009, pp. 1-8.

[14] *DIgSILENT Technical Documentation: DC/DC converter*, DIgSILENT GmbH, 2007.

[15] L. A. Kojovic and S. Member, “Coordination of Distributed Generation and Step Voltage Regulator Operations for Improved Distribution System Voltage Regulation,”

in *Power Engineering Society General Meeting, 2006. IEEE*, Quebec, Canada, 2006, vol. 53126, pp. 1-6.

[16] F. Bignucolo, R. Caldon, and V. Prandoni, “Radial MV networks voltage regulation with distribution management system coordinated controller,” *Electric Power Systems Research*, vol. 78, no. 4, pp. 634-645, 2008.

[17] L. L. Grigsby, *Electric Power Transformer Engineering, Second Edition*. chapter 8

[18] A. Kulmala, A. Mutanen, A. Koto, S. Repo, Ja, x, and P. rventausta, "RTDS verification of a coordinated voltage control implementation for distribution networks with distributed generation," in *Innovative Smart Grid Technologies Conference Europe (ISGT Europe), 2010 IEEE PES*, Gothenburg, pp. 1-8.

Chapter 6

Harmonic mitigation in Distribution Networks with High Penetration of Converter-connected DG

6.1 Introduction

The number of DG and consumer loads interfaced by power electronic converters has increased considerably over the last two decades. Due to their non-linear characteristic, power converters generate harmonic pollution into the distribution network. Although Grid Codes limit the total harmonic distortion (THD) at the point of common coupling (PCC) of converter-connected DG or non-linear loads, the connection of a new converter unit can cause the rise of THD not only at its PCC but in other buses too. Consequently, the level of voltage THD on the MV network sometimes exceeds the statutory limit (5% for IEEE 519-1992 [1] and 8 % for IEC 61000-3-2 [2]). This increase in the harmonic distortion will limit the penetration level of converter-connected DG, and additional harmonic correction devices will be required to maintain the THD level within statutory limits.

This chapter presents a harmonic mitigation technique that uses the existing devices in the network as a first option, rather than installing new components (i.e. active filters that may be costly and may require complex studies to determine their optimal location). The harmonics from converter units can be reduced by improving the converter structures such as multi-legs or multi-level converter and switching control, as described in Section 2.6. However, bearing in mind converters may come from different manufacturers and have different specifications, the mitigation techniques should adopt a generic approach avoiding modifications on the structure and control of conventional converter units.

A potential harmonic mitigation solution is to use the phase-shifting control technique in the transformer of each converter unit to reduce the level of harmonic distortion across the network, which is successful in terms of reducing the harmonics emitted from a group of non-linear loads in the low-voltage system [3]. This technique reduces the harmonic content in a selected order (focusing on those harmonics causing the highest harmonic distortion). The phase-shifted transformer can be operated off-line by changing the vector group of

transformers in order of integer multiples of 30° (from Yy0 to Dy11). Although the on-load phase-shifting transformer (PST) can be used if on-line phase-shifting operation is required [4], this paper aims to use off-line operation as it avoids having to install a new type of transformer, and just changing the winding connection of the transformer to a new vector group will suffice to achieve the required phase shift. In addition, the converter units will be clustered into many smaller areas according to the network topology, and number and location of converter units.

The 17-bus medium voltage network is chosen as test system. The location, type and number of converter-connected DG or non-linear loads are determined. The THD level across the network is investigated via harmonic load flow analysis and assessed under different scenarios with and without the proposed harmonic mitigation technique.

6.2 Phase-shifting technique for harmonic reduction

The phase-shifting technique can be used to eliminate the harmonic injection from parallel harmonic sources. Where a number of harmonic sources are connected through transformers with different vector groups, the self-reduction of harmonics emitted from different sources occurs due to their vector summation of symmetrical components. This effect is explained in the following section.

6.2.1 Harmonic sequence based on symmetrical components

The symmetrical components are developed to analyse an unbalanced three-phase system. Any three-phase system can be represented by a set of three balanced vectors called positive, negative and zero sequence components. The space-phasor formed of the three-phase fundamental waveforms (taking into account harmonic order) is explained in [5] using formula (6.1).

$$\vec{f}(t) = \hat{f}_1 e^{j\omega t} + \vec{f}_h(t) \tag{6.1}$$

Therefore, $\vec{f}_h(t)$ is the harmonic term which is from

$$\vec{f}_h(t) = \left(\frac{\hat{f}_h}{3}\right)\left[1 + e^{-j(h-1)\frac{2\pi}{3}} + e^{-j(h-1)\frac{4\pi}{3}}\right]e^{jh\omega t} + \left(\frac{\hat{f}_h}{3}\right)\left[1 + e^{j(h+1)\frac{2\pi}{3}} + e^{j(h+1)\frac{4\pi}{3}}\right]e^{-jh\omega t} \tag{6.2}$$

where $\hat{f}_1$ is the amplitude of the fundamental frequency, h is the harmonic order, ω is an angular velocity and $\hat{f}_h$ is the amplitude of the harmonic. From (6.1), the harmonic term $\vec{f}_h(t)$ corresponds to the harmonic component, and the direction of its rotation depends on the harmonic order. Therefore, harmonics with orders multiple of 3 are called "zero-sequence harmonics", corresponding to $\vec{f}_n(t) = 0$. Otherwise, the $\vec{f}_n(t)$ corresponds to $\hat{f}_h$ and rotates with the angular frequency $h\omega$ which depends on the harmonic order. A positive sequence harmonic has a harmonic order $h = 3n\text{-}2$ (where n=1, 2, 3,…) and rotates counter-clockwise. Similarly, a negative sequence harmonic rotates clockwise and is determined by the harmonic order $h = 3n\text{-}1$ (where n=1,2,3,…). The representation of symmetrical components is shown in Figure 6.1, and a set of positive and negative-sequence harmonics are listed in Table 6.1.

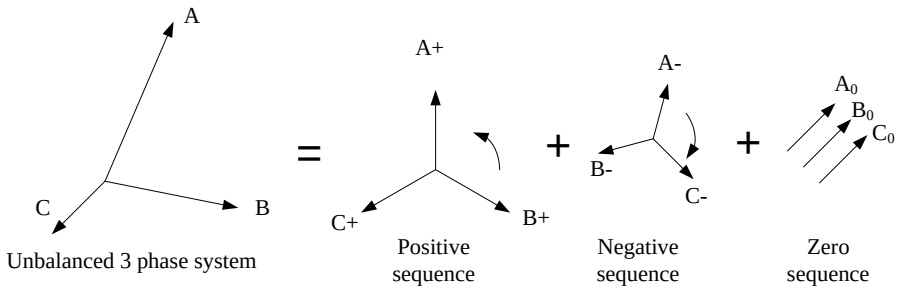

Figure 6.1. Representation of symmetrical components.

Table 6.1. Positive- and Negative-Sequence harmonics.

Positive sequence harmonic	Negative sequence harmonic
h = 1	h = 2
4	5
7	8
10	11
13	14
19	17
22	20
25	23
28	26
31	32

6.2.2 Self-harmonic reduction

Positive and negative sequence currents are the key for self-mitigation from different harmonic sources. The phase-shift between harmonic currents aims to position the harmonic

components, which need to be eliminated, in opposite direction (anti-phase). In addition, the phase-shifted angle is determined from the harmonic order and sequence component. For example, if the 22nd harmonic is identified as the order to be eliminated from the harmonic source A and B, a 60°-phase shift at the fundamental frequency causes the 22nd harmonic component in (6.1) to be $\hat{f}_{22}e^{j22(\omega+60°)t}$, whilst the phase angle of the 22nd harmonic of source B to be shifted by 22×60°=1320° which is equivalent to 240° (counter clockwise). Therefore, the 22nd harmonic of these two sources are in opposite direction causing the reduction of the amplitude of the 22nd harmonic (but also 4th, 10th, 16th…). Figure 6.2 illustrates how the phase difference results in the reduction of the 22nd harmonic.

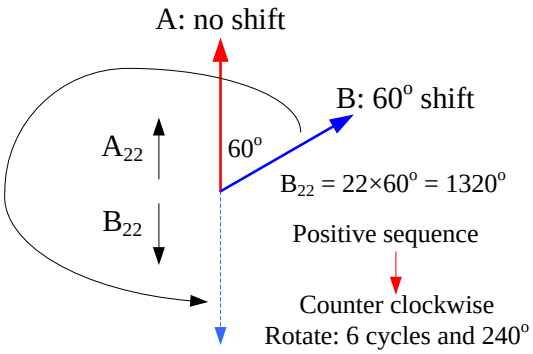

Figure 6.2. A 60°-phase shift between 2 sources results in cancellation of 22nd harmonic current.

6.2.3 Off-line Phase-shifting operation

This research develops the off-line phase shifting technique, for the harmonic mitigation, to the group of harmonic sources that connect to the network though the transformers. Self-compensation of the harmonic currents supplied through transformers in different connection groups will decrease the level of harmonic injection into the network. The vector group of the transformer provides the phase shift between primary and secondary side in multiples of 30° (from 30° to 330°) depending on the winding connection patterns (from Yy0 to Dy11). The examples of phase shifts in different winding connections are illustrated in Appendix J, referred from [6].

A modern distribution transformer such as the resin dry type transformer facilitates a relatively easy access to change its winding connection at the high-voltage (HV) side of the transformer, either wye (Y) or delta (D), as can be seen in Figure 6.3. Apart from changing

the winding connection, swapping the phase sequence at the winding terminals, from *abc* to *bca* or *cab*, also affects the vector group of the transformer. The relationship between phase sequence and vector group of the transformer is demonstrated in Appendix J (Section J.1). Meanwhile, the change of winding connection and phase sequence can be operated off-line to give the transformer the desired vector group, without installing new equipment. However, this technique provides the fixed phase shift between harmonic sources without the ability to follow and react to the change of harmonic distortion.

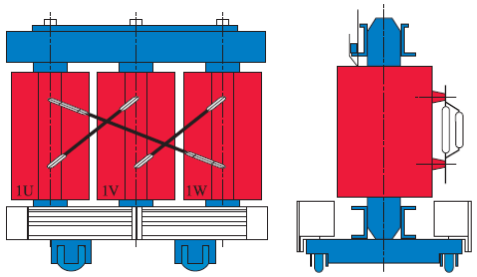

Figure 6.3. Example of a cast resin dry type transformer (GEAFOL cast-resin transformers, SIEMENS [7]).

In case of the low-voltage (LV) side being Y0 connected, the change of winding connection and phase sequence at HV side provides the range of vector groups between 30^{o} and 330^{o} as shown in Table 6.2. It is also similar when the LV side is Y6 connection.

Table 6.2. Vector group of transformer in different winding connection and phase sequence at the HV side.

Winding connection		Phase sequence		
HV side	LV side	*abc*	*bca*	*cab*
D1	Y0	Dy1	Dy5	Dy9
D11	Y0	Dy11	Dy3	Dy7
Y0	Y0	Yy0	Yy4	Yy8
Y6	Y0	Yy6	Yy10	Yy2

6.3 Harmonic load flow and harmonic domain modelling of a distribution system

In this section, the concept of harmonic load flow calculation is explained. The harmonic domain modelling of distribution systems is introduced as a convenient, precise representation for harmonic analysis.

6.3.1 Harmonic load flow

The harmonic current generated from harmonic sources such as power converter units, represented as a current source injecting harmonic current at each bus, is used to calculate the harmonic voltage at frequency $f_h = h \cdot f_1$ (where h is not necessarily an integer and f_1 is the fundamental frequency) using the set of linear equations [8]:

$$\mathbf{I_h} = \mathbf{Y_h V_h} \tag{6.3}$$

where $\mathbf{I_h}$ is the vector of the nodal harmonic current injections, $\mathbf{V_h}$ is the vector of the resulting harmonic voltages and $\mathbf{Y_h}$ is the network admittance matrix at considered frequency f_h . In addition, the $\mathbf{Y_h}$ is using characteristic equations of all network elements (such as lines, transformers and loads). The sequence equivalents (positive, negative and zero) of the network components are used, and then (6.3) can be solved for the three sequence components simultaneously. However, if the system is assumed balanced, only positive sequence component can be considered.

The results of the harmonic load flow at each frequency can be used to determine the level of total harmonic distortion. Therefore, the total harmonic distortion of the bus voltage (THD_V) and the total current harmonic distortion (THD_I) injected into the bus, are calculated from (6.4) and (6.5) respectively.

$$THD_V = \frac{\sqrt{V_2^2 + V_3^2 + V_4^2 + \cdots}}{V_1} \times 100\ \% \tag{6.4}$$

$$THD_I = \frac{\sqrt{I_2^2 + I_3^2 + I_4^2 + \cdots}}{I_1} \times 100\ \% \tag{6.5}$$

The harmonic injections are from converter-connected DG and non-linear loads. New DG technology is interfaced with voltage source converters (VSC), whilst most existing nonlinear loads in industry use current source converters (CSC) as rectifier units. The characteristic of harmonic injection from these two harmonic sources can be found in Section 2.2.4.

6.3.2 Harmonic domain modelling of a distribution system

The model of the distribution system for harmonic analysis is different from models used in load-flow and transient studies. All main system elements are modelled following a change of frequency. The harmonic domain models based on DIgSILENT *PowerFactory* can be found in [8]-[10].

6.3.2.1 Overhead line and underground cable

Overhead lines and underground cables are modelled as π-equivalent circuits. The distributed line parameters for harmonic analysis are shown in Figure 6.4. As the length of the line in distribution networks is relatively short, the shunt capacitance can be neglected.

The conductor resistance is frequency dependent due the skin effect. It can be expressed by using the frequency polynomial characteristic, $y(f_h)$ as

$$R(f_h) = R \cdot y(f_h) \tag{6.6}$$

where $y(f_h)$ is $(1-a)+a\left(f_h/f_1\right)^b$ where typical values of *a* and *b* are 1 and 0.5, respectively.

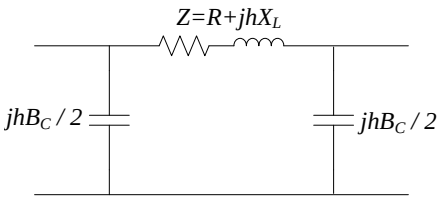

Figure 6.4. Equivalent π circuit model of line and cable.

6.3.2.2 Transformers

For an accurately high-frequency model of transformers (above 5 kHz), additional stray capacitances (C_{HV}, C_{LV} and $C_{HV\text{-}LV}$) are considered into the T equivalent transformer model as shown in Figure 6.5. Additionally, these capacitances are equivalent capacitances of the model and not actual winding capacitances. Therefore, this model can provide an accurate frequency response with respect to voltages and currents at the transformer terminals. However, the effect of internal stress is not included.

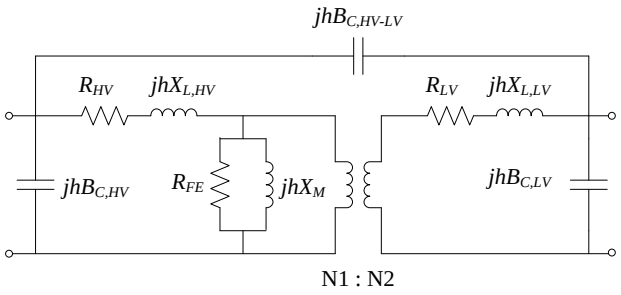

Figure 6.5. Equivalent high-frequency model of the transformer.

From Figure 6.5, R_{HV} and R_{LV} are winding resistances. X_{HV} and X_{LV} are the leakage reactances of the HV and LV sides, respectively. X_M is the magnetising reactance and R_{FE} is the iron loss resistance.

6.3.2.3 Passive load

In harmonic analysis a single-phase passive load is represented as an *RC* circuit as shown in Figure 6.6. Furthermore, three single-phase loads can be connected as Y or Δ for 3 phase analysis.

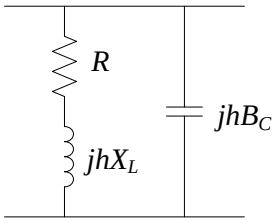

Figure 6.6. Harmonic model for the system load.

6.3.2.4 Shunt filter

The high-pass filter in Figure 6.7(a) is used in this paper to filter the high-order harmonics from the converter-connected DG. The range of harmonic elimination depends on the quality factor, Q_f, where typical values are $0.5 < Q_f < 2$ [11]. The model of the three-phase shunt filter in delta connection is shown in Figure 6.7(b). Additionally, it is possible to include a susceptance to ground (B_g) in μ siemens.

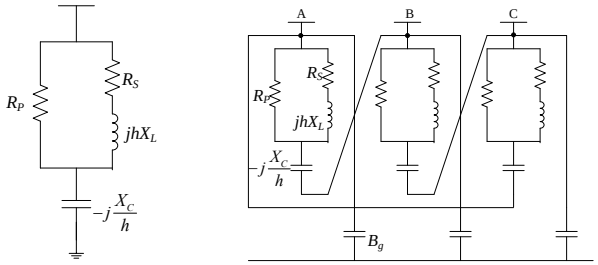

Figure 6.7. High-pass shunt filter.

6.4 Test system and base-case

The THD emission from high penetration of converter-connected DG in MV networks is investigated based on power system simulations. The typical 17-bus, 10-kV Dutch MV network presented in [12] has been chosen as the test system and modelled in DIgSILENT *PowerFactory* software. Details of the test system, including line parameters and load connections, are provided in Appendix K (Section K.2). The total load demand in the base case is 3.98 MW, 0.9 lagging power factor. In addition, the harmonic model of the distribution system, found in Section 6.3.2, is applied to analyse harmonic load flows and to calculate the THD across the network.

Three 1-MW, converter-connected DG units, which amount to 76% penetration level, are connected to the network to show the effect of an increasing amount of converter-connected DG on the level of THD across the network. The location of DG is determined based on the voltage profile and minimum network loss by using the algorithm described in Appendix K (Section K.2.2), adapted from [13]. It is found that the 1st DG (DG1) connects at bus 15, the 2nd DG (DG2) connects at bus 7 and the 3rd DG (DG3) connects at bus 5. The test system with DG connections is shown in Figure 6.8.

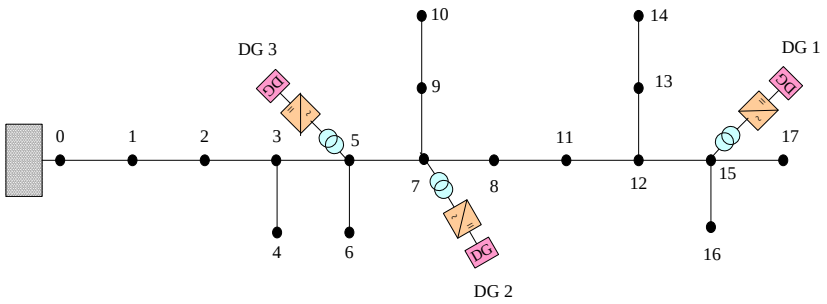

Figure 6.8. Typical 17-bus, 10-kV Dutch MV network with DG connection.

For the base-case, all converter-connected DGs based on VSC operate at 1-kHz switching frequency and are connected using transformers in the same vector group (Dy1). The harmonic voltage waveform (in p.u.), and its spectrum at the converter unit modelled as an ideal harmonic current source (before passing through series reactance, transformer and shunt filter), are shown in Figure 6.9(a) and Figure 6.9(b), respectively.

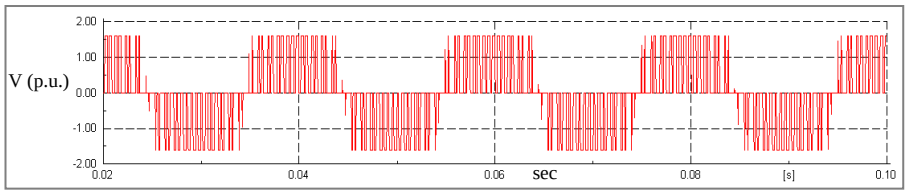

(a) Voltage waveform

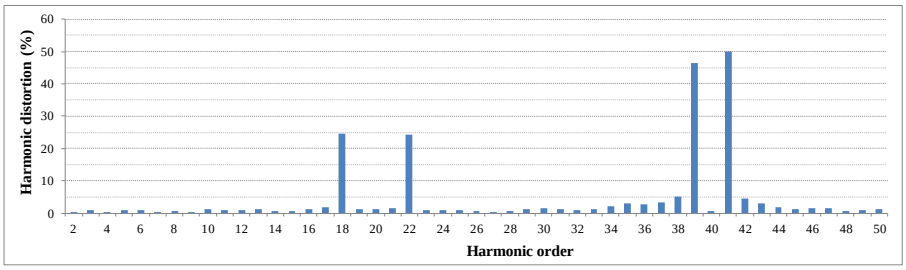

(b) Harmonic spectrum

Figure 6.9. Voltage waveform and harmonic spectrum of VSC-based DG.

From the harmonic load flow simulation, the spectrum of harmonic voltage at PCCs (2^{nd} to 50^{th} order), and the increase on THD due to the connection of a new converter-connected DG (starting from DG1 up to DG3) are shown in Figure 6.10(a) and Figure 6.10(b), respectively. It is found that the series reactance (e.g. line and coupling transformer) and the nature of the power network in the frequency domain can reduce the injection of harmonic components especially the high frequency components.

It is found that the level of THD increases when a new converter-connected DG is added to the network. When the 3^{rd} DG is connected to the network, it causes the THD level of the existing PCCs at bus 7 and 15 (connected to DG2 and DG1, respectively) to exceed the statutory level (5% for IEEE 519-1992), although the THD at PCC of the 3^{rd} DG (bus 5) can be controlled within the standard limit. Furthermore, due to all converters in the base case being operated at 1 kHz, the main harmonic distortion is due to the 22^{nd} harmonic (the side-band of switching frequency at 20^{th} harmonic, see Section 2.2.4), which is the positive sequence harmonic. In addition, bus 15 connected with DG1 has the highest percent of the 22^{nd} harmonic compared to the other PCCs.

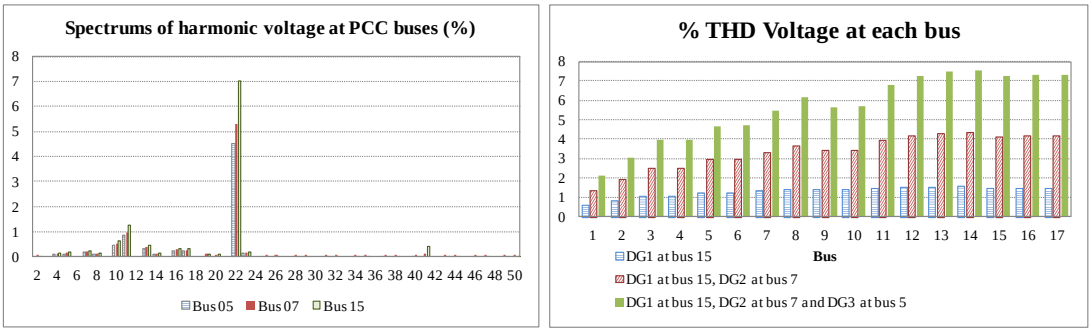

(a) Harmonic voltage spectrums (3 DGs) (b) Bus THD voltage

Figure 6.10. Harmonic spectrums and bus THD voltage in case all DG's converters have the same switching frequency and transformers' vector group.

From the example in Section 6.2.2, the mutual mitigation of the 22nd harmonic can be done by shifting the phase between harmonic sources by 60°. Therefore, if the transformer of DG1 remains unchanged, the transformers of DG2 and DG3 need to change the vector group connection from Dy1 to Dy3 or Dy11 to provide the phase shift of 60° with respect to DG1. In this case, the transformers of DG2 and DG3 are changed to Dy3 and Dy11, respectively. The result in Figure 6.11(a) confirms that when using the phase-shifting technique the 22nd harmonic is reduced. Moreover, the THD level across the network is mitigated to the value below the statutory limit as can be observed in Figure 6.11(b).

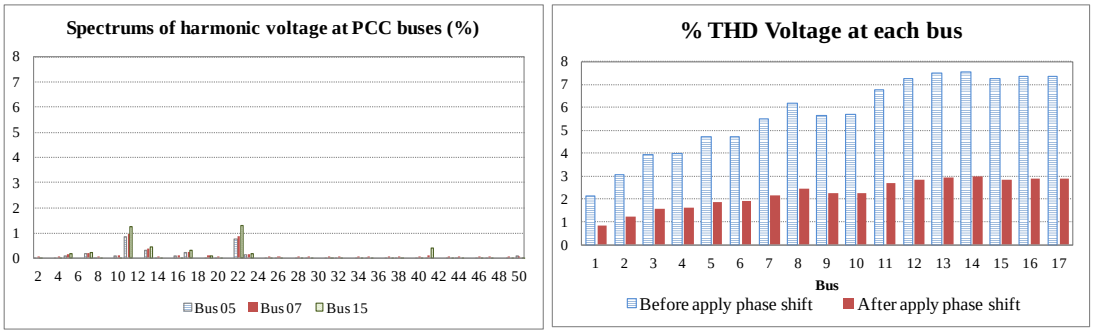

(a) Harmonic voltage spectrums (b) Bus THD voltage

Figure 6.11. Harmonic spectrums and the bus THD voltage after applying the phase-shifting technique.

The electromagnetic voltage waveforms at HV and LV sides of the DG's transformer after applying the phase-shifting technique are shown in Figure 6.12. It is found that the voltage outputs from these three DG units (at LV side of transformer) have phase angle 60° differences between them (using voltage at phase *a*, see Figure 6.12(a)). This effect can

improve the voltage waveform quality at PCC (HV side of transformer), as shown in Figure 6.12(b).

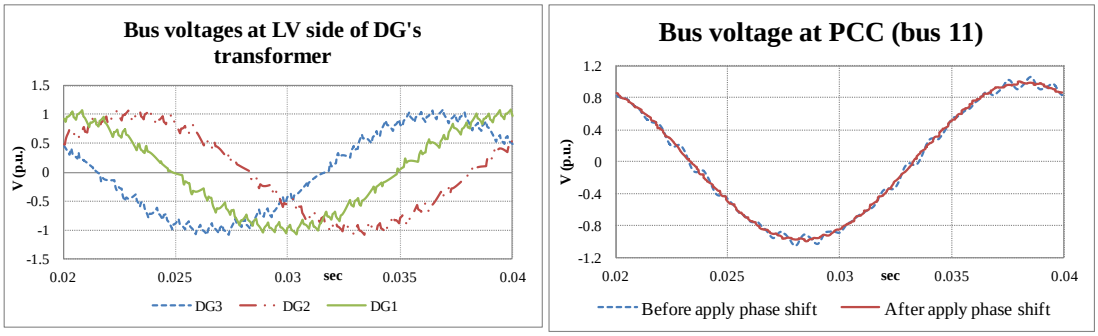

(a) Voltage waveforms from DGs (b) Voltage waveforms at PCC (bus 15)

Figure 6.12. Voltage waveforms at DG's transformers after apply phase shifting.

6.5 Case studies and simulations

The test system is also examined in four different scenarios to explore the effect of using the phase-shifting technique to mitigate harmonic pollution, as follows:

Case 1: All DGs operate with different switching frequencies, e.g. DG1 at 1 kHz, DG2 at 0.8 kHz, and DG3 at 1.2 kHz.

Case 2: All DGs operate with different switching frequencies (as defined in case 1) and the loads connected at buses 6 and 7 are non-linear industrial loads, such as adjustable speed drive, ASD, and induction furnace with static frequency converter, respectively, as presented in Table 6.3.

Case 3: The DGs and non-linear loads are operated as in case 2, but the total load demand is different than in case 2, which aims to examine the phase-shifting technique under light and heavy load conditions.

Case 4: The DGs and non-linear loads are operated as in case 2, but the size of each DG's converter unit is increased 50 %, aiming to examine the phase-shifting technique under very high DG penetration conditions.

Table 6.3. Magnitudes of harmonic currents of selected three-phase loads [3, p. 209]

Harmonic order	Induction furnace (with static frequency converter) [%]	ASD (PWM) [%]
1	100	100
5	20.9	25
7	12.7	11
11	7.8	7.5
13	7.2	5.0
17	4.3	4.4
19	4.9	3.2
23	2.6	2.6
25	3.6	2.0
29	1.7	1.7
31	2.7	1.3
35	1.2	1.0
37	2.0	0.8
41	0.8	0.6
43	1.4	0.5
47	0.5	0.4
49	1.0	0.3

6.5.1 Case 1: All DGs operate with different switching frequencies

The harmonic voltage spectrum at PCCs is shown in Figure 6.13(a) for the case without phase-shifting between harmonic sources. Then, the phase-shift angle (in degrees) between harmonic sources is applied to decrease the content of the highest harmonics. It is found that the 14^{th} and 22^{nd} harmonics create the two highest distortions compared to other harmonics. These two harmonic orders can be cancelled by applying a 60° phase shift. Consequently, if the transformer of DG1 is Dy1, both transformers of DG2 and DG3 can have vector group Dy3 or Dy11. The bus voltage THD in Figure 6.13(c) shows that the phase shifting can reduce the THD across the network to a value below the statutory limit of 5 %. The harmonic voltage spectrums after applying the phase-shifting technique are illustrated in Figure 6.13(b).

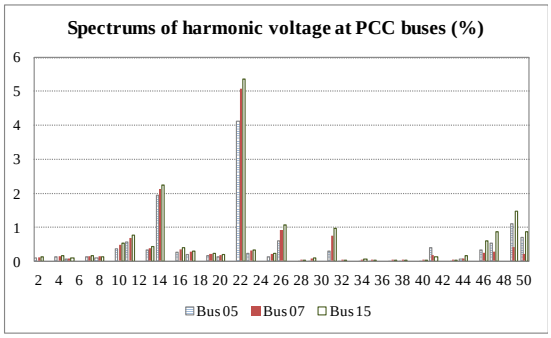

(a) Harmonic voltage spectrums before apply phase shifting

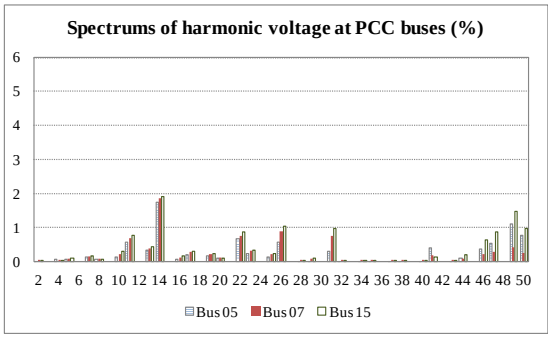

(b) Harmonic spectrum at DG buses after applying 60° phase shift

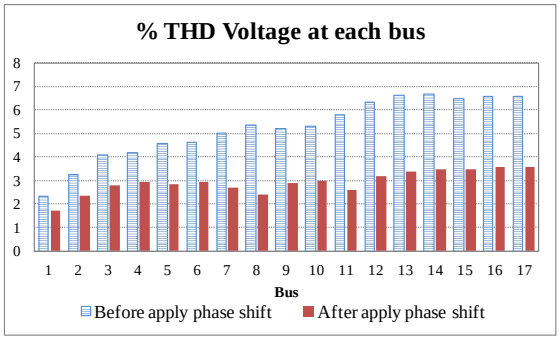

(c) Bus THD voltage

Figure 6.13. Harmonic spectrums at PCCs and the bus voltage THD across the network in case 1 comparing before and after applying the phase-shifting technique.

6.5.2 Case 2: All DGs operate with different switching frequencies, and non-linear loads are present (normal condition)

The new test system and voltage waveforms of non-linear loads at the LV-side of bus 6 and 7 (without DG connection) are shown in Figure 6.14(a) and Figure 6.14(b), respectively. When these two non-linear loads are operated in a network with high penetration of DG, they cause the increase of THD level at other buses including the PCCs of the three existing converter-connected DGs. From Figure 6.15(a), it is found that, without applying phase shifting, the non-linear loads raise the 5^{th} and 7^{th} harmonics compared with case 1, and all PCCs have the voltage THD level above the statutory limit. These two harmonics can be self-compensated by the 30° shift between the harmonic sources.

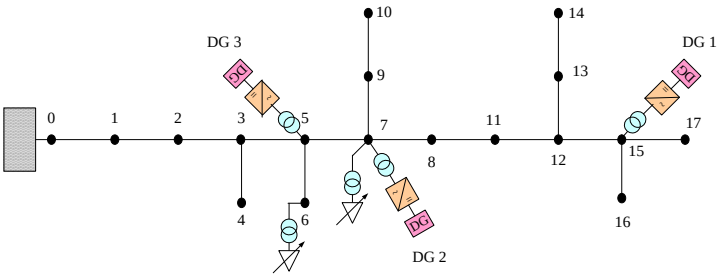

(a) Test system with non-linear loads

(b) Voltage waveforms of non-linear loads at LV side of bus 6 and 7

Figure 6.14. Test system with non-linear loads and harmonic voltage spectrum of non-linear loads.

Because the main harmonic distortion of the 22nd order comes from the DG units, which are the main harmonic source compared with non-linear loads, the 60^{o} phase shifting between transformers connecting the DGs, as in case 1, is sufficient for reducing the THD level across the whole network as can be seen in Figure 6.15(d). However, the addition of the 30^{o} phase shift between the pair of those non-linear loads, apart from the phase shifting among DG units, can enhance the harmonic mitigation (5th, 7th and 31st harmonics are cancelled). Meanwhile, if one transformer connected with non-linear load has the vector group Dy1, the other one can be Yy0 or Yy2. The harmonic voltage spectrums when 1) applying 60^{o} phase shift only among DG units are shown in Figure 6.15(b), and 2) applying 60^{o} phase shift among DG units and 30^{o} among non-linear loads are shown in Figure 6.15(c).

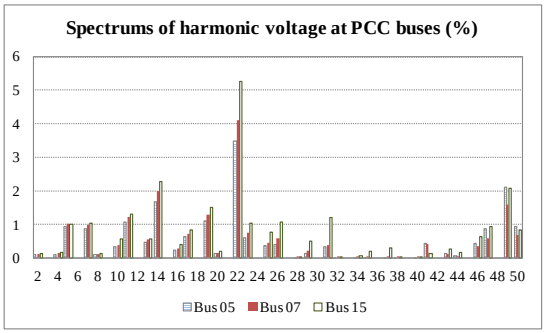

(a) Harmonic voltage spectrums before apply phase shifting

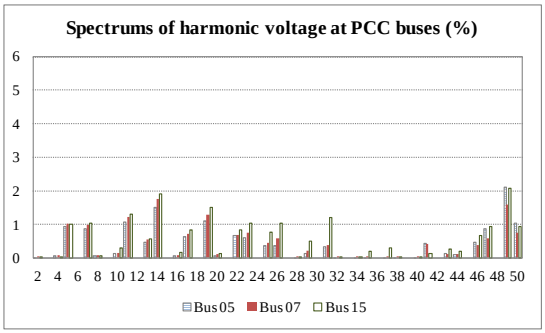

(b) Harmonic spectrum at DG buses after applying phase shift between DGs

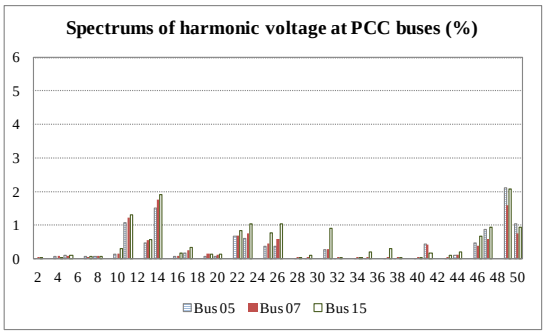

(c) Harmonic spectrum at DG buses after applying phase shifts between the groups of DGs and non-linear loads

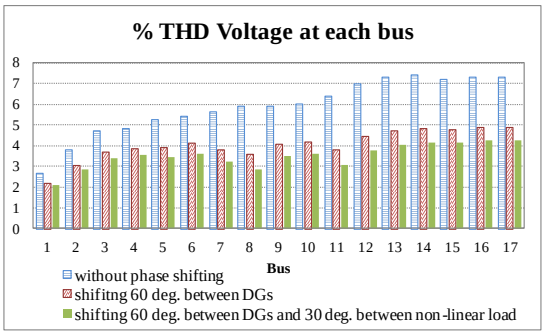

(d) Bus THD voltage

Figure 6.15. Harmonic spectrums at PCCs and the bus THD across the network in case 2.

6.5.3 Case 3: All DGs operate with different switching frequencies, and non-linear loads are present under different load conditions

As the change of total load demand in the network also affects the level of harmonic distortion, the phase-shifting technique may be not sufficient to maintain the level of harmonics within the statutory limit especially under the heavy load condition. In this case, the phase-shifting solution applied in case 2 will be further examined in light and heavy load conditions, while all DGs remain supplying 1 MW. An additional filter may be required in some specific locations of the network to ensure that the level of harmonic distortions across the network is in the statutory limit all the time.

6.5.3.1 Light load condition

The light load condition can occur during the night time due to the small load consumption in the network. The case study is set up as the demands of residential and commercial loads are reduced by about 80%, compared with case 2, while the industrial loads (buses 1, 6 and 7 which are assumed as non-linear loads) remain unchanged. Therefore, the total load demand decreases from 3.98 MW to 1.74 MW (i.e. decreased by about 56%). On the other hand, the level of DG penetration increases from 76% to nearly 168%. Figure 6.16 shows the results from harmonic load flow simulations comparing with case 2. It is found that the harmonic mitigation by using the phase-shifting technique is sufficient to maintain the level of THD voltage across the network within the statutory limit. Additionally, the voltage THD of each bus in the case of light load condition is very similar to case 2, where the 14th is the highest harmonic.

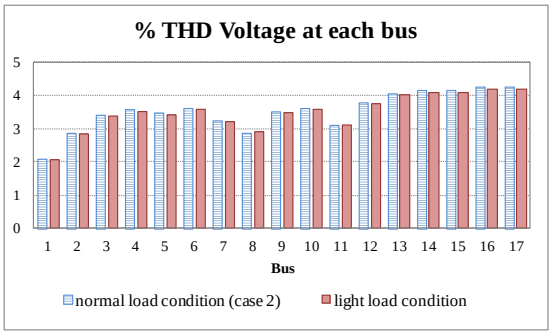

(a) Bus THD voltage

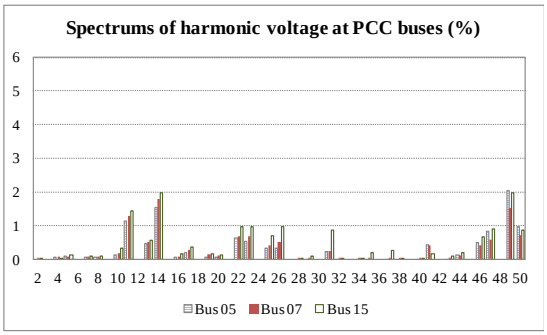

(b) Harmonic spectrum at DG buses after applying phase shifts between the groups of DGs and non-linear loads

Figure 6.16. THD voltage and harmonic spectrums at PCCs under the light load condition.

6.5.3.2 Heavy load condition

In this case, the demand of all connected loads increases by about 180%, compared to case 2. Therefore, the total load demand, including line losses, increases from 3.98 MW to 7.24MW. On the other hand, the level of DG penetration drops from 76% to about 41.4 %. The simulation results in Figure 6.17(a) illustrates that the level of voltage THD increases according to the increase of power flowing in the network. The 11th, 23rd and 25th harmonics at PCCs are obviously increased compared to case 2, as shown in Figure 6.17(b). It is found that using only the phase-shifting technique is insufficient to prevent the harmonic emissions

to be above the statutory limit. An additional filter may be required to enhance the harmonic mitigation rather than only applying phase shifts among harmonic sources.

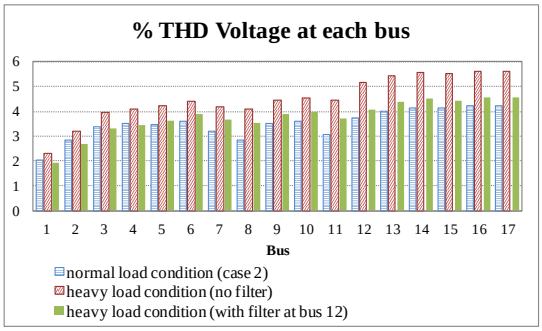

(a) Bus THD voltage

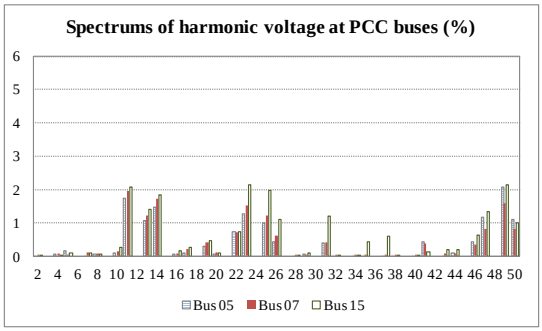

(b) Harmonic spectrum at DG buses after applying phase shifts with no additional filter

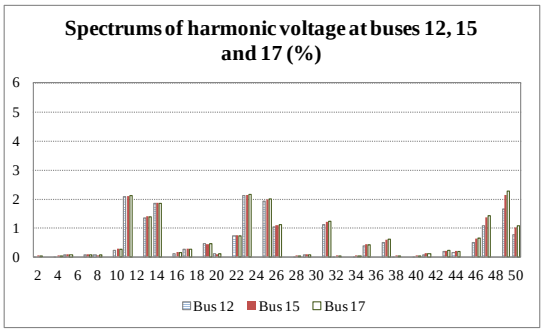

(c) Harmonic spectrum at buses 12, 15 and 17 after applying phase shifts with no additional filter

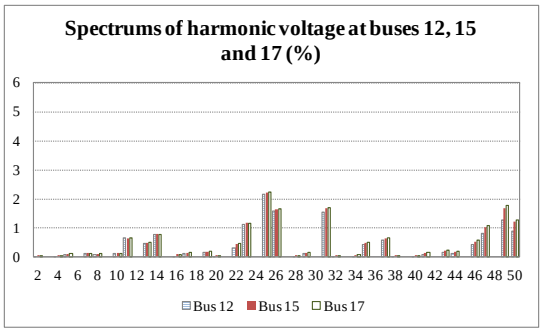

(d) Harmonic spectrum at buses 12, 15 and 17 after applying phase shifts with an additional filter at bus 12

Figure 6.17. THD voltage and harmonic spectrums at specific buses under the heavy load condition.

From Figure 6.17(a), it is found that the level of voltage THD is over the limit from bus 12, to bus 17. As the test system has a radial structure, a high-pass filter can be installed at bus 12 to prevent the harmonic currents from flowing through the buses located behind this bus (e.g. buses 13 to 17). Figure 6.17(c) shows that the main harmonic distortion at bus 12 is due to the 11^{th} harmonic. Therefore, the 0.4 MVar high-pass filter is assumed to be installed at bus 12. The design of this filter follows the calculation procedure in [11],[14]. The corner frequency of this filter is at the 11^{nd} harmonic and the quality factor, Q_f, is set to 2. The simulation result in Figure 6.17(d) shows that this filter can reduce the level of the 11^{th}, 13^{th}, 14^{th}, 22^{nd} and 23^{rd} harmonics in the group of buses 12 to 17. Consequently, the level of bus THD voltage of those buses is reduced to below the statutory limit, as shown in Figure 6.17(a).

6.5.4 Case 4: All DGs operate with different switching frequencies, and non-linear loads are present with very high penetration of DG

In this case the level of DG penetration is made higher by increasing the power output of each DG unit from 1 MW to 1.5 MW under normal load conditions, similar to case 2. Therefore, the total power output of these DG units is raised from 3 MW to 4.5 MW and the level of DG penetration is increased from 76% to 113%. The results from the simulation in Figure 6.18 show that the increase of power generation from DGs (i.e. harmonic sources) slightly impacts on the increase of the voltage THD level at some buses especially between buses 12 to 17. However, the level of bus THD voltage across the network is still staying within the statutory limit and the additional filter may not be required.

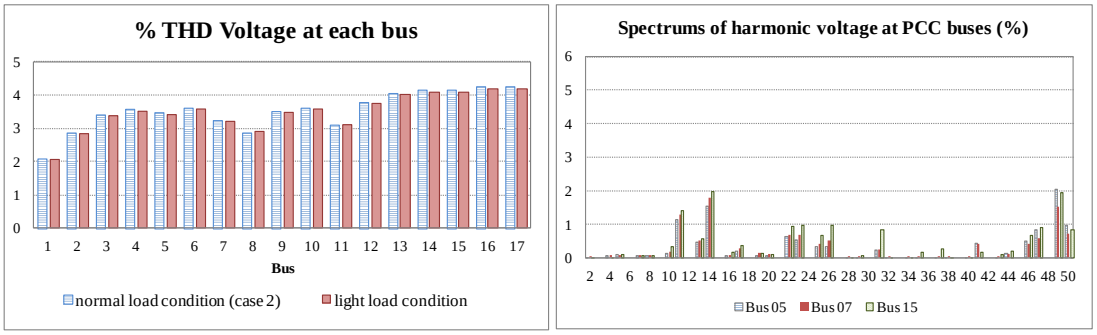

(a) Bus THD voltage

(b) Harmonic spectrum at DG buses after applying phase shifts between the groups of DGs and non-linear loads

Figure 6.18. THD voltage and harmonic spectrums at specific buses under the highly DG penetration condition.

6.6 Discussion

To apply the phase-shifting technique, the network needs to have more than one harmonic source connected in the same feeder. This method is effective when the main harmonic frequencies between harmonic sources are not much different, and the expected harmonics to be eliminated will not disperse to too many frequencies. The procedure of applying the phase-shifting technique to mitigate harmonics in distribution networks with DG connections can be summarised as follow:

1. Review the information of harmonic distortions of individual harmonic sources, which can be found in the data sheet of non-linear devices such as the inverter or variable speed machine.

2. Analyse the harmonic spectrums of voltage at each PCC when harmonic sources connect to the network. Additionally, the harmonic spectrums can be found by computer simulation or real-time power quality monitoring (in practice).

3. Select the harmonic order that provides the highest % of harmonic distortion. Using the information from data sheets to determine what possible devices can produce that harmonic order.

4. Pairing or grouping the devices that can produce the highest harmonic distortion. Then, the values of phase angle to shift between those devices are calculated.

5. Change the winding connection of transformers interfaced with those harmonic sources to the new vector group according to the value of the phase-shift angle. Then, the harmonic spectrums of voltages at PCCs are re-analysed.

6. Find more harmonics which may be cancelled by using the other pair or group of harmonic sources. Re-process again steps 3 to 5.

7. In case that the phase-shifting technique cannot mitigate harmonic distortions successfully an additional filter is required. The size and location of the filter depend on the characteristic of the harmonic distortions and the network topology.

6.7 Conclusions

The phase shifting between harmonic sources, either converter-connected DG units or non-linear loads, can reduce harmonic injection into the network. The phase can be shifted by changing the vector connection of transformers interfaced with harmonic sources in case that more than one harmonic source connects to the network. In addition, the change of vector connection can be done off-line without changing the main structure of the transformer or adding new equipment. The distribution system operator can use this technique to choose the suitable transformer vector group for new converter-connected DGs, which will be connected into the network, to preserve the increase of converter-connected DG penetration and keep the level of harmonic distortion across the network within statutory limits. Furthermore, this technique should be effective especially for harmonic sources that operate

steadily and continuously, due to the fact that the phase shift is fixed and tracking of the change of harmonic distortion is not possible.

6.8 References

[1] "IEEE recommended practices and requirements for harmonic control in electrical power systems," *IEEE Std 519-1992*, 1993.

[2] "Electromagnetic Compatibility (EMC) – Part 3-6: Limits – Assessment of emission limits for the connection of distorting installations to MV, HV and EHV power systems", *IEC/TR 61000-3-6*, Ed. 2.0, Feb. 2008.

[3] A. Baggini, *Handbook of Power Quality*, 1 ed.: John Wiley & Sons, 2008, chapter 7.

[4] J. Verboomen, D. Van Hertem, P. H. Schavemaker, W. L. Kling, and R. Belmans, "Phase shifting transformers: principles and applications," *in Future Power Systems, 2005 International Conference on*, Amsterdam, 2005, pp. 1-6.

[5] A. Yazdani and R. Iravani, *Voltage-Sourced Converters in Power Systems*, 1 ed.: Wiley, 2010. Chapter 4, pp. 81-82.

[6] L. Lawhead, R. Hamilton, and J. Horak, "Three phase transformer winding configurations and differential relay compensation," Basler Electric Company 2006.

[7] SIEMENS. (2012, July.). GEAFOL Cast-Resin Transformers: Planning Guidelines. [Online].Available:https://www.cee.siemens.com/web/slovakia/sk/corporate/portal/produkty/divizie/energetika/ponuka/transformatory/PublishingImages/transform-geafol-projektovanie-en_2000001264471.pdf

[8] S. A. Papathanassiou and M. P. Papadopoulos, "Harmonic analysis in a power system with wind generation," *Power Delivery, IEEE Transactions on*, vol. 21, pp. 2006-2016, 2006.

[9] J. Wasilewski, W. Wiechowski, and C. L. Bak, "Harmonic domain modeling of a distribution system using the DIgSILENT PowerFactory software," *in Future Power Systems, 2005 International Conference on*, Amsterdam, 2005, pp.1-7.

[10] PowerFactory User Manual, ver 14.0, 2010

[11] E. Acha and M. Madrigal, *Power Systems Harmonics: Computer Modelling and Analysis* Wiley-Blackwell, 2001, chapter 3, pp. 65-66.

[12] S. Bhattacharyya, Z. Wang, J. F. G. Cobben, J. M. A. Myrzik, and W. L. Kling, "Analysis of power quality performance of the dutch medium and low voltage grids," *in Harmonics and Quality of Power, 2008. ICHQP 2008. 13th International Conference on*, Wollongong, 2008, pp. 1-6.

[13] A. Kazemi and M. Sadeghi, "Distributed Generation Allocation for Loss Reduction and Voltage Improvement," *in Asia-Pacific Power and Energy Engineering Conference*, 2009 (*APPEEC 2009*), Wuhan, pp. 1-6

[14] *DIgSILENT Technical Documentation: Filter/Shunt*, DIgSILENT GmbH, 2007.

Chapter 7

Conclusions and Suggestions for Further Research

7.1 General conclusions

The impact on power quality when the amount of DG, especially the inverter-interfaced type, has increased in the distribution network has been investigated. The voltage level rise, during light load conditions, and harmonic pollution are two main issues which can limit the number of DG that can connect to the network.

This thesis investigated the performance of automatic voltage control based on hierarchical distributed control structure in order to improve the voltage level in the network, either short- or long-term voltage change. It was identified that converter-connected DG is the key device to provide active decentralised voltage control instead of using conventional compensation devices or power conditioners. The integrated Volt-Var control between DG and other voltage controllable devices was implemented with the aim to enhance voltage controllability and to expand the voltage control area. Harmonic mitigation by applying phase shifts between harmonic sources via the off-line changing of transformer's vector group was also addressed in this thesis.

Significant benefits to distribution networks with DG connections from power quality enhancement by these proposed methods are:

1. Increase the level of DG penetration which means increasing the power generation into the network.
2. Reduce the installation of new compensation devices.
3. Support advanced distribution automation technology for future smart grids in terms of voltage level control.

Details of each contribution in this thesis are summarised as follow:

1) The hierarchical distributed voltage control structure was developed to facilitate the autonomous integrated Volt-Var control in distribution networks with DG connection. The voltage support is obtained from the combination of decentralised and centralised

voltage controls. Additionally, the DG, either synchronous- or converter-based DG is used as the primary voltage support, to provide the active decentralised voltage control by *Q* control (while *P* remains constant). The secondary voltage support is from slower voltage controllers such as the voltage regulator or the substation's OLTC, which can provide voltage control to cover a wider area. Real-time measurements, high-performance computer and communication links are needed in this voltage control structure to fulfil the distribution automation capability.

The LCZ was identified to illustrate the voltage controllable area of DG, by assessing the voltage sensitivity and the available *Q* reserve of DG units, applying also the *thresholding operation* technique. The LCZ are typically used for real-time monitoring and display under the distribution automation environment. It can be adapted to follow the change of network conditions and topology by using information from the real-time state estimation. The zone performance was examined by steady-state and transient simulations. The results showed that the bus members of an LCZ can receive voltage support from DG efficiently. Furthermore, voltage interactions among LCZs were also observed, but these interactions were not significant. The zones operation and control remained very much independent of each other. Results from load flow and transient simulations demonstrated that the LCZs can be adapted to handle changes in the network under different scenarios. However, the accuracy of zone identification is very much dependent on the performance of the state estimator.

2) From the transient simulations, it was find out that converter-connected DG can provide better voltage control response, especially when dealing with short-term voltage variations, compared with conventional synchronous generator-based DG. Therefore, the main decentralised voltage support should be from VSC-based DG, while the synchronous generator-based DG may be used only for steady-state voltage control or as a back-up.

   The VSC-based DG's control system was implemented in the *dq* reference frame and the sinusoidal PWM was employed as the switching technique. The voltage control speed of the VSC-based DG is less than 1 second, which is relatively fast, similar to using power conditioning devices. The DG voltage controller is developed to allow DG to operate in 2 modes; *PQ* and *PV* modes. The robustness of the control system was tested and demonstrated under several scenarios. Results from transient simulations showed that the fast voltage controllability of converter-connected DG makes it successful when dealing

with the most significant voltage disturbances, including sag, swell, slow flicker (<1 Hz), voltage imbalance, under and over voltages, which occurred inside the LCZ. The level of voltage compensation can be determined by the ratio of voltage sensitivity or *V*-*Q* curves, which depend on the value of available *Q* reserve and network topology. The DG can enhance voltage control directly to specific locations in the LCZ via the remote control, such as at the flicker source bus or the bus at end of the feeder, which aims to enhance the flicker mitigation and to provide long-term voltage control, respectively.

3) Interactions between DGs were observed when more than one DG supports voltage control in the same LCZ at the same time. In addition, voltage interactions among these DGs increase the level of voltage variations after clearing a disturbance, which causes difficulty to control their *Q* and *V* outputs and return them to the satisfactory condition. The coordinated controller approach was proposed to reduce the number of voltage-supporting DG units by allowing DG units to provide voltage support based on a ranking order with a time lag in each control sequence. However, it was observed from simulations that this method reduces the fast voltage compensation capability of DGs. Alternatively, an additional *V*-*Q* droop controller was then used to reduce the voltage oscillations due to interactions between DG units in the same LCZ. The simulations showed that adding a proportional–derivative (PD) droop controller gives good performance in terms of voltage interactions mitigation, and reduces the time to bring the voltage back to the steady-state condition after the disturbance has been cleared.

   The coordinated voltage control between DG and other voltage controllable devices can enhance the voltage quality in the distribution network depending on the type of voltage controller. The coordinated controller can increase the integrated Volt-Var controllability, apart from only using optimal steady-state voltage regulation which normally updates new set-points of DG and substation's OLTC, every several to 15 minutes. The voltage control coordination between DG and other controllable devices can be summarised as follows:

   a) The transient simulations showed that the DSTATCOM-based ESS (e.g. battery) can provide fast voltage controllability similar to VSC-based DG by compensating either *P* or *Q* into the network. The voltage supporting time is limited by the size of the energy storage, so it may be suitable only for short-term voltage compensation. Moreover, the voltage support capability inside the LCZ is increased when DG and ESS provide voltage compensation together.

Nonetheless, the coordinated voltage controller with a time lag or *V*-*Q* droop controller is required to mitigate the voltage interactions between DG and ESS if they are located in the same LCZ.

b) The modern OLTC distribution transformer and solid-state transformer (SST) can increase decentralised voltage controllability of specific locations in the network. The simulations showed that these transformers can improve the voltage level of the LV side efficiently. Additionally, the SST also increases voltage controllability to the MV network by using its grid-side converter (e.g. VSC type) similar to the DG's grid-side converter. However, the *V*-*Q* droop controller should be added into the voltage controller to avoid voltage interactions between the SST and DG when they provide *Q* compensation together in the same LCZ.

c) The voltage regulator (VR) and substation's OLTC can provide the secondary voltage support to LCZs, when *V*/*Q* compensation from DG is insufficient. Only long-term voltage variations can be compensated by these two controllable devices due to the slow control response of the tap-changing mechanism. The VR can support voltage control to the area located behind the secondary side. The buses in that area which do not belong to any LCZs can receive voltage support directly from the VR, if the remote voltage control between VR and those buses is available. This can enhance voltage level control to the buses that cannot receive the voltage support from DG. On the other hand, the substation's OLTC is the central controller, which can give the secondary support to LCZs and specific locations, across the network, via remote control system similar to the VR. The interactions between controllable buses must be addressed and ensure that other buses do not exceed their limits after the tap position is changed. The coordinated voltage controller between DG and VR, or substation's OLTC, is developed by applying the margin gap between voltage control set-points. This can prevent the simultaneous operation of these devices. The simulations showed that the coordinated controller can enhance the long-term voltage controllability with small interactions among controllable devices.

4) From harmonic load flow calculations, it is found that a generic approach using the phase-shifting technique can reduce the harmonic injection from the group of converter-connected DG units and non-linear loads, without modifying the structure and control of conventional converter units (and avoiding the installation of new compensation). The

transient simulations showed that changing the vector group of transformers (interfaced with harmonic sources) can provide the phase shifts among harmonic sources. The self-harmonic mitigation, resulting from the phase shifts, helps reducing the voltage harmonic distortions at PCCs. Hence, the voltage THD of buses across the network is decreased to below the statutory limit. However, it was found that the harmonic mitigation by phase shifting is insufficient in case of heavy load conditions. In these conditions additional compensation devices are required in specific locations to ensure the THD level remains within the standard limits.

5) All case studies were developed in DIgSILENT *PowerFactory*. The test system in case of voltage level control is based on IEEE 33-bus distribution system. The performance of voltage support from individual DG, or coordinated DG and other controllable devices were examined via steady-state and transient simulations. The voltage response of specific buses in the network was assessed to demonstrate the impact of those voltage controllable devices. It is found that the proposed voltage control structure that consists of decentralised and centralised voltage controls can enhance voltage quality in the network effectively.

   The typical 17-bus Dutch MV network (i.e. radial system) is used as the test system in case of harmonic mitigation studies. The harmonic components of VSC-based DG are created from the voltage output waveform via Fast Fourier Transformation. The THD of bus voltages, across the network, are calculated to assess the performance of harmonic mitigation by using the proposed technique. The level of THD is calculated by harmonic load flow analysis based on harmonic domain modelling.

7.2 Research findings

The research findings of the thesis are summarised as follow:

1. An evaluation of hierarchical distributed voltage control structure that can provide both dynamic and static voltage support under the active distribution network environment. The Volt-Var controllers are integrated via communication links to fulfil the advanced distribution automation function. All controllable devices are assumed as autonomous voltage controllers which have the degree of intelligence to deal with real-time voltage changes in the network with small interactions.

2. The VSC-based DG provides fast voltage control by *Q* support, dealing with both short- and long-term voltage variations in the distribution network effectively. The performance of active voltage control by converter-connected DG is similar to the use of power conditioning devices. Using DG as decentralised voltage controller gives the following benefits: 1) reduces the installation of new compensation devices, 2) saves the voltage control operation of the central control such as the tap changing of substation's OLTC and 3) increases the level of DG penetration while voltage level is still adequate. Only small voltage variation could be mitigated by using DG, due to the limit of *Q* of each converter unit. However, future distribution networks will present higher voltage control capability due to the higher penetration of converter-connected generation that can be included in the voltage control system.

3. The LCZ is defined to illustrate the DG voltage controllable area. The LCZs can enhance the network and DG visibility to the distribution management system. For example, the network operator can use the historical information about changes in LCZs for the purposes of planning and operating the active network in terms of voltage control and identification of the preferred locations for additional DG connections.

4. The interactions between controllable devices are addressed when those controllable devices can provide fast voltage support together in the same LCZ. This impact increases the level of voltage variations after clearing a disturbance which makes it difficult to control their *Q* and *V* outputs and return them to the satisfactory condition. The interactions can be mitigated by applying a coordinated controller or by adding a *V*-*Q* droop controller.

5. The smart voltage controllable devices, which are autonomous and have communication capability, can be integrated with DG to enhance voltage quality in the distribution network. The new distribution transformer technology such as the solid-state transformer can provide fast voltage control to both MV and LV networks. The VSC-based ESS can give voltage support similar to the DSTATCOM. In case these devices are located in the same LCZ with DG, the coordinated voltage controller between DG and other controllable devices is necessary to minimise the interactions between them.

6. The VR and substation's OLTC can be used for wide-area voltage control, but they can support only slow voltage variations. In case of using these devices to support voltage control in the LCZ, the VR and substation's OLTC provide voltage support only if the support from DG is insufficient, to prevent the interactions among them. During the

voltage control operation, the voltage level of other buses is also checked via real-time monitoring, to ensure that the control operation of the VR and substation's OLTC does not cause them voltage problems.

7. The distribution network operator can use the phase-shifting technique to choose the suitable transformer vector group for new converter-connected DGs, which will be connected into the network, to facilitate converter-connected DG penetration, and to keep the level of harmonic distortion across the network within statutory limits.

7.3 Suggestions for future work

Suggestions for further research are as follow:

1. This thesis assumes that the communication links are ideal (i.e. fast and reliable) for the simulations. However, the development of a practical communication system is required to allow voltage controllable devices in the hierarchical distributed voltage control structure to deal with fast voltage changes and communicate with other devices. In addition, the communication system should be fast, reliable, secure and with high bandwidth capacity. In this context the wireless system is preferred to make the data transmission more flexible.

2. The role of LCZ controller in this work is only acting as the communication gateway to exchange the information to other LCZs and to the substation. However, it is also implemented as the sub-master station which has a high degree of intelligent to manage DGs' operation inside the zone with the minimum support from the master station (at the substation). This role of LCZ controller can enhance decentralised voltage control capability in the network and it can be used to deal with other applications such as electricity market mechanism and islanding operation.

3. In this thesis, the state estimation of the network is not included and the sensitivity matrix is directly extracted from the load flow engine for the LCZ identification process. New measurement devices and communication links are expected to be installed more in the near future which can provide results from the state estimation, including voltage profiles and Jacobian matrix, with high degree of accuracy. The state-estimation process should be fast (e.g. less than 15 minutes is desirable to catch up the network changes on time) and requires a significant number of real-time measurement devices in the network.

4. Normally, a *V-Q* droop controller will be added into converter-connected DG only for stability purposes. From the study in this thesis, it is found that, if DG can provide voltage control, the *V-Q* droop controller should be included in the grid-side converter of DG even though it is operated under grid-connected conditions, to reduce voltage interactions from other voltage controllable devices based on VSC.

5. Investigate the optimal value of *Q* support of DG that should be established in Grid Codes. The value of extra *Q* may be different depending on size, type and location of DG. Moreover, the aggregated value of *Q* reserve from existing DG located in the same LCZ with new additional DG unit can be counted into the optimisation process.

6. The harmonic mitigation by using phase-shifting technique is effective especially for the harmonic sources that operate steadily and continuously because the phase shift is fixed and tracking of the change of harmonic distortion is not possible. Additional harmonic filtering equipment may be required. An optimal algorithm to find the suitable type (i.e. active or passive filter), size and location of filter is required.

Appendix A: Power Quality in Distribution Networks

The definition of power quality in distribution networks and origins of voltage quality disturbances are summarised in this section.

Table A.1. Power quality disturbances in distribution networks based on IEEE Std. 1159-2009 [A.1].

Categories	Typical Spectral Content	Typical duration	Typical voltage magnitude
1.0 Transients			
1.1 Impulse			
1.1.1 Nanosecond	5 ns rise	< 50 ns	
1.1.2 Microsecond	1 µs rise	50 ns - 1 ms	
1.1.3 Millisecond	0.1 ms rise	> 1 ms	
1.2 Oscillatory			
1.2.1 Low frequency	< 5 kHz	0.3-50 ms	0-4 pu
1.2.2 Medium frequency	5-500 kHz	20 µs	0-8 pu
1.2.3 High frequency	0.5-5 MHz	5 µs	0-4 pu
2.0 Short-duration variations			
2.1 Instantaneous			
2.1.1 Sag		0.5-30 cycles	0.1-0.9 pu
2.1.2 Swell		0.5-30 cycles	1.1-1.8 pu
2.2 Momentary			
2.2.1 Interruption		0.5 cycles-3 s	< 0.1 pu
2.2.2 Sag		30 cycles-3 s	0.1-0.9 pu
2.2.3 Swell		30 cycles-3 s	1.1-1.4 pu
2.3 Temporary			
2.3.1 Interruption		3 s - 1 min	< 0.1 pu
2.3.2 Sag		3s - 1 min	0.1-0.9 pu
2.3.3 Swell		3s - 1 min	1.1-1.2 pu
3.0 Long-duration variations			
3.1 Interruption, sustained		> 1 min	0.0 pu
3.2 Undervoltage		> 1 min	0.8-0.9 pu
3.3 Overvoltage		> 1 min	1.1-1.2 pu
4.0 Voltage imbalance		steady state	0.5 - 2%
5.0 Waveform distortion			
5.1 DC offset		steady state	0-0.1%
5.2 Harmonics	0-100th H	steady state	0-20%
5.3 Inter-harmonics	0-6 kHz	steady state	0-2%
5.4 Notching		steady state	
5.5 Noise	broad-band	steady state	0-1%
6.0 Voltage fluctuations	< 25 Hz	intermittent	0.1-%
7.0 Power frequency variations		< 10 s	

Table A.2. Summary of origins of voltage quality disturbances [A.2]

Disturbances	Voltage dips	Overvoltages	Harmonics	Unbalance	Voltage fluctuations
Origin of disturbance					
1. Power System					
- Insulation fault, break of the neutral conductor					
- Switching, ferro-resonance					
- Lightning					
2. Equipment					
- Asynchronous motor					
- Synchronous motor					
- Welding machine					
- Arc furnace					
- Converter					
- Data processing loads					
- Lightning					
- Inverter					
- Capacitor bank					

Occasional phenomenon

Frequent phenomenon

References

[A.1] "IEEE Recommended Practice for Monitoring Electric Power Quality," *IEEE Std 1159-2009*, 2009.

[A.2] P. Ferracci, "Power Quality," *Schneider Electric Cahier Technique no. 199*, p. 36, 2000.

Appendix B:

Power Flow Analysis using a Simple Radial System and the Newton Raphson Method

The power flow (or load flow) analysis is used to examine the power system conditions (e.g. voltage and current) in steady state. The concept of power flow calculation can be explained by using a simple radial system. Moreover, the Newton-Raphson is a widely used method for solving the more complex power flow calculations.

B.1 Load flow study in a simple radial system

Figure B.1.1(a) shows the power flow between two buses from the sending- to the receiving-end. The apparent power (in complex form), S, at the sending-end bus bar is

$$\mathrm{S} = P + jQ = \mathrm{V_S I^*} \tag{B.1.1}$$

Therefore, the flow of current between these two buses is

$$\mathrm{I} = \frac{P - jQ}{\mathrm{V_S^*}} \tag{B.1.2}$$

The voltage at the receiving-end is

$$\mathrm{V_R} = \mathrm{V_S} - \mathrm{I}\left(R + jX\right) \tag{B.1.3}$$

Combining (B.1.2) and (B.1.3) and assuming $\mathrm{V_S}$ is the voltage reference whose angle is zero ($\mathrm{V_S} = V_S \angle 0°$)

$$\begin{aligned} \mathrm{V_R} &= V_S - \left(R + jX\right)\left(\frac{P + jQ}{V_S}\right) \\ &= V_S - \left(\frac{RP + XQ}{V_S}\right) - j\left(\frac{XP + RQ}{V_S}\right) \end{aligned} \tag{B.1.4}$$

From (B.1.4) and the phasor diagram shown in Figure B.1.1(b), the voltage drops which are in phase with $\mathrm{V_S}$ and perpendicular to $\mathrm{V_S}$ are shown in (B.1.5) and (B.1.6), respectively.

$$|\Delta V| = \left(\frac{RP + XQ}{V_S} \right) \tag{B.1.5}$$

$$|\delta V| = \left(\frac{XP + RQ}{V_S} \right) \tag{B.1.6}$$

Additionally, $|\delta V|$ is normally neglected as the angle between V_S and V_R is very small, for the distribution network. This allows a simple voltage drop (rise) approximately, $|\Delta V|$.

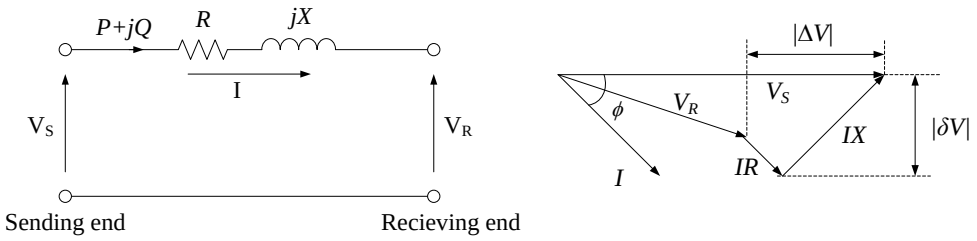

(a) Network equivalent (b) phasor diagram

Figure B.1.1. Two buses radial system.

These calculations are possible only if the sending-end voltage and the sending power are known. However, V_S and apparent power at the receiving-end are only often known. Therefore, if active and reactive powers of the receiving-end are P_L and Q_L respectively, then

$$\mathrm{I} = \frac{P_L - jQ_L}{\mathrm{V_R^*}} \tag{B.1.7}$$

Combining (B.1.3) and (B.1.7), then

$$\mathrm{V_R} = V_S - (R + jX)\left(\frac{P_L + jQ_L}{\mathrm{V_R^*}} \right) \tag{B.1.8}$$

It is found that the solution of (B.1.8) requires iterations, where the initial value of $\mathrm{V_R^*}$ is usually taken as 1 p.u. to start the iterative calculation. Then $\mathrm{V_R^{(n)}}$ is calculated and substitute into the right-hand side to calculate $\mathrm{V_R^{(n+1)}}$. The iterative process is continued until $\mathrm{V_R}$ converges.

B.2 Load flow study by Newton-Raphson method

The Newton-Raphson is the most widely used method for solving simultaneous nonlinear algebraic equations in power flow calculations. Additionally, the Newton-Raphson provides the Jacobian matrix which can be transformed into the form of sensitivity matrix used to illustrate the change of voltage magnitude and voltage angle related to a change of active and

reactive power. In consequence, the information from sensitivity matrix can be employed in the local controllable zone (LCZ) identification process.

B.2.1 Newton-Raphson Method

The Newton-Raphson method is a successive approximation based on an initial estimate of the unknown and then uses the Taylor's series expansion [B.1]. It can be explained by using the nonlinear equation given by,

$$f(x) = c \tag{B.2.1}$$

If $x^{(0)}$ and $\Delta x^{(0)}$ are an initial estimate of the solution and a small deviation from the correct solution, respectively. Then, (B.2.1) can be written as

$$f\left(x^{(0)} + \Delta x^{(0)}\right) = c \tag{B.2.2}$$

The Taylor's series is applied to the left-hand side of (B.2.2), which results in

$$f\left(x^{(0)}\right) + \left(\frac{df}{dx}\right)^{(0)} \Delta x^{(0)} + \frac{1}{2!}\left(\frac{d^2 f}{dx^2}\right)^{(0)} \left(\Delta x^{(0)}\right)^2 + \ldots = c \tag{B.2.3}$$

The higher order terms in (B.2.3) can be neglected, if the error $\Delta x^{(0)}$ is assumed as very small. It is found that,

$$\Delta c^{(0)} \simeq \left(\frac{df}{dx}\right)^{(0)} \Delta x^{(0)} \tag{B.2.4}$$

where $$\Delta c^{(0)} \simeq c - f\left(x^{(0)}\right) \tag{B.2.5}$$

In case of the *n*-dimensional equations, similar to (B.2.3), the linear equations after applying the Taylor's series and neglecting all other higher terms can be expressed as

$$\begin{aligned}
&(f_1)^{(0)} + \left(\frac{\partial f_1}{\partial x_1}\right)^{(0)} \Delta x_1^{(0)} + \left(\frac{\partial f_1}{\partial x_2}\right)^{(0)} \Delta x_2^{(0)} + \cdots + \left(\frac{\partial f_1}{\partial x_n}\right)^{(0)} \Delta x_n^{(0)} = c_1 \\
&(f_2)^{(0)} + \left(\frac{\partial f_2}{\partial x_1}\right)^{(0)} \Delta x_1^{(0)} + \left(\frac{\partial f_2}{\partial x_2}\right)^{(0)} \Delta x_2^{(0)} + \cdots + \left(\frac{\partial f_2}{\partial x_n}\right)^{(0)} \Delta x_n^{(0)} = c_2 \\
&\vdots \\
&(f_n)^{(0)} + \left(\frac{\partial f_n}{\partial x_1}\right)^{(0)} \Delta x_1^{(0)} + \left(\frac{\partial f_n}{\partial x_2}\right)^{(0)} \Delta x_2^{(0)} + \cdots + \left(\frac{\partial f_n}{\partial x_n}\right)^{(0)} \Delta x_n^{(0)} = c_n
\end{aligned} \tag{B.2.6}$$

These equations can be written in matrix form as

$$\begin{bmatrix} c_1-(f_1)^{(0)} \\ c_2-(f_2)^{(0)} \\ \vdots \\ c_n-(f_n)^{(0)} \end{bmatrix} = \begin{bmatrix} \left(\frac{\partial f_1}{\partial x_1}\right)^{(0)} & \left(\frac{\partial f_1}{\partial x_2}\right)^{(0)} & \cdots & \left(\frac{\partial f_1}{\partial x_n}\right)^{(0)} \\ \left(\frac{\partial f_2}{\partial x_1}\right)^{(0)} & \left(\frac{\partial f_2}{\partial x_2}\right)^{(0)} & \cdots & \left(\frac{\partial f_2}{\partial x_n}\right)^{(0)} \\ \vdots & & & \\ \left(\frac{\partial f_n}{\partial x_1}\right)^{(0)} & \left(\frac{\partial f_n}{\partial x_2}\right)^{(0)} & \cdots & \left(\frac{\partial f_n}{\partial x_n}\right)^{(0)} \end{bmatrix} \begin{bmatrix} \Delta x_1^{(0)} \\ \Delta x_2^{(0)} \\ \vdots \\ \Delta x_n^{(0)} \end{bmatrix} \tag{B.2.7}$$

which can be re-written into the short form as

$$\Delta \mathbf{C}^{(k)} = \mathbf{J}^{(k)} \Delta \mathbf{X}^{(k)} \tag{B.2.8}$$

or
$$\Delta \mathbf{X}^{(k)} = \left[\mathbf{J}^{(k)}\right]^{-1} \Delta \mathbf{C}^{(k)} \tag{B.2.9}$$

where k is the iterative sequence, and k=0 means the initial condition. Therefore, the Newton-Raphson algorithm for the n-dimensional case is

$$\mathbf{X}^{(k+1)} = \mathbf{X}^{(k)} + \Delta \mathbf{X}^{(k)} \tag{B.2.10}$$

where

$$\Delta \mathbf{X}^{(k)} = \begin{bmatrix} \Delta x_1^{(k)} \\ \Delta x_2^{(k)} \\ \vdots \\ \Delta x_n^{(k)} \end{bmatrix} \text{ and } \Delta \mathbf{C}^{(k)} = \begin{bmatrix} c_1-(f_1)^{(k)} \\ c_2-(f_2)^{(k)} \\ \vdots \\ c_n-(f_n)^{(k)} \end{bmatrix} \tag{B.2.11}$$

$$\mathbf{J}^{(k)} = \begin{bmatrix} \left(\frac{\partial f_1}{\partial x_1}\right)^{(k)} & \left(\frac{\partial f_1}{\partial x_2}\right)^{(k)} & \cdots & \left(\frac{\partial f_1}{\partial x_n}\right)^{(k)} \\ \left(\frac{\partial f_2}{\partial x_1}\right)^{(k)} & \left(\frac{\partial f_2}{\partial x_2}\right)^{(k)} & \cdots & \left(\frac{\partial f_2}{\partial x_n}\right)^{(k)} \\ \vdots & & & \\ \left(\frac{\partial f_n}{\partial x_1}\right)^{(k)} & \left(\frac{\partial f_n}{\partial x_2}\right)^{(k)} & \cdots & \left(\frac{\partial f_n}{\partial x_n}\right)^{(k)} \end{bmatrix} \tag{B.2.12}$$

$\mathbf{J}^{(k)}$ is called the Jacobian matrix and it is found that $\mathbf{J}^{(k)}$ has an inverse during each iteration.

B.2.2 Power Flow Equation

To solve the power flow problem, the system is assumed as a balanced system, with four quantities associated with each bus: voltage magnitude $|V|$, phase angle δ, active power P and reactive power Q. The network buses are classified into three types as follow:

- Slack bus (known as slack or swing bus): It is the reference bus where the magnitude and phase angle of the voltage are constant. In case of distribution network, the point of common coupling between transmission and distribution networks can be assumed as the slack bus.

- Load bus (known as *P*-*Q* bus): This bus has the specific value of active and reactive power. However, the magnitude and phase angle of the bus voltage is unknown. As DG typically supplies constant active and reactive power, the bus that connects with DG can be assumed as the negative *P*-*Q* bus where active power is a negative and it flows in the opposite direction compared with a conventional load bus.

- Regulated bus (known as generator bus or *P*-*V* bus): It is a voltage controlled bus where voltage remains constant over time. The active power and voltage magnitude are knows whilst the voltage phase angle and the reactive power are unknowns to be determined.

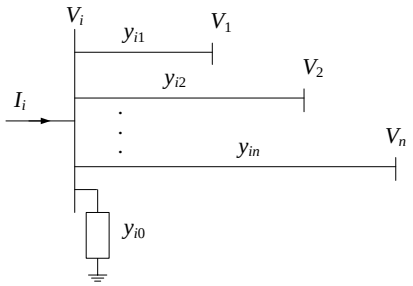

Figure B.2.1. Typical bus of a power system.

Consider the power flow equations for the typical power system in Figure B.2.1, where impedances are converted to admittances. From the Kirchhoff's current loop, it is found that

$$I_i = y_{i0}V_i + y_{i1}\left(V_i - V_1\right) + y_{i2}\left(V_i - V_2\right) + ...y_{in}\left(V_i - V_n\right) \tag{B.2.13}$$

$$I_i = \left(y_{i0} + y_{i1} + y_{i2} + ... + y_{in}\right)V_i - y_{i1}V_1 - y_{i2}V_2 - ... - y_{in}V_n \tag{B.2.14}$$

$$I_i = V_i\sum_{j=0}^{n} y_{ij} - \sum_{j=1}^{n} y_{ij}V_j \qquad j \neq i \tag{B.2.15}$$

The above equation can be rewritten in terms of the bus admittance matrix as

$$I_i = \sum_{j=1}^{n} Y_{ij} V_j \tag{B.2.16}$$

where j includes bus i. $Y_{ii} = \sum_{j=0}^{n} y_{ij}$ (when $j \neq i$) and $Y_{ij} = Y_{ji} = -y_{ij}$.

Alternatively, (B.2.16) can be expressed in polar form where $|Y|$ and θ are the magnitude and angle of the bus admittance matrix, as

$$I_i = \sum_{j=1}^{n} |Y_{ij}||V_j| \angle \theta_{ij} + \delta_j \tag{B.2.17}$$

The complex power at bus i is

$$P_i - jQ_i = I_i V_i^* \tag{B.2.18}$$

Substituting from (B.2.17) into (B.2.18), it is found that

$$P_i - jQ_i = |V_j| \angle -\delta_j \sum_{j=1}^{n} |Y_{ij}||V_j| \angle \theta_{ij} + \delta_j \tag{B.2.19}$$

The real and imaginary parts of the above equation are

$$P_i = \sum_{j=1}^{n} |V_i||V_j||Y_{ij}| \cos\left(\theta_{ij} - \delta_i + \delta_j\right) \tag{B.2.20}$$

$$Q_i = -\sum_{j=1}^{n} |V_i||V_j||Y_{ij}| \sin\left(\theta_{ij} - \delta_i + \delta_j\right) \tag{B.2.21}$$

Applying the Taylor's series and neglecting all higher-order terms, (B.2.20) and (B.2.21) can be transformed into a set of linear equations as

$$\begin{bmatrix} \Delta P_2^{(k)} \\ \vdots \\ \Delta P_n^{(k)} \\ \cdots \\ \Delta Q_2^{(k)} \\ \vdots \\ \Delta Q_n^{(k)} \end{bmatrix} = \begin{bmatrix} \frac{\partial P_2}{\partial \delta_2}^{(k)} & \cdots & \frac{\partial P_2}{\partial \delta_n}^{(k)} & | & \frac{\partial P_2}{\partial |V_2|}^{(k)} & \cdots & \frac{\partial P_2}{\partial |V_n|}^{(k)} \\ \vdots & \ddots & \vdots & | & \vdots & \ddots & \vdots \\ \frac{\partial P_n}{\partial \delta_2}^{(k)} & \cdots & \frac{\partial P_n}{\partial \delta_n}^{(k)} & | & \frac{\partial P_n}{\partial |V_2|}^{(k)} & \cdots & \frac{\partial P_n}{\partial |V_n|}^{(k)} \\ - & - & - & + & - & - & - \\ \frac{\partial Q_2}{\partial \delta_2}^{(k)} & \cdots & \frac{\partial Q_2}{\partial \delta_n}^{(k)} & | & \frac{\partial P_2}{\partial |V_2|}^{(k)} & \cdots & \frac{\partial P_2}{\partial |V_n|}^{(k)} \\ \vdots & \ddots & \vdots & | & \vdots & \ddots & \vdots \\ \frac{\partial Q_n}{\partial \delta_2}^{(k)} & \cdots & \frac{\partial Q_n}{\partial \delta_n}^{(k)} & | & \frac{\partial P_2}{\partial |V_n|}^{(k)} & \cdots & \frac{\partial P_n}{\partial |V_n|}^{(k)} \end{bmatrix} \begin{bmatrix} \Delta \delta_2^{(k)} \\ \vdots \\ \Delta \delta_n^{(k)} \\ \cdots \\ \Delta |V_2^{(k)}| \\ \vdots \\ \Delta |V_n^{(k)}| \end{bmatrix} \tag{B.2.22}$$

From the above equation, bus 1 is assumed as the slack bus. The Jacobian matrix illustrates the linearised relationship between small changes in magnitude and angle of bus voltage with the small changes in active and reactive powers. In case of the generator buses, the voltage magnitudes are known. Therefore, the reactive power equation, (B.2.21), of these buses will be involved in (B.2.22).

A set of linear equations can be written in the short form as,

$$\begin{bmatrix} \Delta P \\ \Delta Q \end{bmatrix} = \begin{bmatrix} J_1 & J_2 \\ J_3 & J_4 \end{bmatrix} \begin{bmatrix} \Delta \delta \\ \Delta |V| \end{bmatrix} \tag{B.2.23}$$

The number of buses in the network is n and the number of generator bus is assumes as m. It is found that ΔP and $\Delta\delta$ are of the order (n-1)×1, while ΔQ and $\Delta|V|$ are of the order (n-1-m)×1. The Jacobian matrix is of order (2n-2-m)×(2n-2-m). J_1 is of the order (n-1)×(n-1), J_2 is of the order (n-1)×(n-1-m), J_2 is of the order (n-1-m)×(n-1) and J_4 is of the order (n-1-m)× (n-1-m).

From (B.2.22), the elements of J_1 are

$$\frac{\partial P_i}{\partial \delta_i} = \sum_{j \neq i} |V_i||V_j||Y_{ij}| \sin\left(\theta_{ij} - \delta_i + \delta_j\right) \tag{B.2.24}$$

$$\frac{\partial P_i}{\partial \delta_j} = -|V_i||V_j||Y_{ij}| \sin\left(\theta_{ij} - \delta_i + \delta_j\right) \quad j \neq i \tag{B.2.25}$$

The elements of J_2 are

$$\frac{\partial P_i}{\partial |V_i|} = 2|V_i||Y_{ij}| \cos\theta_{ii} + \sum_{j \neq i} |V_j||Y_{ij}| \cos\left(\theta_{ij} - \delta_i + \delta_j\right) \tag{B.2.26}$$

$$\frac{\partial P_i}{\partial |V_j|} = |V_i||Y_{ij}| \cos\left(\theta_{ij} - \delta_i + \delta_j\right) \qquad j \neq i \tag{B.2.27}$$

The elements of J_3 are

$$\frac{\partial Q_i}{\partial \delta_i} = \sum_{j \neq i} |V_i||V_j||Y_{ij}| \cos\left(\theta_{ij} - \delta_i + \delta_j\right) \tag{B.2.28}$$

$$\frac{\partial Q_i}{\partial \delta_j} = -|V_i||V_j||Y_{ij}| \cos\left(\theta_{ij} - \delta_i + \delta_j\right) \qquad j \neq i \tag{B.2.29}$$

The elements of J_4 are

$$\frac{\partial Q_i}{\partial |V_i|} = -2|V_i||Y_{ij}|\sin\theta_{ii} - \sum_{j\neq i}|V_j||Y_{ij}|\cos\left(\theta_{ij} - \delta_i + \delta_j\right) \quad \text{(B.2.30)}$$

$$\frac{\partial Q_i}{\partial |V_j|} = -|V_i||Y_{ij}|\sin\left(\theta_{ij} - \delta_i + \delta_j\right) \qquad j \neq i \quad \text{(B.2.31)}$$

The terms $\Delta P_i^{(k)}$ and $\Delta Q_i^{(k)}$ are known as the power residuals, which is the difference between the scheduled and calculated values

$$\Delta P_i^{(k)} = P_i^{sch} - P_i^{(k)} \quad \text{(B.2.32)}$$

$$\Delta Q_i^{(k)} = Q_i^{sch} - Q_i^{(k)} \quad \text{(B.2.33)}$$

where the scheduled active and reactive powers (P_i^{sch} and Q_i^{sch}, respectively) are the known values of active and reactive power at the load bus or the regulated bus.

The updated magnitude and angle values of bus voltages in the new iteration are

$$|V_i^{(k+1)}| = |V_i^{(k)}| + \Delta|V_i^{(k)}| \quad \text{(B.2.34)}$$

$$\delta_i^{(k+1)} = \delta_i^{(k)} + \Delta\delta_i^{(k)} \quad \text{(B.2.35)}$$

The iteration process is continued until the values of power residuals are less than the specific error value, ε , that is

$$|\Delta P_i^{(k)}| \leq \varepsilon \quad \text{and} \quad |\Delta Q_i^{(k)}| \leq \varepsilon \quad \text{(B.2.36)}$$

References

[B.1] Hadi Saadat, Power System Analysis McGrawHill 2nd edition 2004. Chapter 6.

Appendix C: Analysis of an unbalanced network

A three-phase system under unbalanced conditions can be analysed using the symmetrical components method, introduce by Dr. C. L. Fortescue in 1918. Therefore, from [C.1], the three-phase unbalanced system can be determined as the combination of three-balanced components as follows;

1. Positive-sequence components consisting of a set of balanced three-phase components with a phase sequence *abc*.
2. Negative-sequence components consisting of a set of balanced three-phase components with a phase sequence *acb*.
3. Zero-sequence components consisting of three-single phase components, whose magnitudes and phase angles are equal.

The phasor diagram of phase currents in symmetrical components representation is illustrated in Figure C.1.

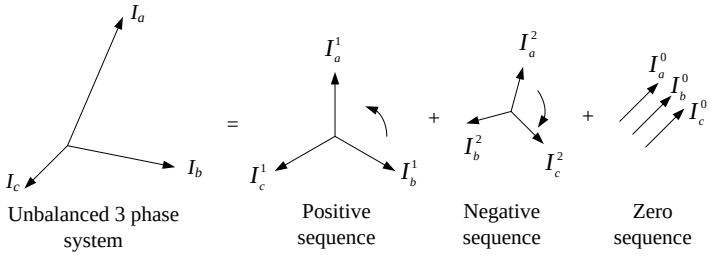

Figure C.1. Representation of symmetrical components of phase currents

From Figure C.1, the positive sequence components can be written as;

$$\begin{aligned} I_a^1 &= I_a^1 \angle 0^\circ \quad = I_a^1 \\ I_b^1 &= I_a^1 \angle 240^\circ = a^2 I_a^1 \\ I_c^1 &= I_a^1 \angle 120^\circ = a I_a^1 \end{aligned} \tag{C.1}$$

From the above definition and Figure C.1, the negative sequence quantities can be written as

$$\begin{aligned} I_a^2 &= I_a^2 \angle 0^\circ \quad = I_a^2 \\ I_b^2 &= I_a^2 \angle 120^\circ = a I_a^2 \\ I_c^2 &= I_a^2 \angle 240^\circ = a^2 I_a^2 \end{aligned} \tag{C.2}$$

Furthermore, zero phase sequence components are represented as

$$I_a^0 = I_b^0 = I_c^0 \tag{C.3}$$

where, the superscripts 1, 2 and 0 are being used to represent positive, negative and zero sequence quantities, respectively.

The three-phase currents in terms of these three symmetrical components would be designed as

$$\begin{aligned} I_a &= I_a^0 + I_a^1 + I_a^2 \\ I_b &= I_b^0 + I_b^1 + I_b^2 \\ I_c &= I_c^0 + I_c^1 + I_c^2 \end{aligned} \tag{C.4}$$

According to (C.1)-(C.3), (C.4) can be rewritten in terms of phase a components

$$\begin{aligned} I_a &= I_a^0 + I_a^1 + I_a^2 \\ I_b &= I_a^0 + a^2 I_a^1 + a I_a^2 \\ I_c &= I_a^0 + a I_a^1 + a^2 I_a^2 \end{aligned} \tag{C.5}$$

From above, it can be rewritten in matrix from and matrix notation as in (C.6) and (C.7), respectively.

$$\begin{bmatrix} I_a \\ I_b \\ I_c \end{bmatrix} = \begin{bmatrix} 1 & 1 & 1 \\ 1 & a^2 & a \\ 1 & a & a^2 \end{bmatrix} \begin{bmatrix} I_a^0 \\ I_a^1 \\ I_a^2 \end{bmatrix} \tag{C.6}$$

The symmetrical components are the inverse of (C.6), it is found that

$$\begin{bmatrix} I_a^0 \\ I_a^1 \\ I_a^2 \end{bmatrix} = \frac{1}{3} \begin{bmatrix} 1 & 1 & 1 \\ 1 & a & a^2 \\ 1 & a^2 & a \end{bmatrix} \begin{bmatrix} I_a \\ I_b \\ I_c \end{bmatrix} \tag{C.7}$$

$$\begin{aligned} I_a^0 &= \frac{1}{3}\left(I_a + I_b + I_c\right) \\ I_a^1 &= \frac{1}{3}\left(I_a + a I_b + a^2 I_c\right) \\ I_a^2 &= \frac{1}{3}\left(I_a + a^2 I_b + a I_c\right) \end{aligned} \tag{C.8}$$

From (C.8), it is found that there is no zero sequence current in three-phase balanced systems as the sum of phase currents is zero. Similarly, the zero-sequence current cannot exist in a three-phase system with ungrounded neutral.

Similarly, the unbalanced phase voltages in terms of the symmetrical components voltage are,

$$\begin{aligned} V_a &= V_a^0 + V_a^1 + V_a^2 \\ V_b &= V_a^0 + a^2 V_a^1 + a V_a^2 \\ V_c &= V_a^0 + a V_a^1 + a^2 V_a^2 \end{aligned} \quad \text{or} \quad \begin{bmatrix} V_a \\ V_b \\ V_c \end{bmatrix} = \begin{bmatrix} 1 & 1 & 1 \\ 1 & a^2 & a \\ 1 & a & a^2 \end{bmatrix} \begin{bmatrix} V_a^0 \\ V_a^1 \\ V_a^2 \end{bmatrix} \tag{C.9}$$

The symmetrical components in terms of the unbalanced voltages are

$$\begin{aligned} V_a^0 &= \frac{1}{3}\left(V_a + V_b + V_c\right) \\ V_a^1 &= \frac{1}{3}\left(V_a + a V_b + a^2 V_c\right) \\ V_a^2 &= \frac{1}{3}\left(V_a + a^2 V_b + a V_c\right) \end{aligned} \tag{C.10}$$

The sequence impedances are determined as the flow paths of symmetrical components. In addition, the positive sequence impedance offers a path for the flow of positive sequence currents. Also, negative and zero sequence impedances offer a path for the flow of negative- and zero sequence currents, respectively. In addition, the sequence impedances of a three-phase power system can be analysed from the three-phase balanced Y-connected load, as illustrated in Figure C.2.

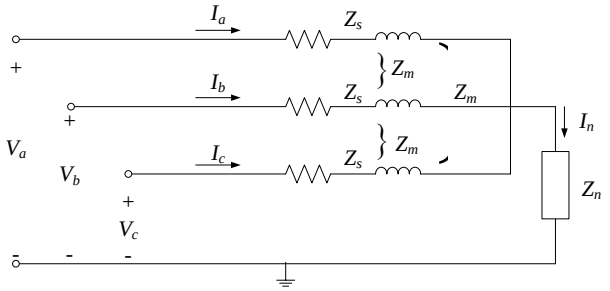

Figure C.2. Three-phase balanced Y connected load system

From Figure C.2, the line-to-ground voltages are

$$\begin{aligned} V_a &= Z_s I_a + Z_m I_b + Z_m I_c + Z_n I_n \\ V_b &= Z_m I_a + Z_s I_b + Z_m I_c + Z_n I_n \\ V_c &= Z_m I_a + Z_m I_b + Z_s I_c + Z_n I_n \end{aligned} \tag{C.11}$$

where, Z_s is the line impedance, Z_m is the mutual impedance between two phases and Z_n is the neutral impedance.

At the load connection point, the neutral current, I_n, is

$$I_n = I_a + I_b + I_c \tag{C.12}$$

Substituting (C.12) in (C.11), the line-to-ground voltages can be written, in matrix form, as

$$\begin{bmatrix} V_a \\ V_b \\ V_c \end{bmatrix} = \begin{bmatrix} Z_s + Z_n & Z_m + Z_n & Z_m + Z_n \\ Z_m + Z_n & Z_s + Z_n & Z_m + Z_n \\ Z_m + Z_n & Z_m + Z_n & Z_s + Z_n \end{bmatrix} \begin{bmatrix} I_a \\ I_b \\ I_c \end{bmatrix} \tag{C.13}$$

From (C.6) and (C.9), the line-to-ground voltages and phase currents can be rewritten in terms of their symmetrical components as

$$\begin{bmatrix} 1 & 1 & 1 \\ 1 & a^2 & a \\ 1 & a & a^2 \end{bmatrix} \begin{bmatrix} V_a^0 \\ V_a^1 \\ V_a^2 \end{bmatrix} = \begin{bmatrix} Z_s + Z_n & Z_m + Z_n & Z_m + Z_n \\ Z_m + Z_n & Z_s + Z_n & Z_m + Z_n \\ Z_m + Z_n & Z_m + Z_n & Z_s + Z_n \end{bmatrix} \begin{bmatrix} 1 & 1 & 1 \\ 1 & a^2 & a \\ 1 & a & a^2 \end{bmatrix} \begin{bmatrix} I_a^0 \\ I_a^1 \\ I_a^2 \end{bmatrix} \tag{C.14}$$

Therefore,

$$\begin{bmatrix} V_a^0 \\ V_a^1 \\ V_a^2 \end{bmatrix} = \begin{bmatrix} 1 & 1 & 1 \\ 1 & a^2 & a \\ 1 & a & a^2 \end{bmatrix}^{-1} \begin{bmatrix} Z_s + Z_n & Z_m + Z_n & Z_m + Z_n \\ Z_m + Z_n & Z_s + Z_n & Z_m + Z_n \\ Z_m + Z_n & Z_m + Z_n & Z_s + Z_n \end{bmatrix} \begin{bmatrix} 1 & 1 & 1 \\ 1 & a^2 & a \\ 1 & a & a^2 \end{bmatrix} \begin{bmatrix} I_a^0 \\ I_a^1 \\ I_a^2 \end{bmatrix} \tag{C.15}$$

Then, the symmetrical components of this system can be written as

$$\begin{bmatrix} V_a^0 \\ V_a^1 \\ V_a^2 \end{bmatrix} = \begin{bmatrix} Z_s + 3Z_n + 2Z_m & 0 & 0 \\ 0 & Z_s - Z_n & 0 \\ 0 & 0 & Z_s - Z_n \end{bmatrix} \begin{bmatrix} I_a^0 \\ I_a^1 \\ I_a^2 \end{bmatrix} \tag{C.16}$$

From (C.16), the sequence impedance matrix is

$$\begin{bmatrix} Z^0 \\ Z^1 \\ Z^2 \end{bmatrix} = \begin{bmatrix} Z_s + 3Z_n + 2Z_m & 0 & 0 \\ 0 & Z_s - Z_n & 0 \\ 0 & 0 & Z_s - Z_n \end{bmatrix} \tag{C.17}$$

where Z^0, Z^1 and Z^2 are the zero sequence impedance, positive sequence impedance and negative sequence impedance, respectively.

If the effect of mutual coupling is not accounted for, i.e. Z_m is zero, the impedance sequence matrix becomes

$$\begin{bmatrix} Z^0 \\ Z^1 \\ Z^2 \end{bmatrix} = \begin{bmatrix} Z_s + 3Z_n & 0 & 0 \\ 0 & Z_s & 0 \\ 0 & 0 & Z_s \end{bmatrix} \quad \text{(C.18)}$$

It is found that the positive and negative sequence impedances are equal, which basically the line impedance. Moreover, the value of the zero sequence impedance depends on the neutral circuit.

References

[C.1] H. Saadat, Power System Analysis, 2nd edition, McGraw hill, 2004, chapter 10.

Appendix D:

An Introduction to Power System State-Estimation

The state-estimation aims to obtain the possible values of magnitude and angle of bus voltages in a power system with limited available network data. The process involves the errors in the measured quantities and the redundant measurements, as described in [D.1]. The estimation is based on a statistical criterion to give the best estimate of the true value of the system state variables (i.e. bus voltage magnitudes and phase angles). In addition, the common used criterion is *the least squares estimation (LSE)*, which minimizes the sum of the squares of the difference between the estimated and the measured values of a function. Furthermore, *the weighted least squares estimation (WLSE)* is a further estimation technique which puts different weights into the process to make the results more reliable and accurate than the basic LSE solution. Meanwhile, the WLSE technique is also used in most practical state- estimation programs.

D.1 Basics of least-squares estimation

This estimation technique tries to estimate the values of unknown variables that relate to the set of measured data with little statistical information being available among them. Following the explanation in [D.2], the method of least-squared error estimation can be demonstrated by using a simple measurement model, assuming no measurement errors, given as

$$b = Ax \qquad \text{(D.1.1)}$$

where x is the system state vector (unknown values) which is the vector of n variables [x_1, x_2,…, x_n]. b is the measurement vector (true, known values) which is the vector of m (m>n) variables [b_1, b_2,…, b_m]. A is the $m \times n$ matrix of non-linear function relating the measurement i (i.e. i=1,…,m), in vector b, to the state vector, x.

It can be seen that (D.1.1) is an over-determined system of non-linear equations, where one equation is for each measurement. The value of the state variables can be estimated by minimising the sum of the squared error between the terms b and Ax. Therefore, the difference, or error is then;

$$e_i = b - Ax \qquad i = 1,\ldots,m \tag{D.1.2}$$

The sum of the squared error is $\sum_{i=1}^{m} e_i^2$, which can be written as

$$\sum_{i=1}^{m} e_i^2 = e_i^T e_i = \left(b - Ax\right)^T \left(b - Ax\right) \tag{D.1.3}$$

The right-hand term in (D.1.3) can be multiplied by $\frac{1}{2}$, to express it in the form of the estimation index, *J*, as

$$J = \frac{1}{2}\left(b - Ax\right)^T \left(b - Ax\right) \tag{D.1.4}$$

Using $\left(Ax\right)^T = x^T A^T$ and $\left[x^T A^T b\right]^T = b^T Ax$, (D.1.4) becomes

$$J = \frac{1}{2}\left[b^T b - 2b^T Ax + x^T A^T Ax\right] \tag{D.1.5}$$

To solve for *x*, it can be done by minimising *J* which can be implemented by setting the gradient of *J* with respect to *x* to zero, as given by

$$\nabla_x J = \frac{\partial J}{\partial x} = \frac{1}{2}\frac{\partial}{\partial x}\left[b^T b - 2b^T Ax + x^T A^T Ax\right] = 0 \tag{D.1.6}$$

Using $\frac{\partial}{\partial x}\left(b^T Ax\right) = A^T x$ and $\frac{\partial}{\partial x}\left(x^T Ax\right) = 2Ax$, the gradient of (D.1.6) can be written as

$$\nabla_x J = \frac{1}{2}\left[-2A^T b + 2\left(A^T A\right)^T x\right] = 0 \tag{D.1.7}$$

Using $\left(Ax\right)^T = x^T A^T$, (D.1.7) can be expressed as

$$\nabla_x J = \frac{1}{2}\left[-2A^T b + 2A^T Ax\right] = 0 \tag{D.1.8}$$

Therefore, this implies the form of a normal equation as

$$A^T b = A^T Ax \tag{D.1.9}$$

The values of *x* can be solved from

$$x = \left(A^T A\right)^{-1} A^T b \tag{D.1.10}$$

$$x = G^{-1}A^T b = A^I b \qquad \text{(D.1.11)}$$

where G is the gain matrix, which $G = \left(A^T A\right)$ and A^I is defined as the pseudo-inverse of A, where $A^I = \left(A^T A\right)^{-1} A^T$.

D.1.1 Real-time measurement model

For the real-time measurements, measurement errors or bad data are included into the set of data of the measurement devices that there are sent to the central control system. In addition, the errors can come from many sources such as meter inaccuracies, communication errors, unbalanced phases and the effect of analogue-to-digital conversions [D.1]. Therefore, the measured values can be written as;

$$z_i = \hat{z}_i + \eta_i \qquad \left(i = 1,...,m\right) \qquad \text{(D.1.12)}$$

where z_i are the measured values, $\hat{z}_i$ are the true or ideal values (unknown) and η_i are the errors (unknown).

Regarding the statistical properties from calibration curves of the measurement errors, it is usually assumed that η_i is a random variable with a normal distribution having zero mean (called Gaussian distribution), as can be seen in Figure D.1.1. Moreover, the standard deviation, σ_i, of each measurement i is calculated to reflect the expected accuracy of the corresponding meter used [D.3]. The larger the standard deviation means the less accurate of that measurement device.

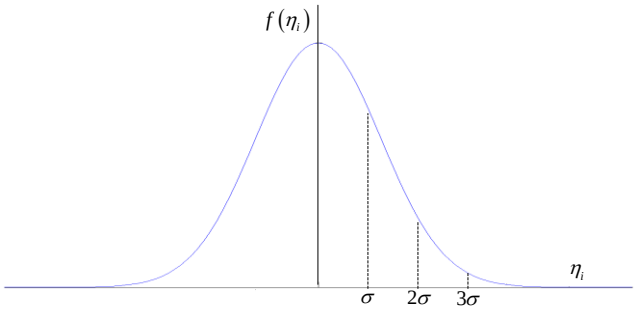

Figure D.1.1. Calibration curves for measuring instruments.

From Figure D.1.1, it is found that the expected value of η_i and η_i^2 are zero and variance (i.e σ_i^2). These values can be expressed as;

$$E(\eta_i) = 0 \qquad \text{(zero mean)}$$
$$E(\eta_i^2) = \sigma_i^2 \qquad \text{(variance)} \tag{D.1.13}$$

Since there are multiple measurement devices in the system, the statistics of one variable will relate to the statistics of other variables. Hence, the errors η_i and η_j for any two measuring devices *i* and *j* can be written in the form of covariance, *Cov*(η_i , η_j), defined as

$$Cov(\eta_i, \eta_j) = E(\eta_i \eta_j) - E(\eta_i) E(\eta_j) \tag{D.1.14}$$

From (D.1.13), when *i=j*, it is found that

$$Cov(\eta_i, \eta_i) = \sigma_i^2 \tag{D.1.15}$$

If measurement errors are assumed as independent, then $E(\eta_i \eta_j) = E(\eta_i) E(\eta_j)$. The covariance between two measuring devices when *i≠j*, is found that

$$Cov(\eta_i, \eta_j) = 0 \tag{D.1.16}$$

The covariance is zero showing two variables are uncorrelated. This means that the variation in one variable has no impact to the other.

The results in (D.1.15) and (D.1.16) can be used to define a covariance matrix, *R*, where the element in position (*i*,*j*) is *Cov*(η_i , η_j), which appear as

$$R = diag\left\{\sigma_1^2 \quad \sigma_2^2 \quad \cdots \quad \sigma_m^2\right\} = \begin{bmatrix} \sigma_1^2 & 0 & \cdots & 0 \\ 0 & \sigma_2^2 & 0 & 0 \\ \vdots & 0 & \ddots & 0 \\ 0 & 0 & 0 & \sigma_m^2 \end{bmatrix} \tag{D.1.17}$$

D.1.2 Weighted least-square estimation

This state-estimation technique aims to eliminate the errors or bad data from the measurements. To achieve this, the weights are added into the state-estimation process where different measuring devices may use different weights, which depend on the value of measurement error of that device.

From (D.1.12), if the correct state x is known, the true values in the measurement model can be considered as

$$\hat{z}_i = h_i(x) \tag{D.1.18}$$

where $h(x)$ is the measurement function matrix that is $m \times n$ dimension.

The measurement equation in form of a vector of function in terms of the state variables, given by

$$Z_i = h_i(x) + \eta_i \tag{D.1.19}$$

From (D.1.19), it is found that the error is $\eta_i = Z_i - h_i(x)$. Similar to (D.1.3), the sum of squared errors can be expressed as

$$J = \frac{1}{2}\sum_{i=1}^{m}\eta_i^2 = \frac{1}{2}\eta^T\eta = \frac{1}{2}\left(z - h(x)\right)^T\left(z - h(x)\right) \tag{D.1.20}$$

The weight is added in (D.1.20) to eliminate the errors of measurements. From the suggestion in [D.3], the good choice of weight is $\frac{1}{\sigma_i^2}$ since a good device has small σ_i^2 or large $\frac{1}{\sigma_i^2}$ whereas the bad device has large σ_i^2 or small $\frac{1}{\sigma_i^2}$. Therefore, (D.1.20) is modified as

$$J(x) = \frac{1}{2}\sum_{i=1}^{m}\frac{\eta_i^2}{\sigma_i^2} = \frac{1}{2}\sum_{i=1}^{m}\frac{\left(z_i - h_i(x)\right)^2}{\sigma_i^2} \tag{D.1.21}$$

From (D.1.17), the matrix R can be substituted in (D.1.21), then

$$J(x) = \frac{1}{2}\sum_{i=1}^{m}\frac{\eta_i^2}{R} = \frac{1}{2}\sum_{i=1}^{m}R^{-1}\left(z_i - h_i(x)\right)^2 \tag{D.1.22}$$

The $J(x)$ is minimised to solving the value of x, demonstrated in the form of

$$g(x) = \frac{\partial}{\partial x}J = 0 \rightarrow \begin{bmatrix} \frac{\partial J}{\partial x_1} \\ \vdots \\ \frac{\partial J}{\partial x_n} \end{bmatrix} = \begin{bmatrix} 0 \\ \vdots \\ 0 \end{bmatrix} \tag{D.1.23}$$

From (D.1.22), the expression of term $g(x)$ in (D.1.23) is

$$g(x) = \frac{\partial J(x)}{\partial x} = \frac{1}{2}\sum_{i=1}^{m}-2R^{-1}\left(z_i - h_i(x)\right)\frac{\partial h_i(x)}{\partial x} = \sum_{i=1}^{m}-\frac{\partial h_i(x)}{\partial x}R^{-1}\left(z_i - h_i(x)\right) \tag{D.1.24}$$

Therefore, (D.1.24) can be written in the matrix form as

$$g(x)=\frac{\partial J(x)}{\partial x}=-\begin{bmatrix} \frac{\partial h_1(x)}{\partial x_1} & \frac{\partial h_2(x)}{\partial x_1} & \cdots & \frac{\partial h_m(x)}{\partial x_1} \\ \frac{\partial h_1(x)}{\partial x_2} & \frac{\partial h_2(x)}{\partial x_2} & \cdots & \frac{\partial h_m(x)}{\partial x_2} \\ \vdots & \vdots & \ddots & \vdots \\ \frac{\partial h_1(x)}{\partial x_n} & \frac{\partial h_2(x)}{\partial x_n} & \cdots & \frac{\partial h_m(x)}{\partial x_n} \end{bmatrix} R^{-1} \begin{bmatrix} z_1-h_1(x) \\ z_2-h_2(x) \\ \vdots \\ z_m-h_m(x) \end{bmatrix} \qquad \text{(D.1.25)}$$

Let us define a matrix $H(x)=\frac{\partial h_i(x)}{\partial x}$ (i.e. $m\times n$ dimension), which is the transpose of the first matrix in (D.1.25). It is found that H is similar to a power flow Jacobian matrix. Hence, it can be called "the measurement Jacobian matrix".

The optimality condition of J can be expressed as

$$g(x)=-H^T(x)R^{-1}\left(z-h(x)\right)=0 \qquad \text{(D.1.26)}$$

Since (D.1.26) is non-linear, it can be solved by using an iterative algorithm such as the Newton algorithm.

A Taylor series is applied to $g(x)$ to prepare for the iteration process. If the high-order terms are ignored, it is found that

$$g\left(x^{(0)}+\Delta x^{(0)}\right)=g\left(x^{(0)}\right)+\nabla_x g(x)\big|_{x^{(0)}}\,\Delta x^{(0)}=0 \qquad \text{(D.1.27)}$$

where x_0 is an initial estimate of the solution and $\Delta x^{(0)}$ is a relatively small deviation from the correct solution.

Therefore, the error $\Delta x^{(0)}$ is found that

$$\Delta x^{(0)}=-\frac{1}{\nabla_x g(x)\big|_{x^{(0)}}}\,g\left(x^{(0)}\right)=-G\left(x^{(0)}\right)^{-1}g\left(x^{(0)}\right) \qquad \text{(D.1.28)}$$

when $G(x)$ is the gain matrix which are the second derivatives of J with respect to the state variables. Then, $G(x)$ can be expressed as

$$G(x) = \frac{\partial g(x)}{\partial x} = \frac{\partial}{\partial x}\left\{-H^T(x)R^{-1}\left(z - h(x)\right)\right\} = H^T(x)R^{-1}\frac{\partial h(x)}{\partial x} \quad \text{(D.1.29)}$$

It is recognised that the term $\frac{\partial h(x)}{\partial x}$ is $H(x)$. From (D.1.27) and (D.1.29), (D.1.28) can be written as

$$\Delta x^{(k)} = \frac{1}{H^T\left(x^{(k)}\right)R^{-1}H\left(x^{(k)}\right)} \times H^T\left(x^{(k)}\right)R^{-1}\left(z - h\left(x^{(k)}\right)\right) \quad \text{(D.1.30)}$$

where k is the iterative sequence, where k=0 is the initial condition.

For the new iteration, the updated state variable, x, is

$$x^{(k+1)} = x^{(k)} + \Delta x \quad \text{(D.1.31)}$$

The iteration process is continued until the values of state variables are less than the specific error value, ε .

From [D.3], the iterative algorithm for WLSE can be summarised as follow:

1. Start iterations, set the iteration index k=0.
2. Initialise the state vector $x^{(k)}$
3. Calculate the gain matrix, $G(x^{(k)})$
4. Calculate the function $g(x^{(k)})$
5. Decompose $G(x^{(k)})$ and solve for $\Delta x^{(k)}$
6. Test for convergence $\Delta x^{(k)} \leq \varepsilon$
7. If no, update $x^{(k+1)}=x^{(k)} + \Delta x^{(k)}$, and go to step 3. Else, stop

The above algorithm essentially involves the following computations in each iteration, k, as;

a) Calculating the measurement function, $h(x^{(k)})$
b) Building the measurement Jacobian, $H(x^{(k)})$

D.2 State-estimation in power systems

In case that the power system has N buses, the state vector will have 2N-1 elements fully observable. In addition, there are N-1 elements of bus voltage phase angles and N elements

of bus voltage magnitudes. If bus 1 is assumed as the reference, the state vector can be written as

$$x^T = [\delta_2 \quad \delta_3 \quad \cdots \quad \delta_N \quad V_1 \quad V_2 \quad \cdots \quad V_N] \tag{D.2.1}$$

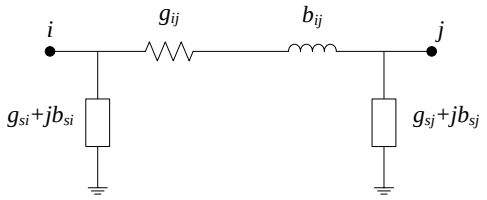

Figure D.2.1. π -model network.

From the general two-port π model network in Figure D.2.1, the measurement function, $h(x)$ includes the line power flows, bus power injections, bus voltage magnitudes and line current flow magnitudes. Follow the explanation in [D.3], the detail of each component is:

Active and reactive power injection at bus i:

$$P_i = V_i \sum_{j \in N_i} V_j (G_{ij} \cos\delta_{ij} + B_{ij} \sin\delta_{ij}) \tag{D.2.2}$$

$$Q_i = V_i \sum_{j \in N_i} V_j (G_{ij} \sin\delta_{ij} - B_{ij} \cos\delta_{ij}) \tag{D.2.3}$$

Active and reactive power flow from bus i to bus j:

$$P_{ij} = V_i^2 (g_{si} + gi_j) - V_i V_j (gi_j \cos\delta_{ij} + b_{ij} \sin\delta_{ij}) \tag{D.2.4}$$

$$Q_{ij} = -V_i^2 (g_{si} + gi_j) - V_i V_j (gi_j \sin\delta_{ij} - b_{ij} \cos\delta_{ij}) \tag{D.2.5}$$

Line current flow magnitude from bus i to bus j:

$$I_{ij} = \frac{\sqrt{P_{ij}^2 + Q_{ij}^2}}{V_i} = \sqrt{\left(g_{ij}^2 + b_{ij}^2\right)\left(V_i^2 + V_j^2 - 2V_i V_j \cos\delta_{ij}\right)} \tag{D.2.6}$$

where V_i, δ_i are the voltage magnitude and phase angle at bus i.

$\delta_{ij} = \delta_i - \delta_j$.

$G_{ij} + jB_{ij}$ is the ij^{th} element of the bus admittance matrix.

$g_{ij} + jb_{ij}$ is the series admittance connecting between buses i and j.

$g_{si} + jb_{si}$ is the shunt admittance connecting at bus i.

N_i is the set of bus members that are directly connected to bus i.

Using the equations in the measurement function, $h(x)$, the measurement Jacobian H can be found that

$$H = \begin{bmatrix} \frac{\partial P_{inj}}{\partial \delta} & \frac{\partial P_{inj}}{\partial V} \\ \frac{\partial P_{flow}}{\partial \delta} & \frac{\partial P_{flow}}{\partial V} \\ \frac{\partial Q_{inj}}{\partial \delta} & \frac{\partial Q_{inj}}{\partial V} \\ \frac{\partial Q_{flow}}{\partial \delta} & \frac{\partial Q_{flow}}{\partial V} \\ \frac{\partial I_{mag}}{\partial \delta} & \frac{\partial I_{mag}}{\partial V} \\ 0 & \frac{\partial V_{mag}}{\partial V} \end{bmatrix} \tag{D.2.7}$$

The expressions for each element in H are;

Elements corresponding to active power injection measurements

$$\frac{\partial P_i}{\partial \delta_i} = \sum_{j=N_i} V_i V_j (-G_{ij} \sin \delta_{ij} + B_{ij} \cos \delta_{ij}) - V_i^2 B_{ii} \tag{D.2.8}$$

$$\frac{\partial P_i}{\partial \delta_j} = V_i V_j (G_{ij} \sin \delta_{ij} + B_{ij} \cos \delta_{ij}) \tag{D.2.9}$$

$$\frac{\partial P_i}{\partial V_i} = \sum_{j=N_i} V_j (G_{ij} \cos \delta_{ij} + B_{ij} \sin \delta_{ij}) - V_i G_{ii} \tag{D.2.10}$$

$$\frac{\partial P_i}{\partial V_j} = V_i (G_{ij} \cos \delta_{ij} + B_{ij} \sin \delta_{ij}) \tag{D.2.11}$$

Elements corresponding to reactive power injection measurements

$$\frac{\partial Q_i}{\partial \delta_i} = \sum_{j=N_i} V_i V_j (G_{ij} \cos \delta_{ij} + B_{ij} \sin \delta_{ij}) - V_i^2 G_{ii} \tag{D.2.12}$$

$$\frac{\partial Q_i}{\partial \delta_j} = V_i V_j (-G_{ij} \cos \delta_{ij} - B_{ij} \sin \delta_{ij}) \tag{D.2.13}$$

$$\frac{\partial P_i}{\partial V_i} = \sum_{j=N_i} V_j (G_{ij} \sin \delta_{ij} - B_{ij} \cos \delta_{ij}) - V_i B_{ii} \tag{D.2.14}$$

$$\frac{\partial P_i}{\partial V_j} = V_i (G_{ij} \sin \delta_{ij} - B_{ij} \cos \delta_{ij}) \tag{D.2.15}$$

Elements corresponding to real power flow measurements

$$\frac{\partial P_{ij}}{\partial \delta_i} = V_i V_j (-g_{ij} \sin \delta_{ij} + b_{ij} \cos \delta_{ij}) \tag{D.2.16}$$

$$\frac{\partial P_{ij}}{\partial \delta_j} = -V_i V_j (g_{ij} \sin \delta_{ij} - b_{ij} \cos \delta_{ij}) \tag{D.2.17}$$

$$\frac{\partial P_{ij}}{\partial V_i} = V_j (g_{ij} \cos \delta_{ij} + b_{ij} \sin \delta_{ij}) + 2V_i (g_{ij} + g_{si}) \tag{D.2.18}$$

$$\frac{\partial P_{ij}}{\partial V_j} = -V_i (g_{ij} \cos \delta_{ij} + b_{ij} \sin \delta_{ij}) \tag{D.2.19}$$

Elements corresponding to reactive power flow measurement

$$\frac{\partial Q_{ij}}{\partial \delta_i} = -V_i V_j (g_{ij} \cos \delta_{ij} + b_{ij} \sin \delta_{ij}) \tag{D.2.20}$$

$$\frac{\partial Q_{ij}}{\partial \delta_j} = V_i V_j (g_{ij} \cos \delta_{ij} + b_{ij} \sin \delta_{ij}) \tag{D.2.21}$$

$$\frac{\partial Q_{ij}}{\partial V_i} = -V_j (g_{ij} \sin \delta_{ij} - b_{ij} \cos \delta_{ij}) - 2V_i (b_{ij} + b_{si}) \tag{D.2.22}$$

$$\frac{\partial Q_{ij}}{\partial V_j} = -V_i (g_{ij} \sin \delta_{ij} - b_{ij} \cos \delta_{ij}) \tag{D.2.23}$$

Elements corresponding to voltage magnitude measurements are;

$$\frac{\partial V_i}{\partial V_i} = 1,\ \frac{\partial V_i}{\partial V_j} = 0,\ \frac{\partial V_i}{\partial \delta_i} = 0,\ \frac{\partial V_i}{\partial \delta_j} = 0 \tag{D.2.24}$$

Elements corresponding to current magnitude measurements (the shunt admittance is ignored)

$$\frac{\partial I_{ij}}{\partial \delta_i} = \frac{g_{ij}^2 + b_{ij}^2}{I_{ij}} V_i V_j \sin \delta_{ij} \tag{D.2.25}$$

$$\frac{\partial I_{ij}}{\partial \delta_j} = -\frac{g_{ij}^2 + b_{ij}^2}{I_{ij}} V_i V_j \sin \delta_{ij} \tag{D.2.26}$$

$$\frac{\partial I_{ij}}{\partial V_i} = \frac{g_{ij}^2 + b_{ij}^2}{I_{ij}} (V_i - V_j \cos \delta_{ij}) \tag{D.2.27}$$

$$\frac{\partial I_{ij}}{\partial V_j} = \frac{g_{ij}^2 + b_{ij}^2}{I_{ij}} (V_j - V_i \cos \delta_{ij}) \tag{D.2.28}$$

References

[D.1] F.C. Schweppe, J. Wildes, "Power System Static-State Estimation: Part I, Part II and Part III", *Transactions on Power Apparatus and Systems*, Vol. 89, No. 1, 1970 p.p. 120-135.

[D.2] J. McCalley. (2012, May, 1). *Steady State Analysis: State Estimation* [course online]. Available: http://home.eng.iastate.edu/~jdm/ee553/ee553schedule.htm.

[D.3] A. Abur, A.G. Exposito, Power System State Estimation; Theory and Implementation. Marcel Dekker, Inc, 1st edition, 2004, chapter 2.

Appendix E: Voltage source converter controller

E.1 Space-vector control for VSC

The space-vector control is used for VSC-based DG. This method controls the voltage outputs of converter to track a current injected into the AC system. The control scheme is developed based on the *dq* synchronous rotating reference frame which decouples the control for the real and imaginary current components. This control method consists of two main classes of two dimensional frames, the *αβ*-frame and the *dq*-frame called the stationary frame and the rotating frame respectively. Furthermore, the control signals are assumed as DC waveform under steady state conditions, so the controller can operate under variable-frequency applications.

The detail of the transformations is adopted from [E.1]. The *αβ*-frame is the transformation from *abc* frame into the Cartesian coordinate system where real and imaginary parts of current from the transformation are function of time. If $i(t)$ is the current-controlled signal, that is, time-varying function, the transformation from three phase *abc*-frame into *αβ*-frame can be written as:

$$\begin{bmatrix} i_\alpha(t) \\ i_\beta(t) \end{bmatrix} = \frac{2}{3}\begin{bmatrix} 1 & -1/2 & -1/2 \\ 0 & \sqrt{3}/2 & -\sqrt{3}/2 \end{bmatrix}\begin{bmatrix} i_a(t) \\ i_b(t) \\ i_c(t) \end{bmatrix} \tag{E.1.1}$$

The transformation from *αβ*-frame to *dq*-frame can be represented as:

$$\begin{bmatrix} i_d(t) \\ i_q(t) \end{bmatrix} = \begin{bmatrix} \cos\varepsilon(t) & \sin\varepsilon(t) \\ -\sin\varepsilon(t) & \cos\varepsilon(t) \end{bmatrix}\begin{bmatrix} i_\alpha(t) \\ i_\beta(t) \end{bmatrix} \tag{E.1.2}$$

In case of a constant-frequency VSC system, $\varepsilon = \varepsilon_0 + \omega_0 t$. In addition, ω_0 is the AC system operating frequency and ε_0 is an initial phase angle between the real axis of the *αβ*– and *dq*-frames (constant value). The ε can be obtained by using a phase-lock loop (PLL), in case of a grid–connected VSC system. The coordination system between *αβ*- and *dq*-frame is demonstrated in Figure E.1.1.

On the other hand, the *dq*-frame can be converted back to the *abc*-frame using the inverse transformation of (E.1.1) and (E.1.2) in the following way:

$$\begin{bmatrix} f_a(t) \\ f_b(t) \\ f_c(t) \end{bmatrix} = \begin{bmatrix} 1 & 0 \\ -1/2 & \sqrt{3}/2 \\ -1/2 & -\sqrt{3}/2 \end{bmatrix} \begin{bmatrix} \cos\varepsilon(t) & -\sin\varepsilon(t) \\ \sin\varepsilon(t) & \cos\varepsilon(t) \end{bmatrix} \begin{bmatrix} f_d(t) \\ f_q(t) \end{bmatrix} \quad \text{(E.1.3)}$$

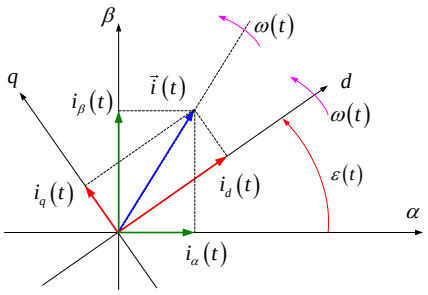

Figure E.1.1. *αβ*- and *dq*-frame coordination system.

E.2 VSC controllers

The details of VSC current control, *P* and *Q* controls and AC voltage control are explained in this section.

E.2.1 VSC current control

The control algorithm of the grid-side VSC is derived from the power transfer across an impedance (see Figure 4.1). The resistance, *R*, and inductance, *L*, combine the impedance of the smoothing reactor and the coupling transformer. The voltage drop between the VSC and the PCC, with the AC system can be written as

$$v_t(t) - v_s(t) = L\frac{di(t)}{dt} + Ri(t) \quad \text{(E.2.1)}$$

The output current of the VSC in *dq* components can be expressed as

$$\begin{aligned} L\frac{di_d(t)}{dt} &= -Ri_d(t) + u_d(t) \\ L\frac{di_q(t)}{dt} &= -Ri_q(t) + u_q(t) \end{aligned} \quad \text{(E.2.2)}$$

where

$$\begin{aligned} u_d(t) &= +L\omega_0 i_q + v_{t,d}(t) - v_{s,d}(t) \\ u_q(t) &= -R_s i_q(t) - L\omega_0 i_d + v_{t,q}(t) - v_{s,q}(t) \end{aligned} \quad \text{(E.2.3)}$$

where ω_0 is the source frequency, u_d and u_q are new control inputs used by the PWM generators. These modified inputs include components obtained from the VSC and feed-

forward terms to eliminate the cross-coupling elements. Therefore, the terms $v_{s,d}$, $v_{s,q}$, $L\omega_0 i_q$ and $L\omega_0 i_d$ can also be considered as disturbance inputs from the control point of view.

From (E.2.3), it is found that the coupled terms are eliminated and independent control of i_d and i_q is achieved. Therefore, the current controller can be sketched in the simplified control block diagram, after Laplace transformation, as shown in Figure E.2.1. The PI controller is used as a compensator to track the change of the output currents, i_d and i_q, compared with the reference currents, $i_{d,ref}$ and $i_{q,ref}$, correspondingly.

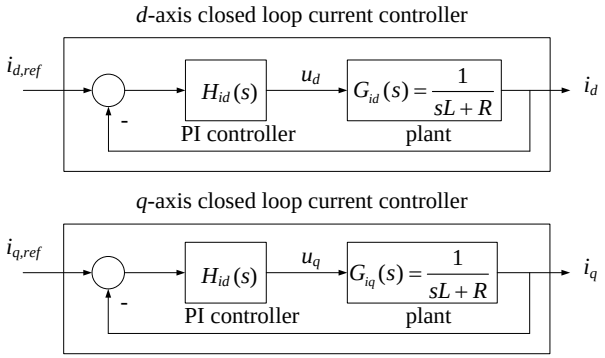

Figure E.2.1. Simplified control block diagram of the VSC current controller.

E.2.2 VSC active and reactive powers control

The dynamic behaviour of the VSC can be analysed by using P and Q as dynamic variables. The analysis of the dynamic model of P and Q is adopted from [E.2]. From Figure E.2.2, the active and reactive powers injected to the ac system at the PCC (in the dq frame) are

$$\begin{aligned} P(t) &= \frac{3}{2}\left[v_{s,d}(t)i_d(t) + v_{s,q}(t)i_q(t)\right] \\ Q(t) &= \frac{3}{2}\left[-v_{s,d}(t)i_q(t) + v_{s,q}(t)i_d(t)\right] \end{aligned} \tag{E.2.4}$$

From the analysis in [E.2], the dynamics of the VSC in terms of active and reactive powers are:

$$\begin{aligned} L\frac{dP(t)}{dt} &= -RP(t) + u_P(t) \\ L\frac{dQ(t)}{dt} &= -RQ(t) + u_Q(t) \end{aligned} \tag{E.2.5}$$

where

$$u_P(t) = -L\omega_0 Q(t) + \frac{3}{2}\left(\left(v_{t,d}v_{s,d} + v_{t,q}v_{s,q}\right) - \left(v_{s,d}^2 + v_{s,q}^2\right)\right)$$
$$u_Q(t) = +L\omega_0 P(t) + \frac{3}{2}\left(v_{s,d}v_{t,q} - v_{s,d}v_{t,q}\right) \quad \text{(E.2.6)}$$

It is found that the dynamics of the VSC in terms of P and Q are similar to the dynamics of i_d and i_q, as found in (E.2.2). The cross-coupling elements between P and Q can also be considered as disturbance inputs. Additionally, P is controlled based on the d-axis current, and Q is controlled based on the q-axis current. The PI controller is also used as a compensator to track the change of P and Q from VSC compared with the reference values, P_{ref} and Q_{ref}, respectively. The decoupled P and Q control block diagrams, in the Laplace domain, are shown in Figure E.2.2.

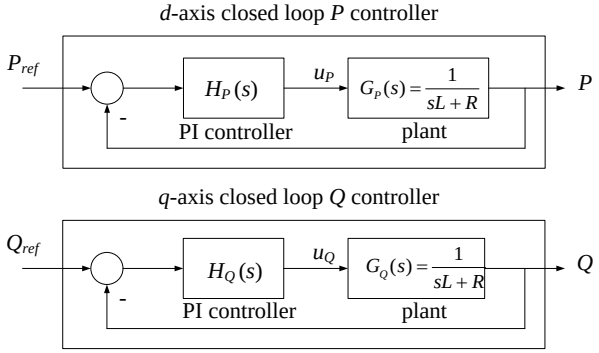

Figure E.2.2. Simplified control block diagram of the VSC P and Q controllers.

E.2.3 AC voltage controller

The AC voltage control can be determined from the voltage drop between the VSC and the PCC. From Figure 4.1, the voltage drop, Δv, over the line impedance can be approximated as

$$\Delta v(t) = v_s(t) - v_t(t) \approx \frac{RP(t) + \omega_0 LQ(t)}{v_s(t)} \quad \text{(E.2.6)}$$

As $R << \omega_0 L$, the value of voltage drop will depend on the flow of reactive power. With this assumption, the AC voltage can be controlled by using Q, decoupled from the P control.

From the above approximation, (E.2.6) can be rewritten as

$$v_s(t) = \frac{\omega_0 LQ(t)}{v_s(t)} + v_t(t) \quad \text{(E.2.7)}$$

where v_t can be considered as a disturbance signal. The instantaneous AC voltage at the PCC can be considered as the sum of an average ac voltage value, v_{s0} and a voltage ripple Δv_s, where $v_s = v_{s0} + \Delta v_s$. However, the voltage ripple should be very small and then Δv_s may be neglected, so $v_s \approx v_{s0}$. The dynamics of the voltage at the PCC bus can be written as

$$v_s(t) = \frac{\omega_0 L Q(t)}{v_{s0}} \tag{E.2.8}$$

where v_{s0} is the average AC voltage at the PCC bus which is a constant value.

Figure E.2.3, shows the schematic block diagram of the AC voltage controller which is the outer loop controller for AC voltage regulation based on the Q controller. The PI controller can be used as the compensator to regulate the AC voltage at the PCC by comparing the measured signal with the reference voltage, $V_{ac,ref}$, which may be set equal to v_{s0}.

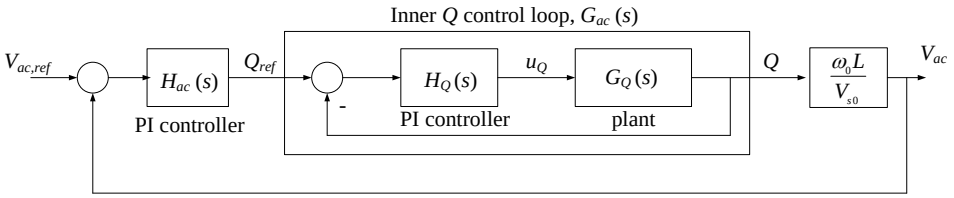

Figure E.2.3. Control block diagram of the outer loop controller for the ac voltage control.

E.3 VSC-based DG parameters and stability analysis

The detail of selecting the size of components to develop the VSC based DG system is discussed. The value of the PI controllers' gains is initially calculated using root-locus and then final values obtained by fine-tuning using trial and error method. The stability analysis is used to examine the DG's controllers to ensure that the control performances (e.g. speed response, robustness and stability) are good enough.

E.3.1 Converter capacity

The conventional VSC-based DG is operated under fixed unity power factor condition where the capacity of the VSC is nearly equal to the active power output rating. However, the

available Q is required to support the voltage control. This means the converter has to be oversized. The capacity of the converter is determined from

$$S \geq \sqrt{P_{rate}^2 + Q_{available}^2} \tag{E.3.1}$$

Where S is the capacity of the converter (rated apparent power), P_{rate} is the rated active power and $Q_{available}$ is the expected available reactive power to support voltage control.

E.3.2 Smooth reactor and coupling transformer

The recommend size of the smoothing reactor (or phase reactor), is usually in the range of 0.1 p.u. to 0.2 p.u [E.3]. From [E.4], the transformer impedance can be calculated based on

$$\begin{aligned} Z_T &= \frac{\%u_k}{100} \cdot \frac{U_T^2}{S_T} \\ R_T &= \frac{\%u_r}{100} \cdot \frac{U_T^2}{S_T} = \frac{P_{Cu}}{3I_{rT}^2} \\ X_T &= \sqrt{Z_T^2 - R_T^2} \end{aligned} \tag{E.3.2}$$

where u_k is the short-circuit voltage of the transformer (in %), u_r is the rated resistive component of the short-circuit voltage (in %) at the rated current, I_{rT}. U_T is rate voltage (LV side), S_T is the rated apparent power, and P_{Cu} is the copper losses.

E.3.3 DC capacitor

The size of the DC capacitor is considered from the level of allowable DC voltage variation, typically 5% [E.5]. From [E.6], the design of the DC-link capacitor of the VSC can be determined from

$$C = \frac{S}{V_{DC} \cdot \Delta V_{DC} \cdot 2 \cdot \omega_e} \tag{E.2.3}$$

where C is DC link capacitor, S is the rated apparent power of the converter, V_{DC} is the nominal DC voltage, ΔV_{DC} is the allowed voltage ripple (peak to peak) and ω_e is the electrical frequency.

E.3.4 VSC-based DG parameters

The size of the VSC, smoothing reactor and coupling transformer are the same for each DG. The different power outputs among DG units can be defined by adjusting the reference values in the individual DG controllers. The parameters of the VSC-based DG system are given in Table E.3.1.

At the initial condition, the DG is set to operate under *PQ* mode, where the AC voltage controller is not connected yet. In case that the DG is operated at unity p.f., the reference value of reactive power, Q_{ref}, in the *Q* controller is set to zero. Moreover, the amount of available *Q* support from DG can be adapted by adjusting the limits of the *Q* output, Q_{min} and Q_{max}, of the PI in the *Q* controller. The limit of *Q* support is ± 1 MVar for this work.

Table E.3.1. Parameters of the VSC-based DG system.

Device	Parameters
Voltage source converter	2 MVA, V_{dc} = 1 kV, v_t = 0.44 kV
DC capacitor	C = 0.063 F (5% peak to peak voltage ripple)
Smoothing reactor	R = 0.0005 Ω, L = 0.0462 mH
Shunt Filter	R = 0.004 Ω, L = 0.0116 mH, C = 0.0018 F
Transformer	2.5 MVA, 0.44/12.66 kV, u_k = 10 %, u_r = 1.27 %

The gain parameters of each PI compensator of VSC controllers are illustrated in Table E.3.2. Initial values calculated using root-locus [E.7] and final values obtained by fine tuning using trial and error method.

Table E.3.2. PI controllers' gains.

Controllers	Gain parameters
i_d controller	K_{id} = 0.2 T_{id} = 0.08
i_q controller	K_{iq} = 0.2 T_{iq} = 0.08
P controller	K_P = 0.7 T_P = 0.1
Q controller	K_Q = 0.6 T_Q = 0.1
V_{ac} controller	K_{Pac} = 10 T_{ac} = 0.1
Droop controller	K_{pq} = 0.05 K_{dq}=0.005

Note that the *V*-*Q* droop controller is added only in case of voltage interactions mitigation.

E.3.5 Stability test

From the VSC-based DG system in the previous section, the stability performance of the inner and outer controllers with the controllers' gains in Table E.3.2., can be investigated by

determining the gain margin and phase margin using Bode diagrams. The stabilities of the inner current controllers (i.e. i_d and i_q), and outer controller (i.e. P, Q, V_{ac} and V_{dc}) are examined based on its control block diagram, as shown in section 4.2. The results from the frequency domain analysis, of each controller, are shown in Figure E.3.1.

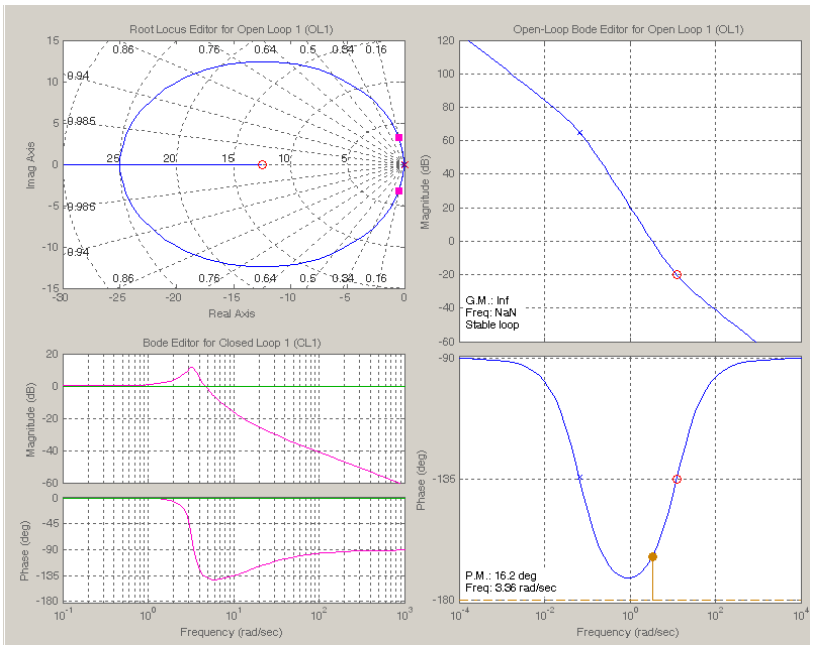

(a) Inner current controller (i_d controller)

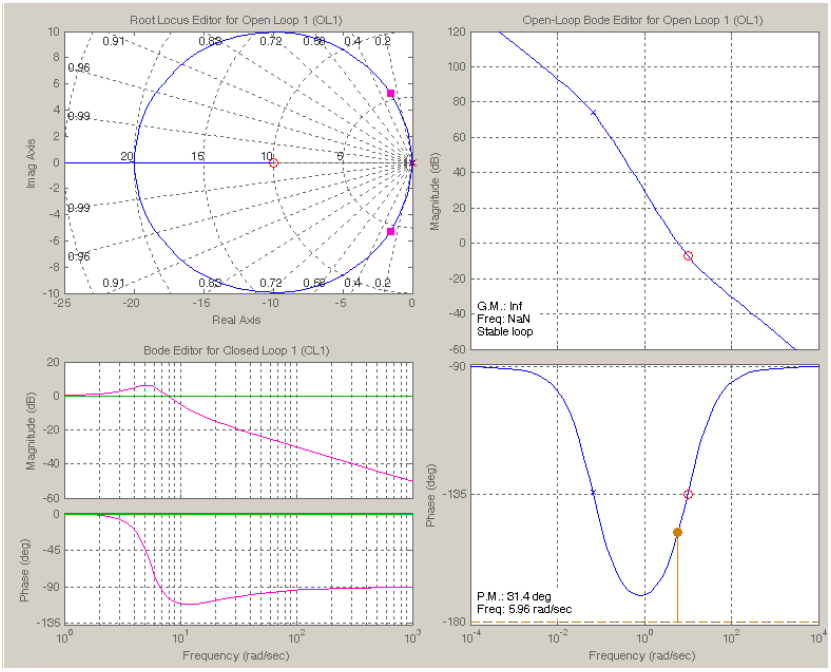

(b) P controller

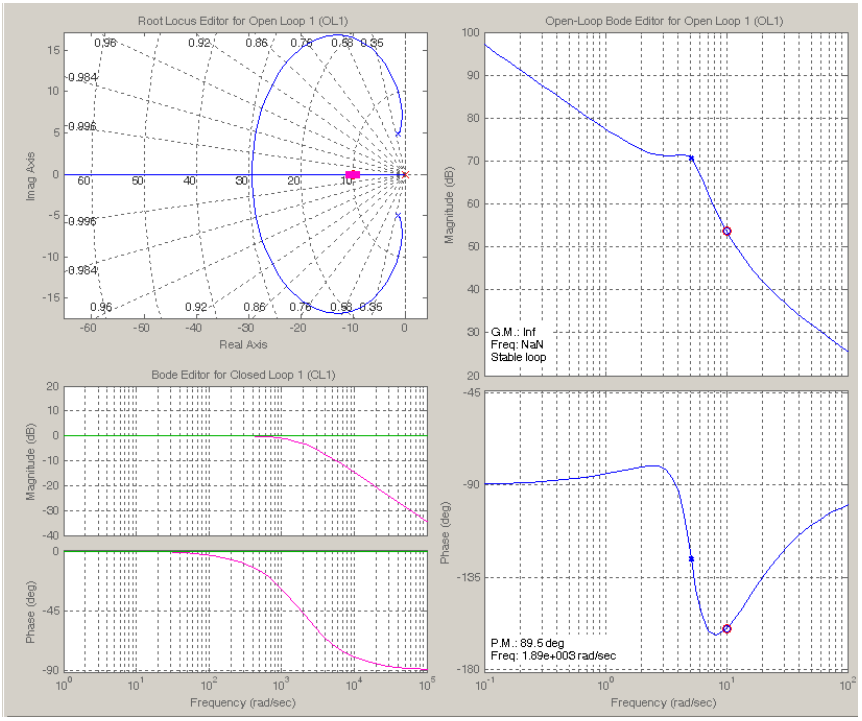

(c) AC voltage controller

Figure E.3.1. Results from the frequency domain analysis of i_d, P and AC voltage controller.

From Figure E.3.1., it was found that the values of phase-shift angle of these three controllers are not over 180°. This means that the controllers are stable. The responses of VSC control in different conditions are examined in the next section.

E.3.6 Adaptability of the VSC-based DG with voltage control under different operating conditions

It is important to mention that the PI controllers' gains in this work are not adaptive, they are fixed, i.e. an adaptive controller is not designed. However, the defined gains are robust to enable a good control system performance under various operating scenarios.

In the following, the robustness of the VSC-based DG controller is examined under several scenarios to ensure it still can work properly under different network conditions. The transient stability of the VSC is analysed by investigating the transient responses of the VSC outputs such as P, Q and AC voltage.

E.3.6.1 Robustness of controllers to system parameters

The robustness of the VSC to system parameters is examined by changing the values of inductor, *L*, of the series reactor, which are 110% and 80% of the base case value. The responses of the VSC to a step change of the VSC reactive power output, from 0 to 1 MVar, are investigated. The simulation results of *P*, *Q* and AC voltage at the PCC are shown in Figure E.3.2. It was found that the VSC controller has a good performance under different system parameters.

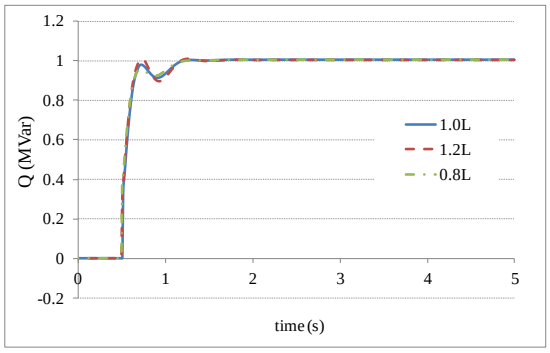

(a) Reactive power from VSC

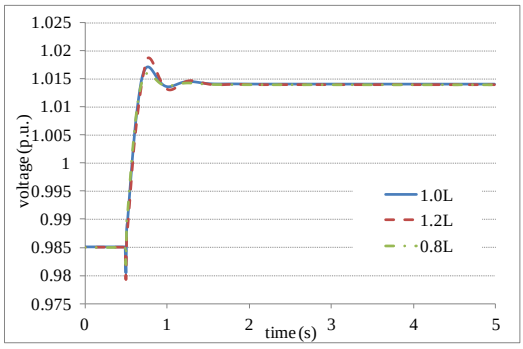

(b) Voltage at VSC

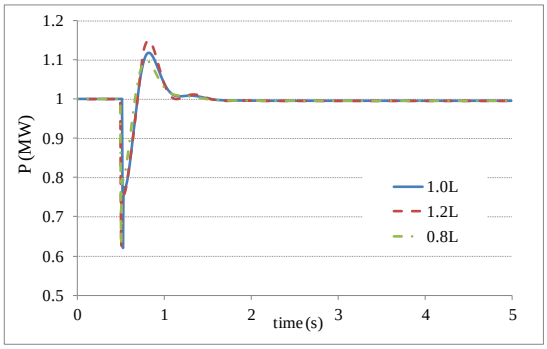

(c) Active power from VSC

Figure E.3.2. System performance when *L* of the series reactor is changed.

E.3.6.2 Robustness of controllers to change in operating point

The VSC operation should be adequate in the event of changes in the operating point when the demand of the network has changed. The transient performance of the VSC is examined under light and heavy load conditions that affect directly to the voltage level of the network, as can be seen in Figure E.3.3. It was found that the VSC controller can perform well in different network conditions.

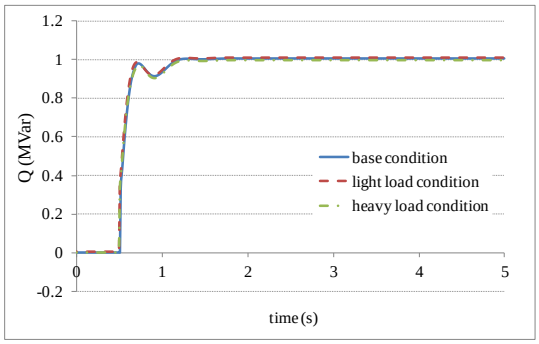

(a) Reactive power from VSC

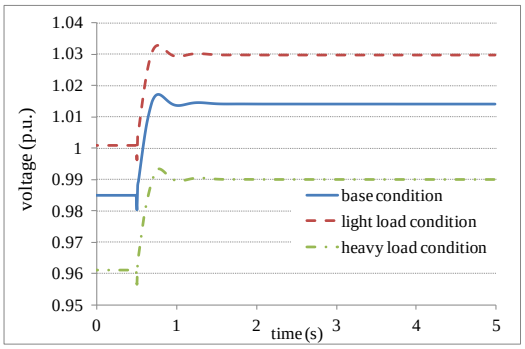

(b) Voltage at VSC

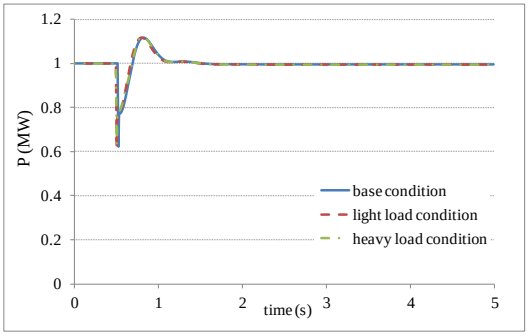

(c) Active power from VSC

Figure E.3.3. System performance under different network's loading conditions.

E.3.6.3 Robustness of controllers to different voltage level disturbances

The performance of the AC voltage controller is examined by applying a disturbance such as voltage sag with different retained voltage levels. In addition, the level of voltage drop affects the change of P and Q from the VSC, as determined from equations (E.3.4) and (E.3.5). Therefore, in case of VSC-based DG, the active power generated from the VSC may change to the new value corresponding to the voltage level during the disturbance. The VSC-based DG performance to changes in the voltage sag level is demonstrated in Figure E.3.4. It can be seen that the VSC controller can operate under different levels of voltage disturbances. The voltage support is sufficient when the level of voltage is small due to the limitation of available Q support from DG. Hence, the voltage controller may be not necessary for the extreme disturbances with very high voltage drops.

$$P \approx \frac{v_s v_t}{X_L} \sin \delta \qquad \text{(E.3.4)}$$

$$Q \approx \frac{v_s^2}{X_L} - \frac{v_s v_t}{X_L} \cos\delta \qquad \text{(E.3.5)}$$

where X_L is the reactance of the series reactor and δ is the phase angle between the voltages at the VSC and the PCC.

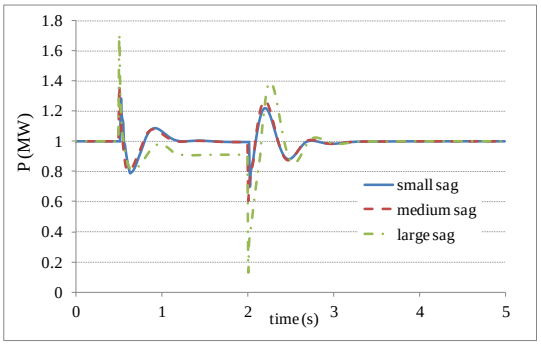

(a) Active power from the VSC

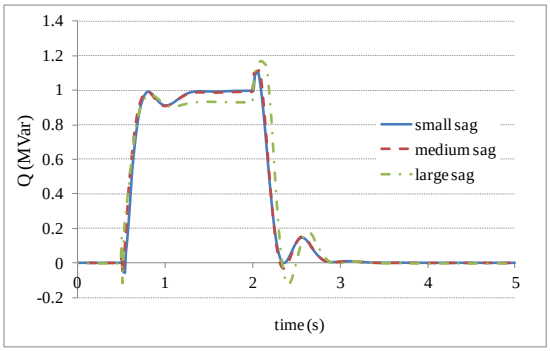

(b) Reactive power from the VSC

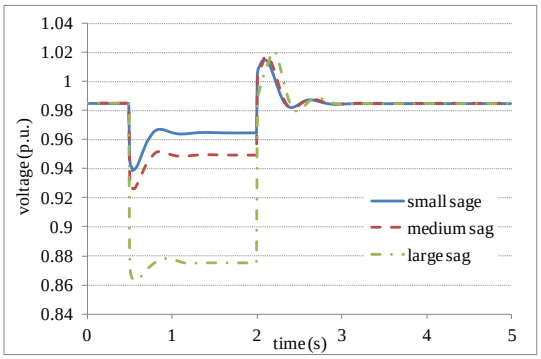

(c) Voltage at VSC

Figure E.3.4. System performances under different voltage sag levels.

References

[E.1] A. Yazdani and R. Iravani, *Voltage-Sourced Converters in Power Systems*, 1 ed.: Wiley, 2010, chapter 3.

[E.2] A. Tabesh and R. Iravani, "Multivariable Dynamic Model and Robust Control of a Voltage-Source Converter for Power System Applications," *IEEE Transactions on Power Delivery*, vol. 24, no. 1, pp. 462-471, Jan. 2009.

[E.3] T. W. Shire, "VSC-HVDC Based Network Reinforcement," Delft University of Technology, 2009, Chapter 3.

[E.4] T. N. Boutsika and S. a. Papathanassiou, “Short-circuit calculations in networks with distributed generation,” *Electric Power Systems Research*, vol. 78, no. 7, pp. 1181-1191, Jul. 2008.

[E.5] A. Constantin, “Advanced Modelling and Control of Wind Power Systems,” Aalborg University, Denmark, 2009, chapter 3.

[E.6] A. D. Hansen, C. Jauch, P. Sørensen, F. Iov, and F. Blaabjerg, “Dynamic Wind Turbine Models in Power System Simulation tool DIgSILENT,” Riso National Laboratory, Riso-R-1400(ed.2). 2003. p.p. 160.

[E.7] D. Xue, Y. Q. Chen, and D. P. Atherton, *Linear feedback control: analysis and design with MATLAB*. Society for Industrial and Applied Mathematics, 2009, chapter 6.

Appendix F: Synchronous machine-based DG

F.1 Synchronous machine parameters

The synchronous generator used in Chapter 4 is assumed as a generator with the steam turbine. This generator is 2 MVA, 0.44 kV and ±0.87 power factor which aims to supply active power at 1.0 MW and available reactive power at ±1.0 MVar to support voltage control. The machine data of this generator is modified from the typical data of 1.5 MVA, 3.3 kV, 50 Hz permanent magnet synchronous generator provided in DIgSILENT *PowerFactory*. The detail of synchronous machine parameters is illustrated in Table F.1.1.

Table F.1.1. Synchronous machine data.

Basic Data					
Nominal Apparent Power : 2 MVA Nominal Voltage : 0.44 kV Power Factor : 0.87 Connection : Delta Rotor type : Round rotor					
Inertia Acceleration time constant : 2 s					
Stator resistances (Leakage reactances)			Synchronous reactances		
rslr	0.0001	p.u.	x_d	1.5	p.u.
xl	0.05	p.u.	x_q	1.5	p.u.
xrl	0	p.u.			
Transient time constants			Transient reactances		
T_d'	0.016667	s	x_d'	0.25	p.u.
T_q'	0.008333	s	x_q'	0.3	p.u.
Subtransient time constants			Subtransient reactances		
T_d''	0.0136	s	x_d''	0.17	p.u.
T_q''	0.005667	s	x_q''	0.17	p.u.

F.2 Turbine governor

The steam-turbine governor model TGOV1 is used to control active power output from the generator. The schematic of the TGOV1 controller is shown in Figure F.2.1. The initial controller gains are referred from [F.1]. Then, a fine-tuning is conducted to obtain the final settings (typically done by trial and error). The gain parameters of this turbine governor are illustrated in Table F.2.1.

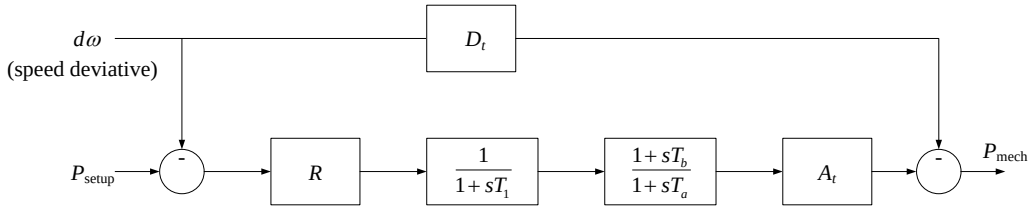

Figure F.2.1. TGOV1 block diagram.

Table F.2.1. TGOV1 gain parameters.

Description		parameter
T_1	Governor time constant (s)	0.1
T_b	Turbine Derivative time constant (p.u.)	0.09
T_a	Turbine delay time constant (p.u.)	0.2
A_t	Turbine power coefficient (p.u.)	1
D_t	Frictional losses factor (p.u.)	0.02
R	Controller droop (p.u.)	0.05
V_{min}	Minimum gate limit (p.u.)	0
V_{max}	Maximum gate limit (p.u.)	1

F.3 Excitation system

The 1981 IEEE type AC1 excitation system model is used for active voltage control of the generator. The block diagram of this excitation system and the gain parameters are shown in Figure F.3.1, and Table F.3.1, respectively.

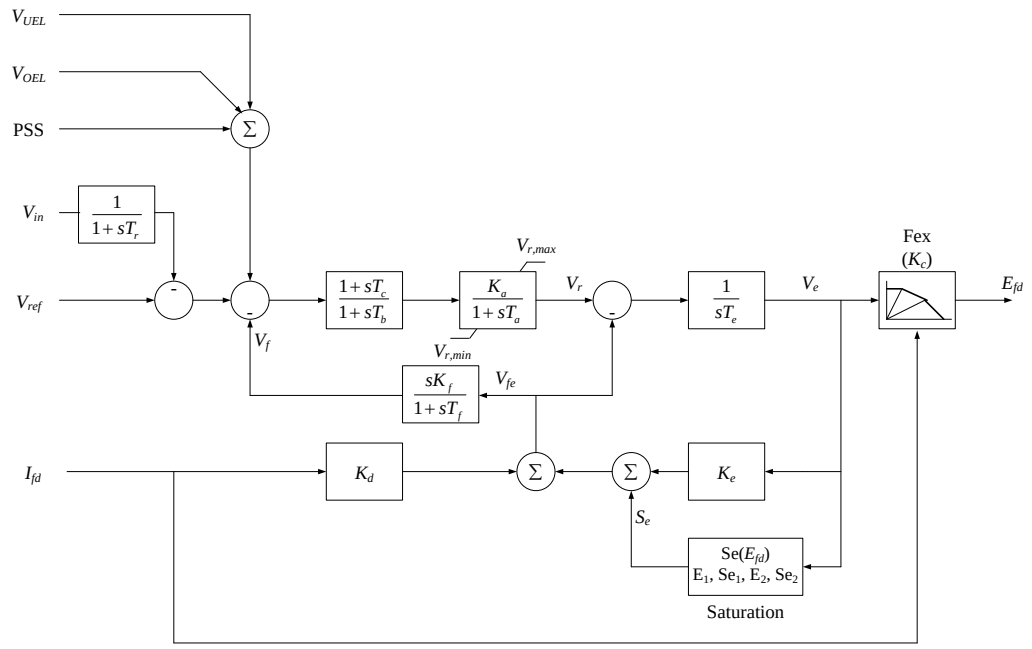

Figure F.3.1. IEEE type AC1 excitation system block diagram.

Table F.3.1. IEEE type AC1 excitation's gain parameters.

Description		Parameter
T_r	Measurement delay (s)	0.01
T_b	Filter delay time (s)	0.1
T_c	Filter derivative time constant (s)	0.1
K_a	Controller gain (p.u.)	250
T_a	Controller time constant (s)	0.095
T_e	Exciter time constant (s)	0.8
K_f	Stabilization path gain (p.u.)	0.03
T_f	Statbilization path delay time (s)	1
K_c	Rectifier regulation constant (p.u.)	0.2
K_d	Exciter Amature reaction Factor (p.u.)	0.2
E_1	Saturation Factor 1 (p.u.)	3.13
Se_1	Saturation Factor 2 (p.u.)	1.73
E_2	Saturation Factor 3 (p.u.)	4.18
Se_2	Saturation Factor 4 (p.u.)	4.3
K_e	Exciter Constant (p.u.)	0.1
$V_{r,min}$	Controller Minimum output (p.u.)	-40
$V_{r,max}$	Controller Maximum output (p.u.)	40

References

[F.1] Siemens, "Dynamic Models Package Standard 1of GMB Dynamic Model for PSS Software Product Suite", revision 1.3, 2010.

Appendix G: The IEC Flicker Meter

The assessment of flicker in the power system is explained in this section. The level of flicker can be measured and assessed by using the standard flickermeter. Additionally, the IEC standard flickermeter (i.e. IEC 61000-4-15 [G.1]) used in this research is discussed.

G.1 Flicker Assessment

Flicker is basically assessed by two parameters, which are;

- P_{st} is a measure of short-term flicker severity obtained for 10 minutes interval. The period of 10 minutes observation is long enough to prevent too much weight to isolate voltage changes and to allow observation of the persistence of the disturbance. A unit of P_{st} corresponds to the threshold of irritability that is independent from the source of the disturbance.

- P_{lt} is a measure of long-term flicker severity obtained for a two-hour period. This means that it is calculated from 12 consecutive values of P_{st}, as given by

$$P_{lt} = \sqrt[3]{\frac{\sum_{i=1}^{12} P_{st,i}^3}{12}} \qquad \text{(G.1.1)}$$

  This parameter provides a criterion for the long term flicker assessment when flicker sources with long and variable duty cycle are concerned. Alternatively, this parameter is used to assess the flicker when several disturbing loads operate simultaneously in a random way.

The limits on the flicker severity are necessary in order to ensure that the flicker is not annoying to the human's eyes. For a power system, P_{st} and P_{lt} should not exceed the planning levels specified by the supply utility for all voltage levels of the system. From IEC 61000-3-7 [G.2], the indicative planning levels of MV and HV systems are shown in Table G.1.1. Furthermore, planning levels for LV and MV systems are equal to or less than the compatibility level which are illustrated in Table G.1.2. Note that the planning levels may take different values from case to case depending on internal quality objectives of individual utilities.

Table G.1.1. Indicative planning levels for P_{st} and P_{lt} in MV, HV and EHV systems.

Flicker Index	Planning levels	
	MV	HV and EHV
P_{st}	0.9	0.8
P_{lt}	0.7	0.6

Table G.1.2. Compatibility levels for P_{st} and P_{lt} in LV and MV systems

Flicker Index	Compatibility levels
P_{st}	1.0
P_{lt}	0.8

G.2 IEC Flickermeter

Standard IEC 61000-4-15 provides the functional and design specification for flicker measurement for all practical voltage fluctuation waveforms. The flickermeter can transform the input voltage fluctuations into an output parameter proportionally related to flicker perception, by simulating the process of physiological visual perception (i.e. lamp-eye-brain chain) based on a 230 V, 60 W, incandescent lamp. In addition, IEC 61000-4-15 is based on the analogue implementations especially models of bulb and human reaction although an instrument is totally or partially digital, which consists of three main compositions as can be seen in Figure G.2.1.

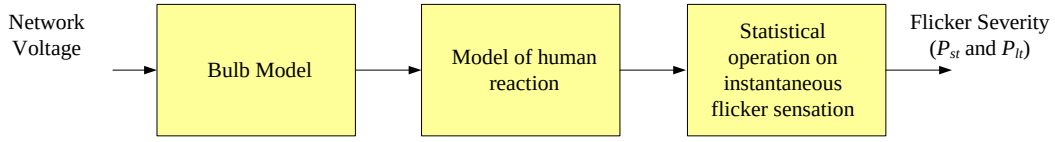

Figure G.2.1. Main block diagram of IEC flickermeter

The architecture of the IEC flickermeter is shown in Figure G.2.2, taken from [G.3]. It is found that the flickermeter can be divided into two parts, which are;

1. Simulation of the response of the lamp-eye-brain chain (blocks 2, 3 and 4)
2. Online statistical analysis of the flicker signal and presentation of results (block 5)

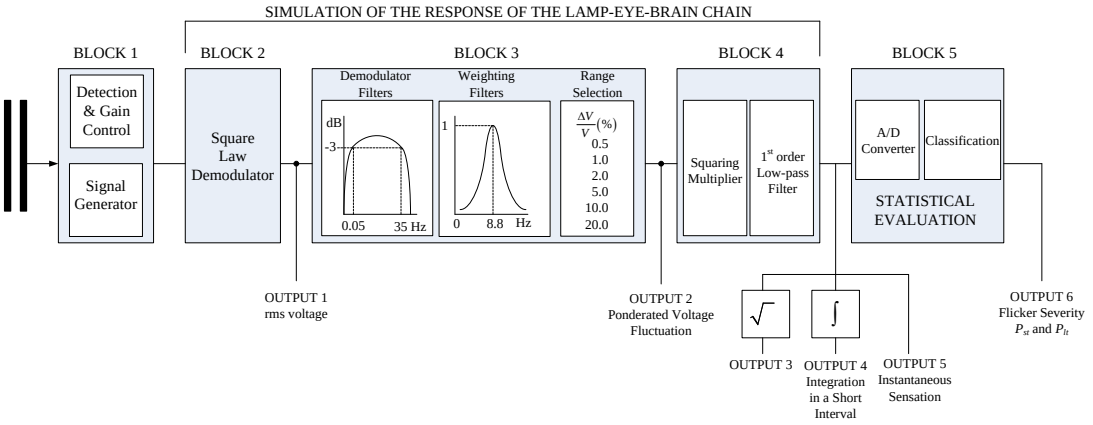

Figure G.2.2. Schematic description of the IEC flickermeter.

Block 1: Voltage Adapting Circuit

Block 1 contains a voltage scaling circuit to scale the input voltage down to an internal reference level independently of the actual input voltage and express as a percent ratio. The input voltage can be averaged by adjusting the gain of the block with a time constant. Additional, the time constant is equal to 1 minute which is long enough to produce the correct voltage change while still allowing following closely slow variation produced by regulation of the supply system [G.3]. Moreover, a signal generator is used for the on-site calibration.

Block 2: Square Law Demodulator

Block 2 is a square law demodulator (or a quadratic demodulator) that recovers the voltage fluctuation by squaring the input voltage, thus simulating the behaviour of an incandescent lamp. From the explanation in [G.3], the operation of a square law demodulation can be explained by using an example of a sinusoidal voltage modulated by a sinusoidal voltage fluctuation as expressed as

$$v(t) = A\cos\omega_p t \cdot (1 + m\cos\omega_m t) \qquad \text{(G.2.1)}$$

where $v(t)$ is the supply voltage with amplitude A at angular frequency ω_p, and m is the amplitude of the sinusoidal voltage fluctuation that modulates the carrier with angular frequency ω_m. Then, applying the square law demodulation to this signal, the output is

$$v_S(t) = \left[v(t)\right]^2 = \frac{A^2}{2}\left(1+\frac{m^2}{2}\right) + \frac{A^2}{2}\left(1+\frac{m^2}{2}\right)\cos 2\omega_p t + \frac{m^2A^2}{8}\cos 2\left(\omega_p+\omega_m\right)t$$
$$+ \frac{m^2A^2}{8}\cos 2\left(\omega_p-\omega_m\right)t + \frac{m^2A^2}{2}\cos\left(2\omega_p+\omega_m\right)t + \frac{m^2A^2}{2}\cos\left(2\omega_p-\omega_m\right)t \qquad \text{(G.2.2)}$$
$$+ mA^2\cos\omega_m t + \frac{m^2A^2}{2}\cos 2\omega_m t$$

Block 3: Demodulator Filter and Weighting Filter

Block 3 is composed of a cascade of two filters which are a demodulator filter and a weighting filter. The demodulator filter eliminates the DC component and the components with frequency higher than ω_p of the demodulator (Block 2) output. The filter incorporates a first order high-pass (suggested 3 dB cutoff frequency at about 0.05 Hz) to eliminate the DC component and a low-pass filter to eliminate the high frequency components, which is a 6th order Butterworth filter with a 3 dB cut-off frequency of 35 Hz for 230 V/50 Hz systems. In case that assuming the output from block 2 is (G.2.2), the voltage signal after through this filter can be expressed as

$$v_F(t) = mA^2\cos\omega_m t + \frac{m^2A^2}{2}\cos 2\omega_m t \qquad \text{(G.2.3)}$$

The weighting filter is the band pass filter which aims to simulate the frequency response to sinusoidal voltage fluctuations of a coiled filament gas-filled lamp combined with the human visual system. A band pass response has a maximum gain for frequencies between 8 and 10 Hz that correspond to the maximum perceptibility of light intensity variations (i.e. 8.8 Hz in Figure G.2.2).

The transfer function of the weighting filter for a 230 V, 60 W, incandescent lamp [G.3] is

$$F(s) = \frac{k\omega_1 s}{s^2+2\lambda+\omega_1^2} \times \frac{1+ s/\omega_2}{\left(1+ s/\omega_3\right)\left(1+ s/\omega_4\right)} \qquad \text{(G.2.4)}$$

Where s is the Laplace complex variable and the values of each parameter can be listed as below [G.1];

k = 1.74802, $\lambda = 2\pi \times 4.05981$, $\omega_1 = 2\pi \times 9.15494$
$\omega_2 = 2\pi \times 2.27979$, $\omega_3 = 2\pi \times 1.22535$, $\omega_4 = 2\pi \times 21.9$

It is found that the combined effect of these two filters in block 3 gives a strong attenuation at frequencies out of the band of 0.05-35 Hz

Block 4: Non-Linear Variance Estimator

Block 4 is the non-linear variance estimator. It consists of a squaring multiplier to simulate the human non-linear visual perception, and a first-order low-pass filter with a time constant of 300 ms to simulate the storage effect of the human brain. The output from Block 4 represents the instantaneous flicker level which is an instantaneous signal proportionally related to the visual sensation of licker. Furthermore, the absolute value of this signal must be converted into per units of perceptibility by scaling it down to a value of the perceptibility threshold. In addition, the perceptibility threshold level is given by a sinusoidal voltage fluctuation of 0.25 % amplitude and 8.8 Hz frequency (i.e. 1 p.u. of perceptibility as the output of block 4). Therefore, the outputs which are higher than the perceptibility threshold level means that flicker is more than perceptible and can become annoying and intolerable [G.3]. The example of the output from block 4 can be seen in Figure G.2.3 (a).

Block 5: Statistical Evaluation

Block 5 is the statistical calculator to perform the on-line analysis of the flicker level over a selected observation period. The outputs of this block are the values of P_{st} and P_{lt} which is mandatory and is connected to a serial digital interface suitable for a printer and other types of recorder The cumulative probability function of the instantaneous flicker sensation over the 10-minute observation period is evaluated by distributing the flicker sensation from block 4 into a certain number of classes. In addition, the IEC requires at least 64 classes for the classifier [G.4]. The counter of each class is incremented by one unit when the sample value of flicker sensation exceeds the threshold value corresponding to that class. Then, the cumulative probability function will be obtained which represents the percentage of the observation time that the sample values belong to those classes. Figure G.2.3 (adopted from [G.3]) shows the cumulative probability function calculation assuming only four classes are used for the classification.

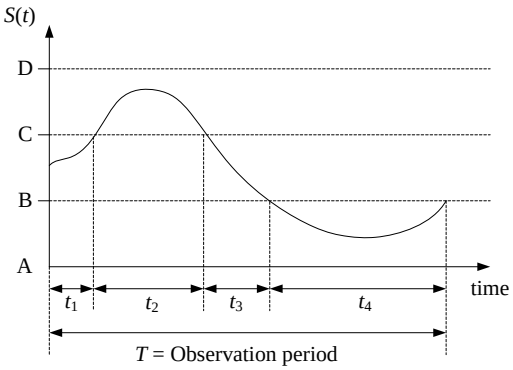

(a) Instantaneous flicker sensation (Output of block 4)

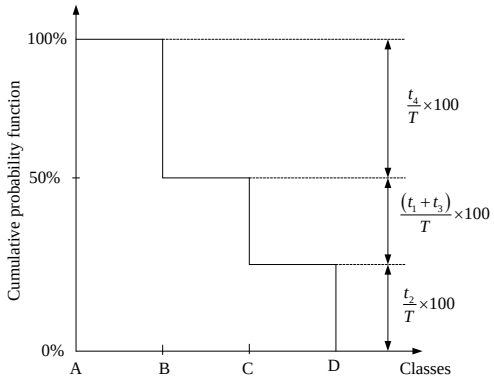

(b) Cumulative probability function (%)

Figure G.2.3. Instantaneous flicker sensation and cumulative probability function calculations.

According to [G.1], the short-term flicker severity, P_{st}, can be calculated by

$$P_{st} = \sqrt{0.0314P_{0.1} + 0.0525P_{1s} + 0.0657P_{3s} + 0.28P_{10s} + 0.08P_{50s}} \qquad \text{(G.2.5)}$$

where $P_{0.1}$, P_{1s}, P_{3s}, P_{10s} and P_{50s} are the percentiles of the flicker levels have been exceed for 0.1%, 1%, 3%, 10% and 50% of the observation time of ten minutes. The suffix '*s*' indicates that the smooth values which the averaging have been applied according to the following equations;

$$P_{1s} = \left(P_{0.7} + P_1 + P_{1.5}\right)/3 \qquad \text{(G.2.6)}$$

$$P_{3s} = \left(P_{2.2} + P_3 + P_4\right)/3 \qquad \text{(G.2.7)}$$

$$P_{10s} = \left(P_6 + P_8 + P_{10} + P_{13} + P_{17}\right)/5 \qquad \text{(G.2.8)}$$

$$P_{50s} = \left(P_{30} + P_{50} + P_{80}\right)/3 \qquad \text{(G.2.9)}$$

The example of a P_{st} recording is demonstrated in Figure G.2.4, taken from [G.5], which the flicker source is an arc furnace connected to the network. It is found that the flicker level is increased dramatically during the furnace operation.

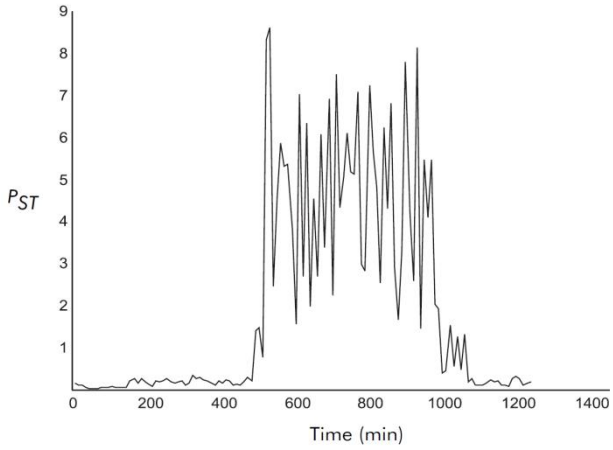

Figure G.2.4. P_{st} valules determined during operation of an arc furnace.

References

[G.1] IEC 61000-4-15 (1997-11), Electromagnetic compatibility (EMC) – Part 4: Testing and measurement techniques – Section 15: Flickermeter – Functional and design specifications.

[G.2] IEC 61000-3-7 (1996-11), Electromagnetic Compatibility (EMC) – Part 3: Limits-Section 7: Assessment of emission limits for fluctuating loads in MV and HV power systems.

[G.3] A. Baggini, *Handbook of Power Quality*. Chichester, UK: John Wiley & Sons, Ltd, 2008, chapter 5.

[G.4] B. Alencar, J. G. Filho, R. Melo, and R. Leao, "A Flickermeter Design on LabVIEW Based on IEC61000-4-15," *12th IEEE International Conference on Harmonics and Quality of Power (ICHQP)*, Cascais, 2006, pp. 1-6.

[G.5] Cooper Development Association, Power Quality Application Guide: Flicker Measurement in Voltage disturbances, Leonardo Power Quality Initiative (LPQI), 2005.

Appendix H:

Parameters of DSTATCOM-ESS and SST controllers

H.1 Parameters of DSTATCOM-ESS

The gain parameters of controllers in DSTATCOM-ESS are illustrated in Table H.1.1 and Table H.1.2 for *V/Q* and *V/P* compensation, respectively.

Table H.1.1. Gain parameters of DSTATCOM-ESS in case of *V/Q* compensation

Controllers	Gain parameters
i_d controller	$K_{id} = 0.2$ $T_{id} = 0.08$
i_q controller	$K_{iq} = 0.2$ $T_{iq} = 0.08$
P controller	$K_P = 0.7$ $T_P = 0.1$
Q controller	$K_Q = 0.6$ $T_Q = 0.1$
V_{ac} controller	$K_{ac} = 10$ $T_{ac} = 0.1$

Table H.1.2. Gain parameters of DSTATCOM-ESS in case of *V/P* compensation

Controllers	Gain parameters
i_d controller	$K_{id} = 0.2$ $T_{id} = 0.08$
i_q controller	$K_{iq} = 0.2$ $T_{iq} = 0.08$
P controller	$K_P = 0.7$ $T_P = 0.1$
Q controller	$K_Q = 0.6$ $T_Q = 0.1$
V_{ac} controller	$K_{ac} = 4$ $T_{ac} = 0.1$

H.2 Parameter of solid-state transformer

The gain parameter of controllers in AC/DC rectifier and DC/AC inverter of SST is shown in Table H.2.1 and Table H.2.2, respectively.

Table H.2.1. Gain parameters of AC/DC rectifier

Controllers	Gain parameters
i_d controller	$K_{id} = 0.4$ $T_{id} = 0.0001$
i_q controller	$K_{iq} = 0.2$ $T_{iq} = 0.01$
P controller	$K_P = 0.01$ $T_P = 0.001$
Q controller	$K_Q = 0.01$ $T_Q = 0.05$
V_{ac} controller	$K_{ac} = 10$ $T_{ac} = 0.1$
V_{dc} controller	$K_{dc} = 0.005$ $T_{dc} = 0.01$

Table H.2.2. Gain parameters of DC/AC rectifier

Controllers	Gain parameters
i_d controller	$K_{id} = 0.1$ $T_{id} = 0.008$
i_q controller	$K_{iq} = 0.1$ $T_{iq} = 0.08$
V_{ac} controller	$K_{ac} = 0.001$ $T_{ac} = 0.01$
V_{dc} controller	$K_{dc} = 0.005$ $T_{dc} = 0.8$

Appendix I: Hunting Detector of Substation's OLTC

The OLTC controller should ensure that the other voltage should not exceed its limit after the tap is changed which causes the controller cannot stop the voltage control operation. The tap should not be changed if the controller can detect that the hunting effect will happen. Additionally, the hunting is checked by determining from the different value, ΔV_{re}, between the other voltage level which is not the one that is controlled by the OLTC, and its OLTC's limit. To avoid the hunting, this different value needs to be higher than the value of voltage change from tap changing 1 step (dV). For example, in case that $V_{re,min}$ will be controlled by the OLTC, if $V_{re,min}$ is lower than $V_{OTLC,min}$, the gap ($\Delta V_{re,max}$)between $V_{re,max}$ and $V_{OTLC,max}$ is determined. Hence, the controller will not allow the tap changer process if the value of $\Delta V_{re,max}$ is lower than the value of dV (see Figure I.1).

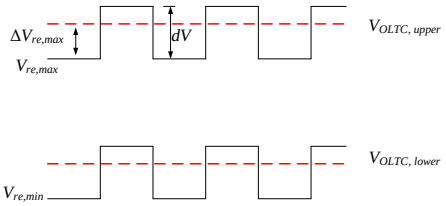

Figure I.1. Hunting effect occurs to $V_{re,max}$ when the OLTC tries to control $V_{re,min}$

The gaps to check the hunting of $V_{re,min}$ and $V_{re,max}$ are in (I.1) and (I.2). The flowchart of hunting effect detector is illustrated in Figure I.2.

$$\Delta V_{re,max} = V_{OLTC,upper} - V_{re,max} \quad \text{(I.1)}$$

$$\Delta V_{re,min} = V_{re,min} - V_{OLTC,lower} \quad \text{(I.2)}$$

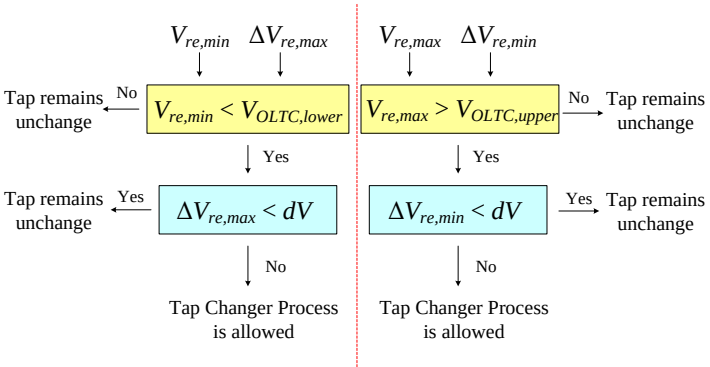

Figure I.2. Flow chart of hunting detector.

Appendix J:

Transformer Winding Configurations and Phase-Shift Determination

J.1 Transformer configurations

There are two main winding configurations for the typical three-phase distribution transformer: wye (or star, Y) and delta (D). The three windings are given names as W_1, W_2 and W_3. A balanced 3-phase positive sequence voltage (*abc* sequence) is applied to three transformer phase bushings: A, B and C respectively.

Moreover, alternate transformer winding configurations are referred to by terms such as Dy# or Yy#, or Yd#, where # is the value of phase-shift counting by clock method (0-12 hour). Phase angle is shifted 30^o per each hour (i.e. 360^o in case of 12 hour). This phase angle is important when one needs a common reference for determining phase shift across the transformer (both sides).

J.1.1 Wye winding configurations

There are 6 different wye connection structures as can be seen in Figure J.1.1(a). In addition, Y0 or Y6 are the most seen in the common practice [J.1]. The use of Y* is for naming each of the configurations which * refers to the phase angle between the voltage across winding W_1 and voltage at A bushing (phase *a* assuming as the reference phase), following a 12 hour clock.

J.1.2 Delta winding configurations

There are 6 different delta connection structures as shown in Figure J.1.1(b). D1 or D11 are the most common used in the normal US market, while D5 and D7 configurations can be seen in some international markets.

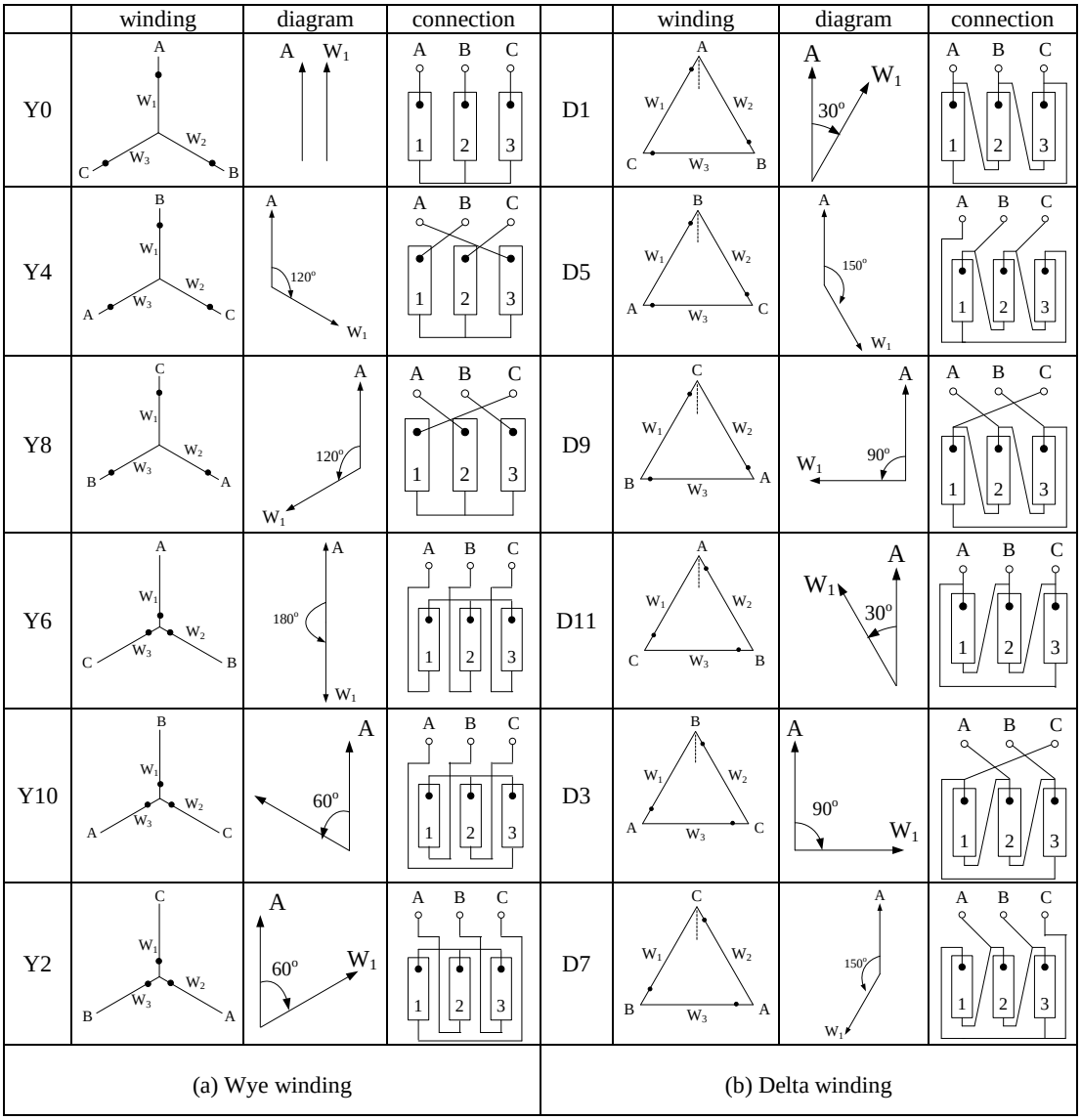

Figure J.1.1. Three phase transformer winding configurations.

J.2 Phase-shift determination

To determining the phase shift, it can be explained from an example which is assuming the primary is D1 and the secondary side is Y0.

J.2.1 Primary side (D1)

The bushing voltages followed a balanced three-phase positive sequence voltages are

$$A_1 = V_1\angle 0°;\ \ B_1 = V_1\angle 240°;\ \ C_1 = V_1\angle 120° \qquad \text{(J.2.1)}$$

where V_1 is the voltage magnitude at the primary side. Note that subscript 1 is referring the primary side of transformer.

From the winding connections in Figure J.1.1(b), the voltage across winding, W_1, can be written as

$$\begin{aligned} W_1 &= A_1 - C_1 \\ &= V_1\angle 0° - V_1\angle 120° \\ &= \sqrt{3}V_1\angle -30° \end{aligned} \qquad \text{(J.2.2)}$$

It is found that the voltage across W_1 is 30° lagging compared with the reference voltage at A bushing, as can be seen from the phasor diagram in Figure J.1.1(b).

J.2.2 Secondary side (Y0)

Similar to the primary side, the bushing voltages of the secondary side are;

$$A_2 = V_2\angle 0°;\ \ B_2 = V_2\angle 240°;\ \ C_2 = V_2\angle 120° \qquad \text{(J.2.3)}$$

where V_2 is the voltage magnitude at the secondary side. Note that subscript 2 is referring the secondary side of transformer.

From Figure J.1.1(a), the voltage across winding, W_1, can be written as

$$W_1 = A_2 = V_2\angle 0° \qquad \text{(J.2.4)}$$

It is found that the voltage across W_1 is in phase with the bushing A voltage, as can be seen from the phasor diagram in Figure J.1.1(a).

J.2.3 Phase shift across the transformer

The phase shift across the transformer (both sides) is found by lining up the voltage across W_1 on different sides of a transformer and seeing how the A bushing voltages on each side compare. The phasor diagram between the voltages at bushing A of primary and secondary

sides is presented in Figure J.2.1. It is found that the phase difference between the primary and secondary voltage is 30° which this winding configuration can be written as Dy1.

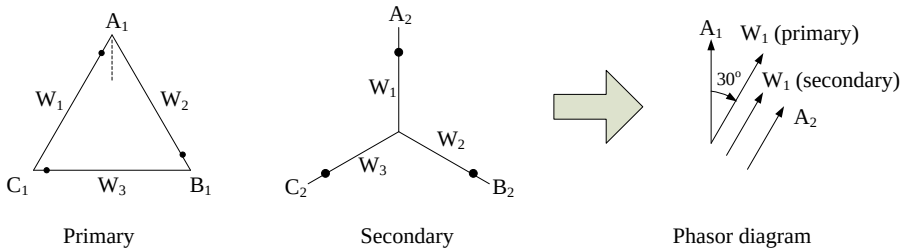

Figure J.2.1. Phasor diagram of voltages between primary and secondary sides (D1 and Y0)

References

[J.1] L. Lawhead, R. Hamilton, and J. Horak, "Three phase transformer winding configurations and differential relay compensation," Basler Electric Company, 2006.

Appendix K: Test System

K.1 33 bus distribution network

The test system is a 12.66 kV distribution system which is referred from [K.1]. It consists of 33 buses and 5 tie lines. The base case is assumed that all tie lines are opened and the total load conditions are 3.75 MW and 2.30 MVar, as illustrated in Figure K.1.1. The detail of load connections and line parameters is shown in Table K.1.1. This test system is used for case studies in Chapter 3 to Chapter 5.

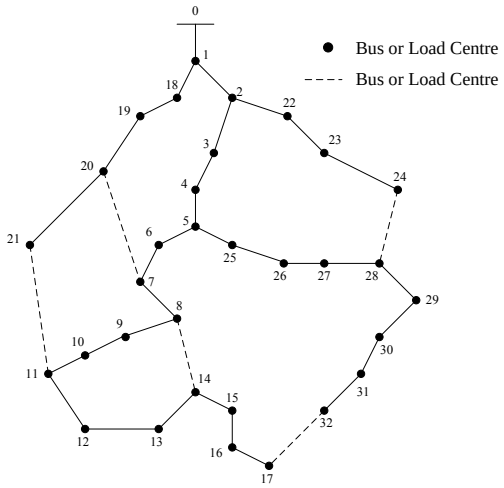

Figure K.1.1. 33 bus distribution network

Table K.1.1. Line parameters and load connections in 33 bus test system.

Bus to Bus	Section Resistance (Ohm)	Section Reactance (Ohm)	End bus real load (kW)	End bus reactive load (kVar)	Bus to Bus	Section Resistance (Ohm)	Section Reactance (Ohm)	End bus real load (kW)	End bus reactive load (kVar)
0-1	0.0922	0.0470	100	60	19-20	0.4095	0.4784	90	40
1-2	0.4930	0.2511	90	40	20-21	0.7089	0.9373	90	40
2-3	0.3660	0.1864	120	80	2-22	0.4512	0.3083	90	50
3-4	0.3811	0.1941	60	30	22-23	0.8980	0.7091	420	200
4-5	0.8190	0.7070	60	20	23-24	0.8960	0.7011	420	200
5-6	0.1872	0.6188	200	100	5-25	0.2030	0.1034	60	25
6-7	0.7114	0.2351	200	100	25-26	0.2842	0.1447	60	25
7-8	1.0300	0.7400	60	20	26-27	1.0590	0.9337	60	20
8-9	1.0440	0.7400	60	20	27-28	0.8042	0.7006	120	70
9-10	0.1966	0.0650	45	30	28-29	0.5075	0.2585	200	600
10-11	0.3744	0.1238	60	35	29-30	0.9744	0.9630	150	70
11-12	1.4680	1.1550	60	35	30-31	0.3105	0.3619	210	100
12-13	0.5416	0.7129	120	80	31-32	0.3410	0.5320	60	40
13-14	0.5910	0.5260	60	10	7-20	2.0	2.0		
14-15	0.7463	0.5450	60	20	8-14	2.0	2.0		
15-16	1.2890	1.7210	60	20	11-21	2.0	2.0		
16-17	0.7320	0.5740	90	40	17-32	0.5	0.5		
1-8	0.1640	0.1565	90	40	24-28	0.5	0.5		
18-19	1.5042	1.3554	90	40					

For transient studies, the short circuit MVA of the upstream network is assumed as 500 MVA, which the *R/X* ratio is approximately 0.2 (see more detail in [K.2]).

The substation transformer is 50 MVA, 115/12.66 kV (YNd5). The short circuit voltage (V_k) is 10.08% and copper loss is 188.098 kW.

K.2 17 bus MV distribution system

The typical MV Dutch distribution network, referred from [K.3], is used for harmonic mitigation studies in Chapter 6.

K.2.1 Typical MV Dutch distribution network

The network is 10 kV which may have 15-25 transformer stations are installed to feed different customers in each feeder. For the based case, the network is assumed that it consists of 17 buses with different types of load connection, as can be seen in Figure K.2.1. In addition, there are three locations where large industrial customer are connected, nine locations for household customer only, four locations where both households and small commercial customers are connected and one location for large commercial customer. The assumptions of designing this network are explained below;

- The short circuit MVA of the MV station is 300 MVA and the voltage at substation is 1.0 p.u.
- The average distance between two buses is 1.2 kilometres.
- Cables are used to connecting between two buses, which line impedance is 0.203 + *j*0.1034 Ω/km.
- Household or small commercial customers or both are loaded by 40-50 % of the transformer rating, which the capacity is 400 kVA. Additionally, the connection of household loads is assumed as balanced connection.
- Large commercial load are fed by 65-70 % of the transformer rating, which the capacity is 630 kVA.
- Industrial loads are fed by their own transformers, which average load demand is 250 kVA each.
- All connected loads have 0.9 lagging power factor.

From above assumptions, the detail of load connections of the based case system can be assumed as in Table K.2.1.

Table K.2.1. Load connections of typical MV Dutch distribution network.

Bus	Type of load	*P* (kW)	*Q* (kVar)	Bus	Type of load	*P* (kW)	*Q* (kVar)
01	Industrial load	0.40	0.19	10	h.h.	0.18	0.09
02	l.c.c	0.40	0.19	11	h.h.+s.c.c	0.18	0.09
03	h.h.	0.18	0.09	12	h.h.+s.c.c	0.18	0.09
04	h.h+s.c.c	0.18	0.09	13	h.h.	0.18	0.09
05	h.h.	0.18	0.09	14	h.h.+s.c.c	0.18	0.09
06	Industrial load	0.40	0.19	15	h.h.	0.18	0.09
07	Industrial load	0.40	0.19	16	h.h.	0.18	0.09
08	h.h.	0.18	0.09	17	h.h.	0.18	0.09
09	h.h.	0.18	0.09				

where, l.c.c is large commercial customer, h.h. is household customer and s.c.c is small commercial customer. Assuming the industrial load is the same consumption as l.c.c to clearly see the impact of harmonic emission from this load type.

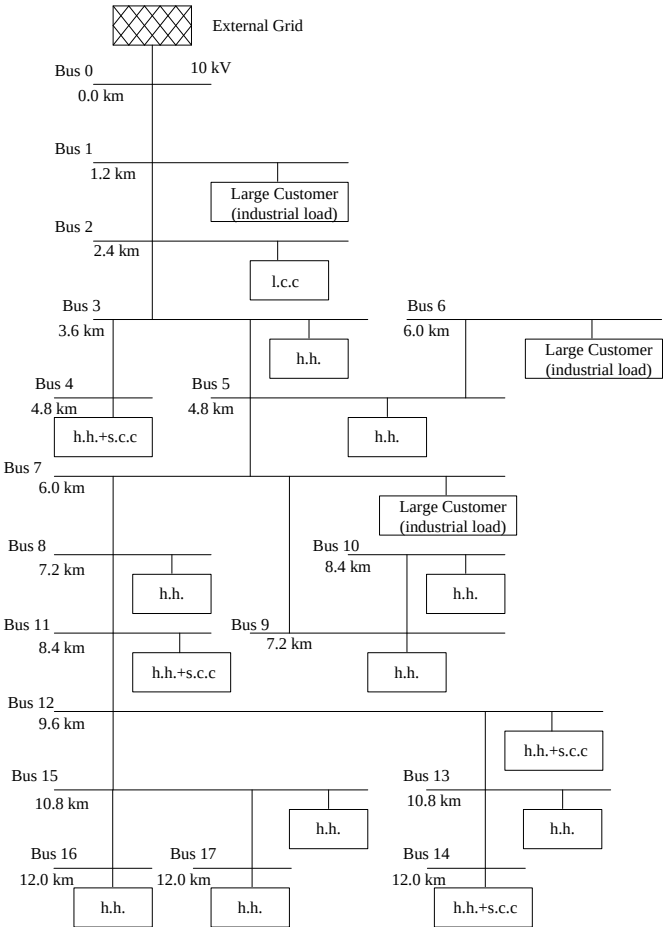

Figure K.2.1. Typical 10 kV Dutch MV feeder.

From load flow calculations, the total load demand using voltage-dependent load models is 3.98 MW and 1.98 MVar (including line losses).

K.2.2 Determining the size and location of DG

The main objective of connecting DG into the system is to reduce loss and improve voltage profile of the system. Therefore, the size and location of DG should provide the minimum grid loss, whilst voltage profile within the statutory limit. The algorithm to find a suitable size and location of DG connection into the distribution network can be explained as below [K.4];

a) Run the base case load flow (using Newton-Raphson method).
b) Consider the active power (*P*) limits of a DG unit.
c) Change active power (*P*) from the minimum value to the maximum value with small steps.
d) In each step of the real power calculation, change the reactive power (*Q*) from 0 to the setting value (such as 80 % of the real power on that step) and then calculate the grid losses and bus voltage
e) Store the reactive power that gives the minimum loss for the related active power, within the voltage limit (normally the statutory limit).
f) Choose the real power with its reactive power that gives the minimum loss for that bus.
g) Repeat these steps for all of the buses and find the best size (active and reactive power) of the DG unit for each bus.
h) Compare the losses of each state find the minimum loss in the distribution system.
i) Store the bus that gives the minimum loss with its DG sizes.
j) Run the base case load flow with DG

In case of determining the DG is operated in unity power factor condition, the reactive power from DG is set as zero (null). Therefore, the step d) can be skipped.

In Chapter 6, the each size of all three DG units is assumed as 1 MW with unity power factor. Therefore, only location of DG is determined by using above algorithm. The location of each DG should provide the minimum power loss whilst all bus voltages are in the statutory limit (i.e. 0.95 – 1.05 p.u.).

From the simulation, it is found that the 1st DG should be connected at bus 15, the 2nd DG should be connected at bus 7 and the 3rd DG should be connected at bus 5. The network loss and voltage profile when an additional DG is connected into the network are shown in Figure K.2.2.

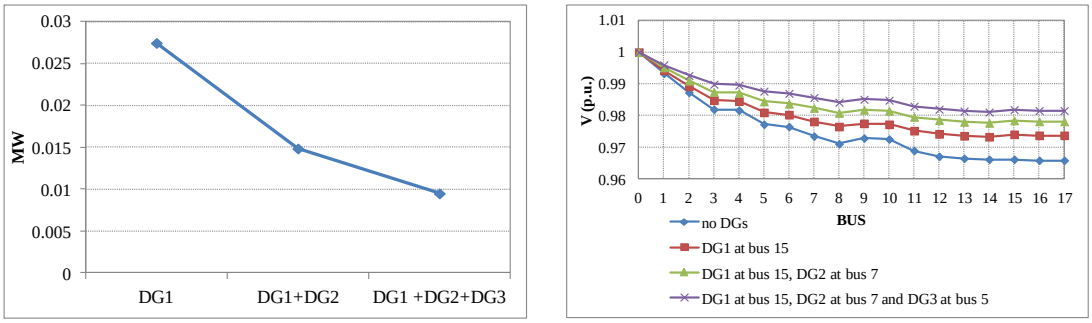

(a) Network losses (b) Voltage profile

Figure K.2.2. Network loss and voltage profile after connecting DGs into the network.

References

[K.1] M. E. Baran and F. F. Wu, "Network reconfiguration in distribution system for loss reduction and load balancing," *Power Delivery, IEEE Transactions*, vol. 4, no. 2, pp. 1401-1407, 1989.

[K.2] B. de Metz-Noblat and F. Dumas, "Cahier Technique no. 158: Calculation of Short-Circuit Currents," in Schneider Electric, updated, no. 158, 2005.

[K.3] S. Bhattacharyya, Z. Wang, J. Cobben, J. Myrzik, and W. Kling, "Analysis of power quality performance of the Dutch medium and low voltage grids," in *Harmonics and Quality of Power, 2008. ICHQP 2008. 13th International Conference on*, Cascais, 2008, pp. 1–6.

[K.4] A. Kazemi and M. Sadeghi, "Distributed Generation Allocation for Loss Reduction and Voltage Improvement," *in Asia-Pacific Power and Energy Engineering Conference*, Wuhan, 2009, pp. 1-6.

Appendix L: Voltage disturbance scenarios

L.1 Voltage sag

The voltage sag scenario is created by applying a three-phase short circuit to ground via a high impedance at a specific bus in the network, as found in Figure L.1. It uses a three-phase short circuit due to the network is assumed as operating under the balanced condition. The value of fault impedance (Z_{fault}) used in this work is varying between 100 to 300 Ω depending on the level of voltage drop in different case studies. Moreover, the temporary voltage imbalance is also created as the same way which is changing from three phase short circuit, to one phase or two phase short circuit to ground or between lines via the impedance (i.e. one or two phase impedance depending on the fault type).

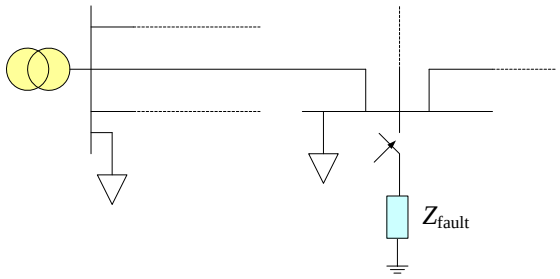

Figure L.3. Voltage sag scenario.

L.2 Voltage swell

The voltage sag scenario is created by injecting additional active power, *P*, (i.e. from the negative load or generator) at a specific bus in the network, as found in Figure L.2. In this work, the value of active power injected into the network is about 1 – 1.5 MW.

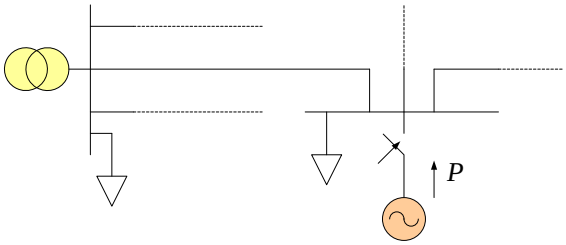

Figure L.4. Voltage swell scenario.